

# Mineral resources of the Precambrian shield of central West Greenland (66° to 70°15'N)

## Part 3. Implications of potential field data for the tectonic framework

Bo Møller Nielsen and Thorkild M. Rasmussen

(1 CD-Rom included)



# **Mineral resources of the Precambrian shield of central West Greenland (66° to 70°15'N)**

## **Part 3. Implications of potential field data for the tectonic framework**

Bo Møller Nielsen and Thorkild M. Rasmussen

(1 CD-Rom included)

# Contents

<b>Contents</b>	<b>3</b>
<b>Abstract</b>	<b>6</b>
<b>Introduction</b>	<b>8</b>
<b>The potential field of the Earth</b>	<b>11</b>
The Earth's magnetic field.....	11
The Earth's gravity field and isostasy.....	11
<b>Petrophysical properties of rocks</b>	<b>14</b>
Magnetic bulk properties .....	14
Magnetisation types .....	15
Classes of magnetic materials in rocks .....	15
Magnetic domains of magnetic mineral grains .....	17
Magnetic properties of rocks .....	18
Densities of rocks.....	20
Application of petrophysical properties in analysis of geophysical data .....	20
<b>Data from West Greenland</b>	<b>21</b>
Aeromagnetic data.....	21
Acquisition.....	21
Gravity data.....	23
Acquisition.....	23
Petrophysical data.....	26
Digital elevation data from West Greenland.....	27
<b>Regional geology of West Greenland</b>	<b>29</b>
Details of the Rinkian and Nagssugtoqidian orogens.....	32
The Rinkian orogen.....	32
The Nagssugtoqidian Orogen .....	34
Northern Nagssugtoqidian orogen.....	34
Central Nagssugtoqidian orogen .....	34
Southern Nagssugtoqidian orogen .....	35
<b>Petrophysical data</b>	<b>36</b>
Petrophysical properties of different lithologies .....	38
Gneiss .....	39
Granite .....	39
Quartz diorite – Arfersiorfik quartz diorite .....	40
Charnockite .....	40

Schist .....	40
Massive sulphides and banded iron formations .....	41
Marble, dolomite and calc-silicate .....	41
Quartzite .....	41
Amphibolite .....	41
Mafic rocks.....	42
Ultramafic rocks .....	42
Granulite and amphibolite facies rocks .....	42
<b>Processing methods for qualitative analysis of potential field data</b>	<b>45</b>
Enhancement of specific wavelengths.....	47
High-pass, low-pass and band-pass filtering .....	47
Enhancement of long-wavelength responses .....	49
Upward continuation and stripping filtering .....	49
Sounding filtering .....	50
Pseudogravity .....	53
Enhancement of short wavelengths.....	55
Downward continuation.....	55
Vertical derivatives – vertical gradients .....	55
Horizontal gradients – directional derivatives.....	60
Curvature analysis .....	61
Curvature of the horizontal gradients .....	61
Terracing operator .....	61
<b>Quantitative analysis of potential field data</b>	<b>62</b>
Euler deconvolution .....	62
Analysis of the analytic signal .....	70
Correlation analysis of gravity and terrain data.....	76
Grids of terrain and gravity data.....	76
Bouguer anomaly and elevation.....	76
Free Air anomaly and elevation .....	78
Residual anomaly.....	83
Discussion on geophysical techniques .....	85
<b>Interpretation and discussion of processed potential field data</b>	<b>86</b>
Responses from different lithologies in general .....	86
Responses from structures in general .....	86
Gravity responses in general .....	87
Regional geophysical patterns and domains .....	87
Southern foreland, southern Nagssugtoqidian Front and southern Nagssugtoqidian orogen.....	88
Southern foreland.....	88
The Southern Nagssugtoqidian Front .....	88
Western SNO .....	90
Middle and eastern part of SNO.....	90

Central Nagssugtoqidian orogen – Ikertôq thrust zone and Nordre Strømfjord shear zone .....	97
Ikertôq thrust zone.....	97
Southern part of the central Nagssugtoqidian orogen .....	97
Middle part of the central Nagssugtoqidian orogen – Nordre Isortoq steep belt (NISB).....	99
Northern part of the central Nagssugtoqidian orogen – northern CNO flat belt ..	101
Nordre Strømfjord shear zone (NSSZ) .....	102
Northern Nagssugtoqidian orogen .....	109
Southern part of the northern Nagssugtoqidian orogen.....	109
Northern part of the northern Nagssugtoqidian orogen .....	110
Northern transition zone of the Nagssugtoqidian orogen .....	117
Northern transition zone of the Nagssugtoqidian orogen .....	118
Akiamiut domain – continuation of the Northern NNO .....	118
Orpissuup Nunaa domain.....	119
Kangilinaaq domain.....	119
The southernmost part of the Rinkian orogen .....	120
Nunatarsuaq domain .....	120
Rodebay domain .....	120
Ataa domain .....	121
Nuussuaq domain .....	131
Mesozoic sedimentary basins .....	131
Conclusions .....	132
<b>Acknowledgements</b> .....	<b>135</b>
<b>References</b> .....	<b>136</b>
<b>Appendix A. – Frequency diagrams of petrophysical properties</b> .....	<b>142</b>
<b>Appendix B – CD-ROM with selected images of potential field data from West Greenland</b> .....	<b>154</b>
Data presentation.....	154
Directory structure of the CD-ROM .....	154
Installing OASIS montaj™ Interface and Adobe Acrobat® Reader.....	155
Opening of maps and toggling between different geophysical data – using Oasis montaj™ Interface.....	156
Create a workspace.....	156
Open a geophysical map.....	156
Toggling between different geophysical data .....	157
Data included in the maps.....	160
Coordinates and scale bar .....	160
Prefix descriptions.....	160
Suffix descriptions .....	161
Abbreviations of thematic maps; M_ .....	162
Abbreviations of geophysical image data; i_ and associated CB_ and T_.....	163
Abbreviations of point/symbol data; Symb_ and associated CB_ and T_ .....	164
Copyright of the data on the CD-ROM .....	165

## Abstract

Magnetic and gravity field data are presented from regional geophysical surveys in central West Greenland that cover the northernmost part of the Archaean North Atlantic craton, the Palaeoproterozoic Nagssugtoqidian orogen and the southernmost part of the Palaeoproterozoic Rinkian orogen. The data are described and interpreted and the results are discussed within the framework of plate-tectonic models established for the region.

The geophysical data are presented as maps in the report and provided as images in digital form on the enclosed CD-ROM in order to facilitate future use and easy access to the data. Enhancement of data signatures is made through the application of geophysical filtering and transformation techniques. The techniques are described in some detail, but the results from the applications are in focus. Foundations of the petrophysical properties of rocks are given and petrophysical data from *in situ* measurements and laboratory work are presented and discussed.

The geology in central West region is well exposed and suitable for correlation with the geophysical data. A pronounced correlation between surface geology and magnetic data is established. This allows the extrapolation and interpolation of geological features from known mapped regions to more cursorily mapped or inaccessible regions.

The course of the southern Nagssugtoqidian front and the Ikertôq thrust zone is delineated and are found to represent the two most pronounced tectonic features in the region. From separation filtering a continuation of these two features to great depths are suggested. From gravimetric data is a thickening of the crust south of the front indicated. Throughout the region are patterns in the aeromagnetic data and gravimetric data linked with geological features.

The geological division into orogenic segments or tectonometamorphic domains is addressed by the use of the potential field data. Geological explanations of the differences in patterns of the potential field anomalies from one segment or domain to another are given. In general, the metamorphic grade is identified as an essential factor for the magnetic responses. For example, the middle and eastern part of the southern segment of the Nagssugtoqidian Orogen is marked by persistent low magnetic gentle responses in the aeromagnetic data. This reflects reworking and retrograde amphibolite facies metamorphism. In contrast, the northern and southern part of the central segment of the Nagssugtoqidian orogen are characterised by high amplitudes and heterogeneous responses in the aeromagnetic data, which reflect prograde metamorphism during the Nagssugtoqidian orogeny. In numerous other cases, the patterns in the potential field data are linked with deformation and metamorphic conditions and events.

The southernmost Rinkian orogen is interpreted to consist of a collage of different domains bounded by zones of tectonic deformation. No persistent trend among the domains is observed and the degree of deformation and tectonic reworking within the domains seems to be lower compared to the Nagssugtoqidian orogen. A boundary between the Nagssugtoqidian orogen and Rinkian orogen is not reflected by the magnetic data.

A correlation analysis of gravity field values and elevation data is also undertaken in order to deduce the isostatic conditions of the region. In general, isostatic compensation is observed for long wavelengths, however, one of the main conclusions arising from this work is that a larger part of Greenland should be considered, as the isostatic phenomenon of nature is a long wavelength phenomenon.

Views on the potential field data and interpretation techniques are given. The techniques are exemplified and their application to the understanding of the tectonic framework is presented for selected geological structures. The data contain numerous other features that are not discussed in detail, but they are of interest in a continued interpretation of the data and the region.

# Introduction

The Geological Survey of Denmark and Greenland (GEUS) launched in 2000 a four-year programme on the assessment of the mineral potential in the central part of West Greenland. The area extends from 66°N to 70°15'N with the exception of Disko Ø and the Palaeogene parts of Nuussuaq (Fig. 1). Age estimates and structural relations in the region have been investigated by several research groups (e.g. Korstgård 1979a; Marker *et al.* 1995; van Gool *et al.* 2002). Magnetic data for the central part of the region have been interpreted by Thorning (1993), Rasmussen & van Gool (2000) and Nielsen & Rasmussen (2002).

The assessment programme includes a compilation of geo-scientific data with the purpose of outlining metallogenetic provinces, address the mineral potential and establishing of the plate-tectonic setting of the region. The interpretation of the potential field data, in the form of aeromagnetic data and gravity data, and their implications on the tectonic framework are an important part of this.

A compilation of other geoscientific data comprises regional, systematically acquired and quality checked data (Schjøth & Steenfelt 2004) is also published under the programme on the assessment of the mineral potential in the central part of West Greenland. The data are presented in a Geographical Information System (ArcView) and are available on a DVD with an accompanying report introducing the data. In addition, a report on the mineral occurrences in the region is available (Stendal *et al.* 2004). All reports can be acquired from the GEUS.

One of the objectives of this report is to provide digital maps of the potential field data together with filtered or transformations of these that are useful for qualitative interpretations, and in some cases for quantitative interpretations. The maps are found on the enclosed CD-ROM. We present our view and interpretations of selected features in the data, but it must be emphasised that the data contain numerous other features that are of interest in a continued interpretation of the data. The report includes explanations of the various filters and transformation techniques applied to the data.

The report is divided into sections as follows:

- General introduction of magnetic and gravity field data and petrophysical properties of rocks.
- Presentation of available geophysical and petrophysical data from West Greenland.
- An overview of the regional geology of West Greenland is given.
- Presentation and evaluation of petrophysical data from West Greenland. The petrophysical data are furthermore presented in order to make these data available as input and support in future quantitative modelling and interpretations.
- Presentation of different geophysical processing techniques with applications to the potential field data from central West Greenland.

- Discussion of the results from the different geophysical techniques and their implications for the interpretation of the tectonic framework of central West Greenland.

It is intended to make this report comprehensible also for readers without geophysical and mathematical tools currently at hand. Some basic principles of potential field interpretation and petrophysical properties of rocks are given. The sections on the different processing techniques focus on the usefulness and the results. Detailed mathematical descriptions of the techniques will not be given. For more detailed information on the potential field data and the processing techniques references are given in the respective sections.

Several approaches are possible in the application of potential field data to the interpretation of the crust. The techniques presented in this report represent a qualitative approach involving the enhancement of certain anomalies. Furthermore, fast data transformations such as Euler deconvolution and analysis of the analytic signal is applied to provide quantitative descriptions of the magnetic sources. In some cases, only minor differences exist between different types of processed data. However, we have included all results to ensure comprehensiveness in the presentation of data.

The A4 paper-size of this report hinder in some cases the accessibility to the details in many of the data shown. Most of the maps in the report (included in appendix A) are consequently included on the enclosed CD-ROM and can be viewed with the personal computer software OASIS Montaj™ Free Interface (which are included on the CD-ROM). A description of the content and directory structure of the CD-ROM can be found in Appendix B.

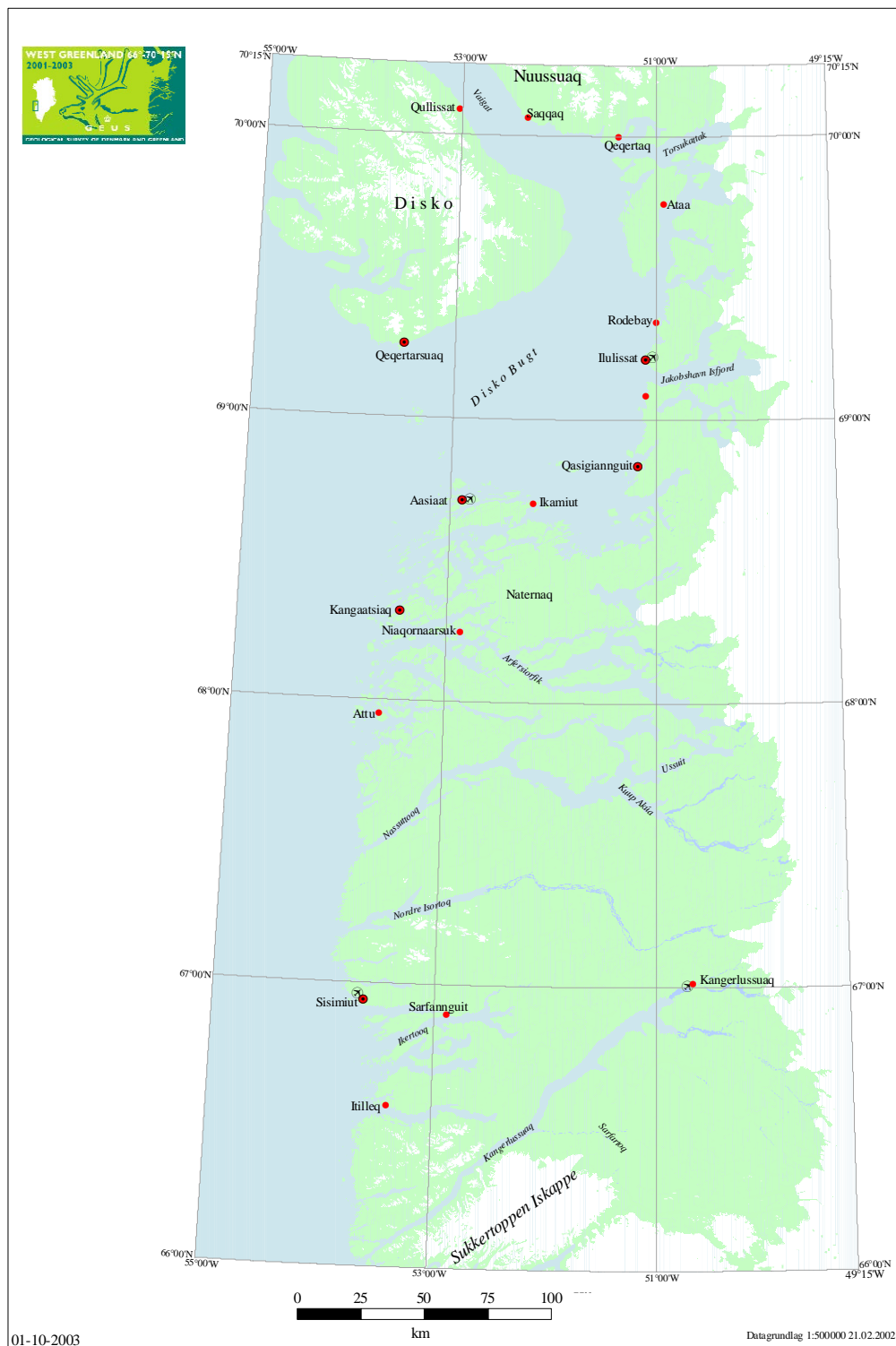


**Figure 1.** Map of the study region for the assessment of the mineral resource potential (66°N to 70°15'N) carried out from 2000 to 2003. Major place names, towns, and airports are indicated.

# The potential field of the Earth

## The Earth's magnetic field

The **Earth's magnetic field** is a superposition or vector sum of contributions caused by several phenomena. The **main field** originates from electric currents in the liquid outer core of the Earth. At the surface of the Earth, the main field contributes approximately 90 % of the field strength. The main field varies slowly with time. The International Geomagnetic Reference Field (IGRF) and the Definite Geomagnetic Reference Field (DGRF) describe the variations mathematically. Both reference models are based on results from a worldwide distribution of magnetic observatories, but recently also results from the Oersted satellite have been used. New reference models are established every fifth year. The IGRF is a prediction of the field whereas the DGRF takes into account the actual observed field variations during the past five-year period. In Greenland, the change of the main field is about – 17 nT/year and the field strength is about 55500 nT. The variations are called the **geomagnetic secular variations**, and they are probably caused by fluid movements in the outer core. The remaining 10% of the field observed at the surface of the Earth originate from short-periodic time dependent variations caused by electric currents in the ionosphere and from magnetic sources in the crust. The short-periodic variations are created by a complicated interaction between the main field of the Earth and the solar wind. The variations consist of **diurnal variations** related to the rotation of the Earth, and temporary magnetic storms, which are created by strong solar winds caused by increased sunspots activity. The contribution of magnetic sources in the crust to the Earth's magnetic field is caused by an induced part related to the presence of an external field or inducing field, basically the main field, and a remanent part independent of the present external field. The remanent part is a record of an earlier external field at the time of formation of the rock. The magnetisation of the crustal sources is determined by the magnetic properties of the minerals forming the rocks and by the history of the rock. In most magnetic surveys, only the field strength or **total magnetic field** (or **magnetic intensity field**) is measured. The **crustal total field anomaly** is calculated from the total field measurement by subtracting the main field (the IGRF or DGRF) appropriate for the date of the measurements and by removing the diurnal variations. Further decomposition of the field into a regional part and residual part is often carried out before quantitative modelling, where the residual field is assumed to represent the response of the local structures to be investigated.

## The Earth's gravity field and isostasy

The gravity pull at a point on the surface of the Earth is dependent on the mass distribution of the material surrounding the point. Consequently, by measuring the variations of the gravity pull from one place to another we can make a judgement of the subsurface of the Earth.

Isolation of gravity anomalies caused by local density variations in the crust involves a series of corrections to the measured gravity. In parentheses the name of the correction is given (based on Blakely, 1996).

The measured gravity field = (1) attraction associated with the reference geoid  
 + (2) effect of elevation above sea level (Free Air)  
 + (3) effect of “normal” mass above sea level (Bouguer and terrain)  
 + (4) time-dependent variations (tidal)  
 + (5) effect of moving measurement-platform (Eötvös)  
 + (6) effect of masses that support topographic loads (isostatic)  
 + (7) effect of crust and upper mantle density anomalies (“geology”)

The Free Air correction describes the decay of the gravity field with respect to height above the geoid. Applications of the Free Air correction give the **Free Air anomaly** that represent the gravity field corrected to sea level. The Bouguer and terrain correction is the gravity effect from masses above sea level. When corrections 1–5 are made, the corrected anomaly is called the **Bouguer anomaly**, which purpose is to give the anomaly due to variations of the densities below the datum. Long-wavelength topographic features, reflecting large regional geological phenomena, are generally compensated by deep-seated masses that isostatically support the topography. This compensation of topographic loads by compensating deeper masses is named **isostatic compensation**.

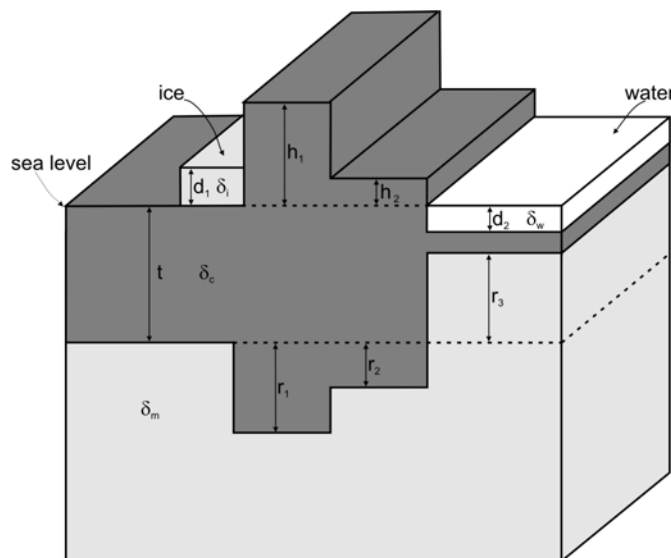


**Figure 2.** Model of Airy's hypothesis of isostatic compensation. Figure modified after Fowler, 1995. The crust has density  $\delta_c$ , the mantle  $\delta_m$ , the ice  $\delta_i$ , and water  $\delta_w$ . Isostatic compensation is achieved by variation in the thickness of the crust: mountains have roots whereas basins have antiroots.

On a regional scale, the Bouguer anomaly often correlates inversely to the topography with respect to the long-wavelength part. Consequently, a method to test if the topography can be seen as fully isostatically compensated (isostatic equilibrium), is to analyse the relationship between the Bouguer anomaly and the topographic height. An Airy model for compensation will be used in the analyses of the gravity field (Fig. 2). In the Airy hypothesis, isostatic compensation is achieved by e.g. mountains having deep roots with smaller density compared to the surrounding material. For more information on the potential field data and isostasy, please refer to Blakely 1996, Fowler 1995, Parasnis 1986 and Telford *et al.* 1998.

# Petrophysical properties of rocks

## Magnetic bulk properties

In all applications of magnetic methods, the measurements represent averaged properties within some volume of the rocks. In case the sensor is placed sufficiently far from a certain rock volume, the magnetic field approximates the field of a magnetic dipole. Therefore, our ability to obtain information about the rocks from magnetic measurements is restricted to the bulk properties of the rocks. The distance at which the magnetic field approximates a dipole increases with increased volume. The **total magnetisation** of rocks is described by the magnetic moment  $\mathbf{M}$  per unit volume and is the vector addition of a **natural remanent magnetic** part  $\mathbf{M}_r$  that exists irrespective of any external magnetic field and an **induced magnetic** part  $\mathbf{M}_i$  proportional to the external magnetic field  $\mathbf{H}$ .

$$\mathbf{M} = \mathbf{M}_r + \mathbf{M}_i = \mathbf{M}_r + \chi \mathbf{H} \quad [1]$$

**Natural remanent magnetisation** can be seen as the ability to retain a magnetisation in the absence of a magnetic field. The natural remanent magnetisation of a rock is a vector sum of several remanent contributions. Usually several sub-populations of magnetic grains exist that carry magnetic moments acquired at different times and therefore generally with different directions. The magnetic moment is highest for acicular sub-micron grains, whereas larger grains have relatively weaker magnetic moments.

The external magnetic field is primarily the magnetic field originating within the core of the Earth and secondarily the magnetic field caused by other rocks near the rock sample. In most cases, the field due to nearby rocks are negligible compared to the core-field. The intensity of the induced magnetic field is related to the external field through a constant of proportionality referred to as **the magnetic susceptibility**  $\chi$  that describes the magnetic moment acquired per unit applied field strength and per unit volume. In this work, the magnetic susceptibility is considered a scalar quantity, i.e. isotropic magnetic properties are assumed. The susceptibility is the ratio between a magnetisation and field intensity and is in the SI-system dimensionless.

The remanent and induced component can be seen as a static and dynamic property respectively. The direction of the induced magnetic moment is in the direction of the external field.

The Königsberger-ratio  $Q$  expresses the ratio between the remanent and the induced magnetic moments:

$$Q = \frac{|\mathbf{M}_r|}{|\mathbf{M}_i|} = \frac{|\mathbf{M}_r|}{\chi |\mathbf{H}|} \quad [2]$$

## Magnetisation types

The magnetic properties of rocks depend on numerous factors. The remanent and the induced magnetic component depend on the amount of magnetic materials, the type and composition of the magnetic materials present, the size, shape, and textures of the magnetic grains.

### Classes of magnetic materials in rocks

A rock is magnetic because it contains magnetic materials (or minerals), which eventually is dependent on the properties, state, and abundance of magnetic atoms forming the minerals. The following introduction to the magnetic properties of minerals and rocks are based on Clark (1997), Blakely (1996) and Putnis (1992). Materials and minerals can be classified according to different configurations and states of the atoms. An overview of the types of magnetic properties for different minerals is given in Table 1.

An electron in an atom spins about its own axis. Because of the electric charge of the electron, the spin creates a magnetic dipole moment. When two electrons in the same orbit, paired electrons, spin in opposite directions, their magnetic moments cancel in the absence of an external magnetic field. In the presence of an external magnetic field, a magnetic moment exists for the atom. In cases, where molecules only contain paired electrons, they are said to be **diamagnetic**. Diamagnetism is present in all materials, but this magnetic type is very weak compared to other magnetic phenomena.

When an electron in an atom or ion is unpaired with other electrons, it gives the atom or ion a magnetic moment. The magnitude of the moment is directly related to the number of unpaired electrons. Molecules containing such unpaired atoms or ions are said to be **paramagnetic**, and have permanent dipole moments. When paramagnetic atoms or ions are incorporated in a crystal structure, their magnetic moments may be randomly orientated and the resulting material has no net magnetic moment. Such material is also termed paramagnetic. If a paramagnetic molecule or material is placed in a magnetic field, the atoms will align with this field to a small degree, causing the material to become weakly magnetised. However, as soon the field is removed, the alignment disappears, so no remanent magnetisation is retained.

In oxides, an exchange interaction via the bonding oxygen takes place. The spins of the atoms become aligned in an antiparallel configuration (i.e.  $\uparrow \text{O} \downarrow \text{O} \uparrow \text{O} \downarrow \text{O} \uparrow \text{O} \downarrow$  where each arrow represents an atom, the direction of the arrow represents the sense of the spin and O is the bonding oxygen). This interaction is named superexchange interaction. If the interactions cancel each other, no net magnetic moment exists and the material is denoted **antiferromagnetic**. The susceptibilities of antiferromagnetic minerals are low and they do not retain any remanent magnetisation.

Magnetically ordered phases possessing a spontaneous magnetisation can be **ferromagnetic sensu stricto** or **ferrimagnetic**. **Spontaneous magnetisation** is the net magnetisation that exists inside a uniformly magnetised microscopic volume in the absence of an

external field. This occurs when the magnetic materials not only have atomic magnetic moments, but also have strong interacting neighbouring moments resulting in a quantum mechanical effect named exchange energy.

When a strong exchange interaction between atoms exists, which is the case for some metals (e.g. Fe, Ni and Co), the atoms align (i.e.  $\uparrow \uparrow \uparrow \uparrow \uparrow \uparrow \uparrow$  where each arrow represents a metal atom) with the same sense, creating a strong permanent magnetic moment. Such material is said to be **ferromagnetic sensu stricto**. Antiparallel interactions between the spins of the atoms are characteristic for a **ferrimagnetic**, but the strength of the spins magnetic moments are unequal (i.e.  $\uparrow \downarrow \uparrow \downarrow \uparrow \downarrow \uparrow \downarrow$ ) and results in a net magnetic moment. Antiferromagnetism is really a case of ferrimagnetism, and is as such an unfortunate term originating from iron-bearing spinels where the effect was first studied.

For simplicity, all strongly magnetic minerals and materials (i.e. ferromagnetic sensu stricto, antiferromagnetic and ferrimagnetic) are referred to collectively as **ferromagnetic**, which also will be the case hereafter. Ferromagnetic minerals will lose their spontaneous magnetisation under heating, because the space between neighbouring atomic magnetic moments is increased and the forces between atoms become insufficient to keep the magnetic moments aligned. At one point the spontaneous magnetisation will drop to zero, this point is called the **Curie temperature**. For magnetite the Curie temperature is 580°C (Fig. 3). Both the induced and the remanent magnetisation will disappear.

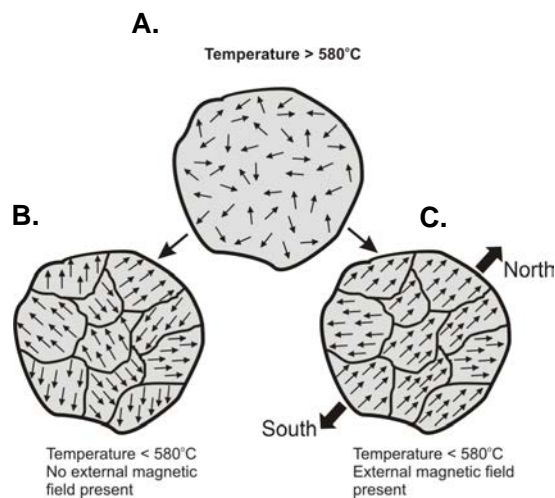


**Figure 3.** Magnetisation of ferromagnetic magnetite is controlled by the temperature. **A.** Above the Curie temperature at 580°C is the vibration of atoms so great that the magnetic poles of individual atoms, shown as arrows, points in random directions. The space between the magnetic dipoles of the neighbouring atoms is large and the magnetite lose its spontaneous magnetisation. Below 580°C will the atoms be arranged in small domains and reinforce each other. **B.** When cooled from a temperature above the Curie temperature to a temperature below in the absence of an external field, the domains are randomly oriented. **C.** In the presence of a magnetic field, most domains tend to be parallel to the external field and the material becomes permanently magnetised.

**Table 1.** Examples of the most important rock forming minerals grouped according to the different magnetic properties and with susceptibility range for these. Table based on Clark (1997).

Magnetic character	Sub-division	Mineral	Magnetic susceptibility SI [x10 <sup>-3</sup> ]
Diamagnetic		Quartz, feldspars and silicates not containing iron	About -0.01 x 10 <sup>-3</sup> SI
Paramagnetic		Olivine, pyroxenes, biotite, silicates containing iron	Max. 100 x 10 <sup>-3</sup> SI, generally less than
Ferromagnetic	Ferromagnetic sensu stricto, Antiferromagnetic, Ferrimagnetic	Magnetite, ulvöspinel, titanomagnetite, maghaemite, pyrrhotite	Variable, from 1 x 10 <sup>-3</sup> SI to 120 SI

The content of ferromagnetic minerals, where magnetite (Fe<sub>3</sub>O<sub>4</sub>) and its solid solution ulvöspinel (Fe<sub>2</sub>TiO<sub>4</sub>) are the dominant ferrimagnetic phases for crustal rocks (Clark & Emerson 1991; Clark 1997; Telford *et al.* 1998), are the dominating factor for the magnetic properties of rocks.

### Magnetic domains of magnetic mineral grains

In order to minimise the magnetic energy of a magnetic mineral the grain will tend to be subdivided into **magnetic domains** of differently orientated magnetic moments. The most important factor that controls the magnetic domain structure is the grain size of the minerals (the effective grain size of homogenous grains, but related to lamella size in heterogeneous grains with exsolution lamellae and size of zones in zoned minerals).

Sufficiently small grains are uniformly magnetised and have **magnetic single-domain** (SD) structure. Ultra-fine magnetic single domain grains (<0.03 µm for magnetite) are disturbed by thermal fluctuations, which cause the orientation of the spontaneous magnetisations to flip rapidly between different directions. This behaviour is called superparamagnetism and the grains are called **superparamagnetic** (SPM). SPM grains cannot retain a stable remanence and their magnetisation shifts rapidly in accordance to any applied field causing SPM grains to have high magnetic susceptibility values. With increasing grain size will the grain, as it is energetically favourable, be subdivided into a number of magnetic domains with differently orientated moments and grains larger than a critical single-domain size have more than one magnetic domain. Such grains can either exhibit **magnetic multi-domain** (MD) behaviour and properties or have a **pseudo-single domain** (PSD) transition grain size with both single domain and multi domain behaviour and properties. The magnetic properties with increasing grain size (above the critical SPM grain size) are summarised by Clark 1997 as: remanence and Königsberger ratio Q decrease and magnetic susceptibility increases slightly.

## Magnetic properties of rocks

Rocks have very variable magnetic susceptibilities. Clark and Emerson (1991), Clark (1997) and Carmichael (1992) give typical susceptibility values for the most common rock types.

The paramagnetism of silicates that determines the background susceptibility of a rock reflects the main mineral content of the rock. Above this background, the content of the ferromagnetic minerals defines the susceptibility (Puranen 1989). The susceptibility of rocks increases with increasing content of mafic minerals.

As magnetite and its solid solution are the minerals that dominate the magnetic properties of a rock, it is highly relevant to evaluate the factors controlling the formation of magnetite. Among the factors controlling the formation of magnetite are redox state, chemical composition of the protholith, cooling history and conditions under deformation. In terms of regional scale effects on the magnetic properties especially the overall oxidation conditions are of importance; conditions that to a large degree are controlled by pressure and temperature, which again is dependant on the depth of formation. A more detailed description, with references, of factors influencing the magnetic properties can be found in Airo (1999). A summary of the factors important on a regional scale interpretation of aeromagnetic data is given below.

1. Middle to deeper crustal levels exposed in Precambrian regions represent originally constant oxidation state and high vapour pressure. Hence, continuous domains of high magnetisation can infer highly oxidative conditions in middle to deep crustal levels.
2. Prograde metamorphism strengthen the original magnetism, although
3. Originally, weakly magnetic rocks can never produce secondary magnetite in such great amounts that they would substantially change the primary magnetisation.
4. In an originally highly magnetic rock, the magnetisation will not be significantly changed due to prograde metamorphic processes, because the relative volumetric concentration of secondary magnetite is still small compared to that of the primary magnetite.
5. The secondary magnetite produced in metamorphic processes of mafic (and intermediate) rocks will be fine-grained or irregularly shaped, and therefore dominated by the remanent magnetisation.
6. The production of secondary magnetite in metamorphic processes of felsic rocks will mainly take place by the increase of titanomagnetite grain size and its composition approaching that of pure magnetite. Then the induced magnetisation increases and the Q-ratio decreases, resulting in an overall high magnetic level and magnetic patterns of more regional nature. The formation of magnetite-bearing felsic rocks needs a precursor having a high concentration of magnetite.
7. Changes in mineral compositions, which involve magnetite and Fe<sup>3+</sup> bearing silicates, require radical changes of either temperature or pressure conditions.
8. The magnetic fabric is a function of the biotite petrofabrics in the rock.

Since several factors can affect the magnetic properties of a rock and the large variability in the susceptibility, even on outcrop scale, a large number of susceptibility measurements of a specific rock type or lithology from several localities are needed to describe the rock. By

averaging a large number of magnetic susceptibility values from several localities, the local variations can be smoothed out.

With many exceptions, the following observation applies generally for the magnetic response of different rock types: On large scales, high magnetic areas are commonly related to large masses of igneous rocks and to crystalline basement consisting of large masses of igneous rocks. Mafic to intermediate igneous rocks can be strongly magnetic to moderately magnetic. In contrast, felsic igneous, metamorphic, altered rocks and especially sedimentary rocks have weaker magnetic responses. The response of metamorphosed sediments is controlled by the composition of the protolith. Metamorphosed carbonates and graphitic meta-pelites are generally weakly magnetic, whereas metamorphosed greywackes and graphite-free pelitic schists may have higher susceptibilities (Grant 1985; Clark & Emerson 1991; Shive *et al.* 1992; Clark 1997; Hildenbrand *et al.* 2001). According to Airo (1999) individual grains or clusters of magnetite have a tendency to align parallel to other crystals such as biotite, and the magnetic response dominated by magnetite will consequently often reflect the grain fabric.

In rocks of sedimentary origin, magnetic properties are continuous along the sedimentary layering and discontinuous across layers. In plutonic rocks and migmatized rocks, the magnetic properties are more variable and often show an unsystematic behaviour. Large variations in the magnetic properties of rocks are possible on locality scale, the variability are generally greater between geological provinces than within them (Clark & Emerson 1991).

Metamorphism has a large effect on magnetic properties. Amphibolite facies metamorphism produces heterogeneous magnetic properties with bimodal susceptibilities. In contrast, granulite facies conditions often produce secondary magnetite that causes increasing susceptibility (Clark & Emerson 1991). Many reactions can form secondary magnetite from different silicate phases under regional metamorphism. The primary controls on how much secondary magnetite that can be formed under metamorphism are the total iron content. The iron content controls the upper limit of the potential production and the oxidation state, and consequently the distribution of iron between oxide and silicate mineral phases (Grant 1985). Carbon acts as a reducing agent that will lower the oxygen fugacity of the rock, which will hinder the formation of magnetite.

Deformation has a varying effect on the magnetic properties depending on whether the induced or remanent magnetisation is changed. Hydrothermal alteration or activity can greatly modify the magnetic properties and magnetic anomaly patterns. Depending on the fluid composition and other factors, can the hydrothermal activity either create or destruct ferromagnetic minerals. The deformation and hydrothermal activity is often concentrated to distinct tectonic zones instead of being regional.

The magnetic anomaly patterns reflecting rock properties are consequently a product of many different factors. And beside the above mentioned will the geometrical factors of the magnetic sources, such as volume, heterogeneity, dip, strike and depth of the magnetic bodies also act as important factors that determine the magnetic signature of the rocks.

Generally, for rocks, the Königsberger-ratio  $Q$  less than 1 implies the presence of larger magnetite grains. Larger  $Q$  values correspond to a dominance of remanent magnetisation and a higher content of small-grained magnetite. In granites and metamorphic rocks the induced magnetisation often dominates over the natural remanent magnetisation (Clark & Emerson 1991).

## Densities of rocks

Most densities of crustal rocks fall in the range from  $1500 \text{ kg/m}^3$  to  $3000 \text{ kg/m}^3$  (Telford *et al.* 1998). Density is a bulk property of the rock with quite small differences from one rock type to another compared to the variability of magnetic properties. An average of  $2670 \text{ kg/m}^3$  is usually quoted for the upper crust.

In general, sedimentary rocks have low densities (average  $2500 \text{ kg/m}^3$ ) causing negative gravity anomalies. In contrast, crystalline metamorphic basement rocks have higher densities (average  $2740 \text{ kg/m}^3$ ) and will consequently produce gravity highs. In addition, the density of the lower crust is higher than the upper crust due to the higher content of intermediate and mafic minerals. However, intrusive igneous granites have lower densities (average  $2640 \text{ kg/m}^3$ ) and thus, produce a negative gravity field anomaly. With increasing metamorphism, density usually increases (Christensen & Mooney 1995) due to the effect of filled pore and recrystallisation to denser rock forms.

## Application of petrophysical properties in analysis of geophysical data

Variations in rock density and magnetisation are as shown in the former sections indicative of geological processes. Therefore, by utilising the petrophysical data, constraints on the interpretations and links to the geological processes are provided. The data can be used either directly by incorporating these in quantitative modelling of the data or indirectly by use as support for qualitative interpretations, e.g. by correlation analysis. Furthermore, petrophysical data can be used in a correlation analysis between airborne measurements and surface outcrop data.

# Data from West Greenland

The geophysical data utilised in this report are primarily the regional aeromagnetic data from surveys by GEUS referred to as the Aeromag programme. References to the individual Aeromag surveys are given by Rasmussen (2002). Gravity data are also utilised. These data are provided by the Danish National Survey and Cadastre (Kort & Matrikelstyrelsen, KMS).

## Aeromagnetic data

### Acquisition

The Aeromag surveys have been conducted over large parts of Greenland since 1992 (Fig. 4). The aeromagnetic data that covers the studied region in central West Greenland originate from the aeromagnetic surveys in 1992, 1997, and 1999. The Aeromag data cover about 20–40 km of the rim of the Inland Ice and continues westwards 10–20 km offshore. An overview over the three surveys and survey parameters are given in Table 2.

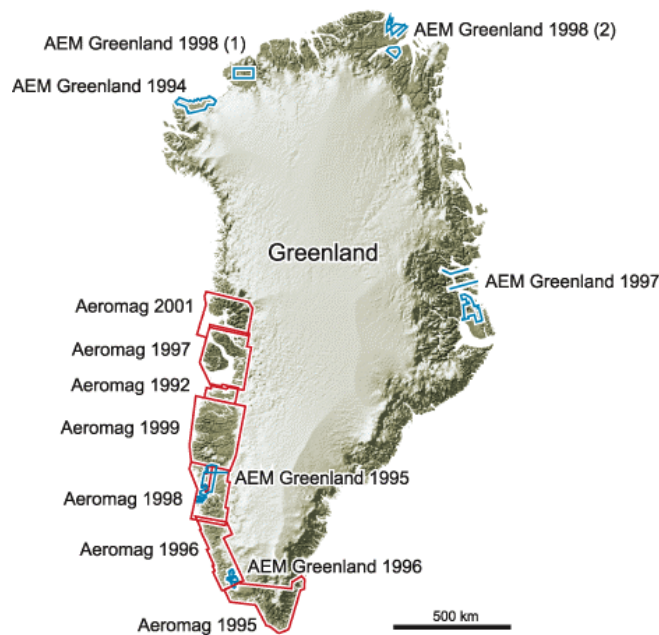


**Figure 4.** Outline of areas covered by regional aeromagnetic surveys (red polygons) from the Aeromag programme. Areas covered by another large airborne survey programme, the ‘AEM Greenland 1994–1998’ with combined electromagnetic and magnetic measurements are outline by blue polygons. The aeromagnetic data used in this report originate from the Aeromag surveys in 1992, 1997, and 1999.

**Table 2.** Survey parameters for the Aeromag 1992, 1997 and 1999 surveys.

Survey parameters	Aeromag 1992	Aeromag 1997	Aeromag 1999
Area	Lersletten, central West Greenland	Disko-Nuussuaq region, central West Greenland	Southern West Greenland
Measurements	Magnetic total field	Magnetic total field	Magnetic total field
Orientation of regular survey lines	N–S	N–S	N–S
Spacing between regular survey lines	1 km	500 m over land, 1000 m over sea	500 m
Orientation of tie-lines	E–W	E–W	E–W
Spacing between tie-lines	10 km	5 km	5 km
Total line kilometres	10062 km	70630 km	141009 km <sup>2</sup>
Terrain clearance	515 m	300 m	300 m
Area extent	8610 km <sup>2</sup>	46390 km <sup>2</sup>	61292 km <sup>2</sup>
Contractor	Geoterrex Ltd.	Sander Geophysics Ltd.	Sander Geophysics Ltd.
Financed by	The Government of Denmark with a contribution from Nunaoil A/S	The Government of Greenland	The Government of Greenland
Selected references	(Schacht 1992; Thorning 1993)	(Murphy & Coyle 1997)	(O'Connor 1999; Rasmussen & van Gool 2000)

Merging of the grids of the magnetic total field from the different Aeromag surveys is done by application of the Geosoft GridKnit™ software with the blending method. In this method, an averaging function is assigned to each grid that determines the weighting of one grid against the other in an overlapping area. This gives a smooth transition from one grid to another. The processing has allowed all data from the Aeromag surveys to be joined into a single grid. The grid cell size in the produced grid is 100 meter. Due to the northern latitude of the survey area the inclination of the magnetic field of the Earth is relatively steep about 80 degrees. Consequently, no reduction to the pole is applied. The International Geomagnetic Reference Field (IGRF) is subtracted from the data.

Reconnaissance magnetic surveys are available from the period before 1992. The magnetic data from the compilation by the Geological Survey of Canada in 1996 (Verhoef *et al.* 1996) for the Arctic and North Atlantic region were used for areas not covered by the regional Aeromag programme. The data from this compilation, 'Magnetic Anomalies of the Arctic and North Atlantic Oceans and Adjacent Land Areas', are in the following abbreviated MAANAOALA.

The data from the MAANAOALA and the regional Aeromag programme were merged (Fig. 5). The merging was done by the Geosoft GridKnit™ software with the use of a blending method. The Aeromag data were upward continued to 1250 m, which is the average flight altitude for the MAANAOALA data over West Greenland.

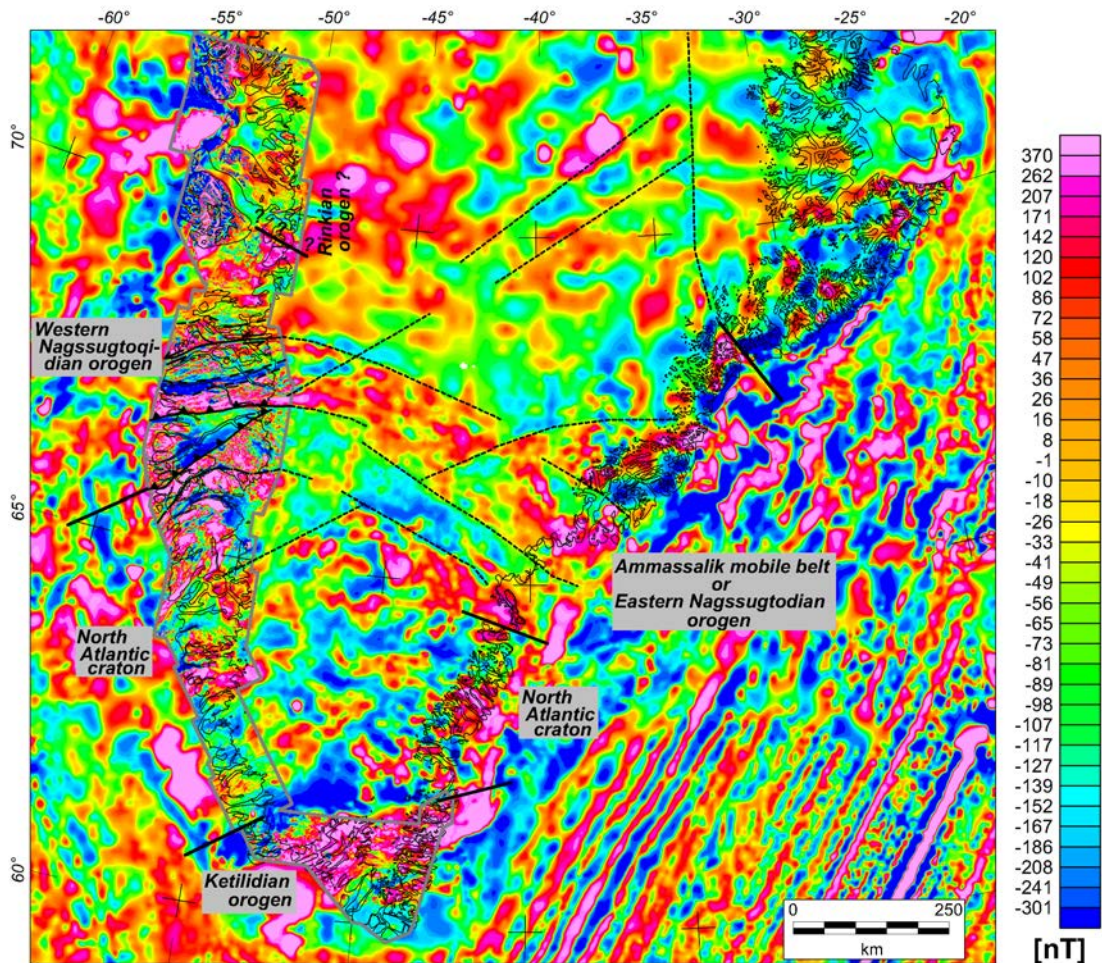


**Figure 5.** The merged total magnetic field from the Aeromag programme (outlined with a full grey line) and MAANAOALA with indications of the gross geological sub-division. Some of the major linear trends observable onshore in the magnetic response that possibly reflect different geological structures beneath the Inland Ice are indicated with dotted black lines. Full black lines delineate the suggested location of boundaries between the different orogens and cratons. The existence of a boundary between the Nagssugtoqidian and Rinkian orogens is debated and is therefore marked with question marks. The geological segmentation of Greenland will be described in the sections on the interpretations. The circumference of the Inland Ice is marked by thin black lines.

## Gravity data

### Acquisition

The surface gravity data for the assessment region were supplied from the database maintained by KMS. A total of 5075 surface gravity stations are located within the study area

(Fig. 6). The data have been collected during several surveys conducted by various organisations. Both ground and marine measurements are included.

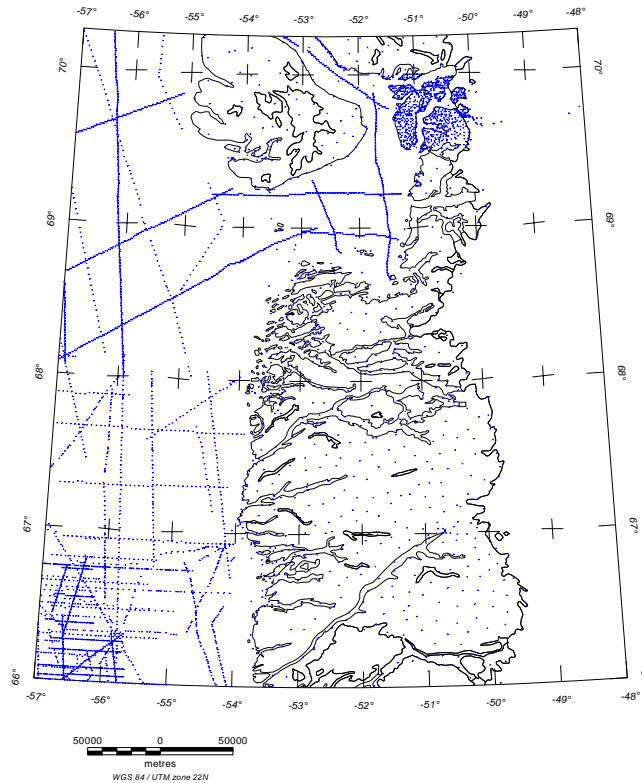


**Figure 6.** Locations of the land and marine gravity stations in the region are shown with blue dots.

The distribution of the surface gravity stations is sparse, with non-uniform station density. Large parts of the area are only very sparsely covered with gravity stations and only a very small number of stations are located on the Inland Ice. Detailed measurements of the gravity field at Arveprinsen Ejland and adjacent areas were carried out by the Geological Survey of Greenland in the late eighties (L. Thorning, personal communication, Sep. 2003). This area is the only area with sufficient density of measurements allowing detailed interpretations of the geological structures from the gravity field.

All data are linked to the IGSN71 reference datum and reduced to Bouguer anomaly values with corrections related to the total mass (using a reduction density of  $2670 \text{ kg/m}^3$ ), the ellipsoidal shape of the Earth, elevation of the gravity stations, and the effect of local topography or bathymetry.

Interpolated and gridded field measurements are shown as the Free Air anomaly and the Bouguer anomaly in Fig. 7 and Fig.8. The gravity anomaly grids are constructed by using a minimum curvature algorithm as the interpolation method. The grid cell size is 2000 m. The non-uniform distribution of gravity stations is inappropriate for a correct sampling of the gravity field. Firstly, the large spacing between stations results in aliasing and improper

presentation of the field. Secondly, areas with a high station density are going to include short-wave features that cannot be represented by the wavelengths sampled by the gridding. In order to obtain a uniform representation in the grid in terms of wavelengths, smoothing by low-pass filtering of the initial grid has been applied. Calculated vertical gradients will be presented in another section.

The study on gravity and isostasy presented here should be considered as a pilot study. The focus region in this report is central West Greenland, but an ideal joint analysis of gravity and isostasy should include a larger part of Greenland and the adjacent sea.

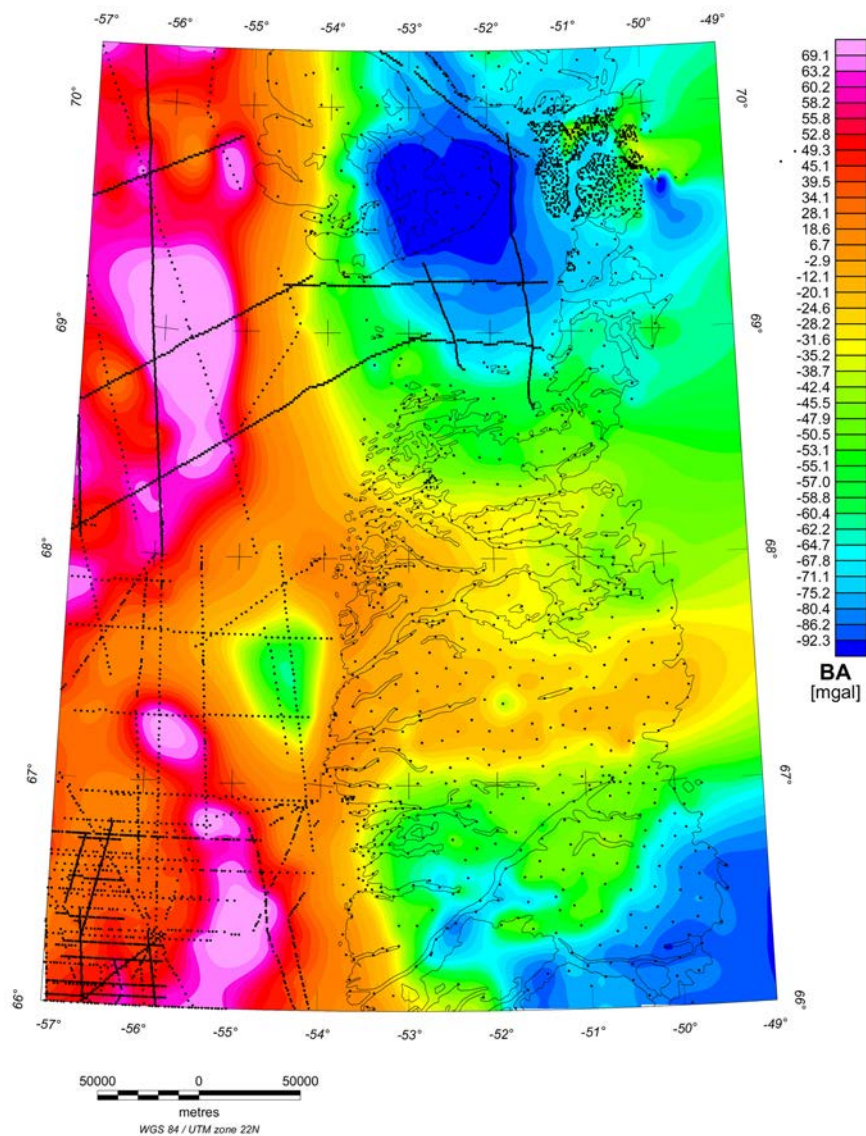


**Figure 7.** Map of gridded Bouguer anomaly field from surface gravity measurements. Black dots show the measuring locations. The grid cell size is 2 km.

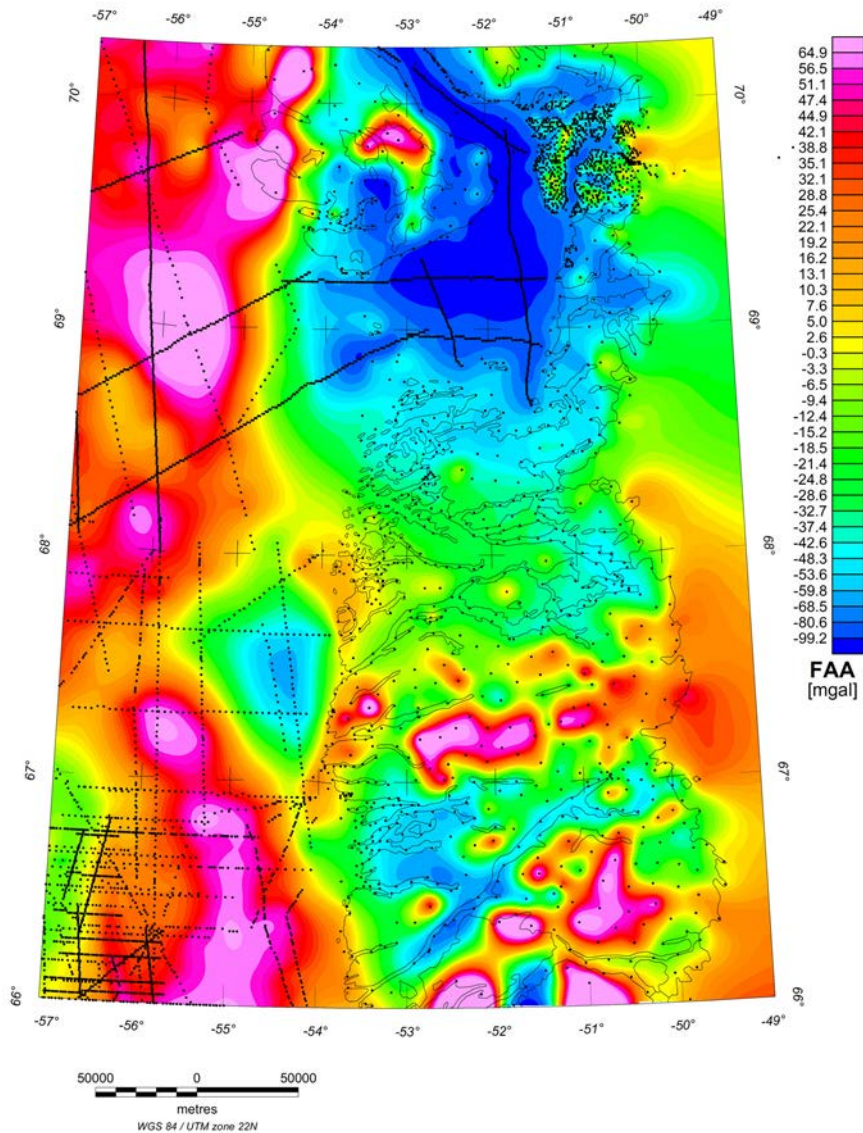


**Figure 8.** Map of gridded Free Air anomaly field from surface gravity measurements. Black dots show the measuring locations. The grid cell size is 2 km.

## Petrophysical data

Determination of the magnetic susceptibility of rocks by use of hand-held magnetic susceptibility metres (models used are Geo Instruments GMS-2, Exploranium KT-9 Kappameter and Exploranium KT-6) has been undertaken during fieldwork in 2001 and 2002 by the authors and other Survey geologists. Laboratory measurements with determination of magnetic susceptibility, remanent magnetisation, and density for 171 selected rock samples have been undertaken by the Geological Survey of Finland (Table 3). All measurements have been compiled into a table with information on lithology.

**Table 3.** Overview of measurements of magnetic susceptibility carried out in the field and grouped according to mapped lithologies.

Lithology type	Localities with SI field measurements	Number of conducted field measurements	Samples with laboratory determined petrophysical properties
Gneiss	197	4186	100
Granite	11	150	4
Quartz diorite	47	1090	3
Schist	37	650	17
Marble, dolomite, calc-silicates	7	120	4
Quartzite	2	20	3
Amphibolite	42	562	24
Massive sulphides	2	20	2
Banded iron formation	1	10	4
Charnockite	6	120	1
Ultramafic rocks	9	280	7
Gabbroic rocks	4	60	2
<i>In total</i>	<i>376</i>	<i>7268</i>	<i>171</i>

Henkel (1991; 1994) and Puranen (1989) have demonstrated the use of different plots and statistical approaches for the analysis of petrophysical properties of crystalline rocks. The suggested approaches are used in this work.

Application and analysis of petrophysical data in the interpretation of aeromagnetic data and gravity data enable an investigation of the correlation between the rock properties and the related field. Furthermore, petrophysical data can be used as constrains in forward or inverse modelling of the anomalies.

## Digital elevation data from West Greenland

The digital elevation model (DEM) is included both to provide a geographic reference for the geophysical maps and to evaluate other data in relation to the terrain of the region. Furthermore, it provides the base for analysis with respect to isostasy.

A digital elevation model have been created for the area. The elevation model covers both the bathymetry and topography of the region and is based on the publicly available ETOPO5 5x5 minute's gridded digital elevation (Data Announcement 88-MGG-02, Digital relief of the Surface of the Earth. NOAA, National Geophysical Data Centre, Boulder, Colorado, 1988) data provided by the National Geophysical Data Centre (<http://www.ngdc.noaa.gov/>) under the National Oceanic and Atmospheric Administration, U.S. Department of Commerce. The accuracy of the data set is difficult to define and Greenland is one of the data-deficient parts. However, it provides a joint bathymetry and topography data set. The 5x5 minute bathymetry and topography grid is shown in Fig. 9. The maximum depth is around 800 m and the maximum topographical height is around 2100 m. Slopes in the Disko Bugt are relatively steep, but otherwise the gradients are mod-

moderate. Shallow water is present outside the coast from Nordre Strømfjord to Sisimiut. Areas with high topography around 500 m to 1000 m are situated approximately 25 km inland in the area between Nordre Strømfjord and south of Nordre Isortoq. Moreover, an area beneath Sukkertoppen Iskappe and south to southeast of Søndre Strømfjord has high topography around 1000 m. The Sukkertoppen Iskappe has a height greater than 2000 m.

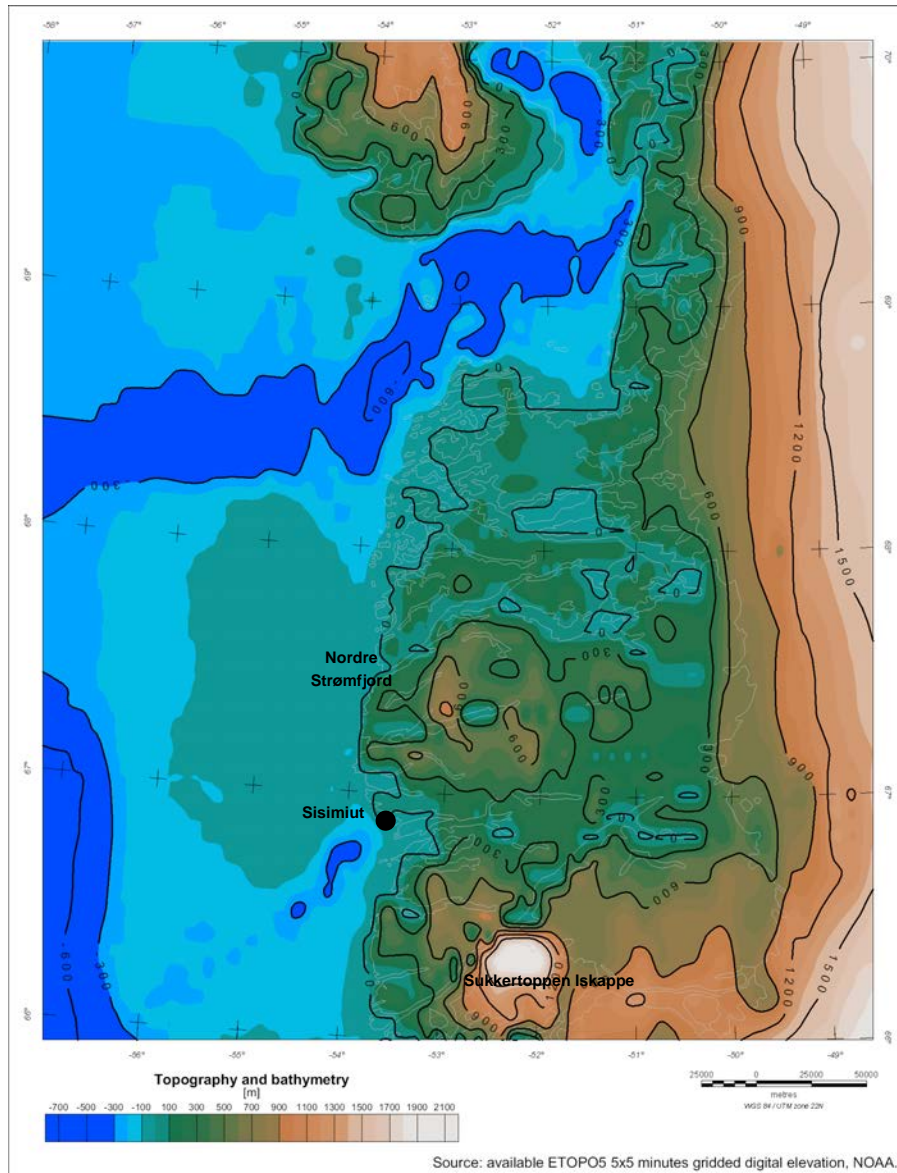


**Figure 9.** Bathymetry and topography from West Greenland based on the publicly available ETOPO5 5x5 minutes grid from NOAA. The contour interval is 500 m.

## Regional geology of West Greenland

A short overview of the regional geological setting of the study region is given in this section. Some detailed information on the regional geology, especially the Nagssugtoqidian and the southernmost part of Rinkian orogen, are given in the succeeding section. The study region constitutes a central position in a system of Palaeoproterozoic orogens stretching from Canada through Greenland, northern Scandinavia, Scotland and the Baltic (Fig. 10) (van Gool *et al.* 2002; Wardle *et al.* 2002b).

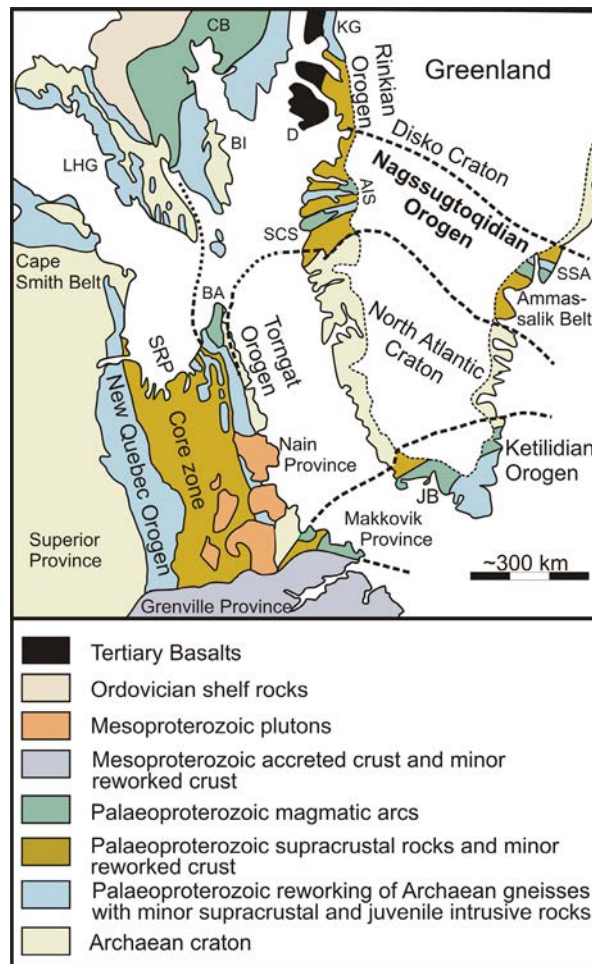


**Figure 10.** Geological correlation of the study region is outlined with a red rectangle. The Disko Island and the Palaeogene parts of Nuussuaq are excluded from the assessment region. AIS, Arfersiorfik intrusive suite; BA, Burwell arc; BI, Baffin Island; CB, Cumberland batholiths; D, Disko Island; JB, Julianehåb batholith; KG, Karrat Group; LHG, Lake Harbour group; SCS, Sisimiut charnockite suite; SSA, Síportôq supracrustal association; SRP, southern Rae Province. Figure modified from van Gool *et al.* (2002).

A geological map of the study region is shown in Fig. 11. The Rinkian orogen (hereafter abbreviated RO, earlier also named the Rinkian mobile belt) forms the northernmost part of the study region. The RO is underlain by Archaean orthogneisses (2835-2758 Ma in Disko Bugt, Nutman & Kalsbeek 1999) intercalated with Archaean supracrustal sequences. Palaeoproterozoic rocks unconformably overlie the basement. Most rocks are in amphibolite facies. Palaeoproterozoic deformation in the RO is characterised by NNW-directed ductile thrusting and fold-napping, succeeded by extensional deformation on low-angle shear zones and large upright folding (Garde & Steenfelt 1999a). The trend of the RO is assumed to be approximately E–W, however this is debated and an N–S trend of the orogen has also been argued for (van Gool *et al.* 2002).

Traditionally, the RO has been considered distinct from the Nagssugtoqidian orogen to the south. However, due to the lack of an obvious boundary between the orogens and similarities in lithologies and structures, the separation between the two orogens is questioned (van Gool *et al.* 2002). It is now argued that the orogens are closely associated with a common geological history and that they perhaps originate in the same continental block. The area north of Jakobshavn Isfjord to 70°15' will in the following be referred as the southernmost part of the Rinkian orogen.

The Nagssugtoqidian orogen (hereafter abbreviated NO) occupies most of the study region. Reworked Archaean gneisses with minor Palaeoproterozoic supracrustal rocks dominate the NO. All rocks within the orogen have been metamorphosed under amphibolite to granulite facies conditions. Marker *et al.* (1995) proposed a structural subdivision of the NO into northern, central, and northern Nagssugtoqidian segments (abbreviated NNO, CNO and SNO respectively hereafter) and the southern foreland. All segments of the NO comprise several large tectonic features, where some of these are identical to the boundaries of the different segments. The most important tectonic elements are the Nordre Strømfjord shear zone; the Ikertôq thrust zone (ITZ) and the southern Nagssugtoqidian front (SNF). The NO has previously been interpreted as both intracratonic (Bak *et al.* 1975a; Watterson 1978) and intercratonic (Bridgwater *et al.* 1973a), but most recently the favoured opinion is that the Nagssugtoqidian orogen developed as a consequence of collision (Fig. 12) between cratonic blocks (Kalsbeek *et al.* 1987; van Gool *et al.* 1996; Connelly & Mengel 2000; van Gool *et al.* 2002).

South of the SNF lies the southern Nagssugtoqidian foreland which comprises the northernmost part of the South Greenland Craton, which is an assembly of Early to Late Archaean terranes of gneiss complexes (Nutman *et al.* 1989; Rosing *et al.* 2001). Directly south of the NO, rocks of the foreland comprise granulite facies orthogneisses and paragneisses that are cut by generally undeformed late Archean granites. The gneisses, which are intruded by Palaeoproterozoic dolerite dykes, e.g. the voluminous Kangâmiut dyke swarm (Escher *et al.* 1975; Bridgwater *et al.* 1995; Cadman *et al.* 2001).

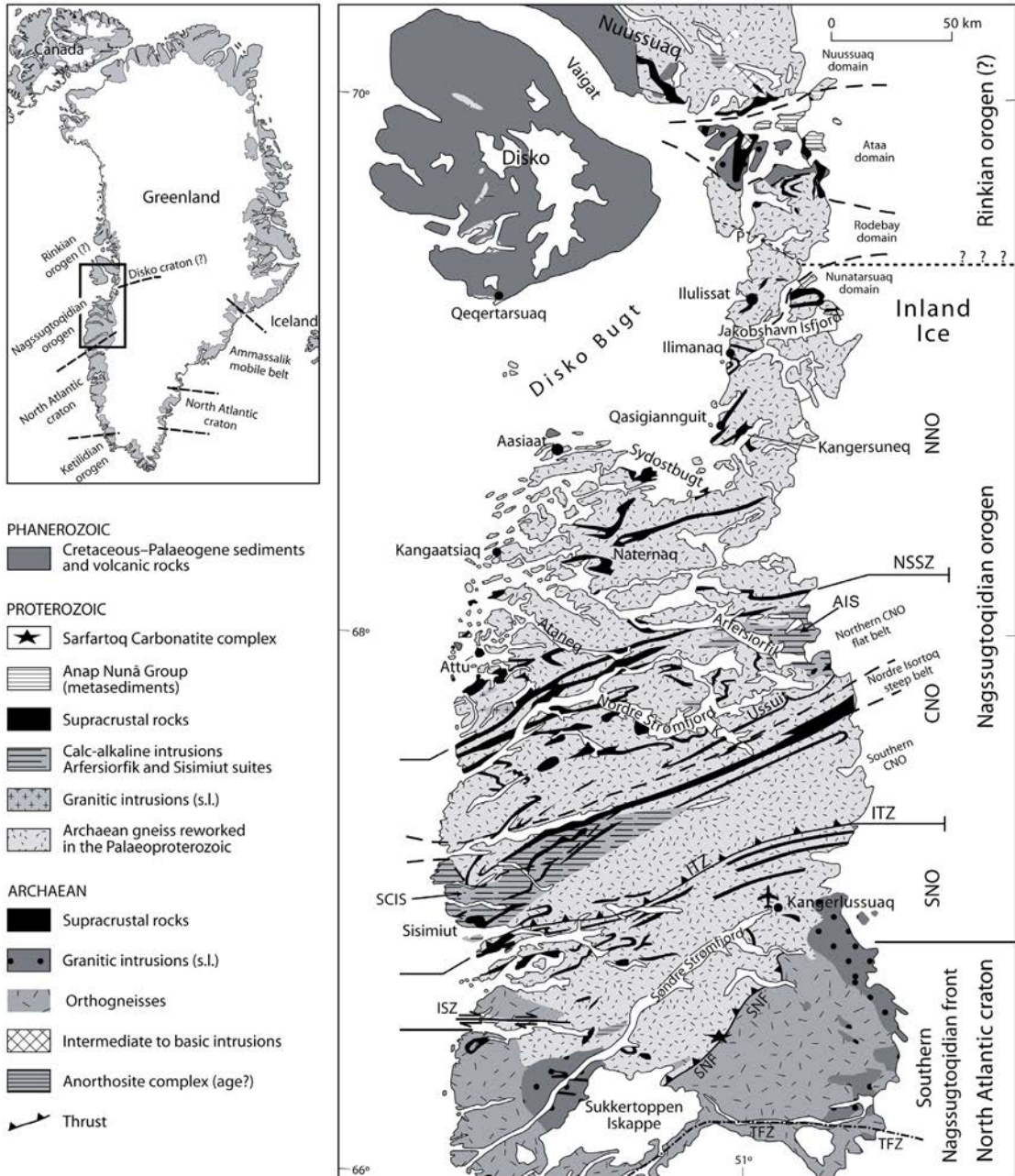


**Figure 11.** Simplified geological map of the main tectonic elements and main lithologies with place names used in the report. Abbreviations: AIS, Arfersiorfik intrusive suite; CNO, central Nagssugtoqidian orogen; ISZ, Itilleq shear zone; ITZ, Ikertôq thrust zone; K, Kuup Akua; NNO, northern Nagssugtoqidian orogen; NSSZ, Nordre Strømfjord shear zone; P, Paakitsoq lineament; SCIS, Sisimiut charnockite intrusive suite; SNF, southern Nagssugtoqidian front; SNO, southern Nagssugtoqidian orogen.

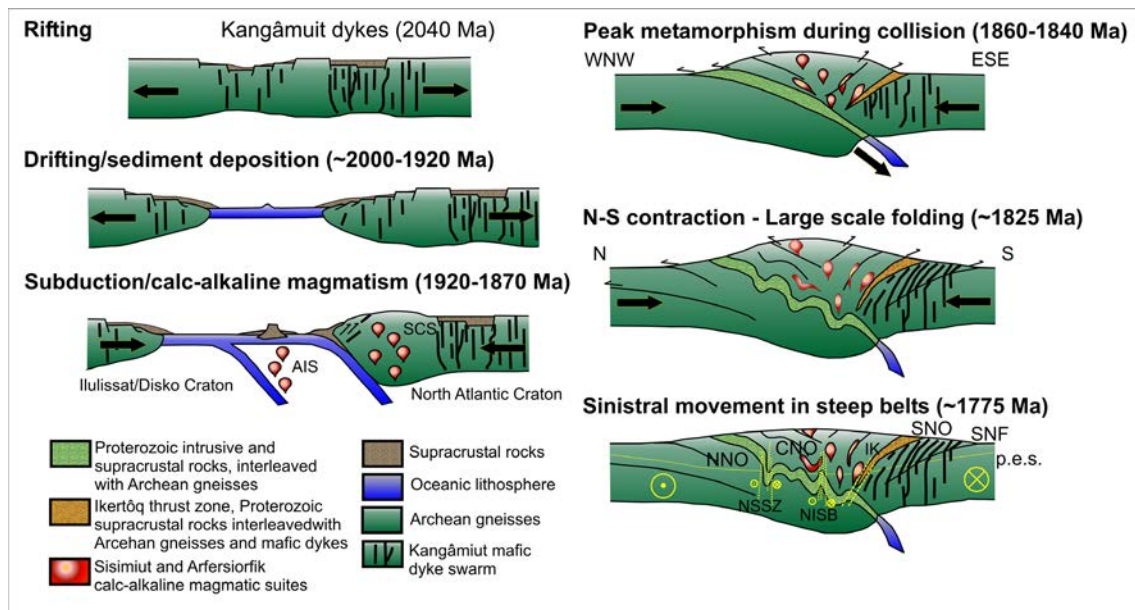


**Figure 12.** Schematic evolution model of the Nagssugtoqidian orogen suggested by van Gool et al. 2002. Abbreviations used in the figure: AIS, Arfersiorfik intrusive suite (Arfersiorfik quartz diorite); SCS, Sisimiut charnockite suite; NSSZ, Nordre Strømfjord shear zone; NISB, Nordre Isortoq steep belt. Slightly modified version of model by van Gool et al. 2002.

## Details of the Rinkian and Nagssugtoqidian orogens

In addition to the overview over the regional geology in the study region, some additional information on the geology of the Rinkian and Nagssugtoqidian orogen will be given in this section. For a geological map over the entire study region, refer to Fig. 11.

### The Rinkian orogen

The area including Jacobshavn Isfjord in the south to the southern shore of Nuussuaq (here referred as the Disko Bugt region) comprises four tectonometamorphic domains; the Nunatarsuaq domain, the Rodebay domain, the Ataa domain and the southern part of the Nuussuaq domain (Fig. 13) (Garde & Steenfelt 1999a).

The Nuussuaq domain comprises Archaean amphibolite facies orthogneisses intercalated with Archaean supracrustal rocks, e.g. the c. 25 km long and 500 m wide Saqqaq supracrustal rocks. The Nuussuaq domain also comprises the Archaean Boye Sø anorthosite complex. Structurally the Nuussuaq domain has been subjected to substantial Proterozoic reworking. NW–SE-trending shear zones are described from the eastern part of Nuussuaq and a ENE–WSW-trending shear zone at Torsukattak (Garde & Steenfelt 1999a, b). The Ataa domain comprises supracrustal rocks of predominant metavolcanic affinities that are intruded by the 2.8 Ga Atâ intrusive complex (Garde & Steenfelt 1999a; Kalsbeek & Skjerna 1999; Kalsbeek & Taylor 1999). The supracrustal rock sequences define a half circle starting at Arveprinsen Ejland, where they form a c. 20 km long and up to c. 10 km wide N–S-trending sequence, over Qqaatsut, Anap Nunaa ending at Eqi and Maniitsoq (Garde &

Steenfelt 1999a; Stendal *et al.* 1999). The Atâ intrusive complex comprises plutonic assemblages of tonalitic, trondhjemitic and granodioritic rocks, which largely have escaped Proterozoic deformation. The southern boundary of the Atâ complex is difficult to establish because of the presence of flat-lying shear zones in the border area. Archaean granodioritic orthogneiss dominate the Rodebay domain. Minor bands of intensely folded amphibolite and schist are found within the orthogneisses. The Nunatarsuaq domain comprises Archaean orthogneiss and an occurrence of Palaeoproterozoic supracrustal rocks north of Jakobshavn Isfjord (Garde & Steenfelt 1999a).

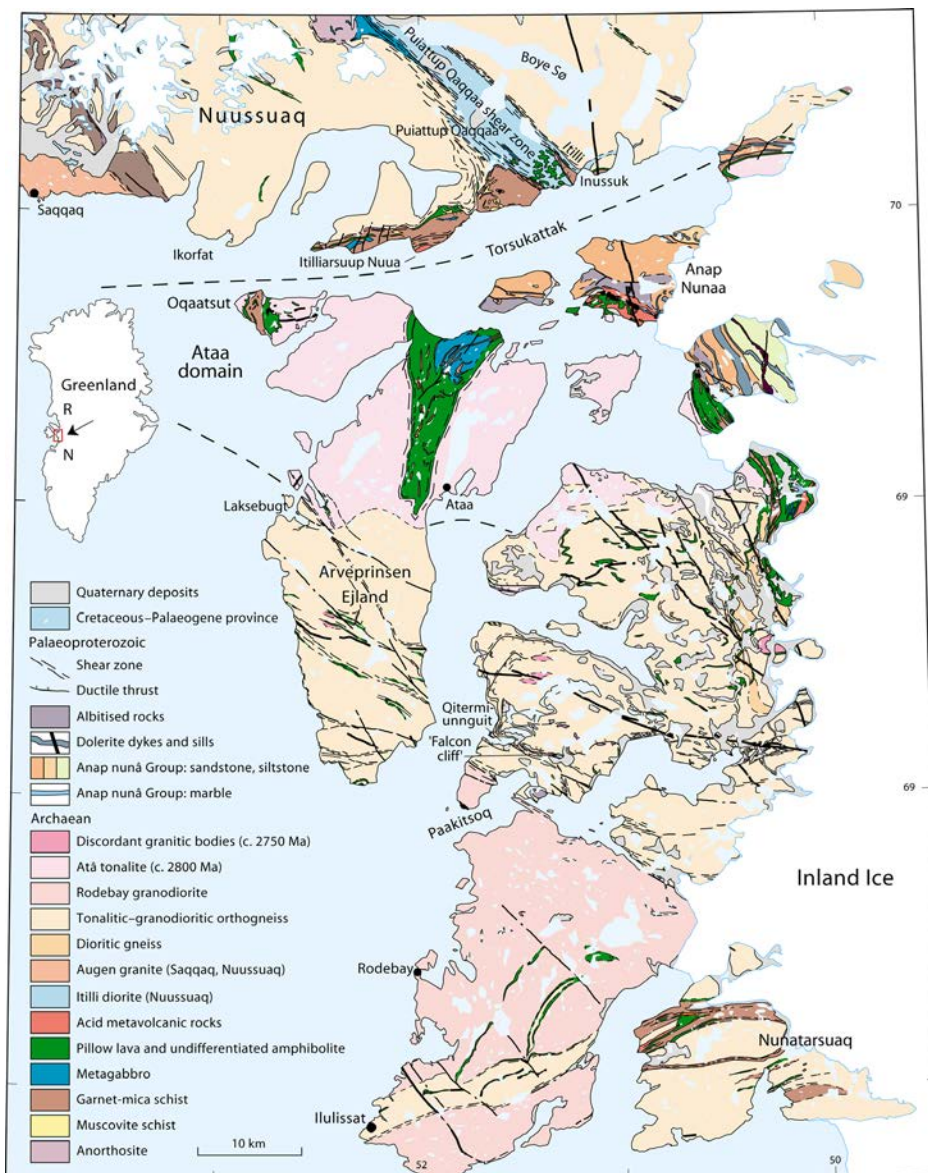


**Figure 13.** Geological map of the northern Disko Bugt area showing the main rock units and domains in the area. Figure modified from (Garde *et al.* 2002).

A boundary or suture between the RO and the NO has not been established and it is questioned if there is one at all (Mengel *et al.* 1998; Connelly & van Gool 2002; van Gool *et al.* 2002). However, if a suture exists between the RO and the NO, the northern Disko Bugt area is considered the most likely location. A possible position of a border has been sug-

gested to be the Paakitsoq lineament in the southern part of Arveprinsen Ejland (Escher & Pulvertaft 1976). This lineament was later found to comprise only a minor offset and was described as a non-penetrative crustal-scale structure (Grocott & Davies 1999).

## **The Nagssugtoqidian Orogen**

### **Northern Nagssugtoqidian orogen**

Archaean amphibolite facies gneisses in the northern part and granulite facies gneisses in the southwestern part dominate the NNO. Several relatively long continuous narrow supracrustal belts are situated in the NNO, often deformed into large-scale fold patterns; e.g. Lersletten. Several belts have an Archaean age but most are of unknown age. Steep- and shallow dipping shear zones, often along contacts between orthogneisses and paragneisses occur throughout the NNO. Presently the extension of the NNO to the north is debated. Recent investigations have shown that the area north of the NNO, around Kangersuneq fjord and Jakobshavn Isfjord, has structures, deformation history and rock ages with considerable similarities to those observed for the Nagssugtoqidian orogen. In lack of a terminology or linking with the NNO, the term northern transition zone of the Nagssugtoqidian orogen (NTZ) will be used for the area between the NNO and the area south of Jakobshavn Isfjord.

To the south is the NNO bounded by the SW–NE orientated Nordre Strømfjord shear zone. The shear zone has formerly been interpreted as a large, crustal-scale sinistral shear zone with large continuous displacement (Bak *et al.* 1975a; Bak *et al.* 1975b; Sørensen 1983). This interpretation has been questioned by several authors and the zone has been interpreted as a non-penetrative crustal shear zone, that records scattered and localised shear with sinistral strike-slip transcurrent motion (Marker *et al.* 1995; Hanmer *et al.* 1997; Connelly & van Gool 2002). However, the most recent publications on the Nagssugtoqidian orogen propose to revert to the term Nordre Strømfjord Shear zone (van Gool *et al.* 2002). The amount of movement along the shear zone can however still be debated.

### **Central Nagssugtoqidian orogen**

The CNO, considered as the core of the orogen, can be divided into three ENE-trending domains; the northern CNO flat belt, Nordre Isortoq steep belt, and southern CNO (van Gool *et al.* 1996).

The northern CNO flat belt is characterised by open and upright folds. The flat belt mainly comprises Archaean gneisses tectonically intercalated with Palaeoproterozoic supracrustals, which are intruded by Palaeoproterozoic quartz-dioritic to tonalitic gneisses of the calc-alkaline Arfersiorfik intrusive suite (Kalsbeek & Nutman 1996a; van Gool *et al.* 1999; van Gool *et al.* 2002). The suite has intrusive ages between 1921 Ma and 1855 Ma. Metasedimentary rocks associated with the intrusive suite have been shown to be of Palaeoproterozoic age (Kalsbeek *et al.* 1987; Kalsbeek & Nutman 1996a; Connelly *et al.* 2000). The Arfersiorfik intrusive suite has been suggested to represent subduction related juvenile Early Proterozoic arc magmatism and to be associated with a cryptic suture in the

orogen (Kalsbeek *et al.* 1987; Kalsbeek & Nutman 1996a). The Arfersiorfik intrusive suite is partly intruded along supracrustal rock belts in the inner part of Nordre Strømfjord, partly as a larger main intrusive body covering several hundreds of square kilometres in the inner part of the Arfersiorfik Fjord. The main body is over 2 km thick and lies above a thin sequence of supracrustal rocks along an intrusive contact (van Gool *et al.* 1999). The gneisses are metamorphosed under Palaeoproterozoic granulite facies conditions in the west and amphibolite facies conditions in the northeast. This change in facies possibly reflects a crustal scale eastward tilt, with deeper crustal levels exposed towards the west (Bak *et al.* 1975b; Thorning 1984; Marker *et al.* 1995). The northern and southern part of the CNO are separated by the Nordre Isortoq steep belt, developed in Archaean orthogneiss interleaved with Palaeoproterozoic paragneisses. The belt comprises an up to five kilometres thick belt of metasediments. The belt crosscuts the southern end of Kuup Akua (south-directed branch of the fjord in the inner part of Nordre Strømfjord) and extends WSW and ESE to the inland ice and the Nordre Isortoq. The Nordre Isortoq steep belt is suggested to be the most likely location of a suture zone between the two colliding continents (Kalsbeek *et al.* 1987; van Gool *et al.* 2002). The southern CNO consists of homogeneous granulite facies large-scale folded Archaean granitoid gneisses in the east and the Palaeoproterozoic Sisimiut charnockite intrusive suite in the west.

The Ikertôq thrust zone (Grocott 1977, 1979; Korstgård 1979b; van Gool *et al.* 1996; Hammer *et al.* 1997) constitutes the southern boundary of the CNO. The thrust zone is defined as a 5–10 km wide belt with penetrative, straight gneissic fabric and isoclinal folding and imbrications. The thrust zone is dominated by Palaeoproterozoic sheets of pelitic and psammitic paragneisses, which are interleaved with Archaean gneisses and deformed Kangâmiut dykes. All structures are transposed into planes with moderate to steep NNW dips. The Ikertôq thrust forms a prominent metamorphic and tectonic boundary and forms the northern limit of the Kangâmiut dykes swarm. The thrust is suggested to be an intense ductile south-directed thrust and is interpreted to have accommodated considerable crustal shortening and uplift of the CNO by thin-skinned thrust stacking that interleave Archaean gneisses with Palaeoproterozoic supracrustal rocks (van Gool *et al.* 2002).

### **Southern Nagssugtoqidian orogen**

The SNO is dominated by amphibolite facies gneisses, with the exclusion of areas to the southwest, which escaped intense reworking and thereby comprises gneisses with Archaean fabric and their original granulite facies metamorphism. The southwestern part of the SNO is subdivided by steeply dipping E–W trending high-strain zones with retrograde shearing and reworking along the Itilleq and Ikertoq fjords (Korstgård 1979b). The southern border of the SNO is defined by an alignment of thrusts termed the southern Nagssugtoqidian front (SNF) thrust (Marker *et al.* 1995). The SNF is recognised as the northward transition of undeformed and discordant Kangâmiut dykes to an area where dykes is penetratively deformed during south-directed shearing (Ramberg 1948; Escher *et al.* 1975; Marker *et al.* 1995). The SNF is located south of Søndre Strømfjord and is mapped from the margin of the inland ice towards southwest to Sukkertoppen Iskappe. The northeast extension of the SNF is cut-off by the Ikertôq thrust zone to the northwest. The SNF is described as discontinuous and consisting of a set of en-echelon, reverse shear zones slightly oblique to the overall trend of the front.

## Petrophysical data

Methods and standard diagrams for analysing petrophysical data have been suggested by Puranen (1989) and Henkel (1991; 1994). Scatter plots of the different properties are used to display the variations in the data. Frequency histograms are used for the general evaluation of the densities.

Localities where field measurements of the magnetic susceptibility have been undertaken and localities of collected rock samples, with additional laboratory determination of magnetic susceptibility and remanent magnetisation are shown in Fig. 14.

The petrophysical properties, without considering lithology type are summarised in the scatter plots and the histograms in Figs. 14 and 15. Petrophysical properties measured in the laboratory exist from 211 rock samples whereof 100 are samples of gneissic rocks. In General a similar distribution of field and laboratory determined magnetic susceptibility values is observed.

Amount, composition, and grain size of ferromagnetic minerals will have a dominating affect on the distribution of the petrophysical results in the scatter diagrams. A bimodal distribution of the magnetic susceptibility can be recognised clearly in the laboratory-determined susceptibility (Fig. 14) and though not so clear, when including all the field measurements (histogram in Fig. 13). This bimodal distribution reflects variations in the content of ferromagnetic and paramagnetic minerals (Puranen 1989; Clark & Emerson 1991; Clark 1997). The first mode has susceptibility values between  $300 \times 10^{-6}$  SI and  $1000 \times 10^{-6}$  SI. The second mode represents susceptibility values between  $5000 \times 10^{-6}$  SI and  $15000 \times 10^{-6}$  SI. Schist, amphibolite, marble, calc-silicate and felsic gneiss generally cause the first mode, whereas mafic rocks, ultramafic rocks, kimberlitic rocks cause the second mode. Results from analyses on felsic rocks with relative low content of mafic minerals predominates the sample set.

From the frequency histograms of density (Fig. 15) can it be seen that the peak for all analysed rocks is between  $2600 \text{ kg/m}^3$  to  $2700 \text{ kg/m}^3$ . This reflects the predominance of felsic rocks (gneisses, granites, charnockite, quartz diorites, schist, quartzite, marble and calc-silicates). Rocks with a density above  $2700 \text{ kg/m}^3$  consist mainly of more mafic rocks (amphibolites, undifferentiated mafic and ultramafic rocks, gabbroic rocks, kimberlite dykes and Kangâmiut dykes). The highest densities (up to  $4026 \text{ kg/m}^3$ ) are caused by rock samples of banded iron formations and massive iron sulphides. The natural remanence of all analysed rocks varies from 0 to  $174920 \text{ mA/m}$  with a mean at  $4541 \text{ mA/m}$ . The lower values originate mostly from felsic gneisses, granite, schist, marble, calc-silicates, and amphibolite. Ultramafic rocks dominate the higher values.

The Q ratio values are below 1 in 55% of the analysed rocks.

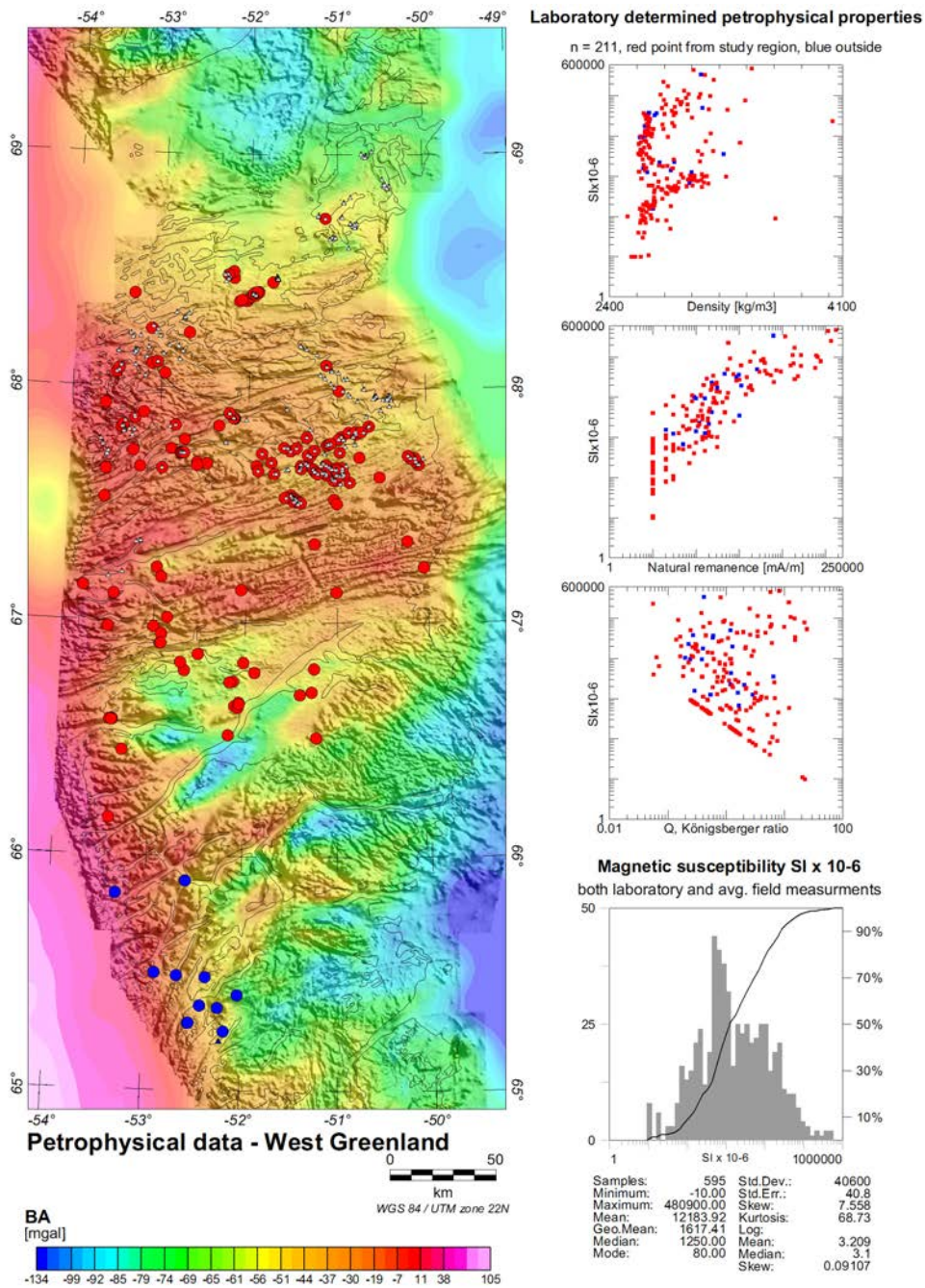


**Figure 14.** Map with combined Bouguer anomaly field (in chromatic colour) and shaded total magnetic intensity field (in grey). Localities where rock samples with later laboratory determined petrophysical properties have been collected are shown with a coloured circle; red for localities within the assessment region, blue for localities outside the assessment region. Localities with field measurements of magnetic susceptibility are marked by a white triangle. Scatter plots of density, natural remanence, and Königsberger ratio summaries the laboratory determined petrophysical properties (see also histograms in Fig. 15). All laboratory and averaged in situ field measurements of the magnetic susceptibility are given in the included histogram.

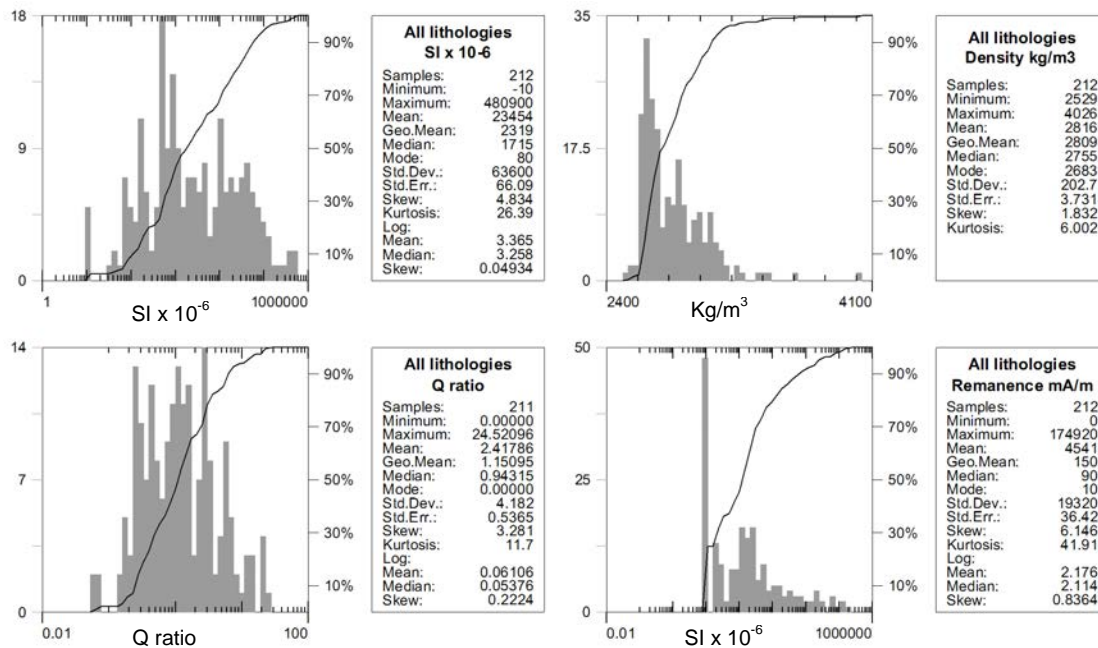


**Figure 15.** Histograms for all samples with laboratory determined petrophysical properties in the assessment region without distinction between types of lithology.

## Petrophysical properties of different lithologies

In general, the majority of the supracrustal rocks from the assessment region show low magnetic susceptibility values from 0.00 to 1000 SI x 10<sup>-6</sup> compared to the surrounding basement gneiss, which yield values from 1000 to 15 000 SI x 10<sup>-6</sup>. The Arfersiorfik quartz diorite shows susceptibility values from 50 to 12 000 SI x 10<sup>-6</sup>. Within the supracrustal sequences the magnetic susceptibility values generally increase in the following order:

- Marble, dolomite, calc-silicate with values from 10 SI x 10<sup>-6</sup> to 130 SI x 10<sup>-6</sup> and a geometric mean at c. 50 SI x 10<sup>-6</sup>
- Quartzite with values from c. 100 SI x 10<sup>-6</sup> to 700 SI x 10<sup>-6</sup>
- Felsic granite with values 10 SI x 10<sup>-6</sup> to 200 SI x 10<sup>-6</sup>
- Schist with values from 40 SI x 10<sup>-6</sup> to 1100 SI x 10<sup>-6</sup> and a geometric mean at c. 450 SI x 10<sup>-6</sup>
- Quartz diorite – Arfersiorfik quartz diorite with values from 50 SI x 10<sup>-6</sup> to 10 000 SI x 10<sup>-6</sup>
- Gneiss (very variable) with values from 50 SI x 10<sup>-6</sup> to 50 000 SI x 10<sup>-6</sup> and a geometric mean at c. 1750 SI x 10<sup>-6</sup>
- Mafic magnetite-bearing granite with values from 1000 SI x 10<sup>-6</sup> to 90 000 SI x 10<sup>-6</sup>
- Amphibolite, gabbroic rocks, mafic rocks and ultramafic rocks with values from 300 SI x 10<sup>-6</sup> to 90 000 SI x 10<sup>-6</sup>
- Banded iron formations with values from 7000 SI x 10<sup>-6</sup> to 300 000 SI x 10<sup>-6</sup>

The histograms of the different lithologies are included in appendix A.

## Gneiss

The petrophysical properties of gneiss lithologies are very variable reflecting the large variation of gneisses observed in the field. The gneisses have minimum susceptibility values around  $10 \text{ SI} \times 10^{-6}$  (one sample  $-10 \text{ SI} \times 10^{-6}$ ) and maximum susceptibility values from  $40000 \text{ SI} \times 10^{-6}$  to  $50000 \text{ SI} \times 10^{-6}$  (one sample  $333560 \text{ SI} \times 10^{-6}$  with very high magnetite content). The mean susceptibility value is  $7200 \text{ SI} \times 10^{-6}$  and the geometric mean is  $1745 \text{ SI} \times 10^{-6}$ . The distribution of the magnetic remanence has two peaks, one peak at  $10 \text{ mA/m}$  and a second peak between  $100 \text{ mA/m}$  and  $300 \text{ mA/m}$ . Densities from  $2600 \text{ kg/m}^3$  to  $2850 \text{ kg/m}^3$  dominate the gneisses. The mean of all gneiss samples is c.  $2700 \text{ kg/m}^3$ . A small number of gneiss samples have lower densities around  $2550 \text{ kg/m}^3$  and higher densities between  $2900 \text{ kg/m}^3$  and  $3100 \text{ kg/m}^3$ . The lower densities correspond to biotite-rich gneisses whereas the high densities correspond to garnet-bearing gneisses. The mean and the distribution of the gneiss densities are comparable with densities for gneisses described in other studies (Puranen 1989; Henkel 1991; Clark 1997; Airo 1999). A clear bimodality is observed for the magnetic susceptibility of the gneisses (Appendix A, Fig. 54). This bimodality is possibly caused by different protholiths, deformation, and metamorphism. Measurements where a distinction between paragneisses and orthogneisses has been made are given in Fig. 16. Susceptibility values for paragneisses are characterized by a clear peak between  $300 \text{ SI} \times 10^{-6}$  and  $400 \text{ SI} \times 10^{-6}$ . Orthogneisses have more variable but higher susceptibility values and have a broad peak between  $5000 \text{ SI} \times 10^{-6}$  and  $9000 \text{ SI} \times 10^{-6}$ . Although overlap exists in the susceptibility values, it seems that the distribution of the values for the two gneiss types can be used in conjunction with other parameters to make distinctions between the two types. No distinction between the two gneiss types can be made from the densities.

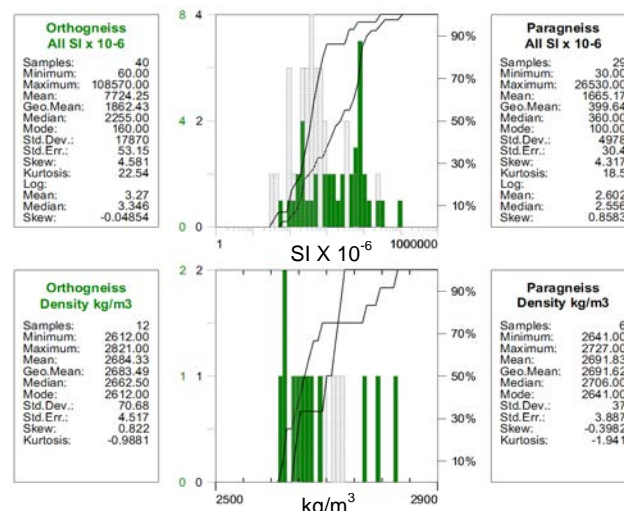


**Figure 16.** Frequency histograms for magnetic susceptibility and density with distinction between orthogneiss and paragneiss. Histogram for paragneisses is shown with grey coloured hatches on top of the histogram for orthogneiss.

## Granite

The granites have magnetic susceptibility values (Appendix A) from  $10 \text{ SI} \times 10^{-6}$  to  $91740 \text{ SI} \times 10^{-6}$ . Most of the higher values originate from granites with visible magnetite grains.

Lower values are dominated by strong felsic mica-rich granite lithologies. Only four samples have been analysed in the laboratory. Three of these samples have densities between  $2600 \text{ kg/m}^3$  to  $2650 \text{ kg/m}^3$  and Q ratios below 1. These values are similar to typical petro-physical values for granites described in the literature (Carmichael 1982; Clark 1997). The highest magnetic susceptibility value, density and Q ratio for the granites correspond to coarser grained porphyric granite with a weak foliation defined by mafic minerals located at the northern shore of Kangasuneq fjord south of Qasigiannuit (Christianshaab). The granite has a high content of magnetite and a pronounced strong positive magnetic anomaly can be seen in the total magnetic field.

### **Quartz diorite – Arfersiorfik quartz diorite**

Susceptibility values for the Arfersiorfik quartz diorite fall in the range from  $20 \text{ SI} \times 10^{-6}$  to  $33\,980 \text{ SI} \times 10^{-6}$ , with a geometric mean at  $3948 \text{ SI} \times 10^{-6}$  (Appendix A). The highest susceptibility values correspond to quartz diorite with very high content of fine-grained acicular magnetite from localities inside the central part of the main Arfersiorfik quartz diorite. Quartz diorites in the Nordre Strømfjord shear zone yield some of the lowest susceptibility values. These differences are also reflected in the aeromagnetics (will be discussed in detail later) where the central part of the Arfersiorfik quartz diorite complex is associated with the highest magnetic anomalies, and the lowest anomalies associated with the Arfersiorfik quartz diorite are located in the Nordre Strømfjord shear zone. The densities for three laboratory analysed Arfersiorfik quartz diorite samples express diversity in their density from  $2682 \text{ kg/m}^3$  to  $3003 \text{ kg/m}^3$ . This diversity possibly reflects a varying content of felsic minerals in the quartz diorite, which also has been observed in the field. The Q ratios of the quartz diorite samples analysed in the laboratory are all below 2.

### **Charnockite**

A small number of charnockites have also been measured (Appendix A). Compared with granite and meta-sediments the magnetic susceptibility values are higher (values from  $150 \text{ SI} \times 10^{-6}$  to  $20830 \text{ SI} \times 10^{-6}$ ). The charnockite lithologies fall in the high end of the susceptibility range for the gneiss lithologies. The locations of the highest susceptibility values are associated with very high anomalies in the aeromagnetics (north of Nordre Isortoq Fjord and north of the outer part of Nordre Strømfjord).

### **Schist**

The susceptibilities of 90% of the schist samples (Appendix A) fall in the range from  $40 \text{ SI} \times 10^{-6}$  to  $1500 \text{ SI} \times 10^{-6}$ . Five schist samples fall outside this range with values from  $2590 \text{ SI} \times 10^{-6}$  to  $343\,580 \text{ SI} \times 10^{-6}$ . The geometric mean is  $455 \text{ SI} \times 10^{-6}$ . Higher susceptibility values are obtained from more mafic pelitic schist types, whereas the lowest susceptibility values are obtained from more felsic, often quartz-rich psammitic, and schist types. The densities of the analysed schist samples are rather dispersing, with values from  $2529 \text{ kg/m}^3$  to  $3088 \text{ kg/m}^3$ . Thirty percent of the samples group in the range from c.  $2600 \text{ kg/m}^3$  to  $2700 \text{ kg/m}^3$  whereas another 25% of the samples group around  $3050 \text{ kg/m}^3$  to  $3100 \text{ kg/m}^3$ . The lower

densities correspond often to more felsic or rust-altered schist types, whereas rocks with higher densities are characterised by garnet-bearing schists. By comparing the schist with the petrophysical properties of the gneisses it can be seen that their range is similar, but that the schist lithologies generally are characterised by lower susceptibility values than the gneiss lithologies.

### **Massive sulphides and banded iron formations**

The susceptibility measurements on massive sulphides (mainly consisting of pyrrhotite, from only four locations) are very varying (Appendix A). The values range from  $90 \text{ SI} \times 10^{-6}$  to  $23940 \text{ SI} \times 10^{-6}$ . The highest susceptibility and magnetic remanence values are from a sample from a massive sulphide occurrence in the Naternaq area (in the NNO) where the pyrrhotite minerals are associated with fine-grained magnetite. The three other samples have susceptibility values below  $10\,000 \text{ SI} \times 10^{-6}$ . The massive sulphides yield some of the highest density values (two samples give densities of  $3608 \text{ kg/m}^3$  and  $4026 \text{ kg/m}^3$ ).

Generally banded iron formations yield some of the highest susceptibility values in the range from  $6830 \text{ SI} \times 10^{-6}$  to  $206\,760 \text{ SI} \times 10^{-6}$  and with a geometric mean at  $40\,277 \text{ SI} \times 10^{-6}$  (Appendix A). All locations with high susceptibility values are associated with well-defined positive anomalies in the aeromagnetics.

### **Marble, dolomite and calc-silicate**

The magnetic susceptibility values of meta-carbonate lithologies (Appendix A) are low with a range  $10 \text{ SI} \times 10^{-6}$  to  $130 \text{ SI} \times 10^{-6}$ . The meta-carbonate lithologies have relative high Q ratios.

### **Quartzite**

As for the meta-carbonate lithologies quartzite lithologies is low magnetic with susceptibility values from  $80 \text{ SI} \times 10^{-6}$  to  $600 \text{ SI} \times 10^{-6}$  (Appendix A). One sample is anomalous with high susceptibility values around  $22\,180 \text{ SI} \times 10^{-6}$ . This sample is from a quartzite with disseminated magnetite. As for the meta-carbonate, the quartzite lithologies are characterised by rather high Q ratios.

### **Amphibolite**

The amphibolites have a distribution with magnetic susceptibility measurements (Appendix A) mainly in the range  $350 \text{ SI} \times 10^{-6}$  to  $8000 \text{ SI} \times 10^{-6}$ . A minor group of samples has low values around  $150 \text{ SI} \times 10^{-6}$  and another 15% of the samples have values between  $13\,000 \text{ SI} \times 10^{-6}$  and  $449\,170 \text{ SI} \times 10^{-6}$ . The distribution of the susceptibilities of amphibolites is comparable to both the values obtained for the gneiss and schist lithologies; however, the susceptibility values for the amphibolites fall in the high end of the distribution of susceptibility for the schists. Over 90% of the analysed amphibolite samples have densities in the

range from 2850 kg/m<sup>3</sup> to 3150 kg/m<sup>3</sup>. Compared with gneiss, granite and meta-sediments, the density of amphibolite is considerably higher. The remanence of the amphibolite lithologies has a rather dispersed distribution.

## **Mafic rocks**

Only 10 localities with mafic rock lithologies (undifferentiated) have been measured (Appendix A). These have magnetic susceptibility values in the range from 760 SI x 10<sup>-6</sup> to 81 370 SI x 10<sup>-6</sup>.

## **Ultramafic rocks**

The ultramafic rock lithologies (hornblendites, pyroxenites, etc.) have high magnetic susceptibility values (Appendix A) in the range from 500 SI x 10<sup>-6</sup> to 77 700 SI x 10<sup>-6</sup> and a geometric mean at 5330 SI x 10<sup>-6</sup>. The high values reflect the high total iron content and the high content of secondary magnetite formed under metamorphism. The densities of the ultramafic rocks are generally very high, from 3100 kg/m<sup>3</sup> to 3400 kg/m<sup>3</sup> and comparable to density values given in the literature (Carmichael 1982).

## **Granulite and amphibolite facies rocks**

The petrophysical properties have been divided into measurements from granulite and amphibolite facies areas (facies boundaries defined accordingly to Escher (1971)). Magnetic susceptibilities for all measured rocks from all lithologies under granulite facies are dominated by high magnetic susceptibility values above 2000 SI x 10<sup>-6</sup> and they have a bimodal distribution with peaks at 600 SI x 10<sup>-6</sup> and 10000 SI x 10<sup>-6</sup>. The geometric mean is 1886 SI x 10<sup>-6</sup>. These values are in accordance with granulite facies values reported from other areas (Schlinger 1985; Olesen *et al.* 1991; Skilbrei *et al.* 1991; Airo 1999). Rocks from all lithologies under amphibolite facies are characterised by generally low susceptibility values and one peak at 600 (coincident with the lowest peak for the measured susceptibility under granulite facies). Magnetic susceptibility values for the gneiss samples under amphibolite or granulite facies conditions display similar characteristics as for all samples, however the distinction between gneisses from the two facies is not so clear. No distinct characteristics between the two facies can be made for the Q ratios or the densities.

The increase in susceptibility values from amphibolite facies to granulite facies is described (Grant 1985) as a result of the production of magnetite on the behalf of the breakdown of hydrous (Fe, Mg) Al-silicates (e.g. biotite, amphibolite) according to the general mineral reaction; hydrous (Fe, Mg) Al-silicates ± SiO<sub>2</sub> ± O<sub>2</sub> ⇌ K-feldspar + (Fe, Mg)-silicates ± magnetite + H<sub>2</sub>O. This is in agreement with the prograde mineral reactions associated with the transition from amphibolite to granulite facies condition suggested by Ramberg (1948) for the study region in West Greenland where Fe-Ti oxides are produced on the expense of silicate assemblages (biotite, hornblende, garnet).

Later retrograde metamorphism under amphibolite facies conditions can cause retrograde reactions where magnetite is destroyed. Magnetite is still stable in upper amphibolite facies but as hornblende is decomposed into biotite, and further into chlorite the magnetite starts to breakdown (e.g. Skilbrei *et al.* 1991; Shive *et al.* 1992; Airo 1999). Retrogression is further enhanced in ductile deformation zones due to higher water content, which oxidize the magnetite. This can account for the general lower magnetic susceptibility values for amphibolite facies rocks and the associated low magnetisation observed in most of the areas under amphibolite facies. The low magnetisation is especially pronounced for the amphibolite facies area of the SNO. This area is also characterised by penetrative strong ductile deformation, providing the possibilities for a high water content, which has enhanced the breakdown of magnetite.

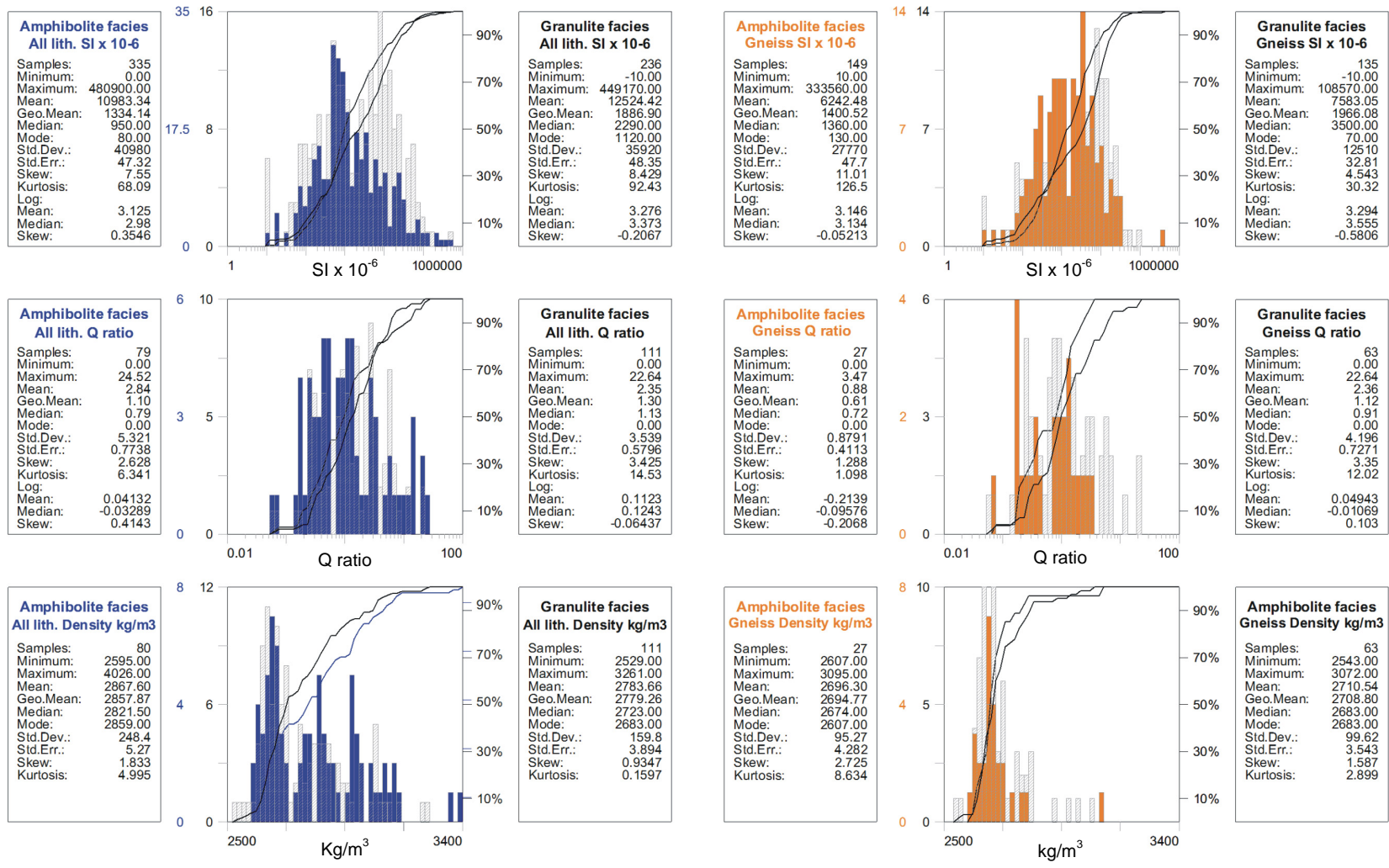


**Figure 17.** Frequency histograms for the petrophysical properties in relation to metamorphic facies. Right histograms are for all lithologies; left histograms are for gneiss lithologies only.

## Processing methods for qualitative analysis of potential field data

Citing Strauss and Corbin (1990, p. 17) qualitative research, broadly defined, represent “any kind of research that produces finding not arrived at by means of statistical procedures or other means of quantification”. Following this, it can be stated that qualitative researchers “seek illumination, understanding, and extrapolation to similar situations” (ct. Hoepfl 1997, p. 2).

Potential field data contain broadband information, where each reading represents a superposition of contributions from various physical sources. In order to enhance and isolate the field from specific sources, a wide range of linear and non-linear filtering and transformation techniques can be applied to the data. As the main objective of the present report is the application of the methods, the mathematical descriptions of the procedures are kept at a minimum. References are provided to more details on the techniques.

The processing methods that are utilised to extract information for the qualitative analysis are solely building on the measured data. The qualitative interpretations require geological knowledge and experience obtained from similar investigations in other areas. The results from the techniques should of course always be critically evaluated and, since every technique is associated with simplifications of a more complex world, precautions in applying the different techniques should be taken.

The following sections will present and discuss the methods used for data processing used to produce contributions to the qualitative interpretations. Most of the methods can be applied to both magnetic field data and gravity field data. Most of the techniques will be illustrated by use of the airborne magnetic data. The total magnetic intensity field is given in Fig. 18.

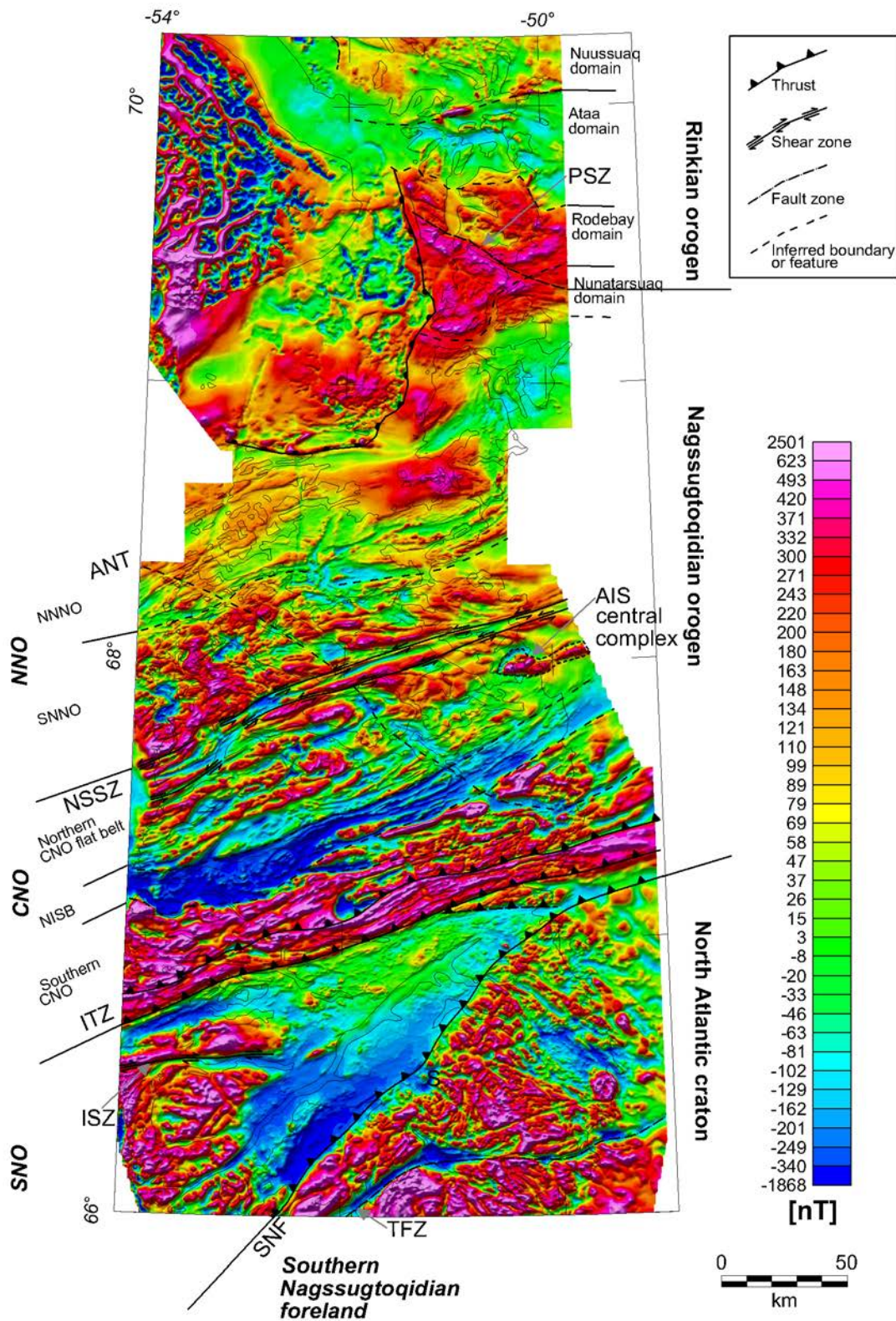


**Figure 18.** Map of total magnetic intensity field for the studied region. The anomaly pattern is shaded by simulating a light source illumination with an inclination of  $45^\circ$  and a declination of  $338^\circ$ . The indicated geological domains and boundaries will be discussed in a later section.

## Enhancement of specific wavelengths

### High-pass, low-pass and band-pass filtering

Standard high-, low-, and band-pass filters that leave a specified range of wavenumbers unchanged and attenuate all other are commonly used in the visualisation of potential field data. An unfortunate property of these filters is that they are not necessarily associated with well-defined physical phenomena, i.e. the filters are generally not physically realisable. The filters are used only as tools in the visualisation of the data for obtaining a suitable dynamic range for the display of the anomalies.

A low-pass filter will only allow wavenumbers below (long wavelengths) a specified value to pass, while a high-pass filter only allows large wavenumbers to pass. A band-pass filter allows wavenumbers within a defined range to pass.

Applying a Butterworth low-pass filter of 8<sup>th</sup> order, with a specific cut-off wavelength enhances the very long-waved features in the magnetic data. Results from a low-pass filtering with cut-off wavelength of 15 km, 25 km, 50 km and 100 km of the total magnetic field are shown in Fig. 19.A–D respectively. A fundamental property of a Butterworth filter is that amplitudes are modified without introduction of phase shifts.

The purpose of these filters is to separate and reject responses of a certain wavelength and thereby separate responses from different geological structures. Specific wavelengths are enhanced and some are suppressed. For example, if an area contains a series of shallow local sources, producing mainly short wavelength anomalies and another series of deeper sources, it is in principle possible to remove the short wavelength anomalies by a low-pass filtering. The effectiveness of the filtering depends on the differences in the responses from the two series of sources and the spectrum contained in the data.

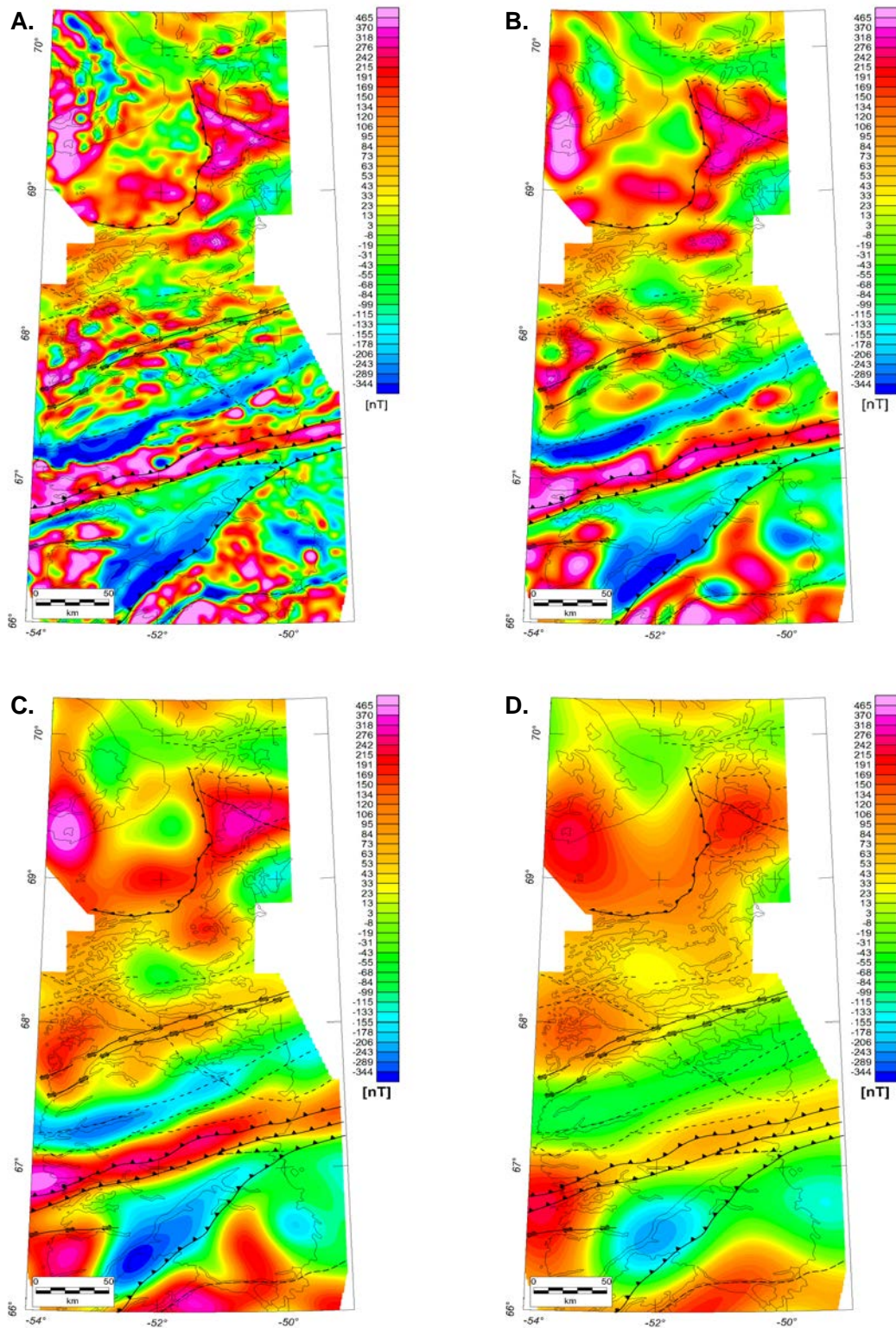


**Figure 19.** Results of low-pass filtering of the total magnetic field with **A.** a wavelength cut-off at 15 km, **B.** at 25 km, **C.** at 50 km and **D.** at 100 km.

## Enhancement of long-wavelength responses

Several techniques, besides the low- and band-pass filtering, can be used to enhance long-wavelength features that originate from regional large-scale geological features. Altogether, the maps emphasising long wavelength features will be denoted long wavelength maps.

### Upward continuation and stripping filtering

Jacobsen (1987) suggested a stripping filter to separate responses from various crustal depth levels. The filter makes use of upward continuation of the field to different heights to separate long-wavelength from short-wavelength.

Jacobsen interprets the wavenumber expression for upward continuation to height  $2z$  above the measurement plane, as the regional field at the surface of the Earth from sources below depth  $z$  (Fig. 20). Applications of the results of the stripping filtering applied to the total magnetic field for the study region are shown in Fig. 21.

The upward continuation of the field to a higher level is an effective way to suppress high frequency anomalies. An advantage of using the upward continuation operator instead of a standard low- and band-pass filtering is that the filter is physically realisable and robust. The upward continuation is produced by Fourier transformation of the potential field data, multiply the transformed data by  $e^{-Kh}$ , where  $h$  is the height and  $K$  is the wavenumber, followed by an inverse Fourier transformation. Because the magnitude of short wavelength features are attenuated more than long wavelength features, an upward continuation is an effective low-pass filter. A full treatment of the upward continuation process can be found in Blakely (1996).

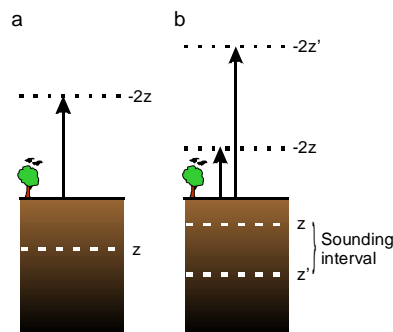


**Figure 20.** Geometrical relationships of (a) stripping filtering, where the subsurface field below depth  $z$  is given as the upward continuation of the field to height  $2z$ , and (b) sounding filtering where the sounding interval between  $z$  to  $z'$  depth is given as  $2z' - 2z$ . Figure modified after Jacobsen (1987).

As Jacobsen points out, the belief that some band-pass filtering can produce the field from the geological structure within a certain depth interval is strictly speaking precluded by the fundamental ambiguity of potential field data. However, in practice, the filtering does work in some sense, but it is important to keep the limitations in mind and only use the results qualitatively. To make the band-pass filtering work is it necessary to make the assumption of a signal weighting downwards through the Earth. In the stripping filtering approach the continuation operator act as the weight function, with its success depending on the differences in wavenumber content of the fields to be separated. Thus, uncertainties and loss of information are possible errors due to mixing of overlapping spectra and wavelength disturbance. Moreover, the magnetic field obtained through these techniques is naturally a simplification of the true geology. Nevertheless, these filtering techniques remain a valuable tool for qualitative anomaly detection and pattern discrimination and have been used with good results (Pedersen 1991; Rutland *et al.* 2001).

The geological application of the stripping filtering is that it is possible to get an indication of the evolution of the potential field caused by sources downward through the Earth.

### **Sounding filtering**

Another approach suggested by Jacobsen (1987), on the separation of wavelengths, is estimation of the surface fields from depth intervals in the subsurface. This approach is denoted as sounding filtering. This filtering is achieved by subtracting data corresponding to different levels of upward continuations, which reflects surface fields from different levels in the Earth (Fig. 20). The limitations in the stripping filtering also apply to sounding filtering.

The results of sounding filtering of the subsurface interval between a depth of 0 to 150 m, 1 to 6 km, 1 to 9 km and 6 to 12 km are shown in Fig. 22.

The geological application of the sounding filtering, again keeping in mind the limitations and highly qualitative nature of the results, is that it allows an evaluation of which depth interval the anomalies originates from.

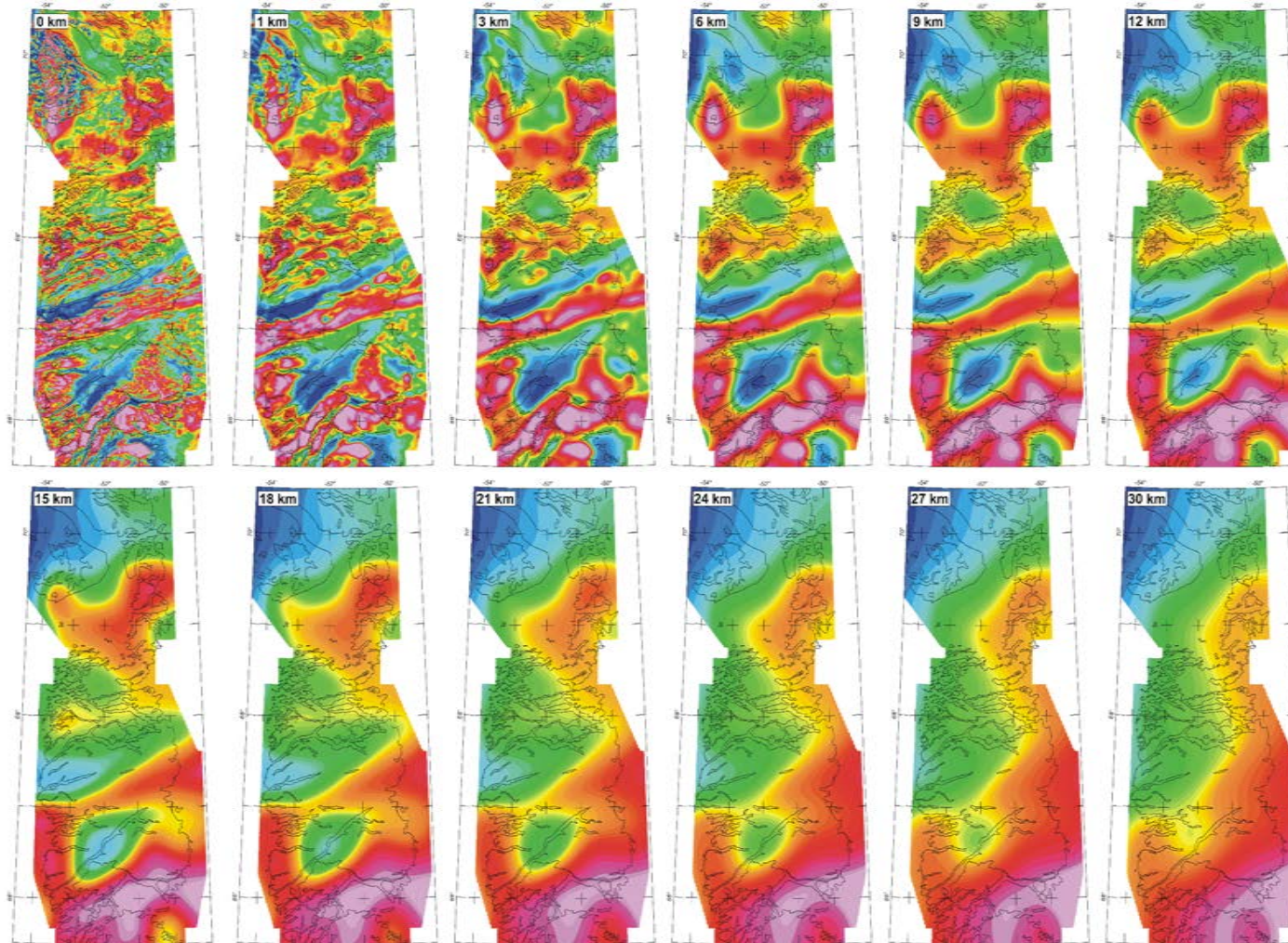
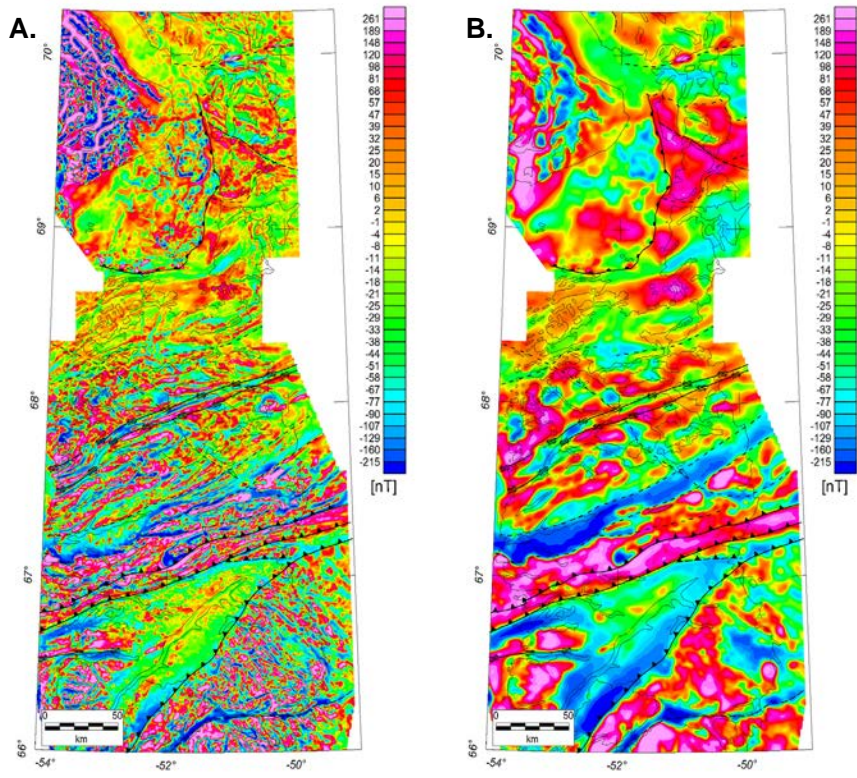
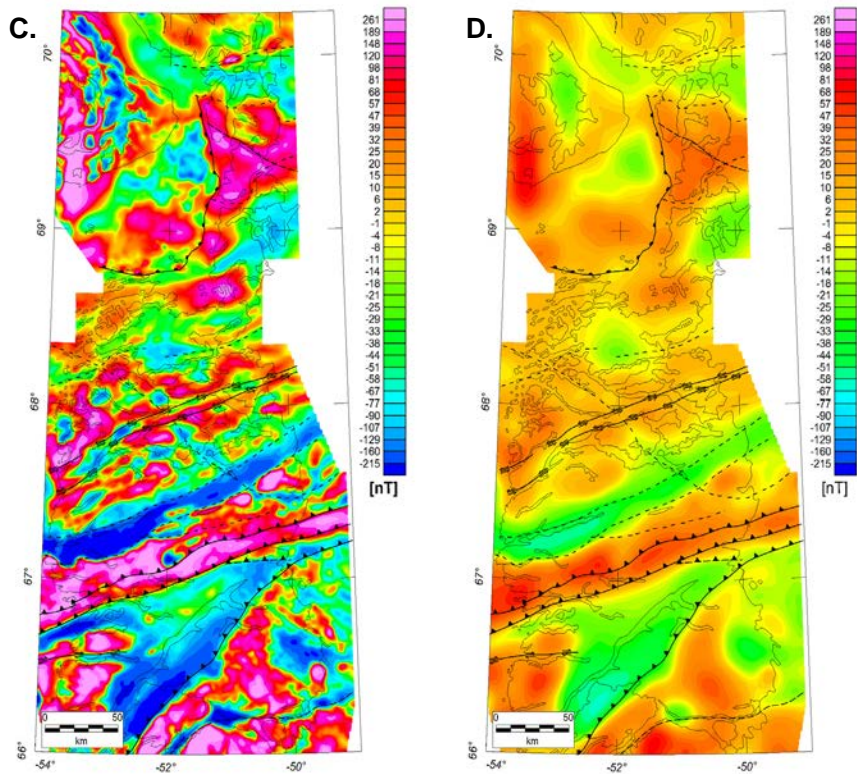


**Figure 21.** Maps of the stripping filtering of the total magnetic field. The maps represent the total magnetic field at the surface of the earth from sources down through the earth below depths of 1 km to 30 km in steps 3 km intervals (besides the first two maps, which are at 1 km steps). The relation that an upward continuation of the field to different heights above the ground corresponds to the field in depths approximately equal to half the heights is utilised. In this way, every map represents an upward continuation of the field at an interval of 6 km.



Nominal sounding interval 0.150 m to 1 km  
TMI UC 0 km – TMI UC 2 km

Nominal sounding interval 1 km to 6 km  
TMI UC 2 km – TMI UC 12 km



Nominal sounding interval 1 km to 9 km  
TMI UC 2 km – TMI UC 18 km

Nominal sounding interval 6 km to 9 km  
TMI UC 12 km – TMI UC 18 km

**Figure 22.** Results from sounding filtering of the total magnetic field.

## **Pseudogravity**

Another way of emphasising responses from long wavelength deep-seated regional features is to convert the total magnetic field into an imitated gravity field that would be observed if the distribution of the magnetisation were replaced with a proportional density distribution (i.e., the ratio between the magnetisation and the density is constant, Blakely, 1996). This conversion is called pseudogravity transformation and the resulting quantity is denoted a pseudogravity anomaly. As pointed out by Blakely (1996), these names may be inappropriate as no masses is involved in the transformation. Blakely suggest that it is more appropriate to talk about a conversion from magnetic field to magnetic potential (where the units are magnetic potential units, which also will be used here as the units for the pseudogravity). The pseudogravity anomaly map is shown in Fig. 23.

The pseudogravity field has similar properties as a gravity field. This means that on a regional scale the maximum of the horizontal gradient is located directly above a vertical physical contact, although an offset of the peak is expected for a dipping contact

The geological application of the pseudogravity field is that the field can be directly compared with the measured gravity field, and permits investigation of similarities between the magnetic and gravity sources. If sources of gravity and magnetic anomalies are the same and proportionality exists between magnetisation and density, then the constructed pseudogravity should be identical to the observed gravity field. The pseudogravity filter is basically a spatial integration and the transformation will suppress short wavelength anomalies.

As pointed out by Blackly (1996), even though the mass distribution and the magnetic distribution are not the same, the pseudogravity anomalies can be very instructive and in some way easier to interpret and quantify than the magnetic anomalies. For tabular bodies will the largest horizontal gradients (will be addressed in a later section separately) of the gravity anomalies be located over the edge of the bodies. This can be utilized in the magnetic interpretation by transformation of the total magnetic intensity field to pseudogravity followed by a calculation of the horizontal gradients. (Cordell & Grauch 1985).

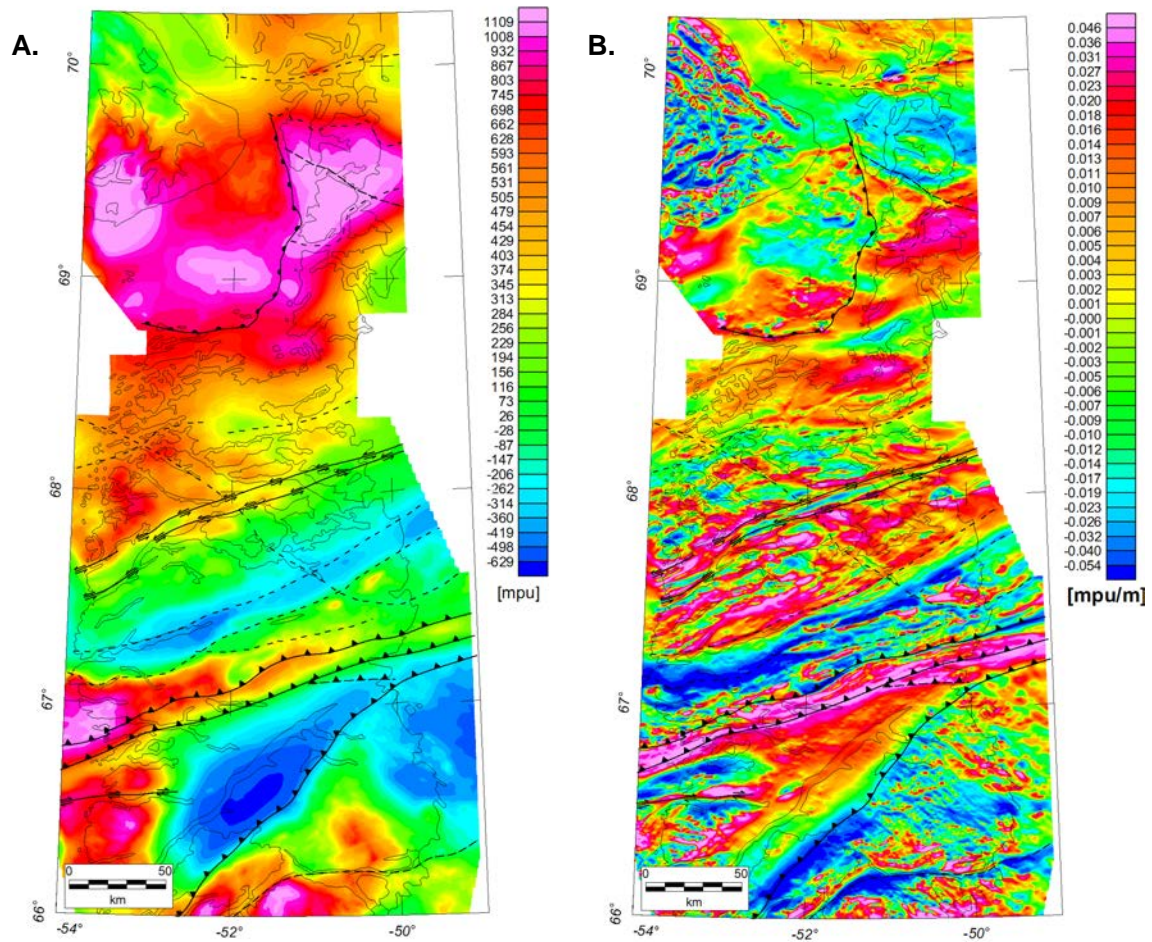


**Figure 23.** **A.** Map of the pseudogravity field derived from transformation of the magnetic total field intensity in Fig. 18. The pseudogravity anomaly is given in arbitrary magnetic potential units (mpu). **B.** The horizontal gradient of the pseudogravity field. The gradient is calculated for a north-south direction.

## **Enhancement of short wavelengths**

Besides high- and band-pass filtering, responses from shallow or sub-outcropping structures can be highlighted through different methods. The maps emphasising short wavelength features will be denoted short-wavelength maps.

### **Downward continuation**

Instead of upward continuation of the field to a higher level it is also possible to downward the field to a level closer to the sources. A downward continuation will enhance the high frequency and hereby the effect of the anomalies originating from shallow sources. However, short wavelength noise are also amplified and it is only practical to downward the field a limited distance. The results and limits depend on the quality and sampling of the data. A downward continuation of the field can be used to enhance the near-surface geological structures, sources and trends.

### **Vertical derivatives – vertical gradients**

A direct way of enhancing the short-wavelength part of the magnetic field is to calculate the vertical gradient (or first order derivative). The calculation is usually done in the Fourier domain. The physical interpretation of the vertical gradient is represented by the measurement of the field at two points directly above each other, subtracting the two obtained values and then dividing by the vertical distance separating the points of measurements. The calculated vertical gradient of the magnetic total field is given in Fig. 24. Some airborne magnetic systems measure the gradient by utilising two magnetic sensors.

The vertical gradient of the gravity field is constructed from a microlevelled Bouguer anomaly field. The microlevelled Bouguer anomaly field (Fig. 24.A) is very similar to the original Bouguer anomaly field (Fig. 24.C) but short-wavelength anomalies are suppressed. Thereby, the vertical gradient calculated from the microlevelled Bouguer anomaly field (Fig. 24.D) is less distorted by aliasing compared to the vertical gradients derived from the original Bouguer anomaly field (Fig. 24.B).

The geological application of the vertical gradient is that it enhances shallow features, sharpens the flanks of the anomalies, and strongly attenuates long-wavelength regional effects. In this way, the vertical gradient of the field is very use full in the interpretation of geological features at the surface.

Differentiation of the field twice in the vertical direction gives the second order vertical derivative, which is the vertical gradient of the first order derivative. The second vertical derivative enhances high-frequency responses even more than the first vertical derivative. However, this property causes also the second vertical derivatives to be more sensitive to noise and this can introduce artificial features. The second order vertical derivative of the magnetic total field is shown in Fig. 26.

The geological application of the second order derivative of the field is that the suppression of the long-wavelength features is even greater than the first order derivative. This can especially be utilised to enhance boundaries and structural trends that are small in the first derivative. However, the complexity and the possible effects of noise are increased.

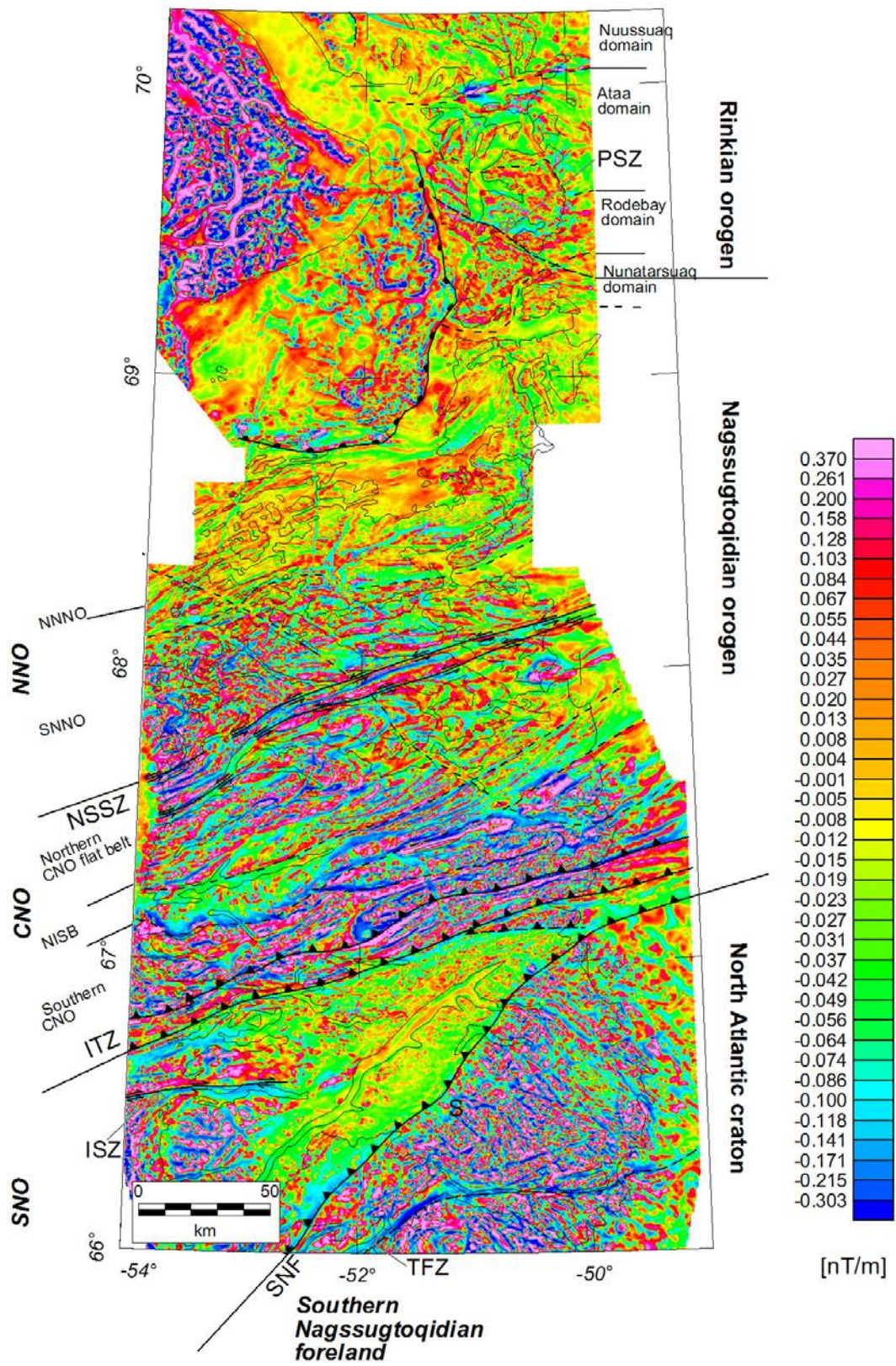
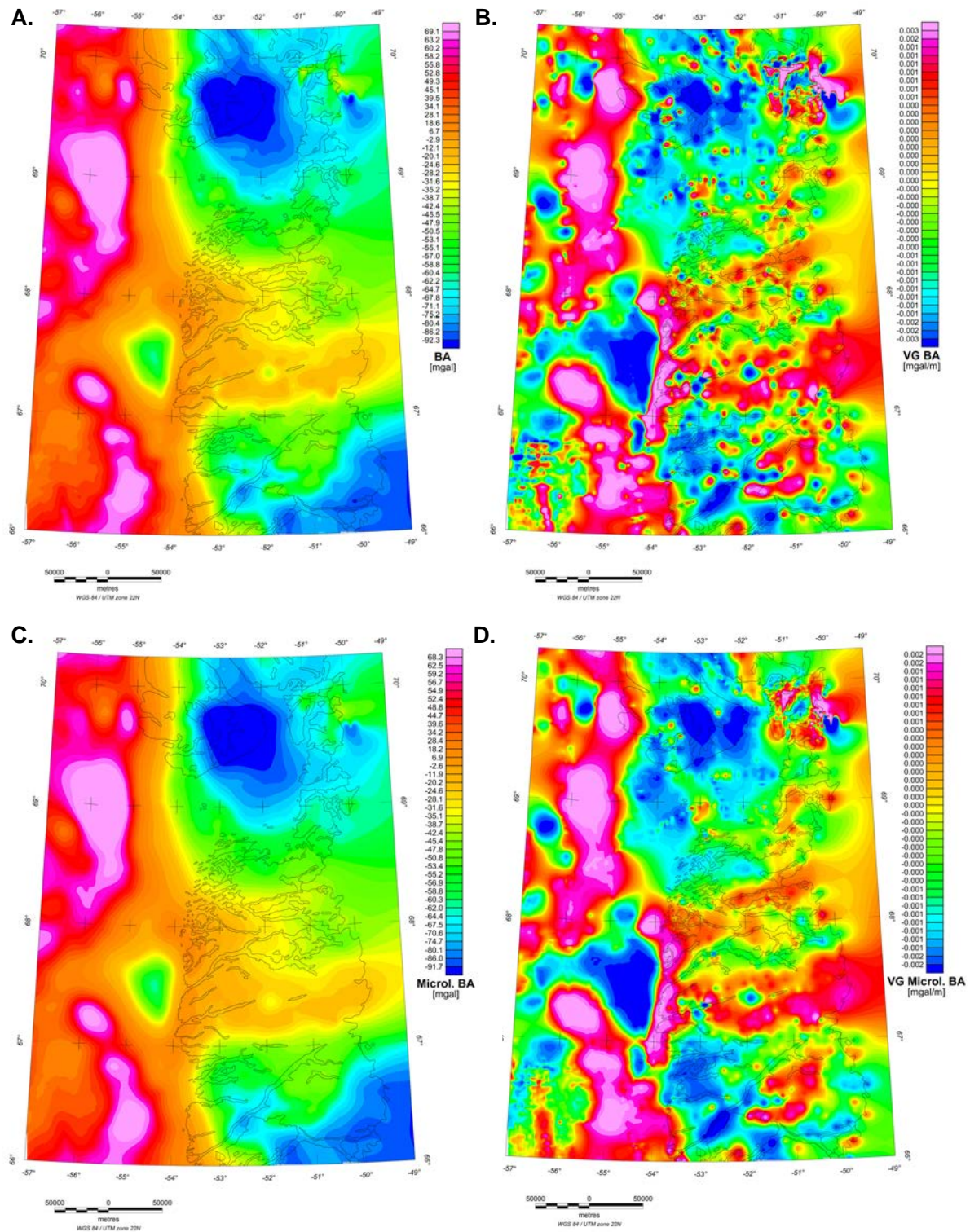
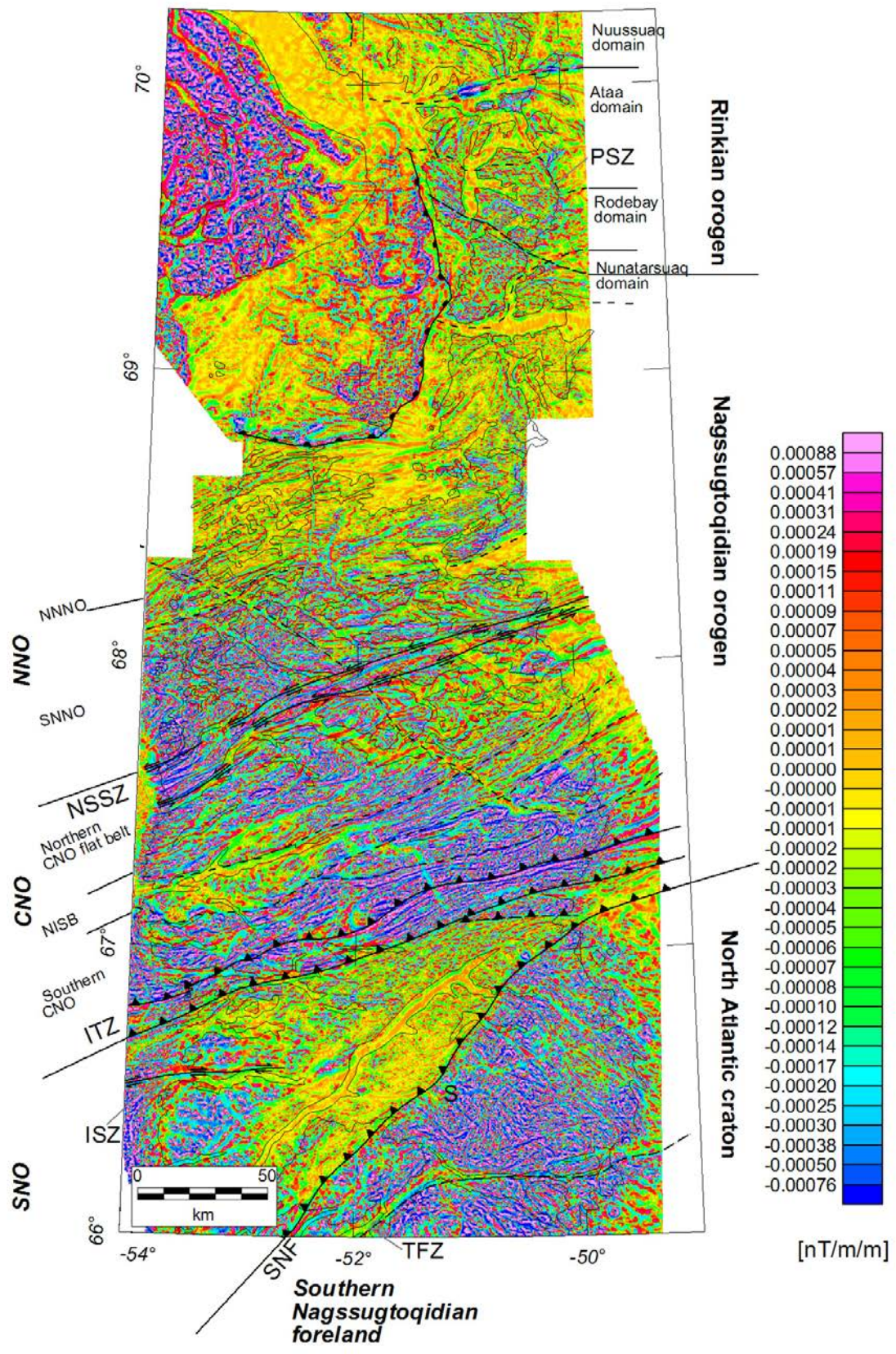


Figure 24. Map of the vertical gradient of the total magnetic field intensity.



**Figure 25.** **A.** Original Bouguer anomaly field (as Fig. 7). **B.** Vertical gradient of the non-microlevelled original Bouguer anomaly field. **C.** Microlevelled Bouguer anomaly field. The micro-levelling process is done with a low-pass filter with a cut-off wavelength of 25 km, which is 2 to 3 times the separation between gravity stations in the most of the study region on land. **D.** Vertical gradient derived from the microlevelled Bouguer anomaly field. All grids are with a 2 km grid cell size.



**Figure 26.** Second vertical derivative of the magnetic field. Very shallow features are further enhanced compared with the first vertical derivative.

## Horizontal gradients – directional derivatives

Horizontal gradients (or derivatives) will show anomalies from structures perpendicular to the direction of differentiation. In this way, it is not only enhancing short wavelength, but it is also a directional filter. The calculation of the horizontal gradients is often done in the Fourier domain. Insufficient sampling of the field across flight lines can create spurious results. In order to suppress this, an upward continuation of the field is applied. The height of the upward continuation is determined visually until aliasing effects become sufficiently suppressed. An upward continuation distance of 500 m was found appropriate. The horizontal gradients in the E–W and N–S directions of the magnetic total field are calculated to accentuate responses from structures that are perpendicular to these directions (Fig. 27).

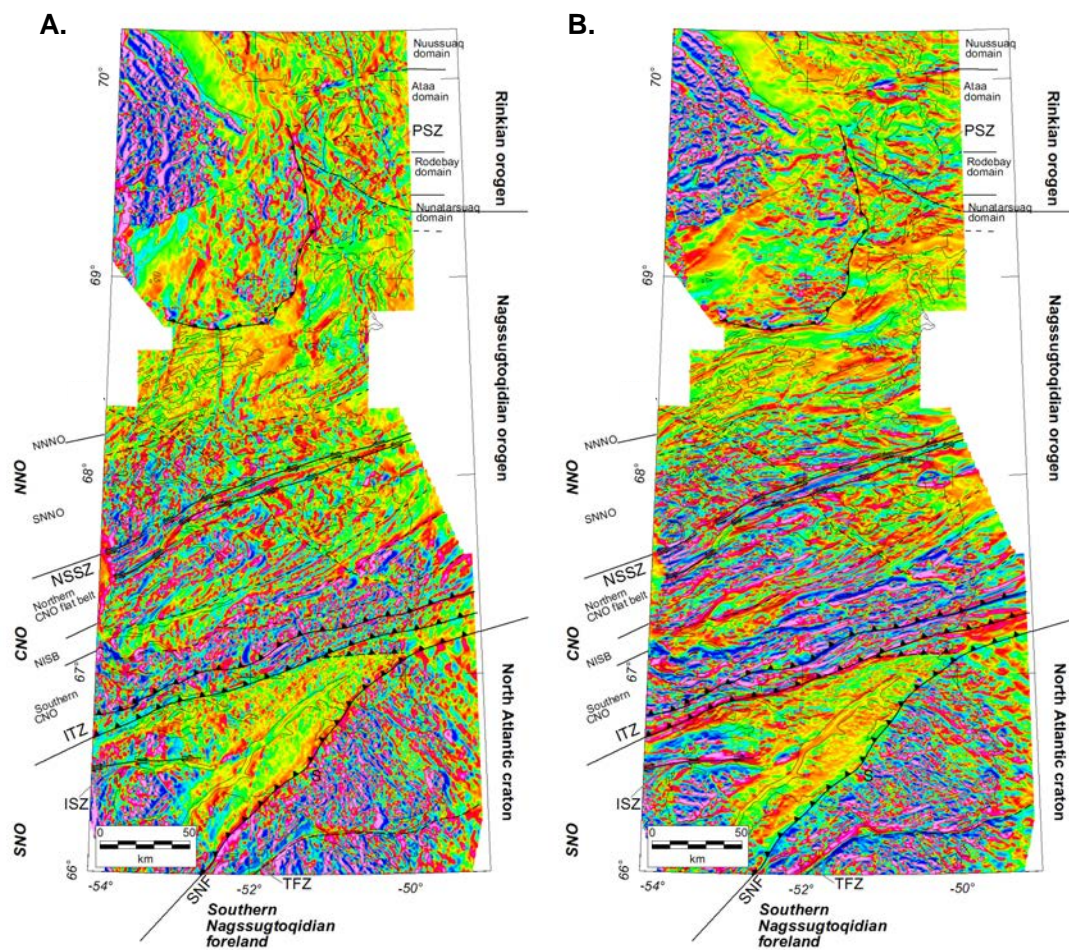


**Figure 27.** Horizontal gradients (or derivatives) and 500 m upward continued total magnetic field. The derivatives in **A.** are calculated for the E–W direction, which enhance features with an N–S orientation, whereas the derivatives in **B.** are for the N–S direction with enhancement of E–W orientated features.

The geological application of the horizontal gradients is that it is possible to enhance shallow geological structures with a specific orientation, such as dykes, structural orientations,

boundaries, and faults. Enhancements of anomalies from structures that are suppressed in the non-filtered responses due to another dominating orientation are hereby possible. Furthermore, anomaly peaks located approximately over edges of wide bodies are obtained by this transformation. These advantages can be utilised to map the outlines of sources.

## **Curvature analysis**

The qualitative methods presented so far have transformed and filtered the data in order to extract specific information from the data. Another method is to investigate the signal of the potential field data strictly mathematically and geometrically.

Abrupt changes in the potential field data, reflecting changes in the distribution of the magnetisation or density, are generally related to three types of geological defined boundaries: 1) lithologies, 2) geological terrains and 3) deformation state. Type 1) and 3) are expressed on a local or regional scale, whereas type 2) is mostly relevant on regional scale. Some automatic methods for locating abrupt changes in the potential field are presented below.

### **Curvature of the horizontal gradients**

A simple first approach is to analyse the curvature of the gravity field data and the pseudo-gravity transformed magnetic data (Cordell & Grauch 1985). As the steepest horizontal gradient of a gravity anomaly of a tabular body is located over the edges of the body, this can be used to examine abrupt lateral changes in the density distribution. The same applies for magnetic data transformed by the pseudogravity transformation, where the steepest horizontal gradients will reflect lateral changes in magnetisation. If the boundaries are not represented by a well defined vertical geological boundary, some offset in the location of the steepest gradient can be expected (Grauch & Cordell 1987). The geological features and boundaries that are extracted through this technique are present in the original total field data, but the analysis can be an aid in the interpretation process and can reveal and clarify features and patterns that might be difficult to identify in the original data.

### **Terracing operator**

Delineation of boundaries can be done by the use of the terracing operator (Cordell & McCafferty 1989). This data-processing technique converts the potential field data into equivalent physical property domains. The operator analyse the local curvature of the data, in a sliding 3 by 3 point window across the data. The maximum value of the data in the window is assigned to the centre point if the local curvature is negative. The minimum value is assigned if the local curvature has a maximum and the centre value is left unchanged if zero curvature is found. The process is iterated until no change is observed in the terraced grid. In this process, the potential field data is terraced into homogeneous domains.

# Quantitative analysis of potential field data

Quantitative analysis seeks causal relations, prediction, and generalization of findings. The causal determination is carried out by the use of models that are able to reproduce the measured data: either by forward or inverse modelling. A forward model is constructed by manually assigning and adjusting the properties and shapes of a model, until the calculated response matches the observed response. An inverse modelling assumes a principal Earth model, where the measured data are used to determine the modifications of the models geometries and properties in an automatic fashion until a satisfactory fit to the measured response is obtained.

The objective of a quantitative processing of potential field data is to estimate source distributions and parameters such as depth, shape, dip and strike. These estimations can then be used as input to the geological models and interpretations.

In most cases are the techniques based on modelling by use of a rather limited number of bodies along a limited number of lines. The techniques are difficult to apply effectively to large data sets as in the case of the data from West Greenland and it is only feasible to model a few lines with selected anomalies.

However, fast and more 'automatic' but less robust quantitative imaging techniques for estimation of source parameters exist that are well suited for large data sets. An advantage of these techniques is that they are not biased by the selection of specific anomalies/lines, but give a more extended picture. The automatic techniques are often applied to gridded data or to a large number of lines. The anomalies and patterns contained in the data are evaluated automatically and estimations on the source parameters are based on simple defined relations between the behaviour of the potential field and the sources. The evaluation of the results and the problems with robustness of the automatic techniques causes some difficulties compared with the manual modelling or inversion of a few selected lines.

In this section, we present results from some of the fast automatic imaging techniques that provide quantitative descriptions of the sources.

## Euler deconvolution

Euler deconvolution has been used for both two-dimensional cases (Thompson 1982; Roest *et al.* 1992) and three-dimensional cases (Reid *et al.* 1990; Zhang *et al.* 2000).

Euler deconvolution is implemented as a linear inversion of the potential field based on Euler's homogeneous differential equation. The expression is

$$(x - x_0) \frac{\partial T}{\partial x} + (y - y_0) \frac{\partial T}{\partial y} + (z - z_0) \frac{\partial T}{\partial z} = N(B - T). \quad [3]$$

where  $x_0$ ,  $y_0$  and  $z_0$  refer to the position of the source (point mass, magnetic dipole, etc.) in a right-handed Cartesian co-ordinate system ( $x$ ,  $y$ ,  $z$ ).  $T$  is the total-field and  $B$  is the regional of the total field. The degree of homogeneity denoted  $N$  is called an Euler structural index, which relates to the decay with distance of a magnetic anomaly originating from an arrangement of magnetic poles or dipoles. The structural indices of different simple geological models are given in Table 4 and Fig. 28. An index of  $N = 1$  corresponds in the gravity case to a pipe and in the case of a magnetic field to either a sill or dyke.

**Table 4.** *Structural index  $N$  for different simple magnetic and gravity models.*

$N$	Magnetic	Gravity
0.0	Contact	Sill/dyke/step
0.5	Thick step	Ribbon
1.0	Sill/dyke	Pipe
2.0	Pipe	Sphere
3.0	Sphere	

Complications and limitations arises when the rate of change of a field with distance is not a constant and when the sources are not 'true' simple models (Blakely 1996). Despite the complications, the Euler deconvolution method is a useful tool for obtaining information on source depth and geometry if the estimates are viewed with appropriate precautions.

A located Euler deconvolution is used in this work. This method makes use of locations of sources from the analytic signal (see next section) whereby offsets between sources and magnetic anomaly peaks are taking into account. In order to find the peaks in the grid, a method suggested by Blakely (1996) was used, where each grid cell value is compared with its eight nearest grid cell values in four directions. For structural indices less than or equal to 2 in the case of magnetics where lineaments are expected, all possible peaks are located where only one direction of neighbouring grid cell values are lower than the central value. For structural indices equal to 3, where isolated single peaks are expected, only locations with all neighbouring grid cell values lower in four directions are selected (Fig. 28).

In order to suppress short wavelength noise the magnetic field was upward continued to 300 m above the flight height. Moreover, smoothing by Hanning filters were applied to the analytic signal so that low amplitude short wavelength features were disregarded. Note that the physical realisable upward continuation filter was applied to the data entering the Euler deconvolution.

Analyses with different structural indices were performed by use of the located Euler deconvolution. An error estimate is given for the depth and the location. Results are sorted according to these estimates and only the most reliable results are presented. The Euler results are given in Fig. 29 to Fig. 33. All Euler deconvolution results with different structural index and thereby structure are included. The colour of a circle in the figures corresponds to the depth to the source of one solution. Thus, dips of two-dimensional features can be inferred in some cases.

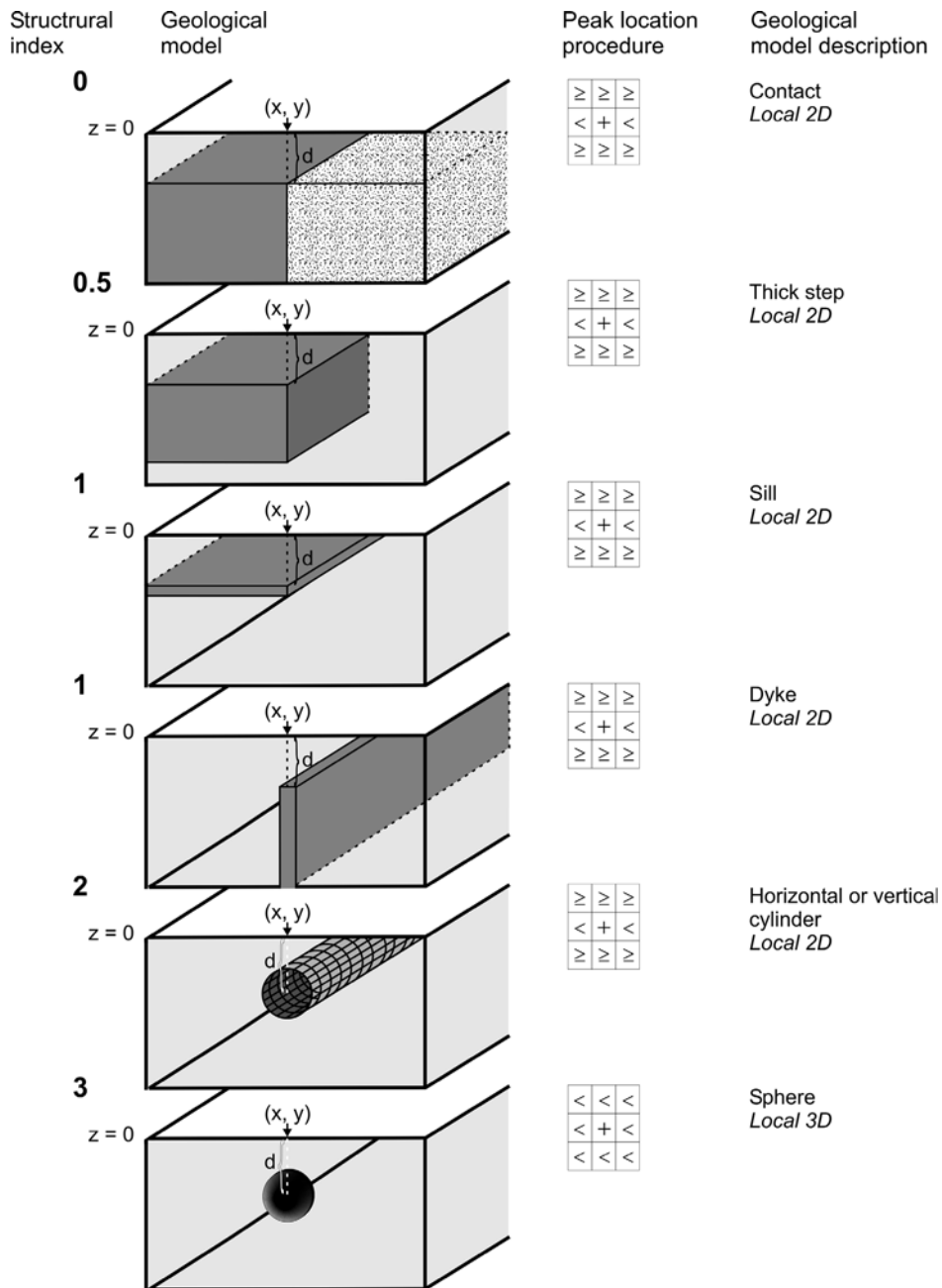


**Figure 28.** Structural indices used in Euler deconvolution and corresponding geological models when applied to a magnetic field. The peak location procedure, as suggested by Blakely, 1996, is also indicated, where each square represent a grid value; + for peak value, < for value less than peak value,  $\geq$  for value equal to or larger than peak value.

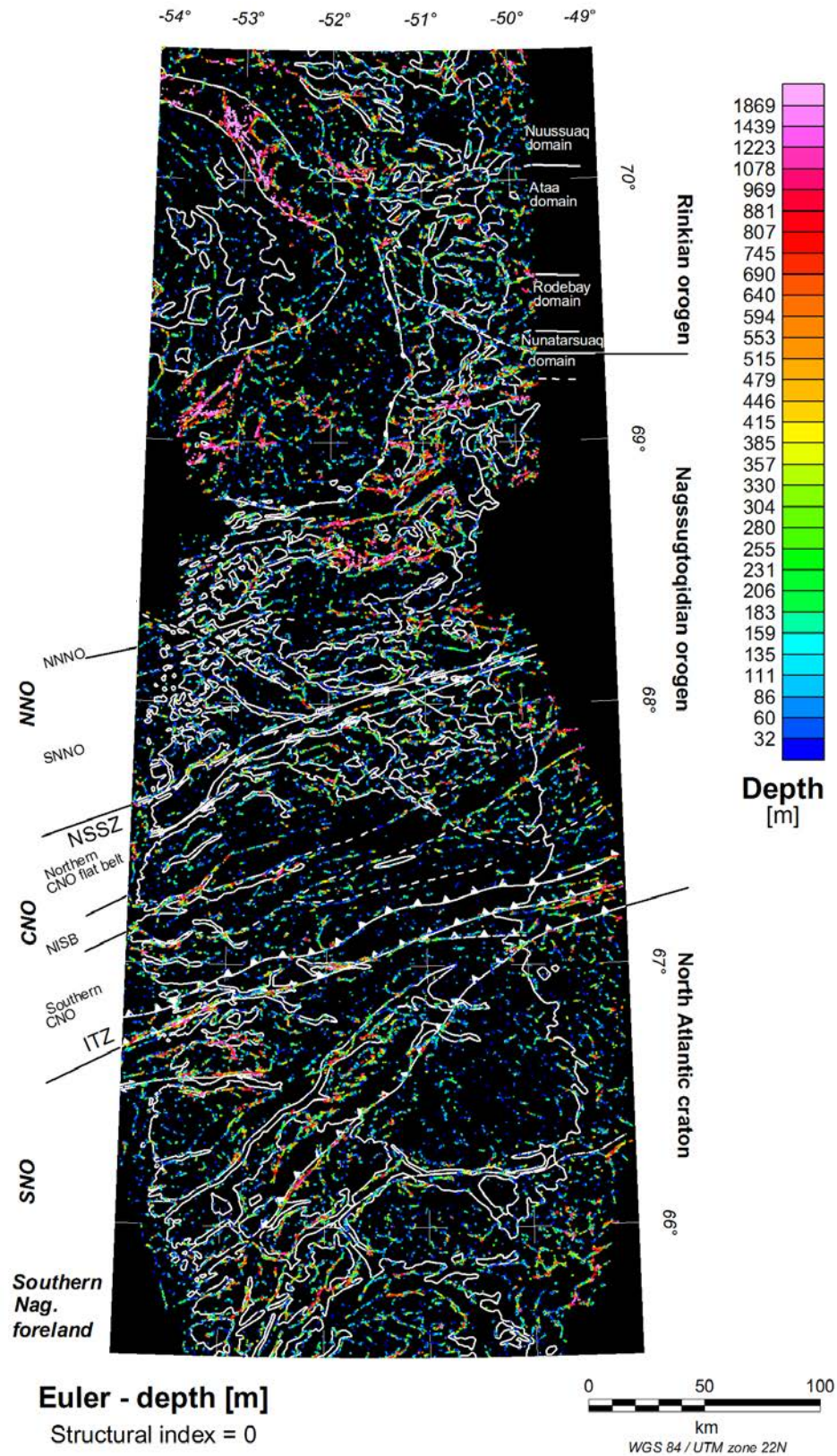


**Figure 29.** Located Euler deconvolution analysis of the magnetic total field intensity field with 0 as structural index, which corresponds to a contact as a geological model. Many known geological contacts are picked-up through this analysis.

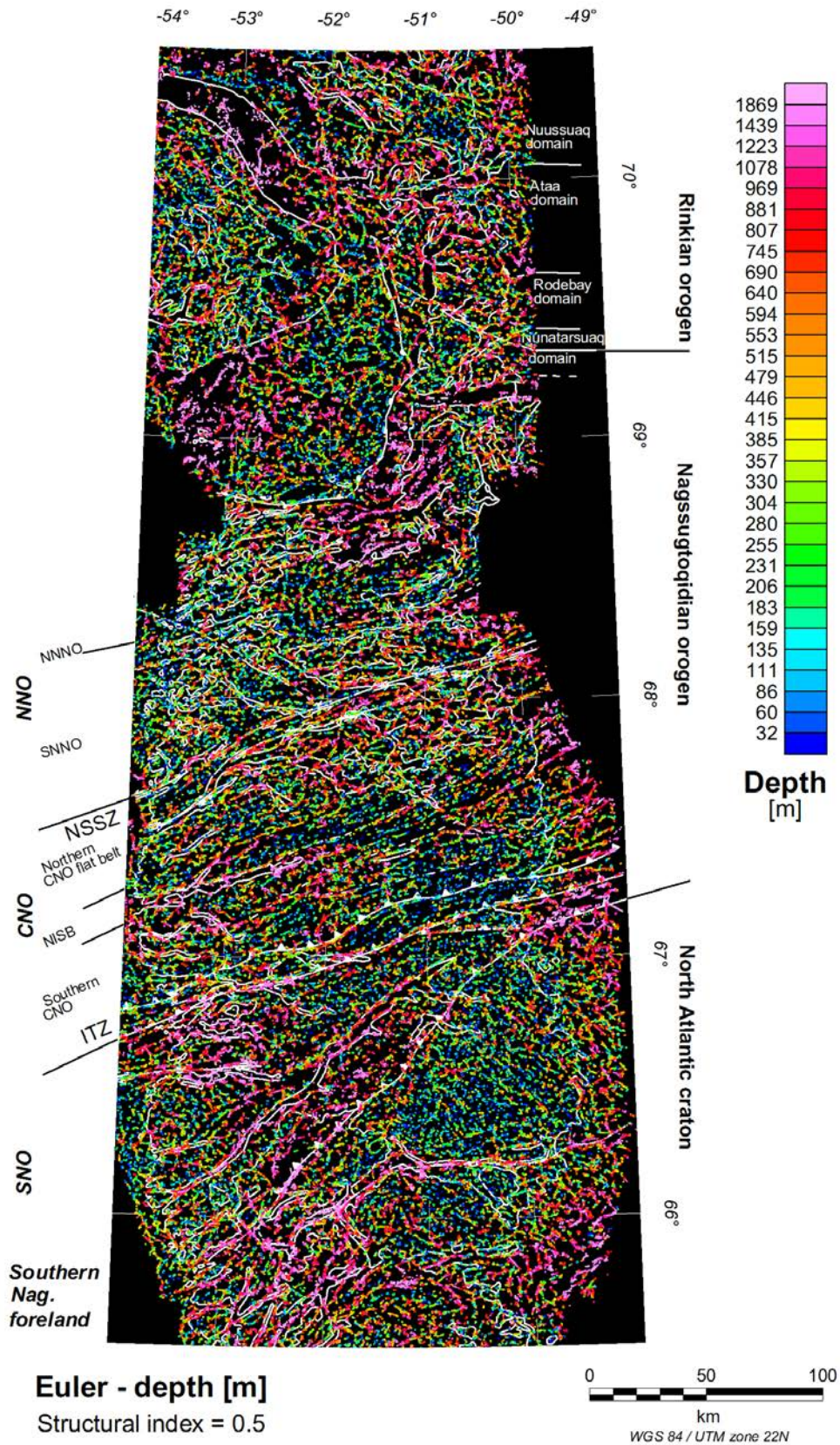


**Figure 30.** Located Euler deconvolution analysis of the magnetic total field with 0.5 as structural index, which corresponds to a thick step as geological model.

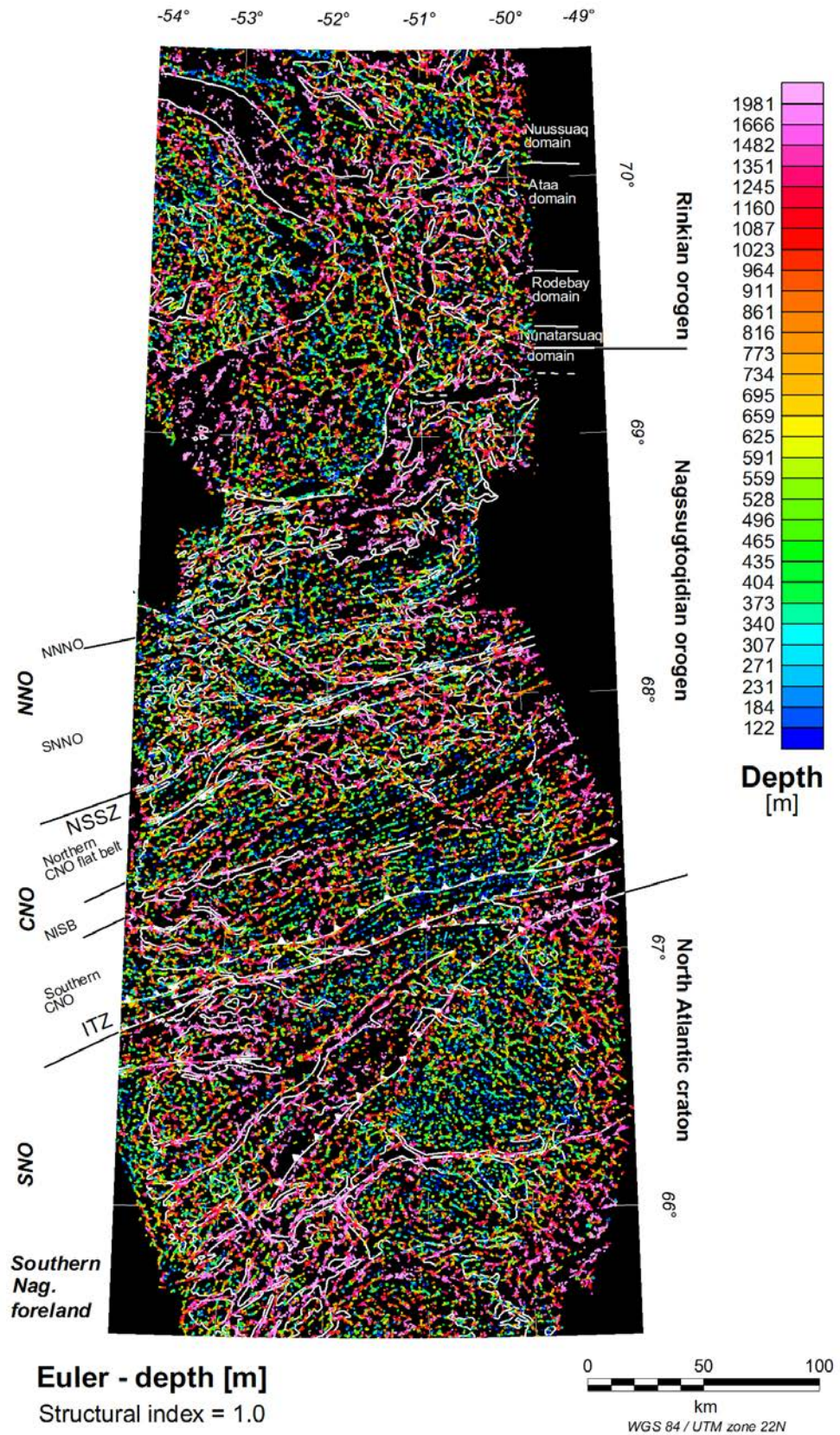


**Figure 31.** Located Euler deconvolution analysis on the magnetic total field intensity with 1 as structural index, which corresponds to a sill or dyke as geological model.

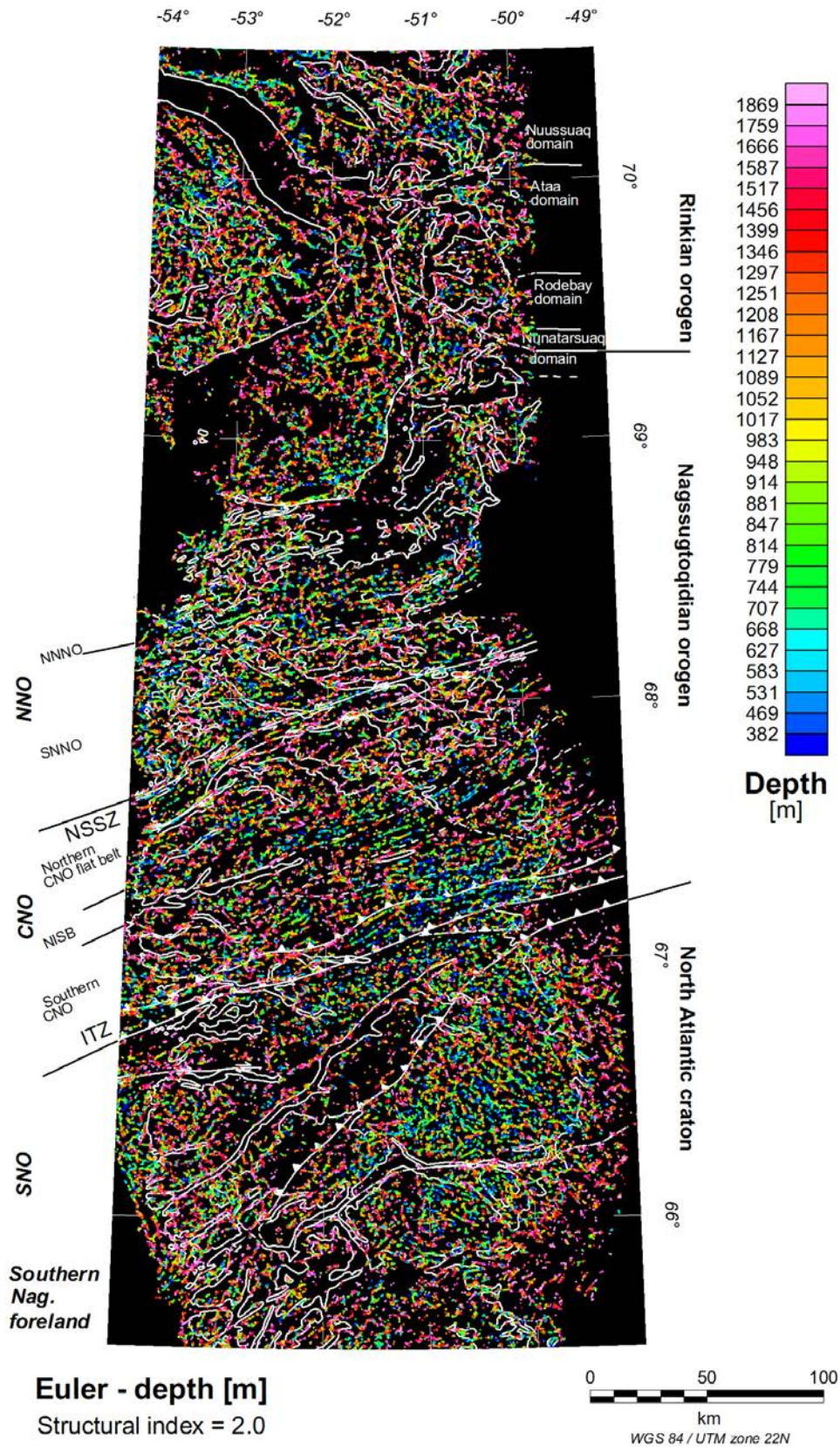


**Figure 32.** Located Euler deconvolution analysis on the magnetic total field with 2 as structural index, which corresponds to a vertical cylinder (pipe) or horizontal cylinder as geological models.

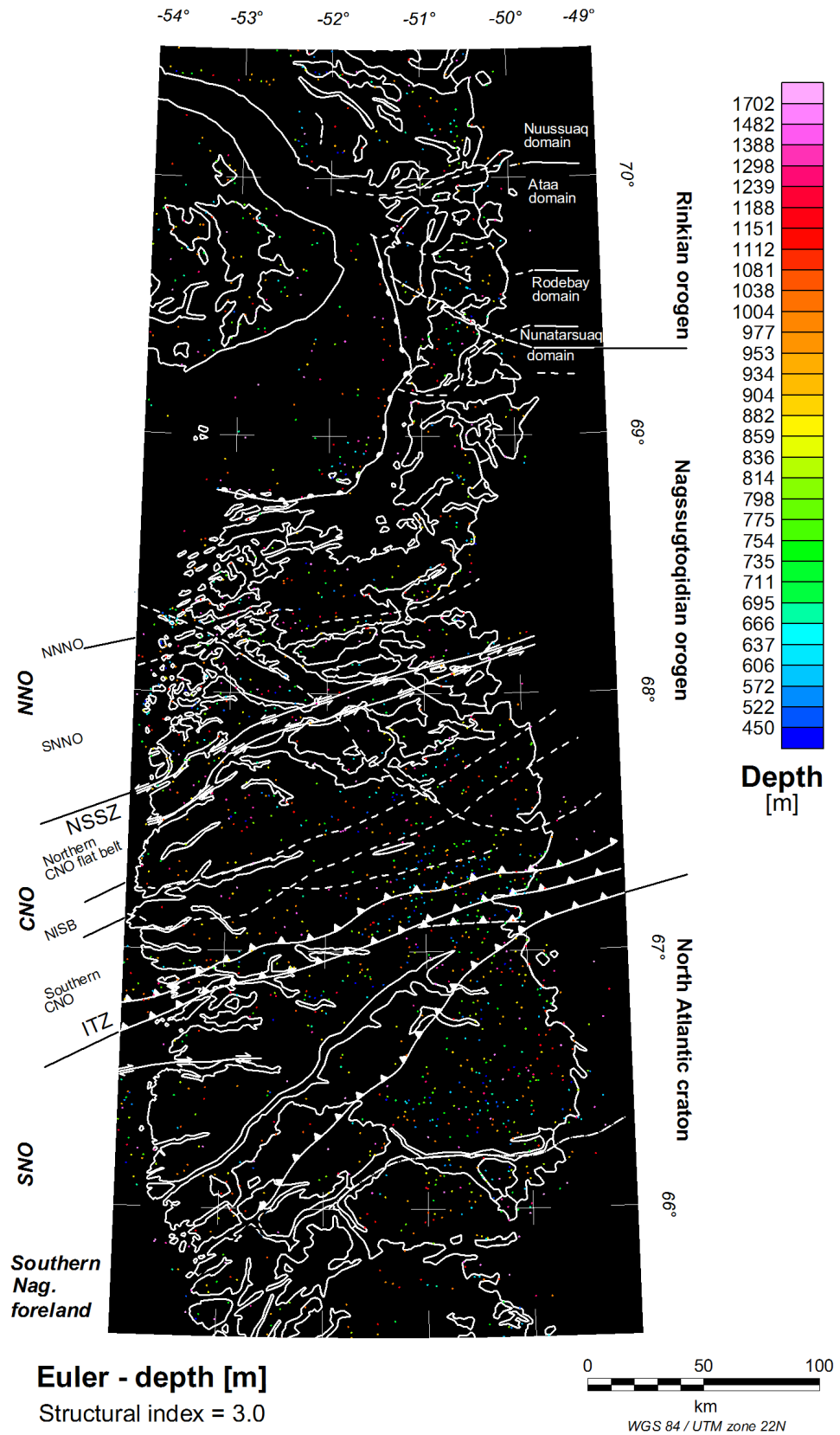


**Figure 33.** Located Euler deconvolution analysis on the magnetic total field with 3 as structural index, which corresponds to a sphere as geological model.

## Analysis of the analytic signal

The analytic signal  $A(x,y,z)$ , given below, is a complex function related to the derivatives of the magnetic field (Nabighian 1972). The analytic signal is given by

$$A(x, y, z) = \frac{\partial T(x, y, z)}{\partial x} + \frac{\partial T(x, y, z)}{\partial y} - j \frac{\partial T(x, y, z)}{\partial z} \quad [4]$$

where  $j = \sqrt{-1}$ ,  $T$  is the magnetic total field anomaly, and differentiation is performed with respect to the two orthogonal and horizontal directions  $x$  and  $y$  and with respect to the vertical direction  $z$ . The analytic signal is a non-measurable parameter, independent of the direction of the magnetisation and the direction of the Earth's field. Therefore, all bodies with the same geometry have the same analytic signal. The position of the source is determined by the location of the maximal amplitude of the analytic signal. The amplitude of the analytic signal is symmetric and the peak occurs directly over edges of wide bodies and centres of narrow bodies. This means that the analytic signal itself in principle provides an interpretation tool with indications of source location. The analytic signal is shown in Fig. 34.

From the analytic signal, it is possible to make estimations of the source parameters, e.g. depth to source, width of source, dip of source, direction of magnetisation, and to outline the source geometry. Nabighian (1972; 1974) initiated application of the analysis of the analytic signal to two-dimensional problems. This method was later developed further by Thurston and Smith (1997, 1999) and Smith *et al.* (1998), Bastani and Pedersen (2001). Application to three-dimensional problems was developed by Nabighian (1984) and Roest *et al.* (1992,a, b).

In the analyses presented in this work, we make use a modified version of the method suggested by Bastani and Pedersen (2001) in which a dyke structure is used as principal model. The modification involves that the technique is applied to a regular grid and that the strike of the source is used to correct the estimates, such that oblique strike angles are taken into account. Furthermore, the analysis can be carried out in two directions, in this case E–W and N–S and the results can then be combined.

A rectangular grid is needed in order to run the analysis. To facilitate this, the magnetic data from the Aeromag surveys were merged with the data from the MAANAOALA data set (Fig. 5). As the MAANAOALA data is of a quality not suitable for an analysis on the analytic signal the area outside the area covered by the Aeromag survey was masked out after the analysis.

A flow diagram of the processing involved in the analysis is given in Fig. 35.

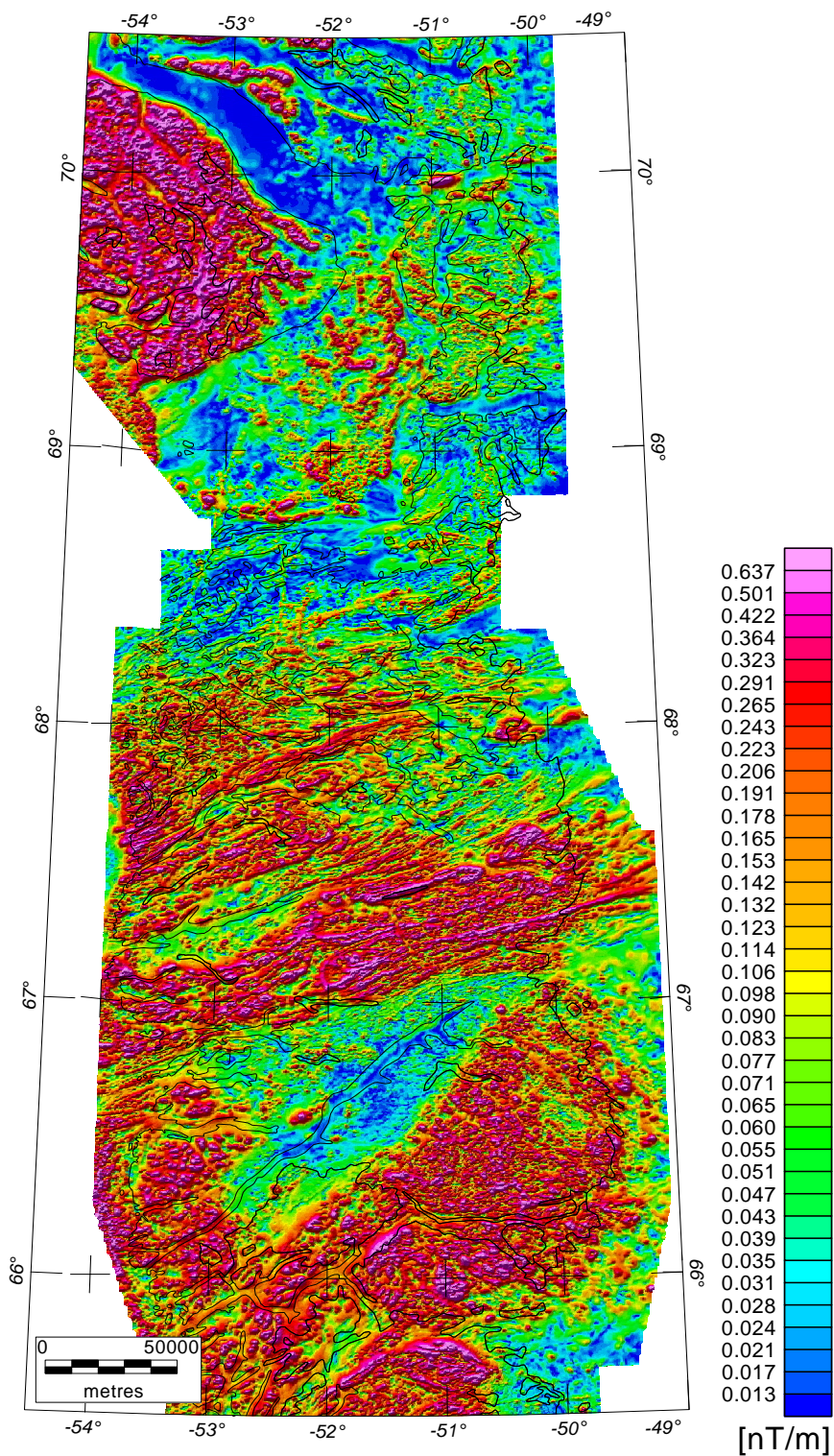


**Figure 34.** *The amplitude of the analytic signal of the total magnetic field constructed from three derivatives of the field. Simulation of a light-source illumination with an inclination of 45° and a declination of 338° shades the function. Structures are enhanced in the analytic signal presentation of the field.*

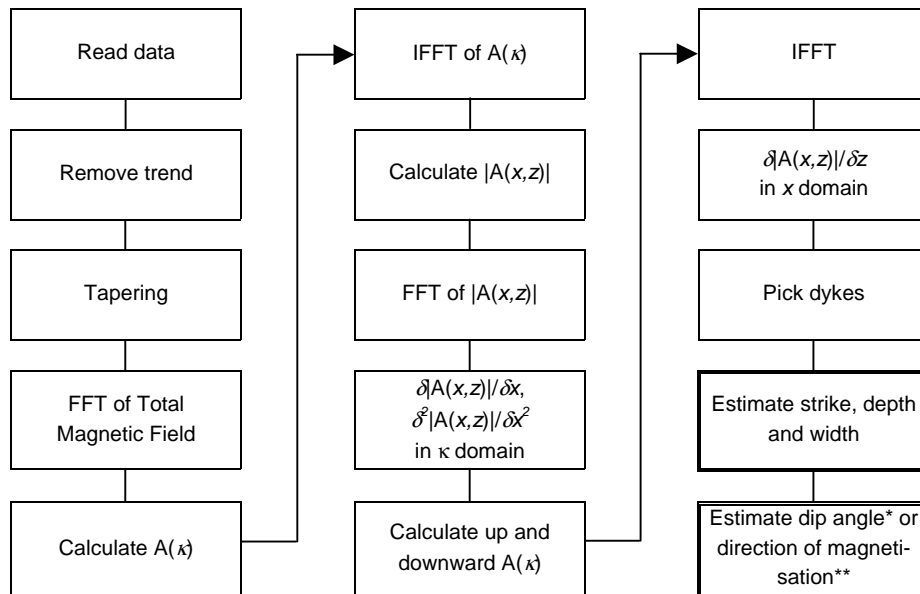


**Figure 35.** Flow diagram for the analysis of the analytic signal. Abbreviations: FFT = Fast Fourier Transformation, IFFT = Inverse Fast Fourier Transformation,  $\kappa$  domain = wave-number domain,  $x$  domain = space domain,  $A(\kappa)$  = analytic signal as function of the wave-number,  $A(x,z)$  = analytic signal as function of  $x$  and  $z$ ,  $\delta A(x,z)/\delta x$  = horizontal derivative of analytic signal,  $\delta^2 |A(x,z)|/\delta x^2$  = second horizontal derivative of analytic signal,  $\delta A(x,z)/\delta z$  = vertical derivative of analytic signal (after Bastani and Pedersen, 2001). \* The dip angle can only be estimated by assuming the direction of the magnetisation is in the direction of the main field (usually induced magnetisation only). \*\* The direction of the magnetisation can only be estimated if the dip angle is known.

The results from the analysis of the analytic signal with respect to strike, depth, width, and dip-angle of the dyke are shown in Figs. 36 to 38. It can be difficult to see all the details due to the scale of the figures, but in digital form, a lot of information can be obtained by zooming to the area of interest. Some edge effects occur along the joint boundary of the merged two aeromagnetic data sets. Some artificial results can also be seen within the region covered by the Aeromag data as results clustering along grid lines.

The results from the analysis correlate well with the strike and dip of the geological structures known from geological mapping in the region. The analysis of the analytic signal is a powerful tool to gain information on unexplored and alluvial covered areas and is very suitable for the data in West Greenland.

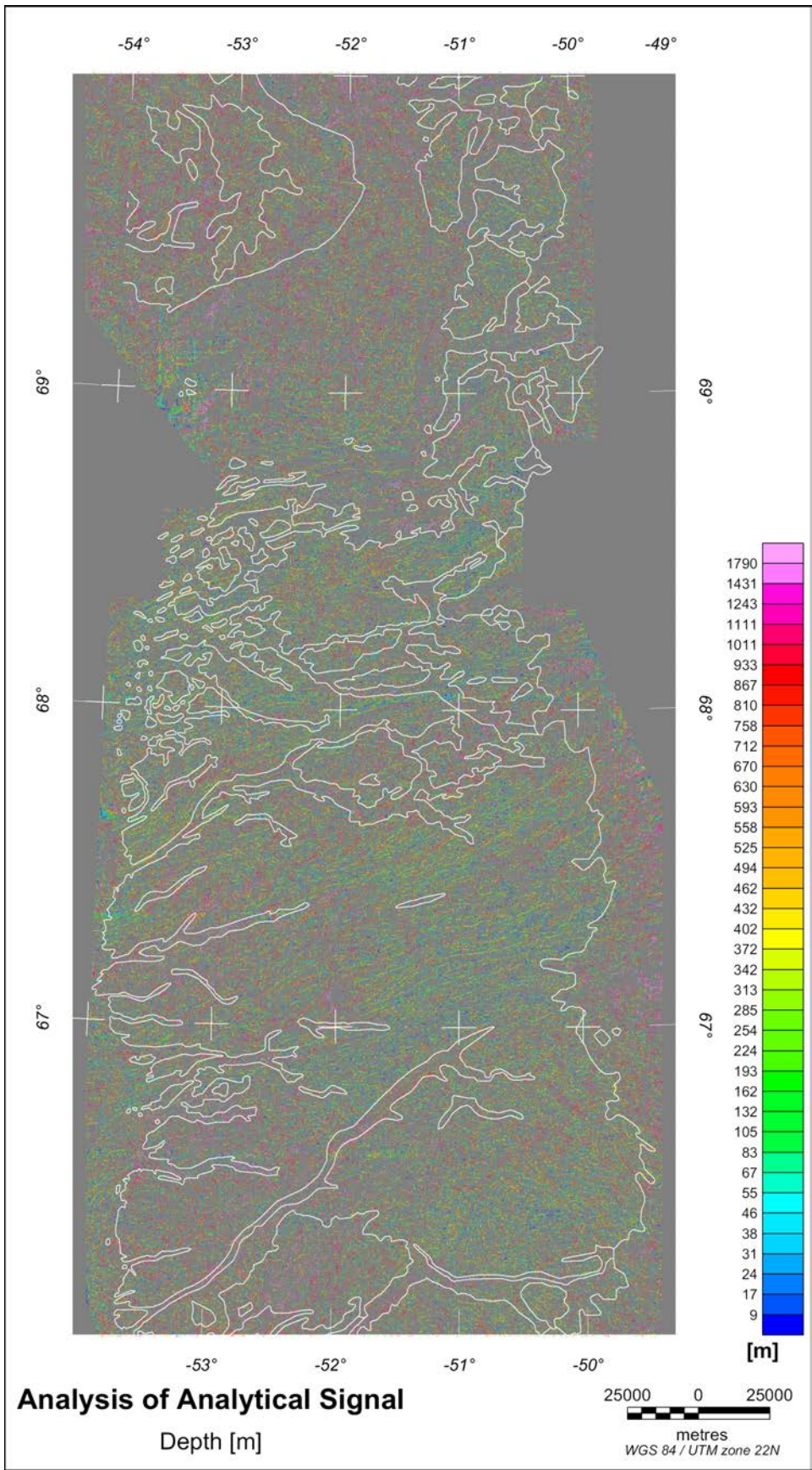


**Figure 36.** Estimates on the depth to the top of the of the dykes. Estimates from analysis run in both E–W and N–S directions.

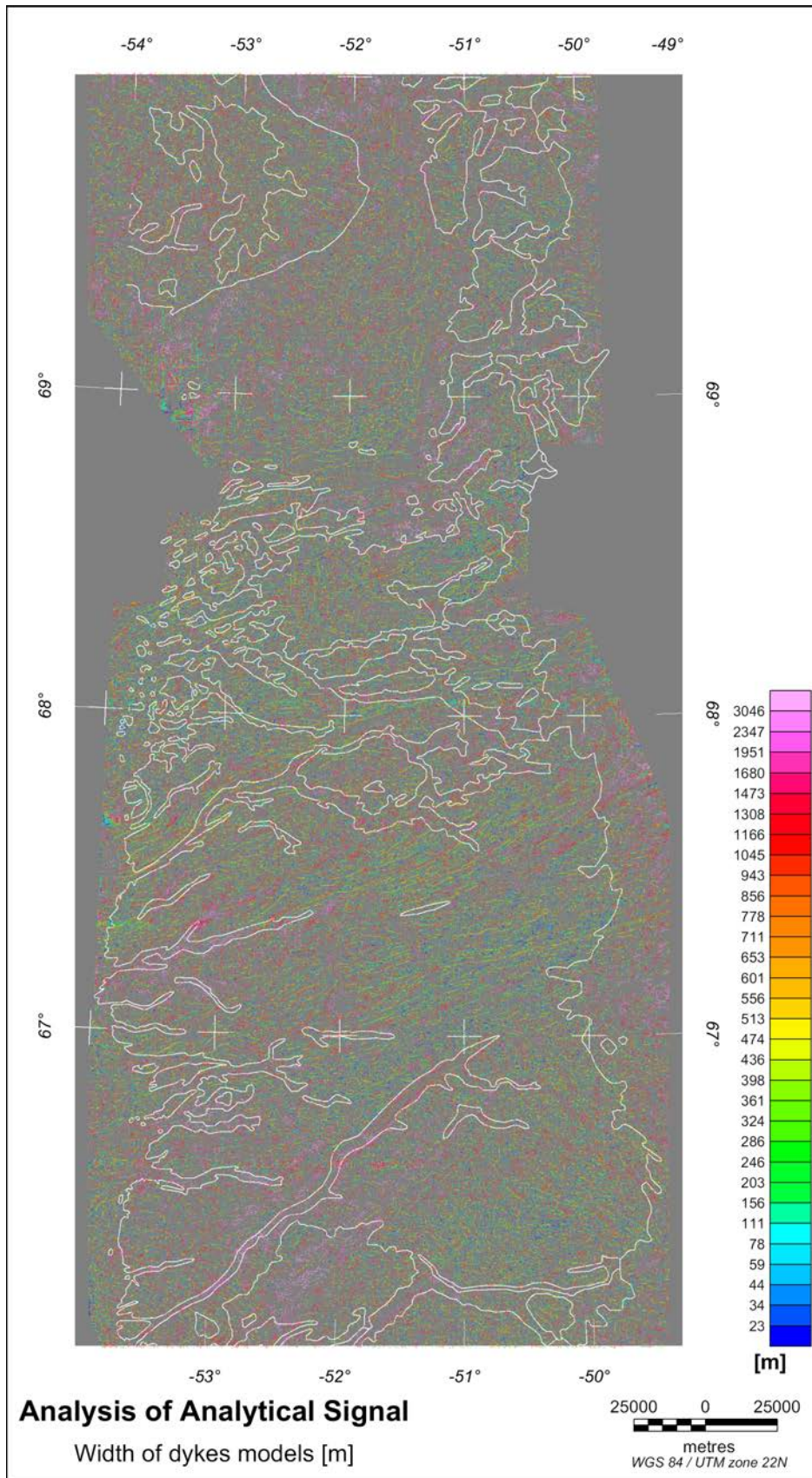


**Figure 37.** Estimates of the width of the dykes. Estimates from analysis run in both E–W and N–S directions.

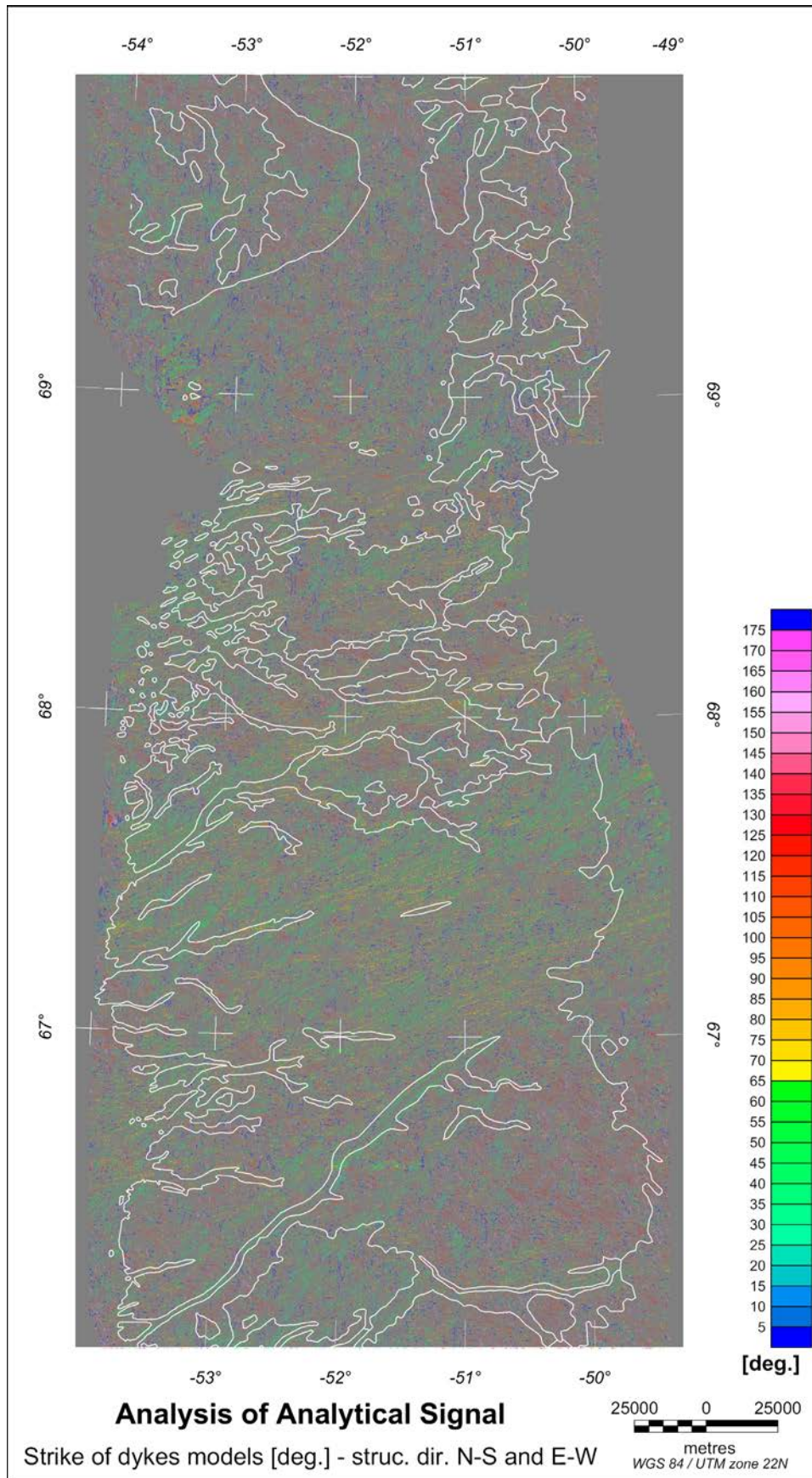


**Figure 38.** *Strike of dykes.*

## Correlation analysis of gravity and terrain data

Relations between terrain and the gravity field can be used to study the crust with respect to isostasy. The steps of the correlation analysis will be presented in the following sections. A pilot study for the assessment region is presented here. One of the conclusions from the pilot study is that a larger area should be investigated, as isostasy is a long-wavelength phenomenon. However, the results provide new information on the isostasy and density variations in the assessment region.

### Grids of terrain and gravity data

The grids have a 2 km cell size. These grids are low-pass filtered with a Butterworth filter (degree of the function filter set to 8) to remove wavelengths below 30 km, 45 km and 60 km. As most of the land-covered areas have a sampling distance between stations around 10 km, which equals a 20 km Nyquist wavelength, a 30 km wavelength cut-off is used to suppress noise due to aliasing. After low-pass filtering, the data in the interpolated grids are excluded from the analysis if they are more than 15 km away from a gravity station. Data from ice-covered regions are also excluded. Finally, the constructed grids of the Bouguer anomaly, Free Air anomaly, and corrected elevation (with equivalent rock mass, see next section) are saved to a database. The data are plotted in scatter diagrams and a linear regression analysis is performed.

A terrain grid, where the water-covered bathymetry is corrected to an equivalent rock mass can be seen in Fig. 39. Through this transformation a smaller depth is obtained, but with the same gravity contribution. The formula used for this transformation is given equation 3.

$$h' = d' - d = d \frac{\rho_w - \rho_c}{\rho_c} \quad [5]$$

where  $h'$  is the corrected bathymetry,  $d' = d \frac{\rho_w}{\rho_c}$  is the thickness of the corrected layer of water and  $d$  is the thickness of the original layer of water,  $\rho_w$  and  $\rho_c$  is the density of the water and crust respectively (1020 kg/m<sup>3</sup> and 2670 kg/m<sup>3</sup>, Telford *et al.* 1998).

### Bouguer anomaly and elevation

The low-pass filtered Bouguer anomalies for cut-off wavelengths of 30 km, 45 km, and 60 km are given in Fig. 40. The Bouguer anomalies as a function of the elevation, uncorrected for the continental area and corrected for the ocean for the different cut-off wavelengths, are shown in Fig. 41. The scatter is relatively large but the overall distribution of the data is retained for the different low-pass filters. Thus, there exist an overall negative correlation between the Bouguer anomaly and the topography in the region (with a gradient obtained from the linear regression around  $-0.089$  mgal/m and an intersection around a Bouguer anomaly of  $-5.3$  mgal). The coefficients and the correlation coefficient of the regression lines are very similar. This suggests that the overall trend is robust.

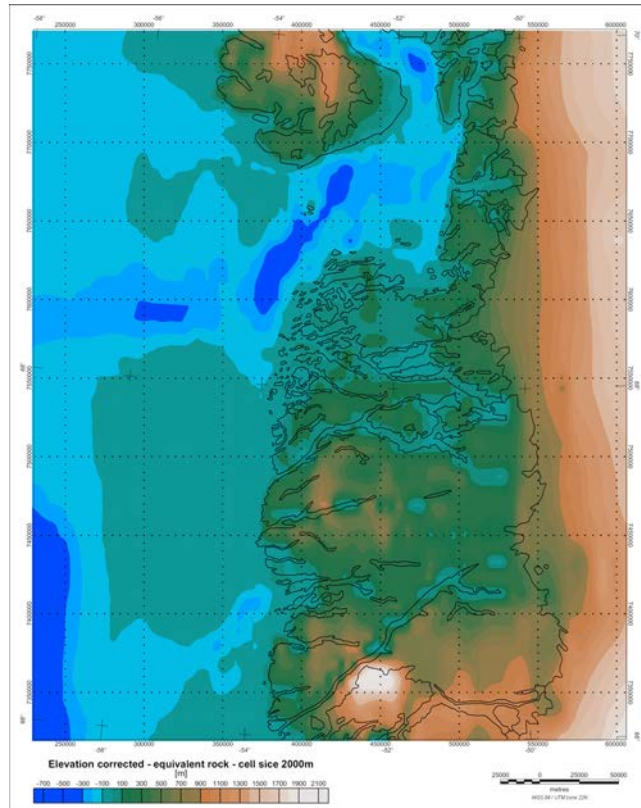


**Figure 39.** Corrected bathymetry where the water columns are corrected to an equivalent rock mass. Cell size is 2 km.

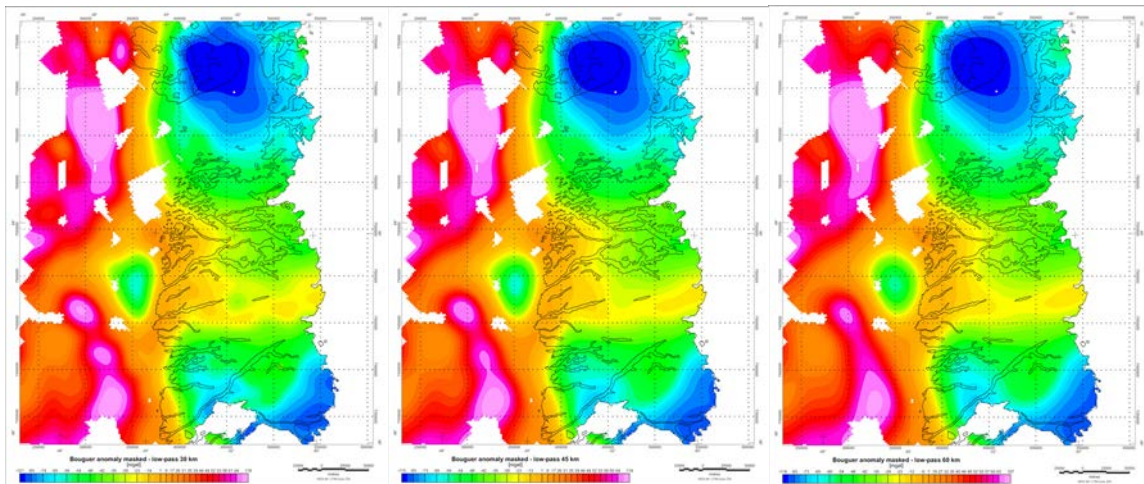


**Figure 40.** The Bouguer anomaly for 30 km, 45 km, and 60 km cut-off wavelength in the low-pass filtering (from left to right). Data over ice-covered areas and grid nodes more than 15 km away from measurement station are excluded (white areas within the maps).

Most of the Bouguer anomaly values scatter for data in the elevation range from 0 to -250 m. The highest Bouguer anomaly values correspond to the large positive anomalous area approximately 50 km southwest of Disko Ø that continues southward as an elongated belt along the entire west coast. The most negative Bouguer anomaly values are located at Disko Ø. This anomalous area extends further SE into the Disko Bugt and into the northern part of Jakobshavn Isfjord. All Bouguer anomalies obtained at elevations above ~1000 m

lies above the regression lines. This indicates that no linear relationship between high topography and Bouguer anomalies exists. Most of these values correspond to values from the area south and southeast of Søndre Strømfjord, an area with relative rough topography. Insufficient terrain correction can explain some of this systematic deviation from the overall trend. Small negative Bouguer anomaly values (between 5 mgal to  $-30$  mgal) above the regression lines in the elevation range from 250 m to 750 m originate from the area between Nordre Strømfjord and Nordre Isortoq, an area that is characterised by an E–W trending anomalous belt. This belt includes also the area between Nordre Strømfjord and Kangaatsiaq (Fig. 40). The Bouguer anomaly values for this area are nevertheless not as negative as the values from the area south of Søndre Strømfjord.

Scatter plots of the Bouguer anomaly values for positive continental elevations only are given in Fig. 43 in order to make a comparison with the trends obtained for the entire region (Fig. 41). The gradient of the linear regression line is more flat and the intersection varies from  $-30.8$  mgal to  $-31.6$  mgal, which is approximated 26 mgal less than the regression lines for both positive and negative elevation. This is a very pronounced difference caused by numerous small negative Bouguer anomaly values at low elevations. The group of relatively small negative Bouguer anomaly values in the elevation range from 250 m to 750 m has now more impact on the results. This group has a positive correlation with topography.

#### **Free Air anomaly and elevation**

The grids of the Free Air anomaly are given in Fig. 42, and corresponding scatter plots with the anomaly as a function of the positive elevation are shown in Fig. 43. As for the Bouguer anomalies, there is a similar overall distribution and scattering of the values for the different low-pass filters. This is also confirmed by the linear regression analysis, which gives comparable results. The intersection is around 31 mgal and the gradient is 0.04 mgal/m.

The high Free Air anomaly values (157 mgal to  $\sim 60$  mgal) obtained at high topographic levels correspond to areas south of Søndre Strømfjord and south to southeast of Nordre Isortoq. Some of the values from the margin of the Sukkertoppen Iskappe might be influenced by the presence of ice.

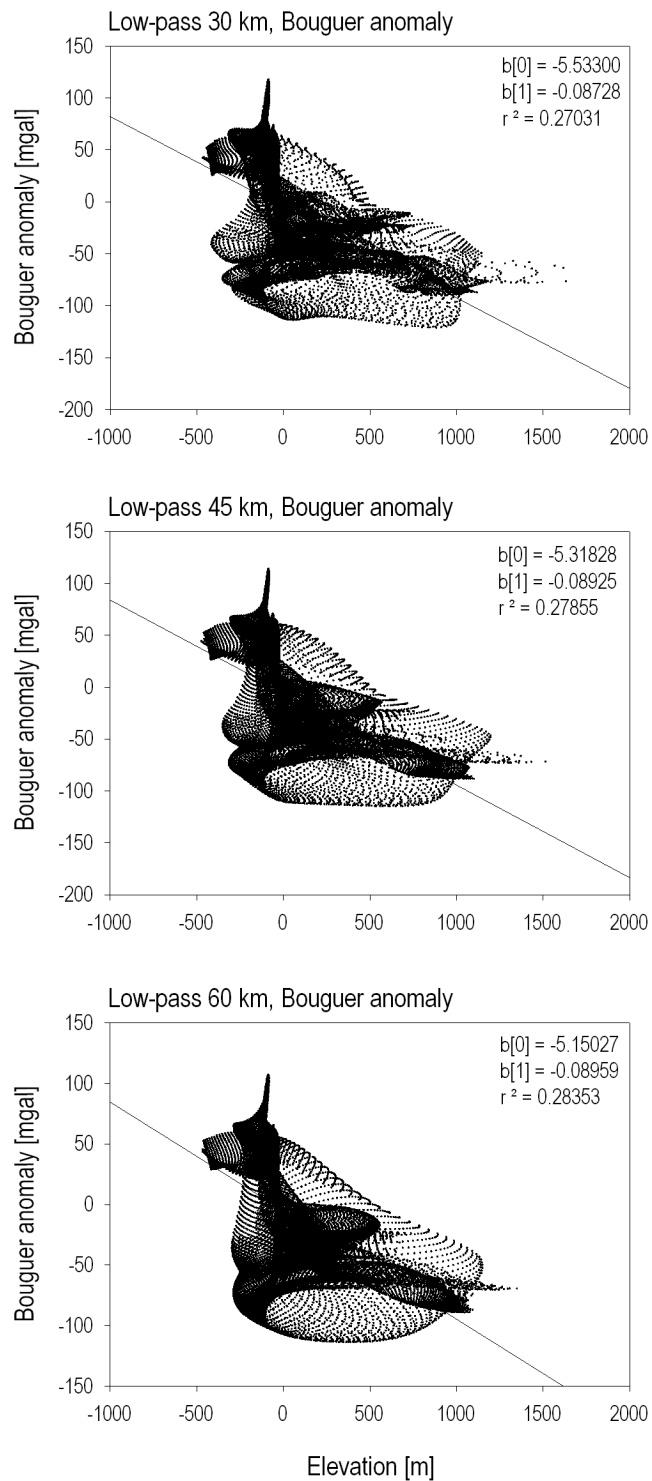


**Figure 41.** Bouguer anomalies as a function of the corrected elevation (positive and negative), and the results of the corresponding linear regression;  $b[0]$  is the intersection with the ordinate-axis,  $b[1]$  is the gradient and  $r^2$  is the correlation coefficients.

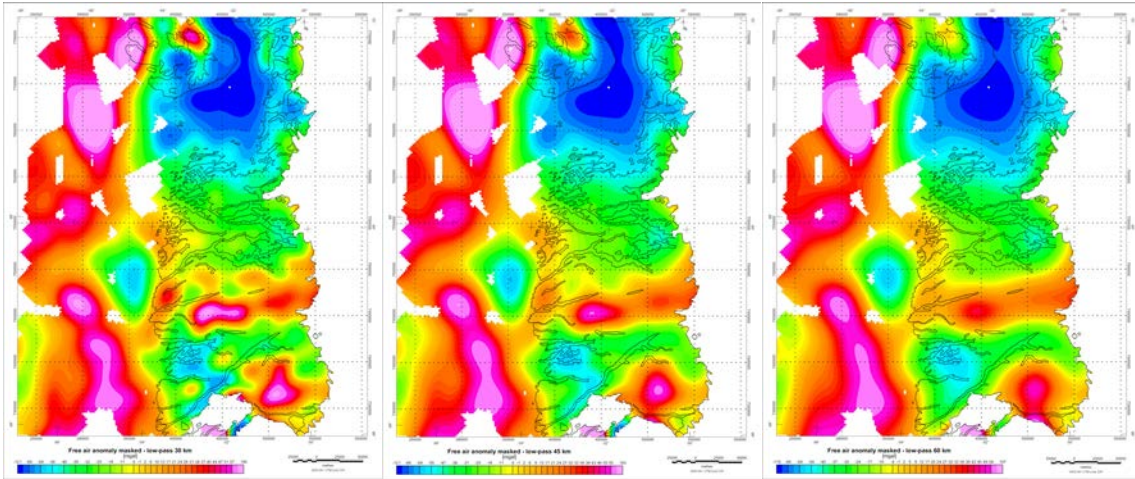


**Figure 42.** Free Air anomaly for 30 km, 45 km, and 60 km as cut-off wavelength in the low-pass filtering (from left to right).

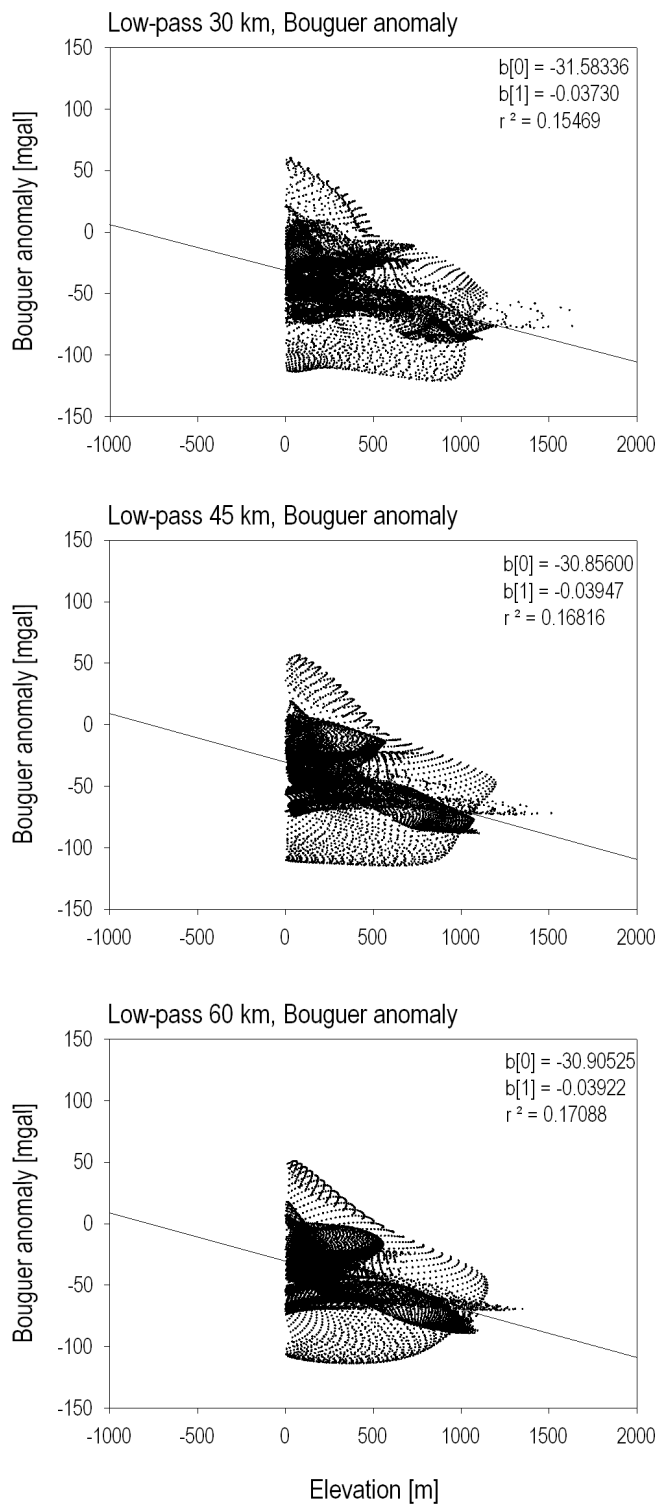


**Figure 43.** Bouguer anomalies as a function of the positive elevation and the results of the corresponding linear regression (parameters as Fig. 41).

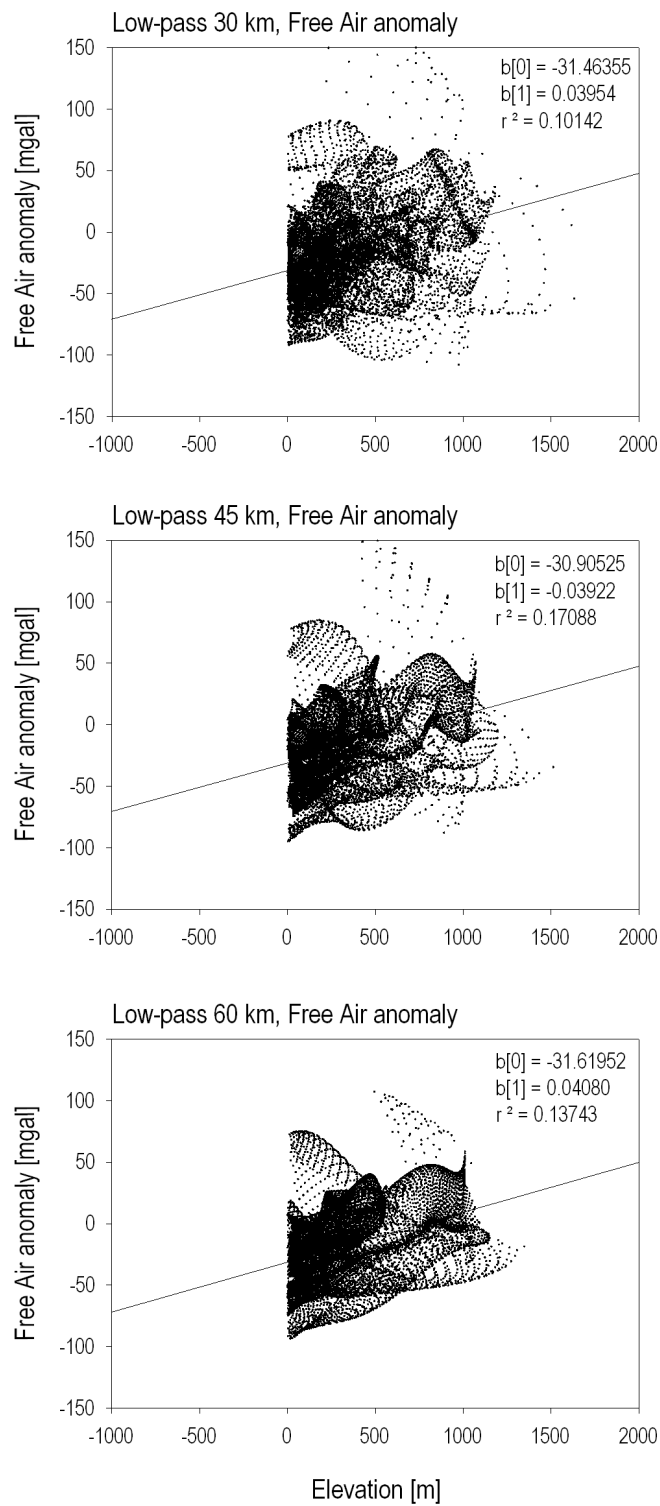


**Figure 44.** Free Air anomaly values as a function of the positive elevation and the results of the corresponding linear regression (parameters as Fig. 41).

### **Residual anomaly**

In order to examine the presence of non-isostatically supported areas, the gravity field that simulates a fully compensated topography is calculated and subtracted from the Bouguer anomaly to produce the residual anomaly. The full compensation is based on the assumption of a linear relation between the gravity field and topography. Theoretically, the residual anomaly should represent the effects of isostatic disequilibria. The residual anomaly is therefore useable to test the extent of isostatic compensation in accordance with the compensation mechanism assumed. Anomalous areas, where negative and positive values in the residual anomaly indicate non-isostatically compensation and/or local mass deficit or excess mass, will be indicated. Fully compensated areas will give a residual anomaly around 0 mgal. The residual anomaly is given in Fig. 45.

The parameters of the regression line from the Bouguer anomalies as a function of both negative and positive elevation (Fig. 41) are used for the calculation of the residual anomaly for the whole region (Fig. 45). The residual anomaly, for the area with positive elevation only (Fig. 46), is calculated by the parameters of the regression line for Bouguer anomaly over positive elevation (Fig. 43). It is difficult to interpret the residual anomaly grids in Fig. 45 over water, because the intersection of the regression lines for positive elevation is very different from the intersection for both negative and positive elevation. The values for the residual anomaly for both positive and negative elevation varies between  $-106$  mgal and  $104$  mgal, whereas the residual anomaly values for positive elevation only varies between  $-77$  mgal and  $85$  mgal (values for 60 km low-pass filtering). The difference in the range is caused by the different intersection of the regression lines.

As for the Bouguer and Free Air anomaly, the area between Nordre Strømfjord and the Ikertôq thrust zone stands out as a pronounced positive anomalous area in the residual anomaly.

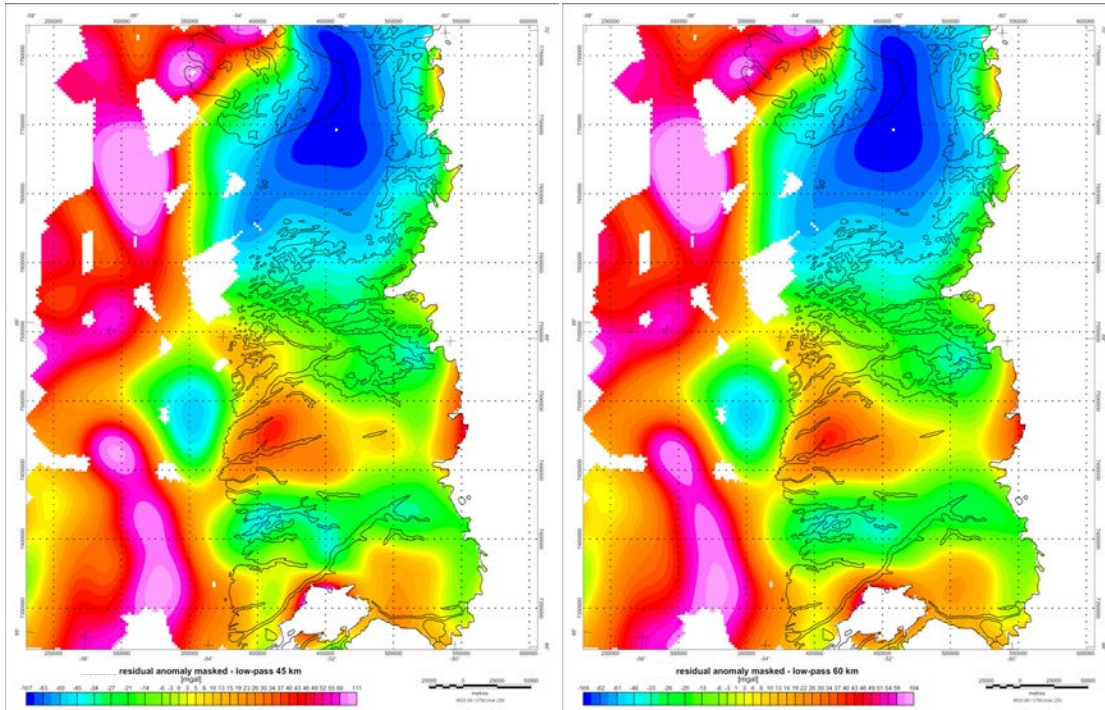


**Figure 45.** Residual anomaly based on linear relation for both negative and positive elevation versus Bouguer anomaly with low-pass filters with 45 km and 60 km cut-off wavelengths.

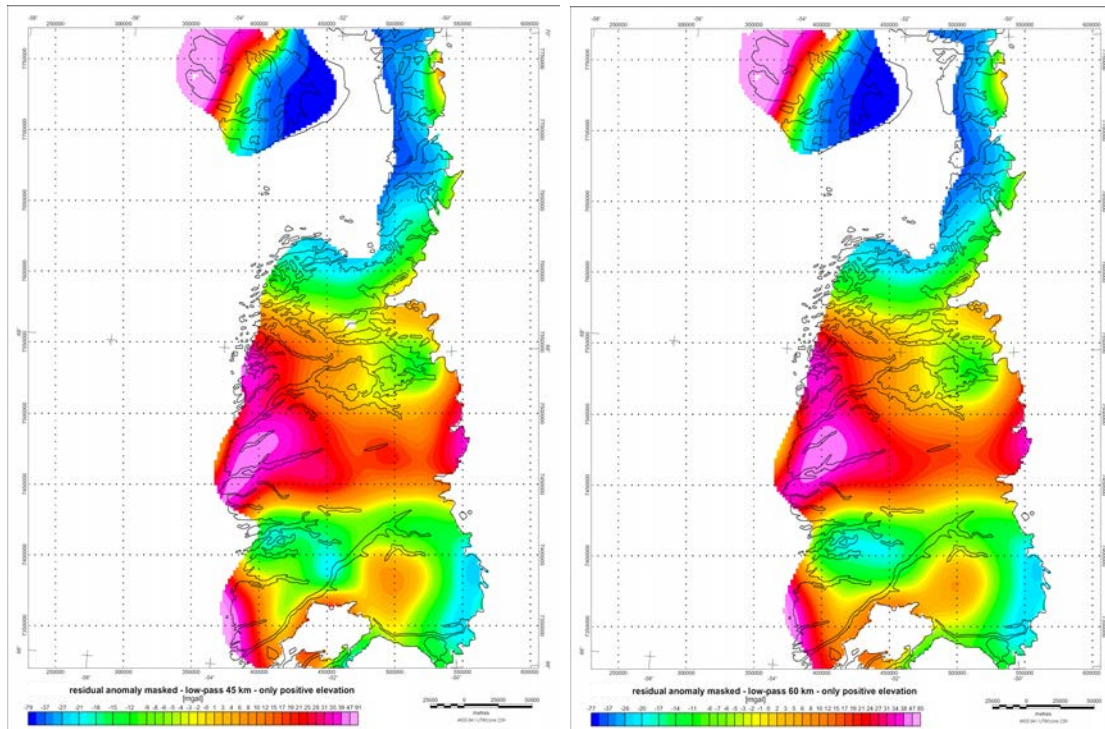


**Figure 46.** Residual anomaly as in Fig. 45, but now for areas with positive elevation only.

## **Discussion on geophysical techniques**

In order to use the geophysical data in the most effective way it is of importance that processing techniques are used to search for, extract, and clarify the information obtained in the data. One of the objectives with the report has been to present some of the processing techniques available to meet this requirement. Furthermore it is intended to present processing techniques, which can be applied to a large data set and large geographical region.

As shown in the former sections, a wide range of processing techniques exists that can be applied to the analyses of the geophysical data. Every technique has its advantages and disadvantages, and the different techniques produce results that should be used integrated in the final interpretation.

The techniques presented originate from two fundamentally different processing approaches: quantitative or qualitative. A qualitative approach is used to produce results that illuminate, clarify, and extrapolate the information available in the data. In contrast, the quantitative approach produces results with estimations of different physical parameters through statistical procedures and comparisons between observed data and calculated model responses.

# Interpretation and discussion of processed potential field data

As one of the objectives with this report is to discuss regional-scale features in context of the potential field data, little attention will be given to local features. Several of the domains and geological features (especially in the CNO and NNO) described and correlated to the potential field data have been investigated during fieldwork in 2001 and 2002 by the authors.

## Responses from different lithologies in general

The total magnetic field intensity (hereafter denoted TMI) for the study region is given in Fig. 18. An examination of the TMI map shows that a good correlation between known surface lithology and structures and the TMI exists. This has also been confirmed during fieldwork in 2001 and 2002 by the authors (Nielsen & Rasmussen 2002).

In general supracrustal belts are seen as banded low magnetic zones, often elongated zones; e.g. the Nordre Isortoq and Nordre Strømfjord supracrustal belts. Amphibolites show both banded linear and irregularly shaped magnetic anomalies of intermediate to very high amplitude. Gneiss zones are often seen as patterns of narrow banded linear magnetic zones of intermediate amplitude, e.g. gneisses of the southern CNO. The granites are internally homogeneous with respect to magnetic properties and produce strong magnetic anomalies. The granites are associated with both high and low anomalies. Mafic to ultramafic lithologies show up as local anomalies of high amplitude. The metamorphic facies conditions are well correlated with the magnetics. Areas under granulite facies conditions are highly magnetised, whereas area in amphibolite facies shows up with lower magnetisation.

## Responses from structures in general

In general, the directional trends in the magnetics of the CNO and NNO are predominated by the ENE-trending structural orientation of the Nagssugtoqidian orogen. The trends in the magnetics of the southern foreland and the western part of the SNO are more heterogeneous and no dominating orientation can be observed. The middle and eastern part of the SNO does not show any directional trends in the magnetics. Several structural orientations are reflected in the magnetics of the northern foreland of the Nagssugtoqidian orogen and the Rinkian orogen. However many of the directional trends in the magnetics for these areas are more northerly orientated than the trends of the CNO and for the NNO no predominating trend can be observed. All major boundaries and lineaments in the region are reflected by the magnetics.

Tectonic features such as faults and fracture zones are generally associated with a decrease in magnetisation and are often observed as a linear zone or lineament that crosses the magnetic anomaly pattern caused by the surrounding rocks. In some cases the lateral

offset can be determined from the anomaly pattern. The decrease in magnetisation is caused by change in the magnetic mineralogy due to the geological processes, which have affected the zone. Moreover, the decrease in the magnetic field can also be caused by or exaggerated by a topographic effect associated with the zone. Other tectonic features such as shear zones and thrust faults often represent geological boundaries of different domains or geological blocks with different deformation style, structures, lithologies, metamorphism etc. These boundaries will be reflected by abrupt changes in the magnetic pattern. In some cases, lineaments defining the tectonic structures in boundary zones are also visible. Conjugated faulting perpendicular to the main tectonic feature and tectonic lenses are recognisable.

Large deep-seated structures generally produce regional, long wavelength anomalies, while restricted shallow bodies are recognized by short wavelength local anomalies. Folding of lithologies, especially when dealing with variably magnetised lithologies, as in the case with supracrustal rocks, will be represented as curved, banded alternating magnetic zones. Separated domains or terranes dominated by similarities in structures, lithologies, deformation etc. can often be outlined from the magnetic field as areas of distinct anomaly patterns with a common expression.

## **Gravity responses in general**

The overall regional division and geological domains of the region, as interpreted from the magnetics (will be described in details in the following sections) and geological data, is in general reflected in the Bouguer gravity field (Fig. 7). The maximum Bouguer anomaly values (~120 mgal) are represented by a spatially large anomaly in the sea southwest of Disko Ø (around 56°W and 69°N). The minimum Bouguer anomaly value (~-131 mgal) is located within a spatially large anomaly covering most of the Disko Ø. Low Bouguer anomaly values (~90 mgal) are obtained in the area south and southeast of Søndre Strømfjord south of SNF.

## **Regional geophysical patterns and domains**

Several geophysical domains, defined as areas with distinct magnetic patterns and abrupt changes to neighbouring areas, are deduced from the map of the total magnetic field intensity (Fig. 18).

Tectonometamorphic and structural domains are characterised by their uniformity in the patterns and distribution of the potential field. The provinces are often bounded by abrupt changes in the patterns. Consequently, elements of the distribution and patterns observed in the potential field data can in many cases be used to deduce and correlate geological domains. A selection of maps of some of the most used processed potential field data will be included in the following sections. However, some interpretations and discussions are also based on some of the processed data already presented and it will sometimes be necessary to refer back to these.

## **Southern foreland, southern Nagssugtoqidian Front and southern Nagssugtoqidian orogen**

### **Southern foreland**

The southern Archaean foreland is highly magnetised and characterised by short wavelengths high amplitude patterns in the total magnetic field intensity. The Bouguer anomaly field of the southern foreland will be discussed in the next section.

The southern foreland is also characterised by a high density of well-defined short wavelength magnetic lineaments with various orientations (Figs. 47, 48.B, 48.G, 48.H, and 48.E). The lineaments are interpreted to originate from fault zones. No lateral displacement is observed for most of them. The main direction for these lineaments, which in almost every case are associated with a decrease in magnetisation, are dominantly NW–SE to NNW–SSE, perpendicular to the SNF. The faults can be interpreted to reflect a conjugated system to the SNF and can be associated with post-compressional relaxation in the area. The lineaments are terminated at the SNF and cannot be observed to continue further north into the SNO.

A very pronounced ENE-trending lineament is situated just north of the Tasersiaq valley (TFZ in Fig. 47). The lineament continues towards the coastal regions with a NE-trending orientation. The lineament along the Tasersiaq valley is situated in an area where retrograde amphibolite facies gneisses are mapped (Allaart & Jensen 1979; Allaart 1982). This lineament corresponds in the coastal part of the area to a fault zone (hereafter denoted the Tasersiaq fault zone, abbreviated TFZ in the figures). Based on the anomaly patterns, the fault zone can be inferred to continue inland. The lineament is relatively well defined, and the feature could correspond to a major fault or shear zone. A rather large distinct circular highly magnetised area is located just north of the TFZ at the margin of the Inland Ice. This anomaly corresponds to a large granite body (Allaart 1982; Rosing *et al.* 2001). Similar anomalies, however with a smaller extent, are located both south and north (beneath the Inland Ice) of the mapped granite.

The southern foreland and the western part of SNO are the most homogenous and highest magnetised domains in the study region. The anomaly patterns of the TMI in the western part of SNO and the southern foreland have similar characteristics in the total magnetic field intensity and the analytic signal (Figs. 48.A and 48.C). The domains display high amplitudes and long wavelengths in the stripping filtering (see Fig. 21). The domains correspond to areas of gneisses in granulite facies, which have escaped retrograde metamorphism.

### **The Southern Nagssugtoqidian Front**

The SNF shows up as a very sharp continuous and well-defined ENE–WSW trending boundary, defining an abrupt change in the magnetic pattern without any offsets (Figs. 48.A and 48.D). Judged from the total magnetic field intensity of the merged Aeromag and MAANAOALA data (see Fig. 5) the Ikertôq thrust zone (will be discussed separately in a latter section) continues to the NE beneath the Inland Ice and truncates the Southern

Nagssugtoqidian Front. The course of the front is described with a ramification towards the NW on the eastern side of the Sukkertoppen Iskappe (Allaart & Jensen 1979). From the magnetics it can be deduced that the SNF continues westward beneath the Sukkertoppen Iskappe (see Fig. 5). No NW ramification of the front east of Sukkertoppen Iskappe can be recognized in the magnetics.

The SNF is described as being formed by anastomosing oblique shear zones with a foreland directed component of ductile thrusting (Hageskov 1995). The SNF is defined by the transition from undeformed, discordant Kangâmiut dykes in the south to deformed dykes to the north in the SNO (Ramberg 1948; Escher *et al.* 1975; Korstgaard *et al.* 1987; Marker *et al.* 1995). In the inner part of Søndre Strømfjord the boundary is described as being a c. 20 km wide transition zone in which retrogression of the Archaean granulite-facies gneisses occur and progressively rotation of the Kangâmiut dykes (Korstgaard *et al.* 1987). Hageskov (1995) furthermore describes the front as a set of en-echelon, reverse shear zones with top-to-the-south displacement. Based on the continuity of the abrupt change in the magnetics pattern it seems likely that the SNF can be seen as a continuous boundary west of Sukkertoppen Iskappe where this transition zone has been described as being more complicated (Bridgwater *et al.* 1973a; Korstgaard *et al.* 1987). The magnetic patterns north and south of the possible SW extension of the SNF have similar characteristics and no abrupt change in the pattern can be observed (Figs. 48.A and 48.B). Furthermore, no lineament in the SW extension of the SNF can be observed in the vertical or horizontal gradient. This suggests that the SNF is terminated or redirected at the western part of the Sukkertoppen Iskappe.

In the maps of the stripping filtering is the SNF picked-up as the most prominent deep-seated crustal scale feature. The SNF is picked-up by the Euler analysis as discontinuous lines of relatively deep-seated estimates (>2000 m, Fig. 30). An interesting feature of the SNF is observed in the low-pass filtering of the magnetics with cut-off wavelengths below 10 km (Fig. 48.F): In the area where the Sarfartoq carbonatite complex is located (Secher 1986; Larsen & Rex 1992) a south-eastward inflection in the lineament of the SNF is observed. This inflection is created by a destruction of the magnetic properties caused by alterations related to the intrusion of the carbonatite complex.

The SNF is also observed as a distinct change in the Bouguer anomaly field (Fig. 40), with Bouguer anomaly values around -30 to -40 mgal north of the SNF (in the SNO) and -90 to -100 mgal south of the SNF (in the southern foreland). The negative Bouguer anomaly south of Søndre Strømfjord shows a negative correlation with topography. This correlation suggests a thickening of the crust along the SNF and south of it. The thickening might be produced by a combination of processes related to possible collisional activity between the Nagssugtoqidian orogen and the North Atlantic craton. South directed up-thrusting (SNF and Ikertôq thrust zone, the latter will be discussed in a later section) of crustal material produced a thicker crust. Moreover, subducted continental material beneath SNF and the southern margin of the North Atlantic craton, during the end-stage of a continent-continent collision would result in a thicker crust. A similar situation is described from the Torngat mountains in the Torngat orogen (Wardle *et al.* 2002a), Labrador, where a preserved crustal root is interpreted from gravity field data and seismic data beneath the boundary between the Nain Craton and the Torngat orogen. The preservation of a crustal root be-

neath SNF and the southern margin of the North Atlantic craton could be explained in the same way as the preserved Torngat root; i.e. by lack of post-orogenic heating and ductile reworking without any post-collisional magmatism in the region. Ellis and Beaumont (1999) describes how the subduction of the continental plate will cease as the inherent buoyancy of the subducted plate overcomes the slab-pull effect. This results in a trapping of the subducted plate beneath the overriding plate. Ellis and Beaumont (1999) describes similar examples of Precambrian crustal roots from the Svecofennian orogen, the Trans-Hudson orogen of western Canada and the Proterozoic orogens in the northwestern part of the Canadian Shield.

### **Western SNO**

The magnetic field of the western SNO is characterised by high short wavelength responses comparable to the magnetic field observed at the southern foreland. Beside two W–E orientated magnetic low lineaments, which correspond to the geologically described Itivdleq and Ikertôq shear zone (Korstgård 1979b), the western SNO is dominated by several well-defined short wavelength low magnetised NW and NE directed lineaments. These lineaments are interpreted to be faults. A small part of the westernmost SNO shows up with a slightly different pattern in the analytic signal and the other maps for structural enhancement of the magnetic field variations (Figs. 48.B, 48.C and 26). This difference could possibly be caused by a N–S orientated fault with vertical uplift.

An explanation on the very pronounced differences in the magnetic responses of the western SNO from the rest of the SNO (will be described later) and the termination of the responses from SNF can perhaps be found in NW directed low magnetised lineaments in the southern part of the western SNO. The lineaments truncate the SNF at its termination (Figs. 26 and 27), and define a boundary from highly magnetised lithologies to the west to very low magnetised lithologies to the east. The lineaments can reflect later faults, which have truncated the SNF and uplifted granulite facies lithologies to the west. The entire fault system in the western SNO could be related to this event. A similar setting is observed south and north of Nordre Strømfjord and at Nuussuaq in Disko Bugt, where an uplift of the basement has occurred. These lineaments are not described geologically and should be investigated closer before a conclusion about the extension and possible role of the lineaments can be made.

### **Middle and eastern part of SNO**

The middle and eastern part of the SNO is characterised by long wavelength very low magnetic field anomalies (Figs. 48.A and 48.F). Several factors are possible causes for the low magnetisation. A rather large body of granodiorite (Fig. 47) occurs along both sides of Søndre Strømfjord immediately northwest of Sukkertoppen Iskappe (Allaart & Jensen 1979). Several later maps do not include the granodiorite. The western and northern outline of the granodiorite is similar to the most demagnetised zone in the southern part of the middle SNO and could be one of the causes for the low magnetisation. The existence of a large granodiorite body is also in agreement with interpretations of the Bouguer anomaly field (Fig. 40) where a triangular shaped low Bouguer anomaly correlates with the suggested granodiorite. Short wavelength anomalies in the middle of the granodiorite body north of Søndre Strømfjord and along the northern margin of Sukkertoppen Iskappe could

originate from described amphibolite horizons in the granodiorite. The magnetic data indicate (Fig. 48.A) that the southern limit of the granodiorite body is identical to the SE extension of the SNF beneath the Sukkertoppen Iskappe.

The proposed metamorphic facies boundaries and deformation phases (Allaart & Jensen 1979; Grocott 1979; Talbot 1979; Allaart 1982; Rosing *et al.* 2001) are drawn on top of the magnetics in Fig. 47. With some modifications, these boundaries correlate with the changes and patterns observed in the magnetics (Fig. 47). Besides the facies variations are the different deformation phases Nag. 1 and Nag. 2 also matching the observed changes and pattern in the magnetics (deformation phases Nag. 1 and Nag. 2 are defined in Bridgwater *et al.* 1973b; Grocott 1979; Talbot 1979; Korstgaard *et al.* 1987). The areas with Nag. 1 deformation are characterised by an overall tendency towards slightly lower and smoother magnetic responses, whereas the areas with Nag. 2 deformation have slightly higher magnetic responses and a higher content of separated short wavelength magnetic anomalies. Nag. 1 deformation is described as Late Archaean transcurrent shearing whereas Nag. 2 deformation is characterised by ductile thrusting. Where the outline of the metamorphic and deformation boundaries is marked as uncertain (e.g. Grocott 1979; Talbot 1979), these can be deduced from the magnetics. For example is the western metamorphic and deformation boundary in the SNO clearly outlined from the magnetics. As described in earlier sections, several metamorphic processes can influence the magnetic susceptibility and a relation between metamorphic facies and measured magnetic susceptibilities from the region is established. The high anomaly amplitudes of areas in Archean and Palaeoproterozoic Nagssugtoqidian granulite facies (in the southern foreland and in the CNO) reflect prograde mineral reaction resulting in production of magnetite. The low anomaly amplitudes of the areas in Palaeoproterozoic Nagssugtoqidian retrograde amphibolite facies (in the SNO) reflect mineral reactions with breakdown of magnetite to silicate mineral phases. The penetrative ductile state in the SNO has had an enhancing effect on the breakdown of magnetite, as more oxidizing water is present under ductile conditions.

A localised short wavelength magnetic anomaly in the middle of the SNO (Figs. 48.A and 48.C) is related to an intrusive body of anorthosite and leucogabbro. Several less pronounced, elongated, and slightly smaller anomalies are observed north of the intrusive body (Fig. 48.C). These anomalies correspond to elongated small belts of schist and amphibolite lithologies. The course of the elongated supracrustal belts in the SNO can be deduced from magnetics (Figs. 48.B and 48.D).

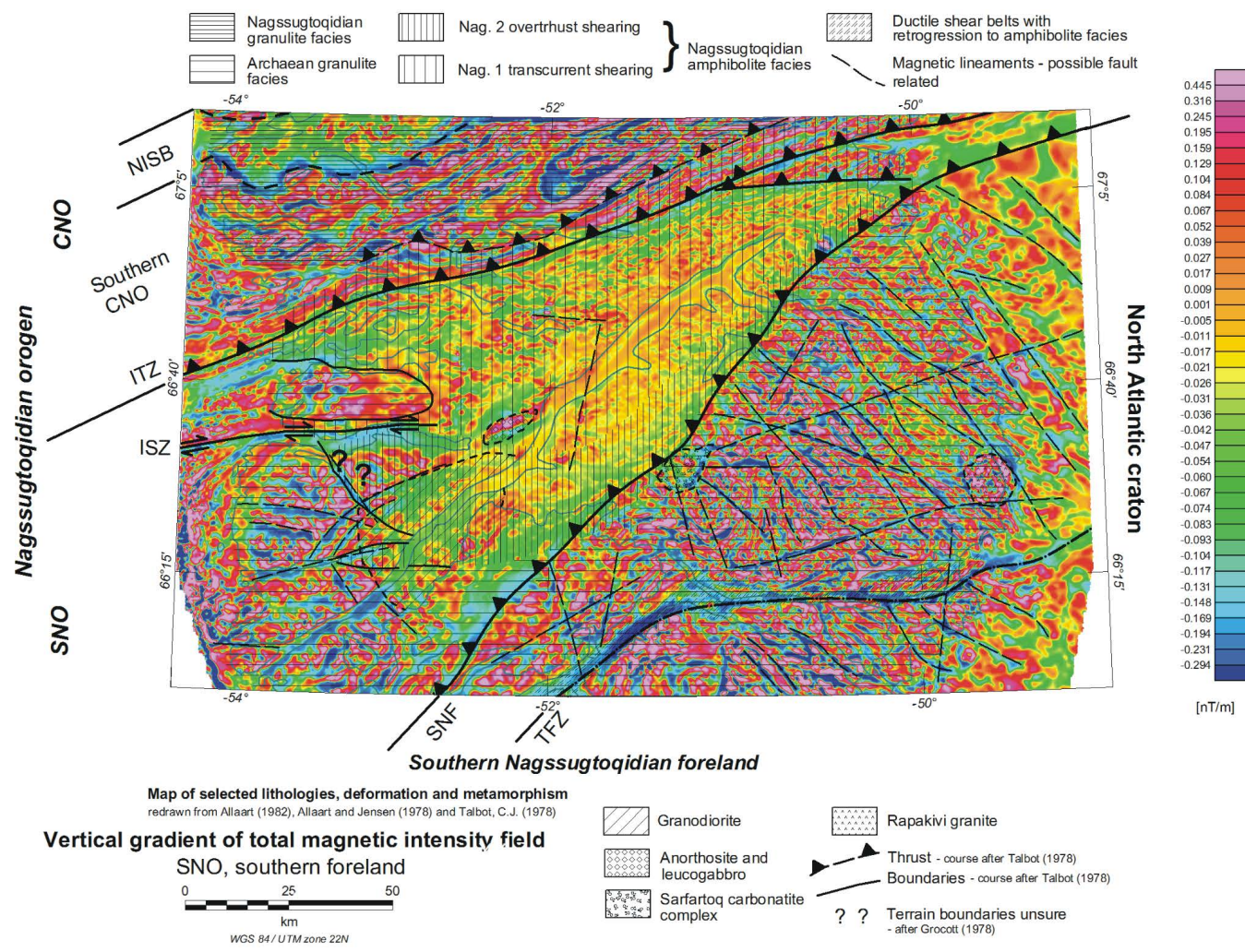


**Figure 47.** Metamorphic and deformation phases after Allaart 1982, Allaart and Jensen 1979 and Talbot 1979 for the southern foreland and SNO are drawn on top of the vertical gradient of the total magnetic field intensity. For abbreviation used in the figure, please refer to Fig.11.

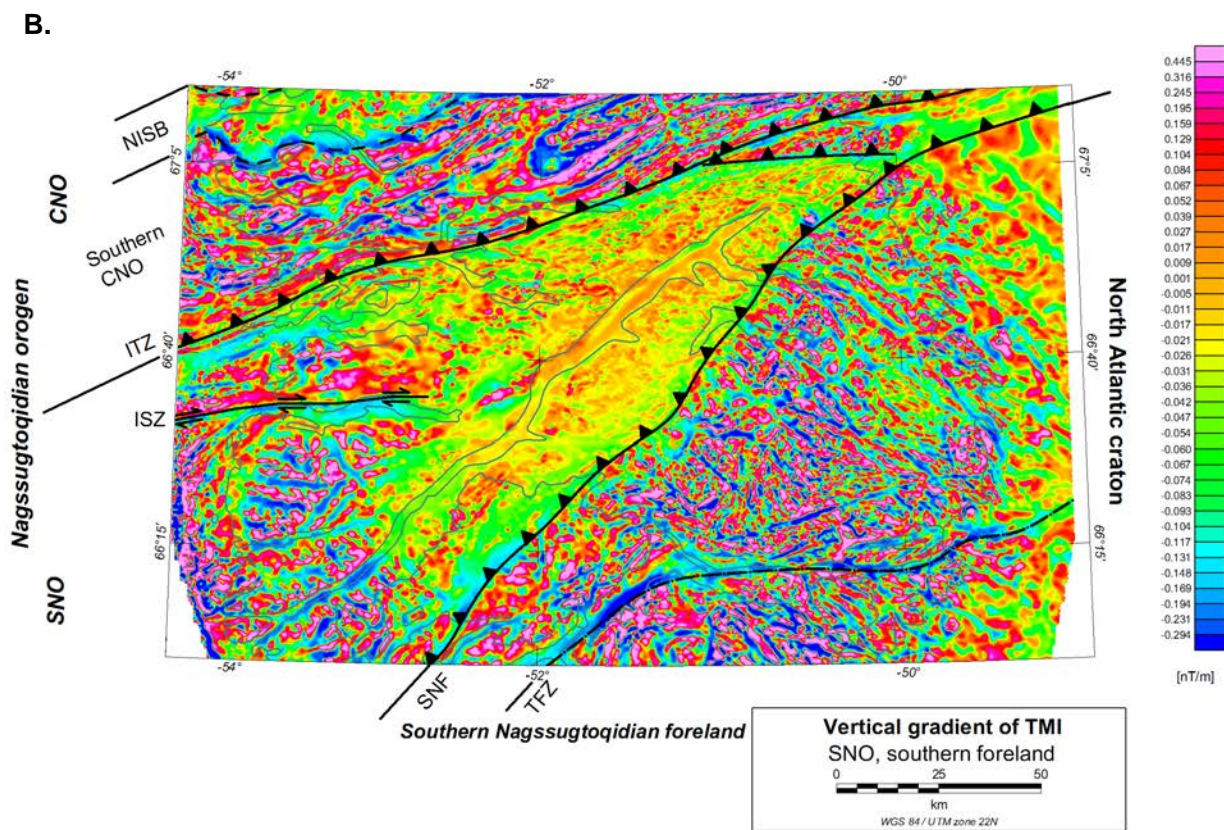
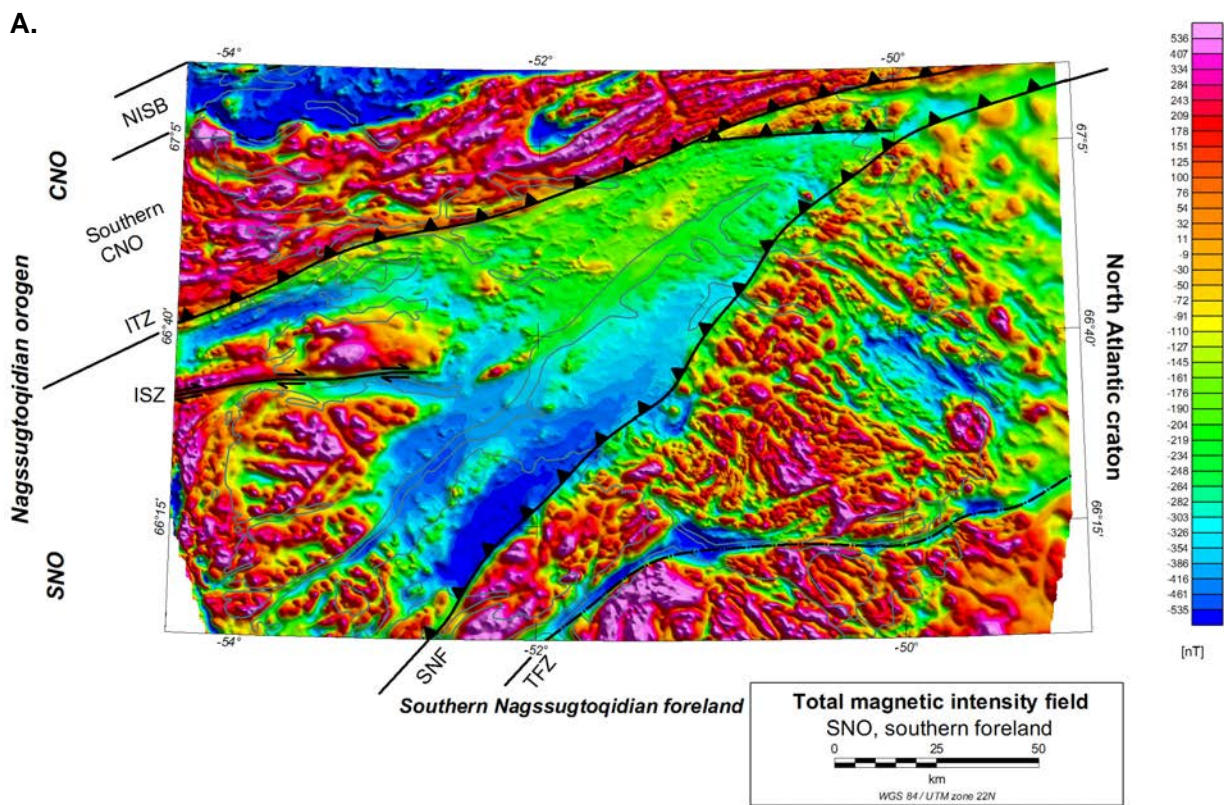


Fig. 48 Continued →

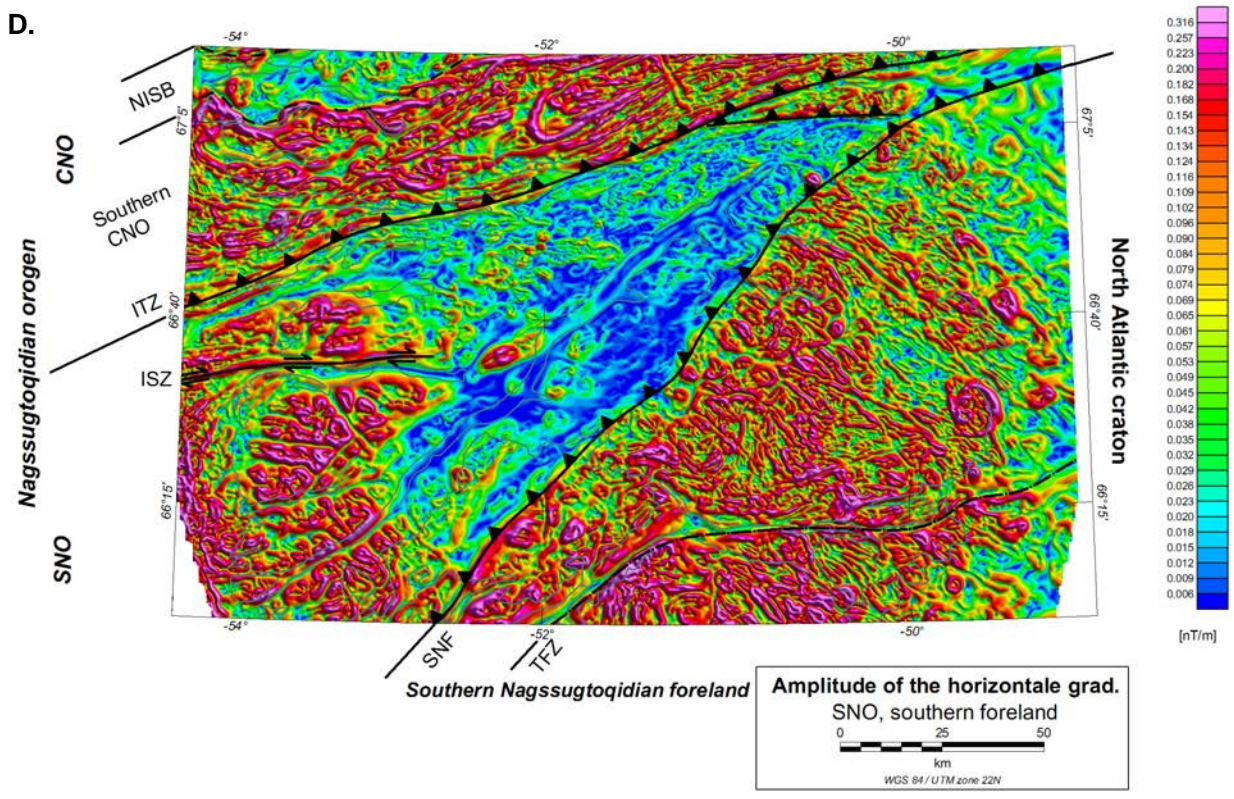
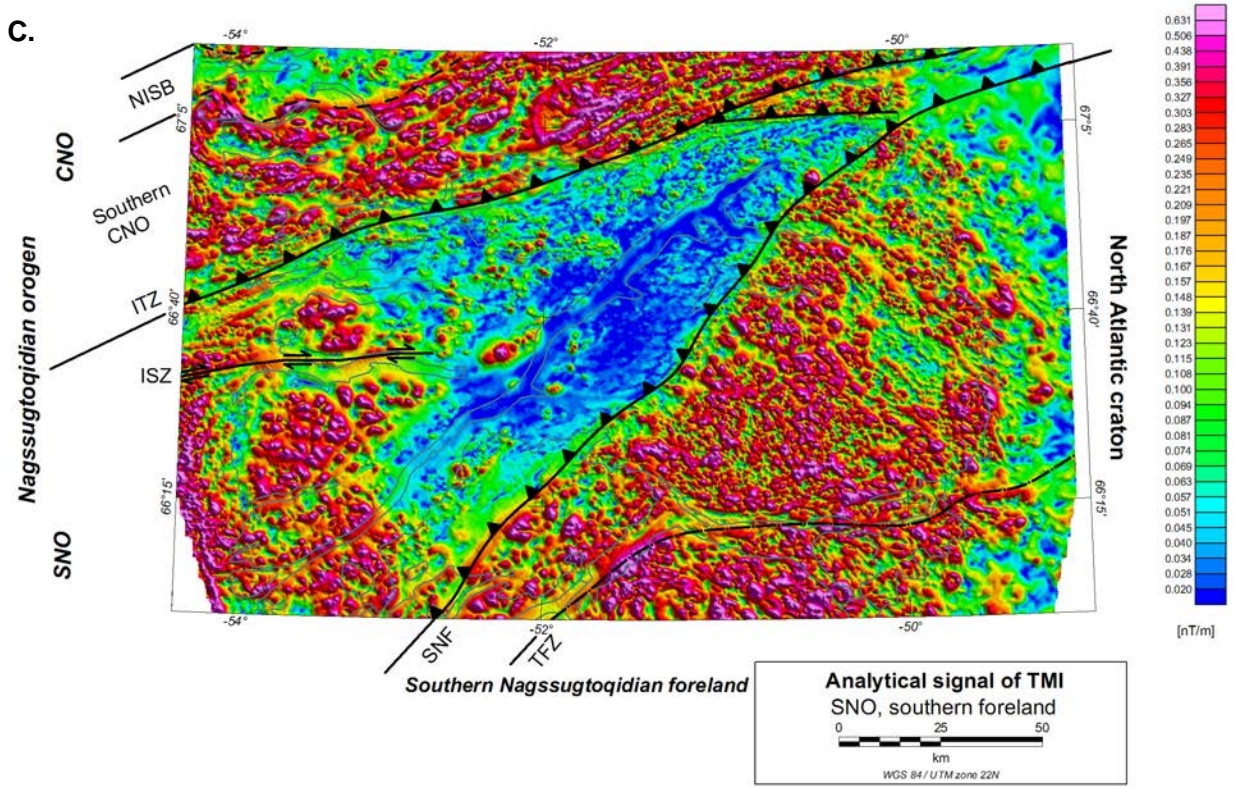


Fig. 48 Continued →

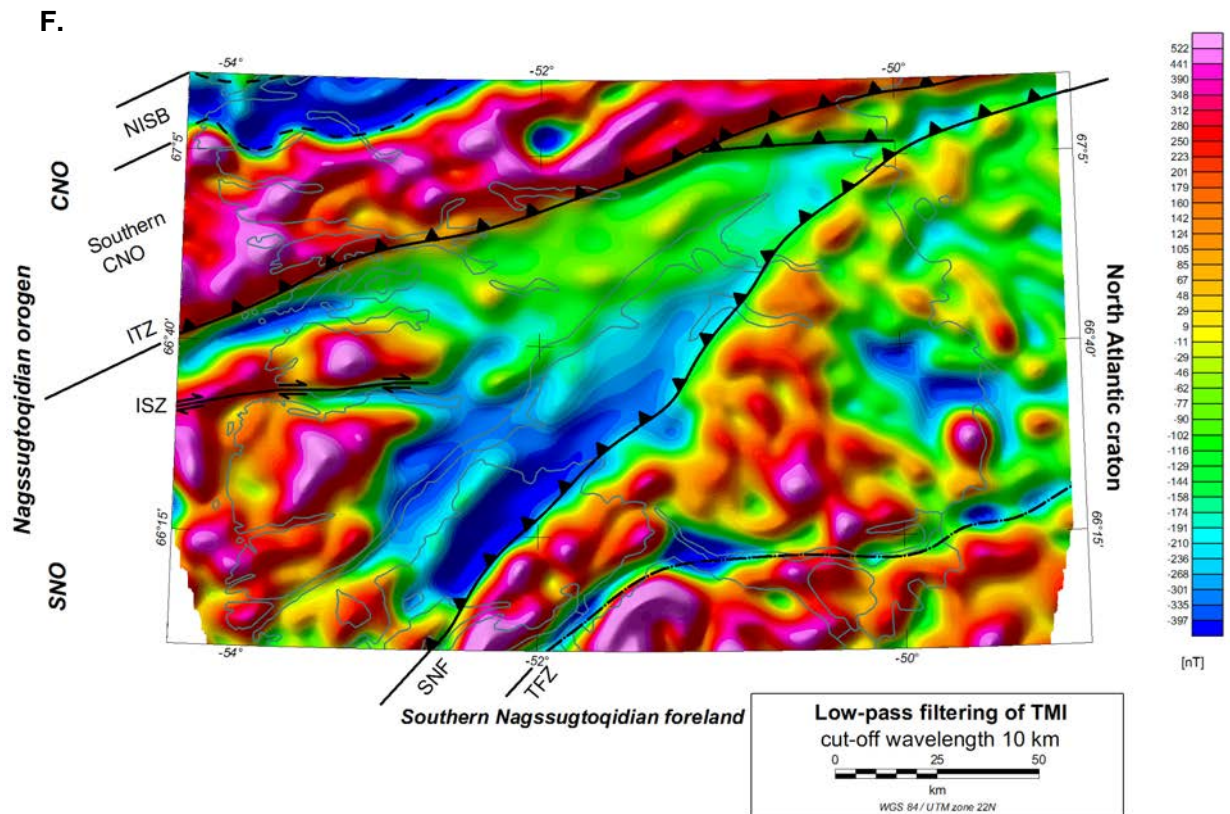
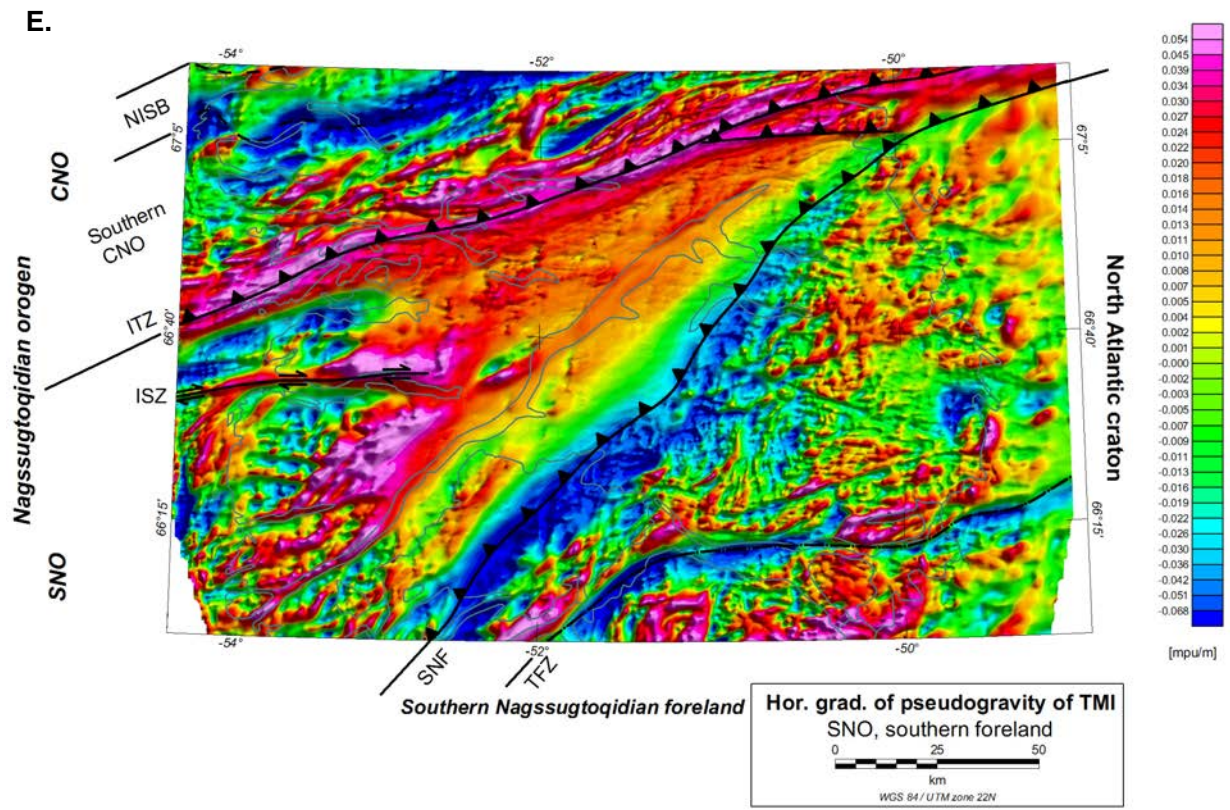


Fig. 48 Continued →



## **Central Nagssugtoqidian orogen – Ikertôq thrust zone and Nordre Strømfjord shear zone**

### **Ikertôq thrust zone**

The Ikertôq thrust zone is reflected in the magnetics as WNW–ESE orientated lineaments with sharp steep gradients and contrast between reworked amphibolite facies gneisses to the south and more magnetised rocks related to the Sisimiut charnockite complex and granulite facies gneisses to the north (Figs. 49, 50.A and 50.I). The orientation of the magnetic anomalies is due to strong planar fabric in the gneiss.

In particular, the thrust zone is clearly defined in the eastern part, whereas the field in the central part becomes more diffuse. Towards the coast, the thrust zone is marked by distinct lineaments, but without a strong contrast between neighbouring areas because of the similarities of the rock types and metamorphic conditions north and south of the thrust. The Ikertôq thrust zone is also clearly defined in the gravity, with a high and low Bouguer field north and south of the thrust zone respectively (see Fig. 40). Individual panels of supracrustal and gneiss lithologies can be viewed along the entire strike of the zone (Fig. 50.B). Judged from the stripping filtering of the total magnetic field intensity (see Fig. 21) is the Ikertôq thrust, together with the SNF, the most penetrative boundaries at depth in the orogen. The SNF and the Ikertôq thrust zone can be followed to a depth of more than 21 kilometres. The thrust zone is very clearly defined by the Euler deconvolution (see Fig. 30) with increasing depth estimates to the west compared with estimates towards the east.

A NNW–SSE trending magnetic lineament perpendicular to the thrust zone cuts the northern part in the middle of the thrust zone. This lineament correlates with the Isortoq Elv valley. The magnetic anomaly is relatively strong and the valley is not characterised by particular steep topographic gradients. It is therefore believed that the lineament can represent late faulting.

### **Southern part of the central Nagssugtoqidian orogen**

The western part of the southern CNO is characterised as a strong magnetised area comprising numerous elongated anomalies (Fig. 50.A). These anomalies originate from the Sisimiut charnockite suite. Geological mapping is described as difficult due to similarities between the Archaean gneisses and the charnockite suite (Kalsbeek & Nutman 1996b; Kalsbeek 2001). However, from the magnetic patterns (e.g. Figs. 50.I. and 50.J) the charnockite can be extended further east compared with the mapped outline of the suite. Results of stripping filtering (see Fig. 21) indicate that the anomalies caused by the charnockite intrusive suite attenuate at a depth of 15 kilometres. The charnockite suite is to the east bounded by a large low magnetic anomaly reflecting an upright fold structure. The area with is unmapped and is largely covered by glacial material. The low magnetisation originates possibly from hitherto non-described low magnetised supracrustal lithologies.

The magnetic pattern of the eastern part of the southern CNO is characterised by relative high amplitude short wavelength anomalies compared with the broader anomalies of the charnockite suite. In particular, this is clear in the vertical gradient of the magnetic field and in the analytic signal in Figs. 50.B and 50.C. Except a pronounced E–W trending orientation of the anomalies, the anomalies pattern resembles the pattern of the southern foreland.

Several NNW to NW trending magnetic lineaments from the eastern part of the southern CNO in the south (Figs. 50.E and 50.A) cut the E–W trending magnetic anomalies and are interpreted as faults. Some of the faults recognisable in the magnetics have also been mapped out (Escher 1971). The faults are to the south bounded by the Ikertôq thrust zone. The faults appear to have a dextral displacement of the magnetic anomalies (Figs. 50.B, 50.D and 50.E).

Isolated elongated high amplitude magnetic anomalies (Figs. 49, 50.A, 50.C and 50.I) are located along the northern boundary of the western part of the southern CNO. These anomalies correlate with described geochemical anomalies (Steenfelt & Dam 1991; Steenfelt 1996; van Gool *et al.* 1996) and a several kilometre wide tract of syn-kinematic granites with ages at c. 1835 Ma (Kalsbeek & Nutman 1996a) and syenitic rocks with ages c. 1900 to 1920 Ma.

A low magnetic lineament is observed with an E–W trend in the eastern part of the southern CNO just north of the Ikertôq thrust zone (Figs. 49, 50.A and 50.B). The lineament cuts the anomalies of the granites and syenitic rocks and can consequently reflect a tectonic event with an age younger than 1835 Ma. The lineament bends towards NNW–SSE at the boundary to the middle CNO (also denoted Nordre Isortoq steep belt, will be described in the next section) and continues further north with a weak negative response into the southern NNO and further NNW into the sea. Further discussion and interpretation of this lineament will be given in the next section.

The southern CNO is characterised by high Free Air anomaly values (see Fig. 42), especially pronounced in the western part. The data from this area show a positive correlation between Bouguer anomaly and elevation (see Figs. 39 and 40). The positive correlation between topography and Bouguer anomaly associated with the high positive Free Air anomaly in the southern part of the CNO is unusual but can be explained as a combination of several phenomena. Since isostasy is a long wavelength phenomenon dependent on the rheological properties of the entire lithosphere, sources causing short-wavelength gravity anomalies are not expected to be isostatically compensated locally. This might be the case for the southern part of the CNO. The existence of a relatively local and dense mass in the crust would explain the positive correlation. This would be in agreement with the proposed tectonic evolution (van Gool *et al.* 2002) of the Nagssugtoqidian orogen, where heavier rocks, in the form of dense oceanic plate, possibly have been transported down in the continental crust during subduction. The isostatic disequilibria could also originate from localised heavy ultramafic/gabbroic bodies. Geochemical anomalies and field observation suggest the presence of such lithologies (A. Steenfelt, GEUS, personal communication, Sep. 2003). Another process leading to an increase in the Bouguer anomaly is a thinner crust under the CNO, where local up-doming of heavier mantle will increase the Bouguer anomaly.

### **Middle part of the central Nagssugtoqidian orogen – Nordre Isortoq steep belt (NISB)**

The middle CNO (hereafter referred to as the Nordre Isortoq steep belt, denoted NISB, following van Gool *et al.* (2002) is characterised by a distinct broad continuous low NE–SW orientated magnetic response (Figs. 50.A and 50.B). The western part of the NISB is uniform and smooth whereas the eastern part is dominated by parallel elongated very short wavelength anomalies (Figs. 49. 50.I and 50.J). The NISB is relatively cursorily mapped and investigated, but it is known to contain the hitherto thickest supracrustal sequence of mainly psammitic and pelitic lithologies (van Gool *et al.* 1996; van Gool *et al.* 2002). This is in agreement with the observed magnetic responses and susceptibility measurements from the eastern part of the NISB (see also Nielsen & Rasmussen 2002). Judged from descriptions and maps of the NISB, the distribution of the supracrustal rocks are more uniform to the west compared to the east, where Archaean orthogneiss are interleaved with Archaean and Palaeoproterozoic paragneiss (van Gool *et al.* 2002). This is reflected by the differences in the magnetic patterns of the western and eastern part of the NISB. Bodies of charnockite are located just south of the inlet to Nordre Isortoq fjord and a little further east at the end of the fjord.

The NISB has been described as the likely place for a suture zone within the orogen (Kalsbeek *et al.* 1987; van Gool *et al.* 2002). The possible location of the suture zone within the Nordre Isortoq steep belt is supported by the presence of sharp horizontal gradients associated with the low magnetic domain and the very different characters of the responses of the adjacent areas. The continuous and distinct nature of the magnetic field from this domain supports this interpretation.

The extension of the low magnetised lineament observed in the eastern part of the southern CNO has a very weak signature in the NISB (Figs. 50.B and 50.F) and is coincident with the Kuup Akua valley. The lineament will be discussed further in the next section.

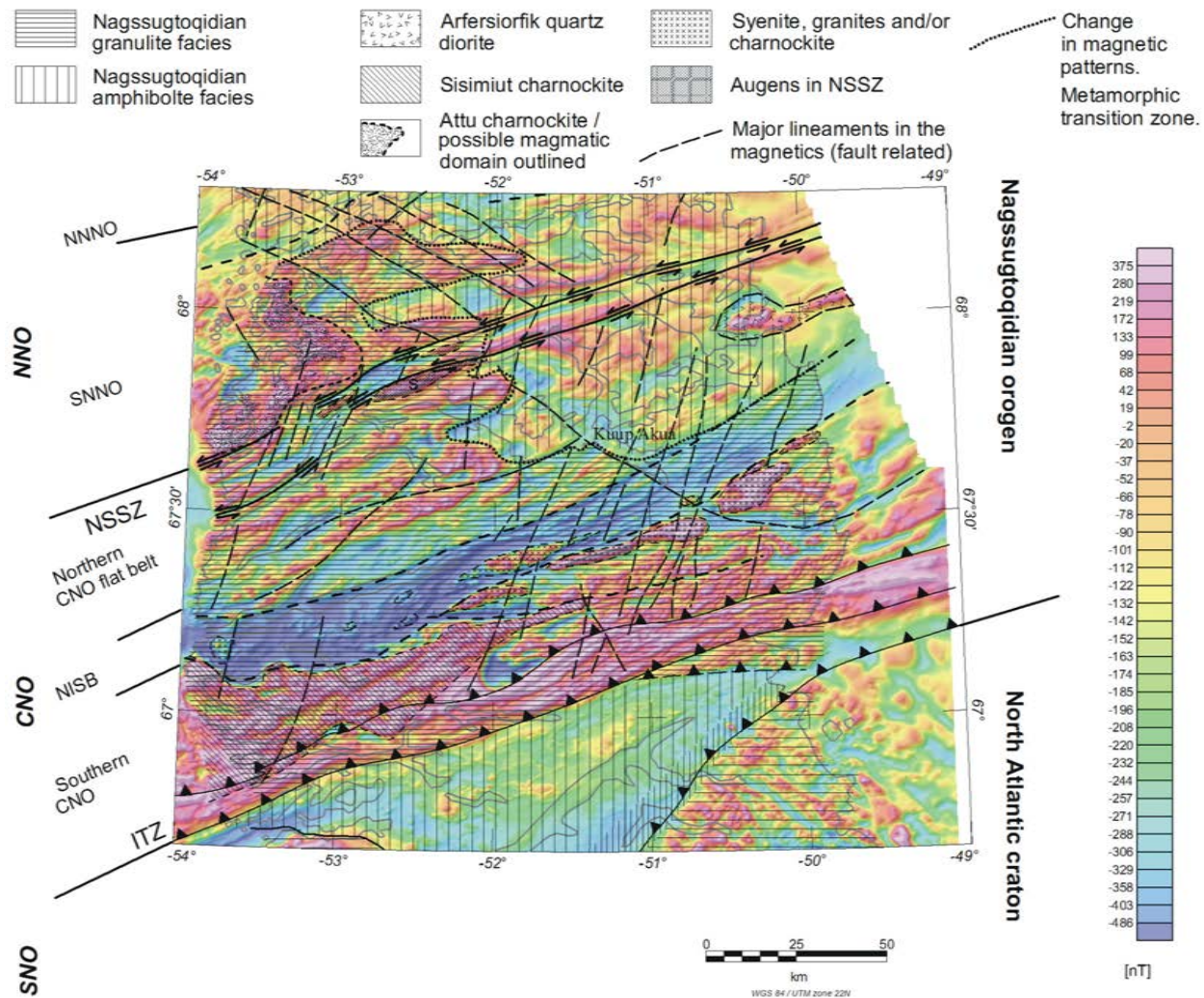


**Figure 49.** Metamorphic boundaries and magnetic lineaments (fault related) together with outline of different distinct features. Furthermore is charnockite and possible other magmatic lithologies outlined south of Attu, together with the outline of a possible Attu magmatic domain. This domain is discussed in the section for the southern NNO. For abbreviation used in the figure, please refer to Fig. 11.

### **Northern part of the central Nagssugtoqidian orogen – northern CNO flat belt**

The northern CNO (also named the northern CNO flat belt by van Gool *et al.* (2002), which will be used hereafter, see Fig. 49) is characterised by several large scale upright fold structures and very varying magnetic anomaly patterns, however, a dominating W–E trend (Figs. 50.A and 50.B) is clearly seen. Most of the moderate to high magnetic anomalies can be correlated to areas with orthogneisses. Low magnetic anomalies can often be associated with supracrustal rocks.

In general, a pronounced correlation between metamorphic facies changes/characteristics of especially the magnetic patterns, but also the gravity field, is observed. The present day exposed metamorphic patterns is a result of southward thrusting in the Ikertôq thrust zone and the southern SNO and regional north-eastward tilting with regional up-down block-faulting, bringing granulite facies lithologies up in the western part of the CNO and the NNO (will be described in a later section) and amphibolite facies lithologies down in the eastern part of the CNO. Consequently, the change in patterns represents different crustal depths and a rotational axis of tilting. The tilting results in a thinner crust towards the west and a consequently up-doming of the mantle. The latter will probably affect a larger region and would be seen as a longer wavelength feature in the Bouguer anomaly. That could be why a positive correlation of the topography and the Bouguer anomaly in parts of the high Bouguer anomaly is observed. Furthermore, the tilting will produce the metamorphic facies transition observed. More magnetised and denser granulite facies rocks were brought up towards the south by thrusting.

The eastern part of the northern CNO flat belt is also characterised by the extension of the NNW to NW orientated faults observed in the southern CNO. Generally, the entire CNO is characterised by the largest density of fault related lineaments compared with the SNO and the NNO.

Deep situated faults and fracture zones in bedrock lithologies are commonly associated with a decrease in magnetisation. This is also the case for the study region. The decrease in the magnetic field associated with these zones is related to both the topographic depression associated with the zone and the production of Fe-bearing hydrous silicates due to alteration and destruction of magnetite. Near surface alterations at low temperature, oxidizing condition and presence of water results in an oxidation of magnetite to hematite (Henkel & Guzmán 1977). In uplifted areas, deeper sections of these zones will be exposed. In these areas have mid-crustal with high pressure and stable oxidation state existed under the formation of the fractures and fault zones. Under these conditions are Fe-bearing hydrous silicates formed at the expense of magnetite in the same mineral reaction (Grant 1985; Clark & Emerson 1991; Clark 1997; Airo & Ruotoistenmäki 2000) The faults are often surrounded by lithologies unaffected by the process in the fault zone and consequently, the zones will likely show a decrease in the magnetisation. Generally, if faulting post-date the main deformation stage and affects consolidated cooled crust, no alteration of the magnetic mineralogy is expected and the faults will not be associated with a pronounced lower magnetisation.

Many of the NNW to NW orientated faults have a brittle nature (observed by the authors during fieldwork in the area) and are not associated with a prominent decrease in magnetisation. The brittle nature and the absent decrease in magnetisation indicate that the faults were formed after the main deformation phase and under upper crustal conditions. The faults define a regional block faulting possibly associated with the eastward tilting.

The Arfersiorfik intrusive suite in the eastern part of the northern CNO flat belt has a rather complex response (Figs. 49, 50.A, 50.B and 50.D). Many of the small thin bands intruded along metasediments are not visible in the magnetics, whereas the larger bands along the metasediments often have low magnetic responses. The major intrusive body of the Arfersiorfik intrusive suite is situated in the inner part of Arfersiorfik fjord. The margin and outer parts of the body has a low magnetic response whereas the central part of the intrusive complex in the innermost part of the fjord has a very pronounced magnetic high. This suggests that the Arfersiorfik intrusive suite consists of different petrological phases. During fieldwork in 2001 and 2002 in the region by the authors this interpretation was confirmed. Several different magmatic phases could be recognised in the quartz-diorite from the inner part of Nordre Strømfjord, Ussuit, and the inner part of Arfersiorfik; e.g., the pronounced positive anomaly in the latter could be correlated with a very magnetite rich part of the quartz-diorite. The anomaly of the intrusive suite attenuates at a depth of 3 km (see Figs. 21, 50.I and 50.J).

#### **Nordre Strømfjord shear zone (NSSZ)**

The Nordre Strømfjord shear zone can clearly be seen in the magnetics as a linear band with low magnetisation. The shear zone comprises a number of rather short wavelength low and high lineaments with several offsets and with similar magnetic responses for the neighbouring areas on both sides. The low magnetisation in the NSSZ is interpreted to be related to the supracrustal rocks in the shear zone and destruction of the magnetite due to higher water pressure in the shear zone. It is believed that this zone is formed under ductile deformation at which higher water pressure in the zone provided conditions for the demagnetisation of the rocks. The zone is later tilted, as described in the former section on the northern CNO flat belt. Anticlockwise and clockwise rotation of the planar structures in the marginal zone north and south of the NSSZ respectively are clearly reflected by the magnetics (Figs. 50.B and 50.D). Low-strain 'augens' of variable size described by Sørensen (1983) are also observed in the western and central parts of the shear zone (Fig. 49).

The anomaly of the Nordre Strømfjord shear zone attenuates from west to east at a stripping depth of 12 kilometres (Fig. 21). This is consistent with the eastward tilting and a wedge-form of the shear zone described by Bak *et al.* 1975. The Euler deconvolution shows the shear zone as a rather shallow feature.

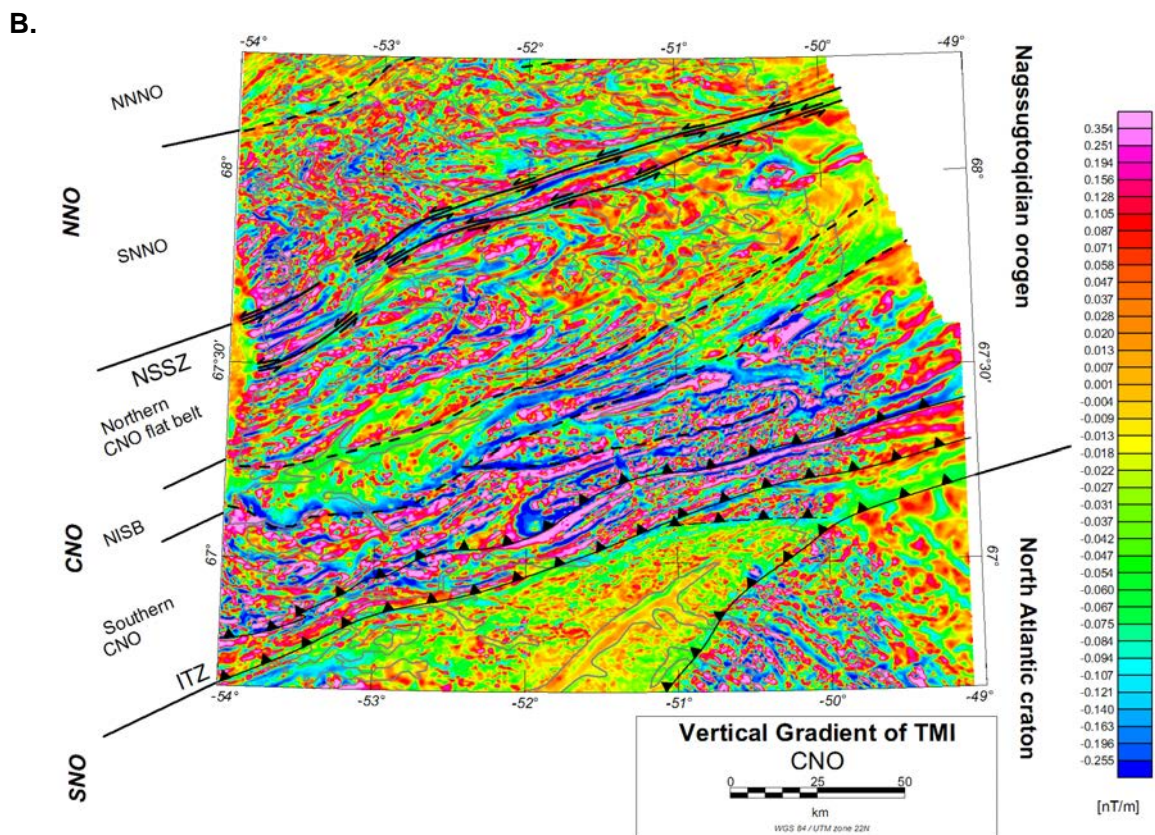
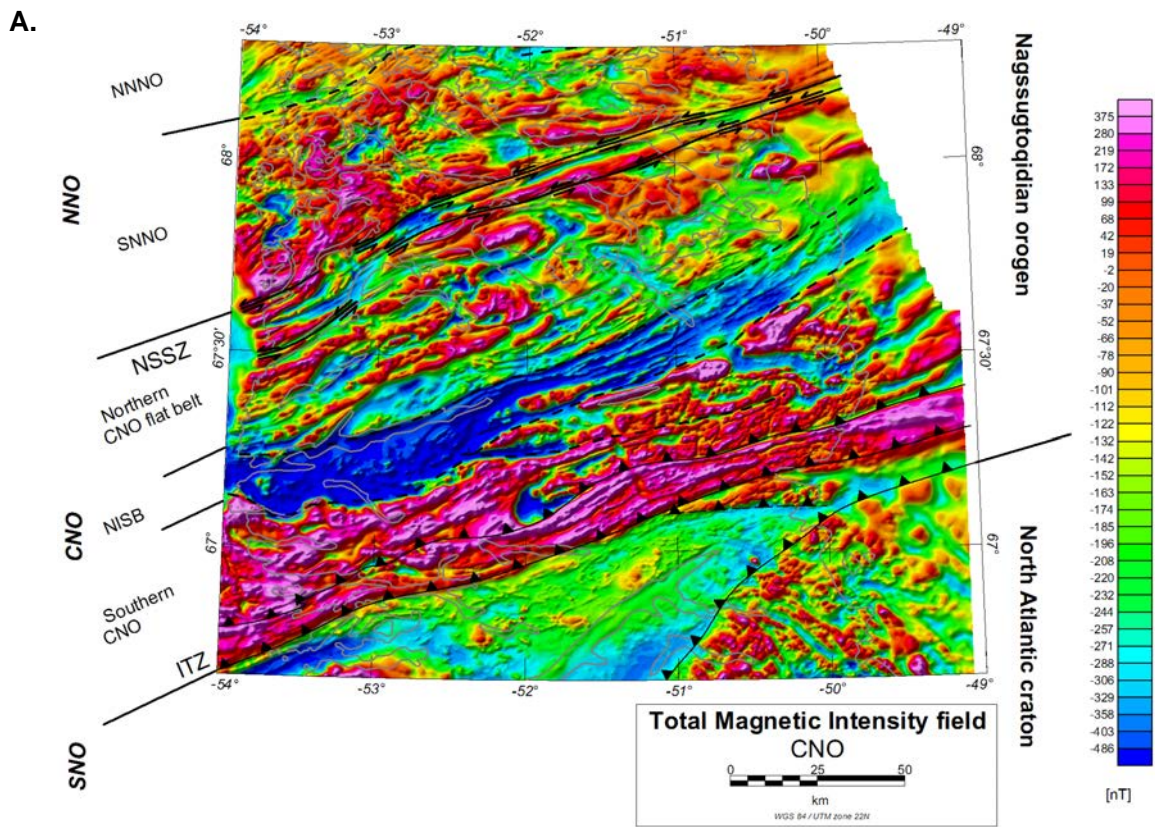
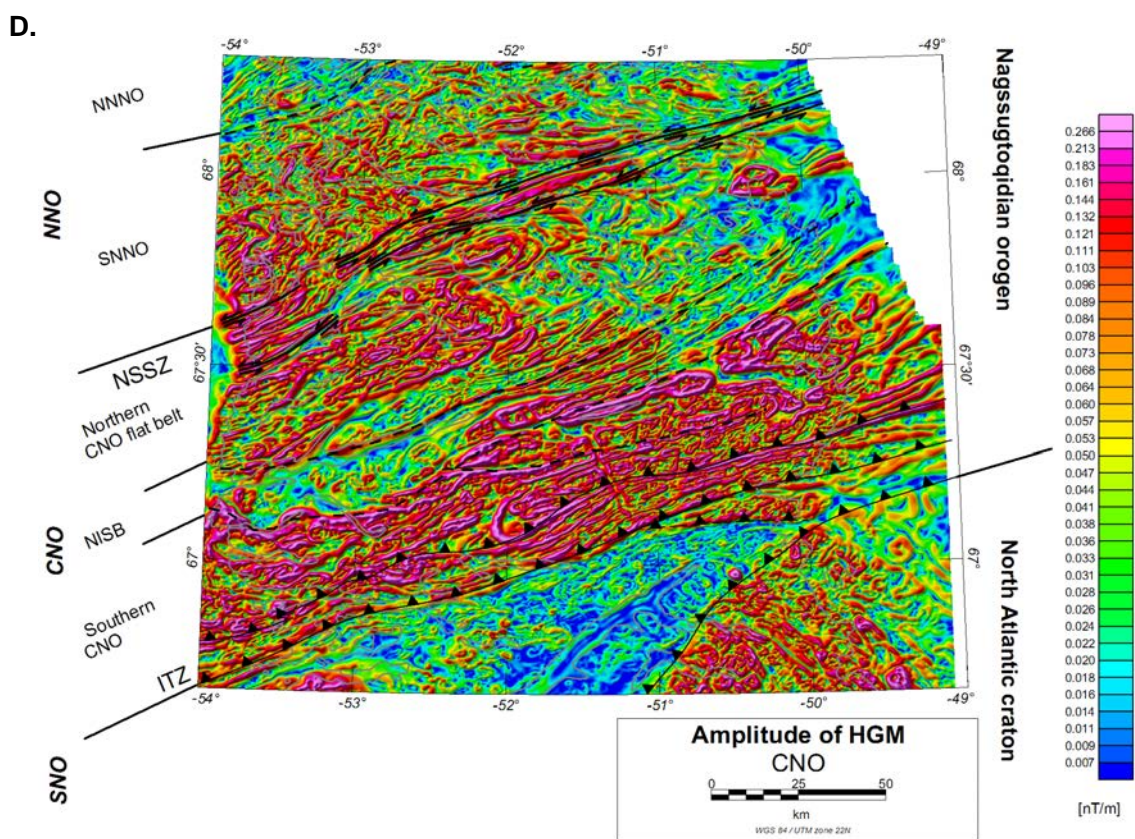
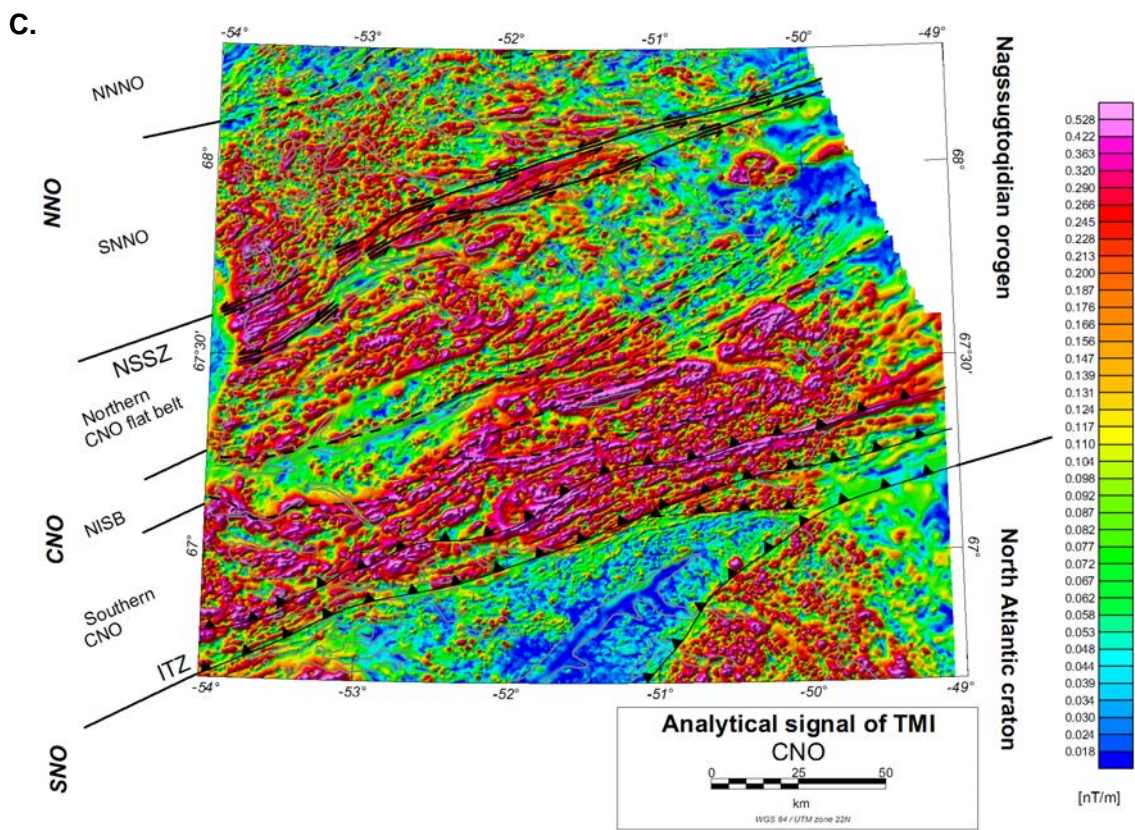


Fig. 50 Continued →



**Fig. 50** Continued →

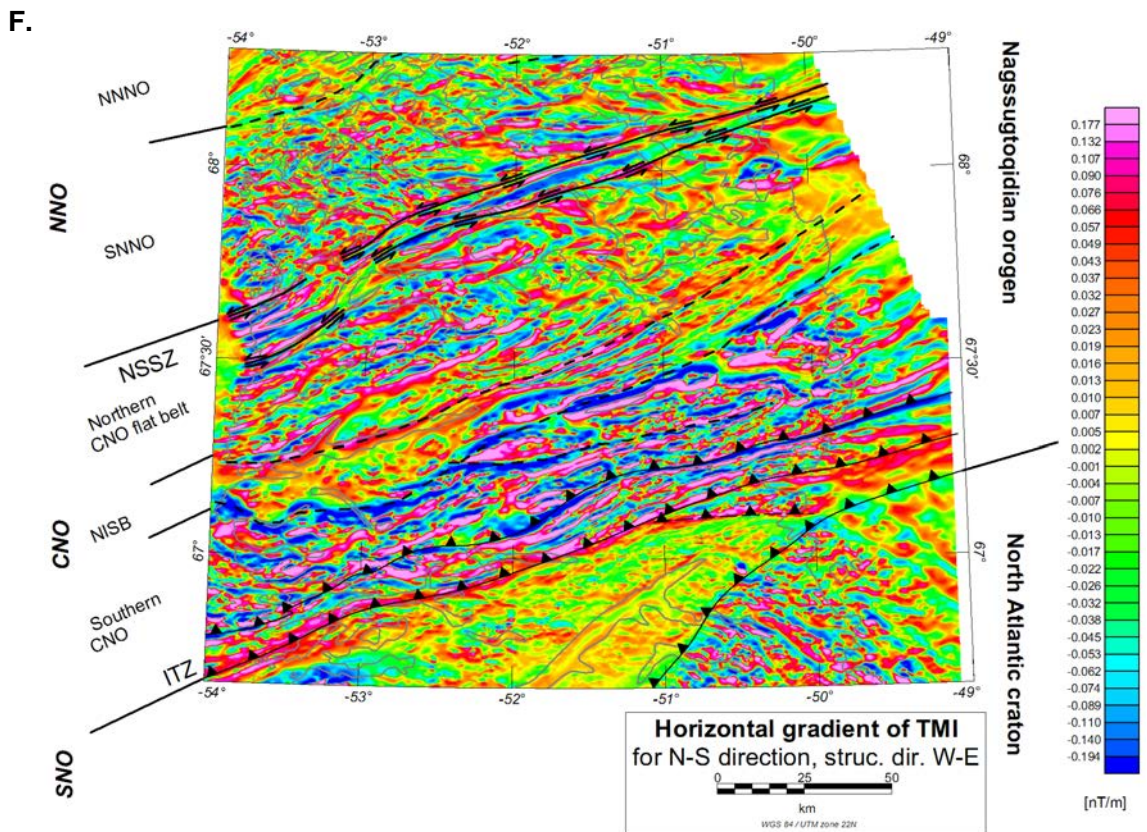
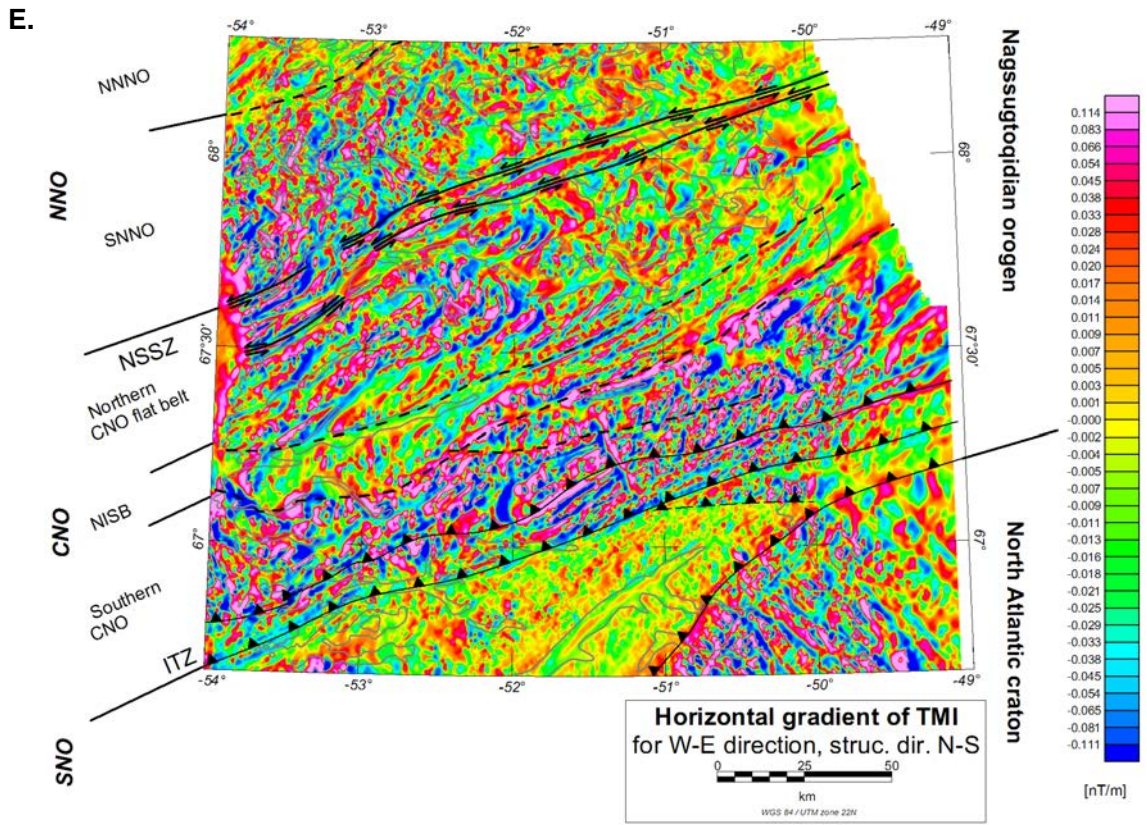
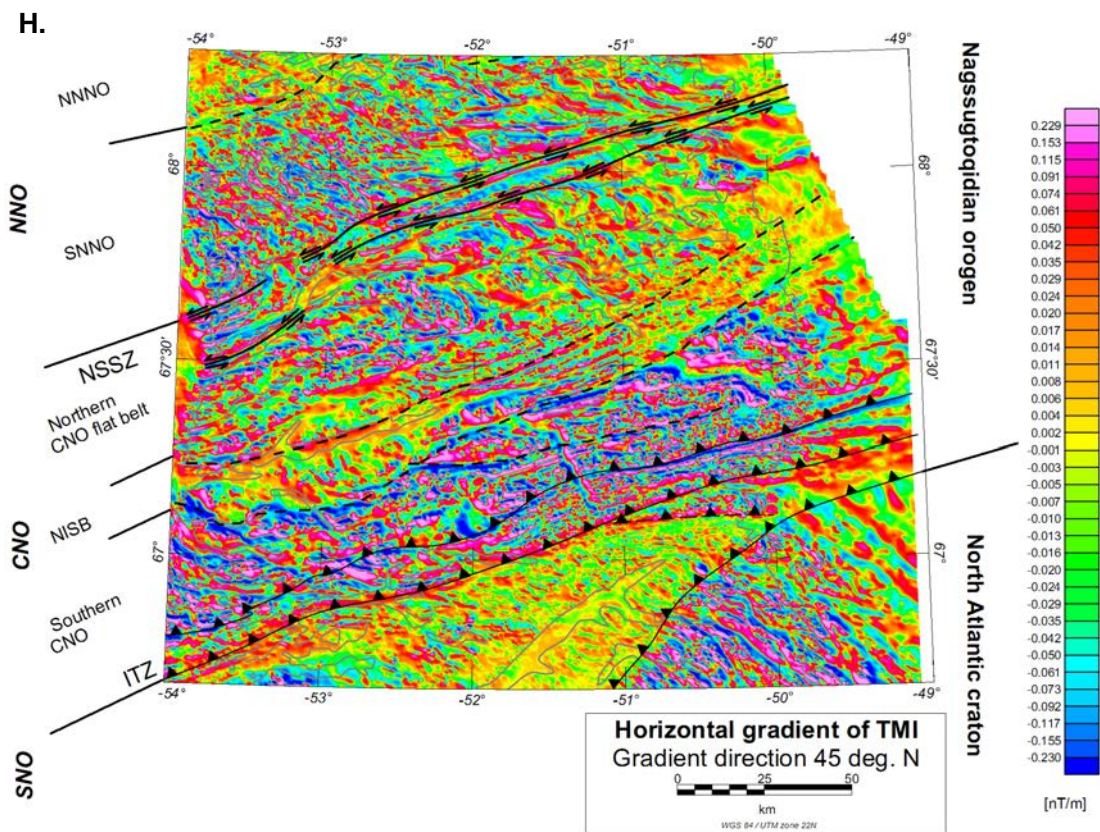
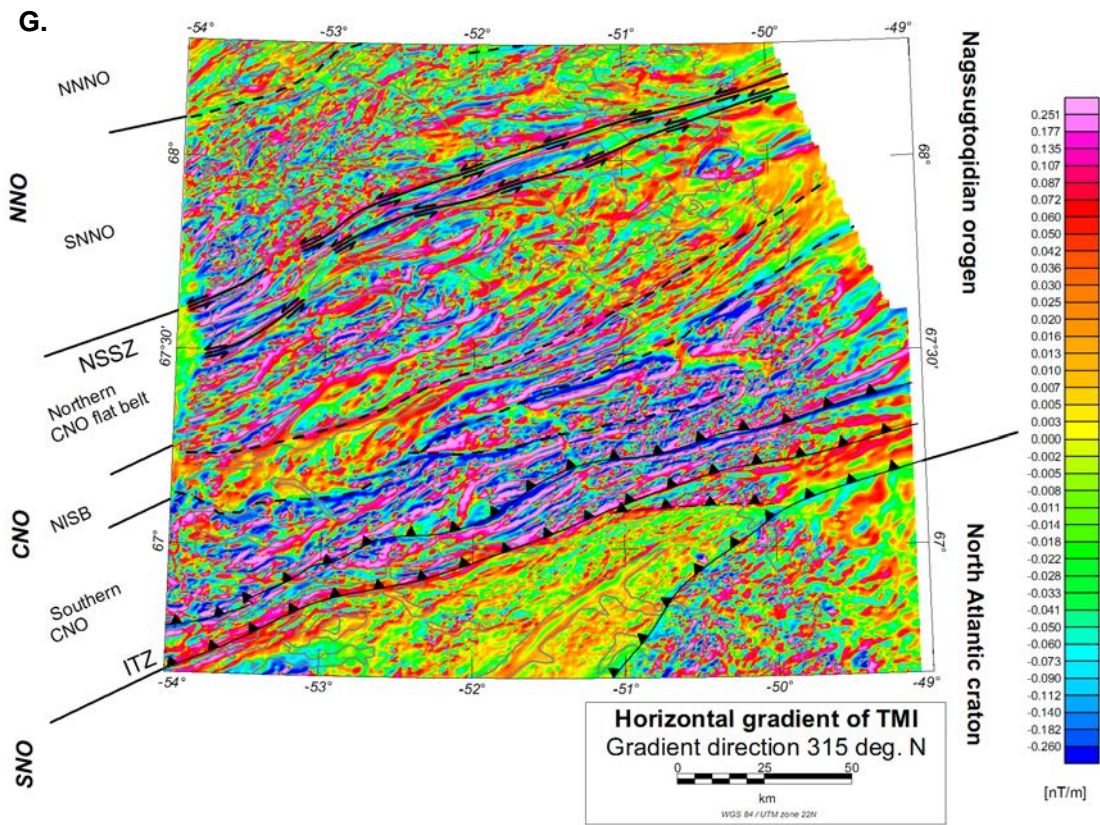
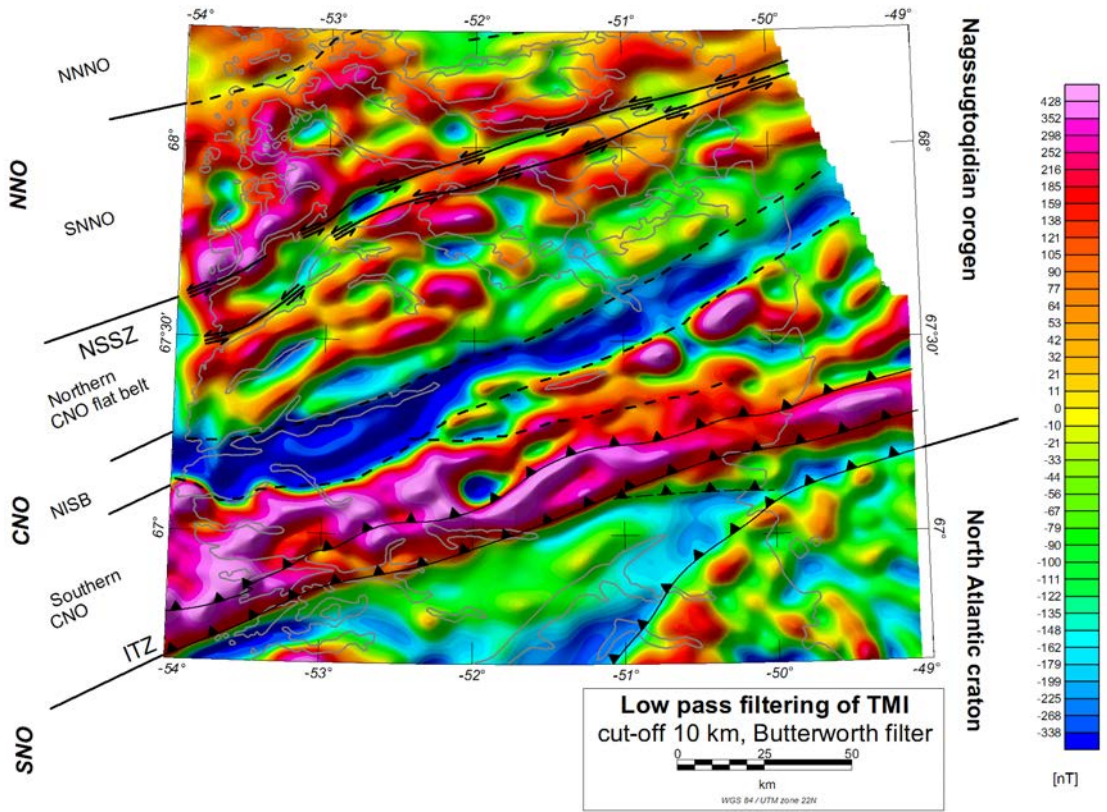


Fig. 50 Continued →



**Fig. 50** Continued →

I.



J.

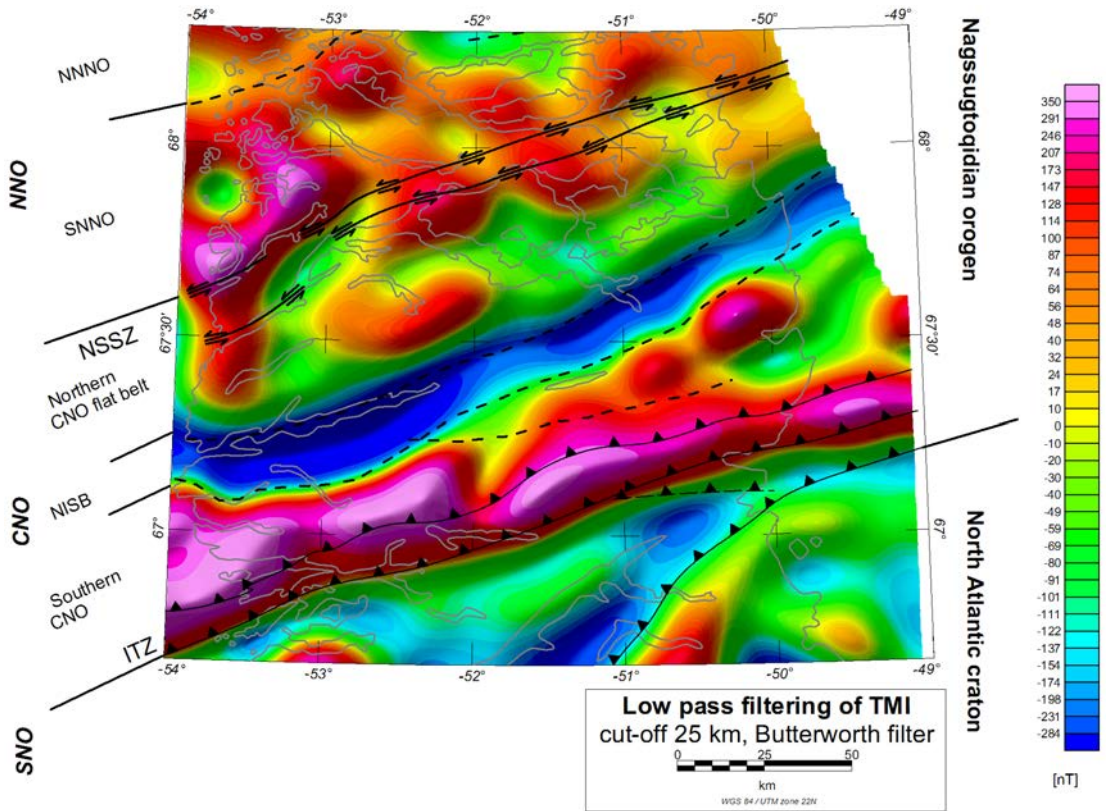
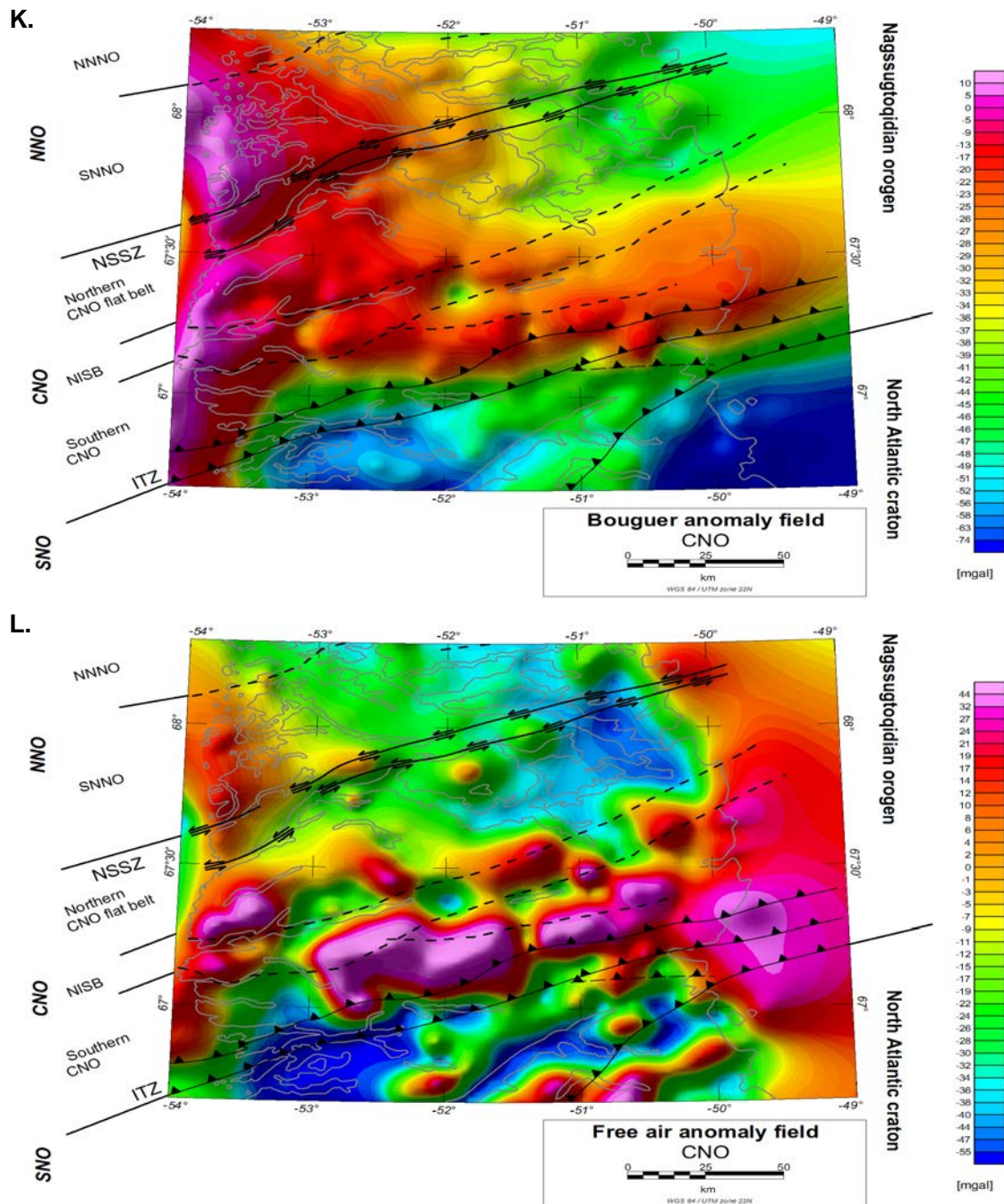


Fig. 50 Continued →



**Figure 50.** Maps showing different processed data for the northern segment of the Nagsugtoqidian orogen (NNO). **A.** Total magnetic field intensity (TMI). **B.** Vertical gradient of TMI. **C.** Analytic signal of TMI. **D.** Amplitude of the horizontal gradient of magnetics (the square root of the sum of squares of the derivatives in the x and y directions). **E.** Horizontal gradient of TMI calculated for W–E direction emphasising N–S structures. **F.** Horizontal gradient of TMI calculated for N–S direction emphasising W–E structures. **G.** Horizontal gradient of TMI calculated for the direction 315°N emphasising structures with a 45°N direction. **H.** Horizontal gradient of TMI calculated for the direction 45°N emphasising structures with a 315°N direction. **I.** and **J.** Low pass filtering of the TMI with 10 km and 25 km as cut-off wavelengths respectively. **K.** Bouguer anomaly field. **L.** Free air anomaly field. For abbreviation used in the figure, please refer to Fig. 11.

## **Northern Nagssugtoqidian orogen**

Based on a marked change in the magnetic pattern from south to north, the NNO can be sub-divided into the southern and northern NNO. The southern NNO is characterised by irregular short wavelength magnetic anomalies whereas the northern NNO is characterised by low amplitude long wavelength patterns with a dominating linear NE–SW trend. The transition from one domain to another is gradual.

### **Southern part of the northern Nagssugtoqidian orogen**

Generally, the magnetic anomaly pattern and trends towards the boundary to the NSSZ are strongly affected by the sinistral displacement of the zone and an increasing anticlockwise orientation of the trends of the magnetic patterns is observed towards the shear zone. Gradually smoother low amplitude magnetic patterns are observed northwards in the southern NNO. This is interpreted to reflect a diminishing in the Paleoproterozoic penetrative deformation and less influence from the shear zone.

Further north the northern NNO is defined by lower amplitude magnetic anomaly patterns than the southern NNO (Figs. 51, 52.A, 52.I and 52.J) and elongated linear magnetic anomalies, which often can be followed for more than 10 to 15 km (Figs. 52.B and 52.D). In a detailed analysis undertaken for an area north of Attu on the boundary between the southern and northern NNO (Piazolo *et al.* 2002; Piazolo *et al.* 2004) was the magnetic data combined with structural, metamorphic, and petrological data in order to investigate the possible presence of high strain zones and metamorphic facies transitions. The elongated linear anomaly belt was interpreted to be related to zones of localised high strain displaying an autochthonous contact between rheological different south and north blocks. The linear belt related to a high strain zone and defining the boundary between the two domains can be followed from west to east. The linear belt is discontinuous, which illustrate the autochthonous nature of the contact. If the contact was a tectonic allochthonous contact, a straight continuous anomaly with a more abrupt change in the magnetic patterns on both sides should be expected. In the middle of the southern NNO swings the elongated linear belts towards SE and continues eastward.

The western part of the southern CNO is generally more magnetised than the eastern part of the CNO (Figs. 51 and 52.A). As for the CNO, this is believed to be associated with the metamorphic facies. The western part of the southern CNO is under granulite facies, whereas the eastern part is under amphibolite facies. In addition, the Bouguer anomaly reflects these conditions (see Fig. 40).

A triangular domain at the coast in the western NNO has higher amplitude anomalies than the rest of the western NNO (Figs. 52.A, 52.K and 52.L). Based on the geological map of the area (Olesen 1984) and fieldwork by the authors in 2002 can the anomalies be related to granitic and charnockitic rocks, in some cases with layers or enclaves of metagabbro. The rocks in the area are generally found to have a very high content of magnetite and especially the amphibolites from this area have a distinct higher content of magnetite com-

pared with neighbouring areas. It is believed, that the area represents a more magmatic dominated area that is referred to as the Attu magmatic domain.

#### **Northern part of the northern Nagssugtoqidian orogen**

A pattern of bending elongated N–S oriented anomalies of high and low field values, which turns into a NE–SW trend in the middle of the northern NNO characterise the northern NNO (Figs. 51, 52.A and 52.B). These elongated anomalies correlate with a relatively large folded supracrustal belt, denoted the Naternaq supracrustal belt. The fold closure is marked by a decrease in magnetisation. Beside the low magnetic response of the pelitic and psammitic metasediments it is believed that partial melting and emplacements of granites in the fold closure can contribute to the decrease in magnetisation and that fluid activity in the closure also could have played a role in the demagnetisation. Amphibolites in the supracrustal belt are marked by high responses. Beside this structure, the other areas of the northern NNO are dominated by NE–SW oriented homogeneous elongated anomaly trends. It is possible, that these anomalies, besides reflecting different lithological panels of NE–SW oriented rocks also reflect localised zones of high strain as observed in the boundary between the southern and northern NNO. Compared with the southern NNO the northern NNO is also characterised by the lack of continuous NNW–SSE directed lineaments in the magnetics. Several smaller lineaments with different orientations can be deduced by detailed investigations of the magnetic patterns (Figs. 52.B, 52.E, 52.F and 26). The north-western part of the northern NNO is characterised by slightly higher elongated anomalies. Many of these responses are related to layers of amphibolite. Two distinct lineaments with magnetic low values in the western part of the NNO can be related to dykes: one onshore and one offshore further west. The onshore dyke are described by Ellitsgaard-Rasmussen (1951) as a composite dolerite dyke with unusual globular structures.

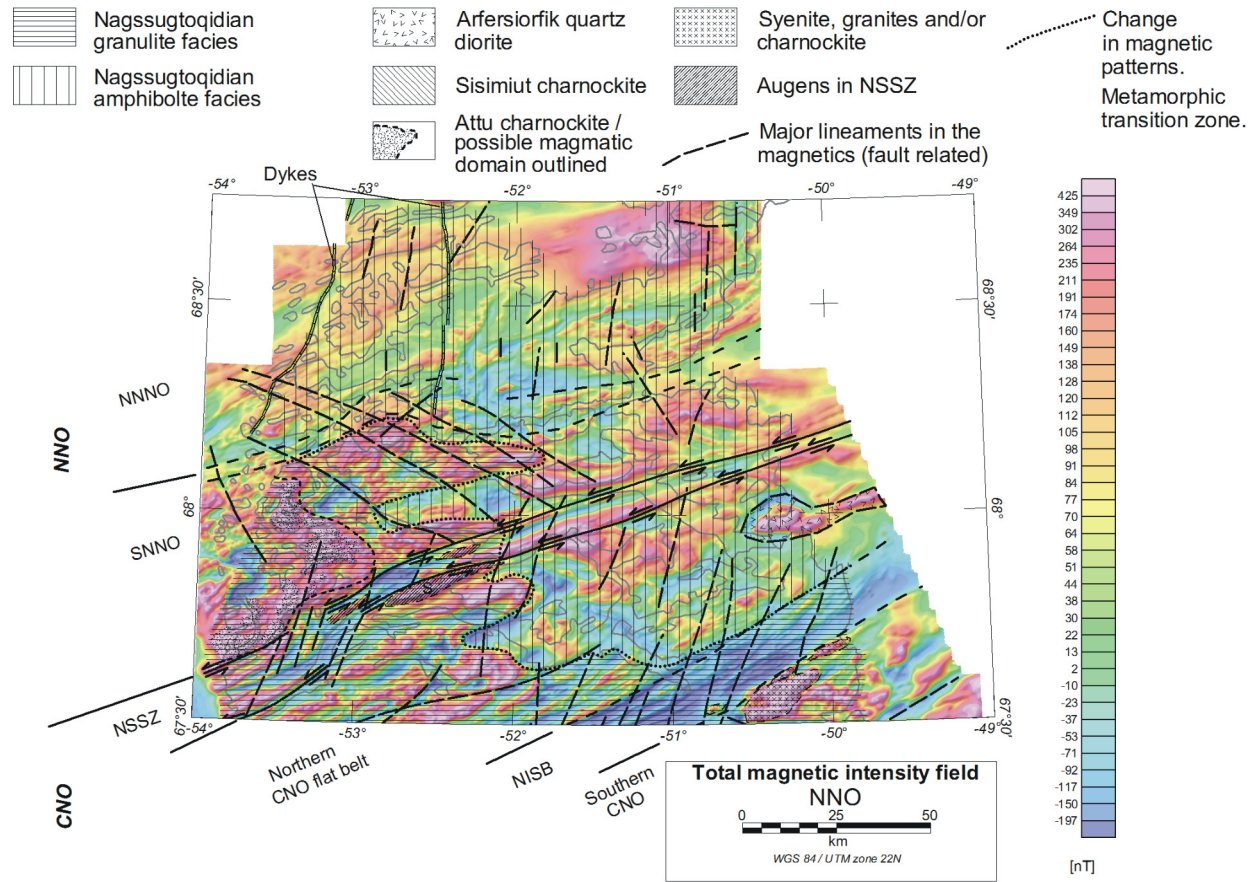


**Figure 51.** Metamorphic boundary and magnetic lineaments (possible fault related) for the NNO. The metamorphic boundary is gradual and Palaeoproterozoic penetrative deformation diminishes northward. The boundary between the southern and northern NNO (SNNO and NNNO) is marked by a shift in the magnetic patterns. The proposed Attu magmatic domain in the southwestern corner of the southern NNO is outlined. Features in the CNO are also included. For abbreviation used in the figure, please refer to Fig. 11.



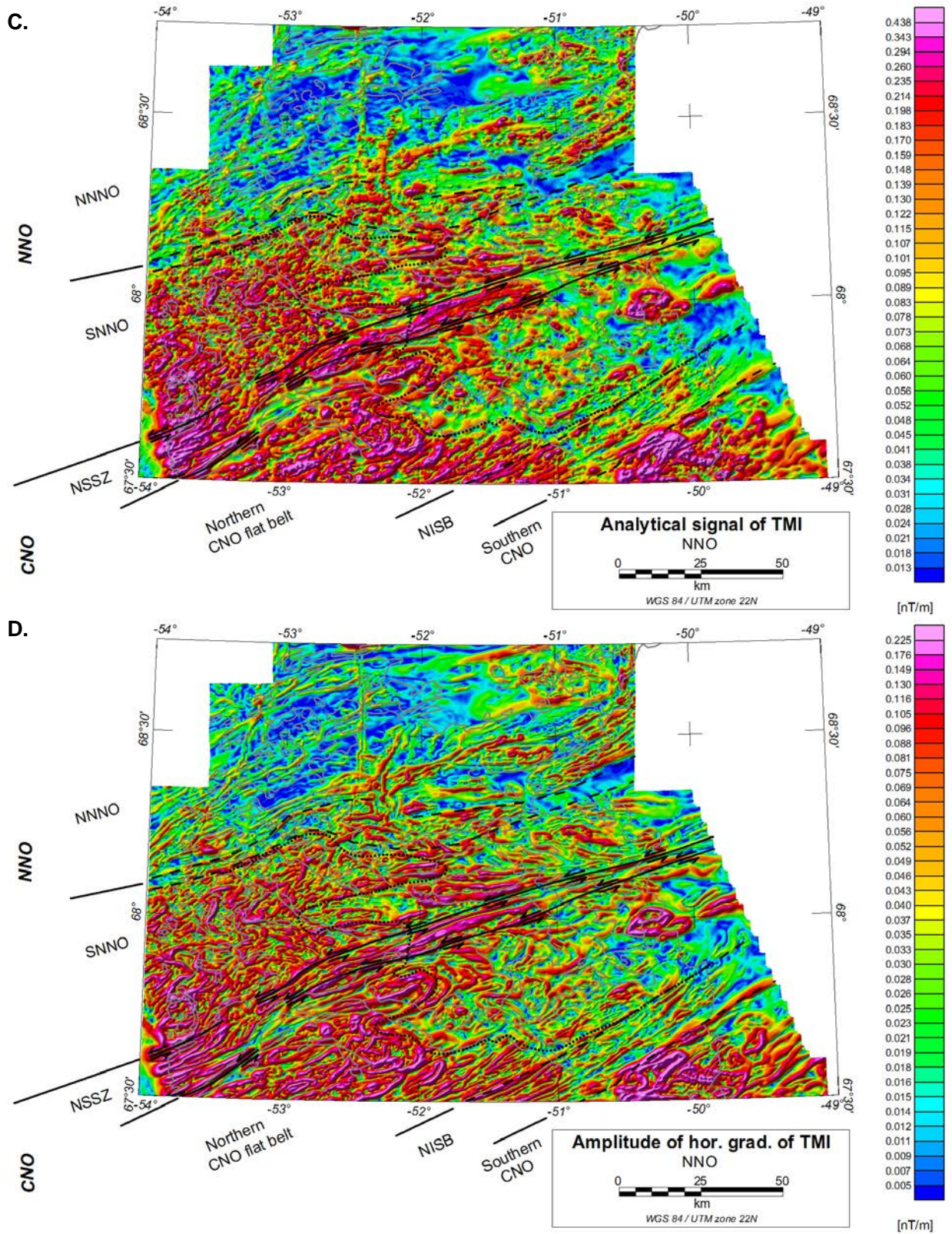


Fig. 52 Continued →

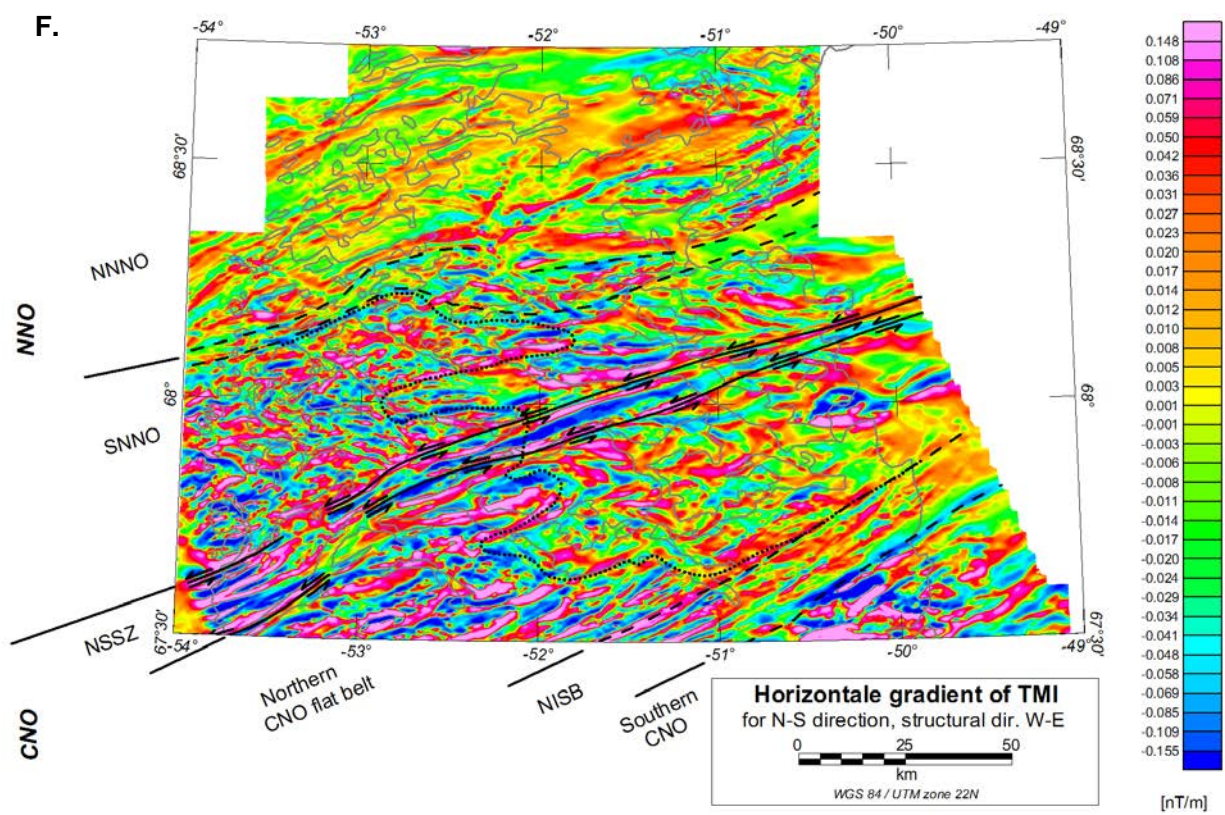
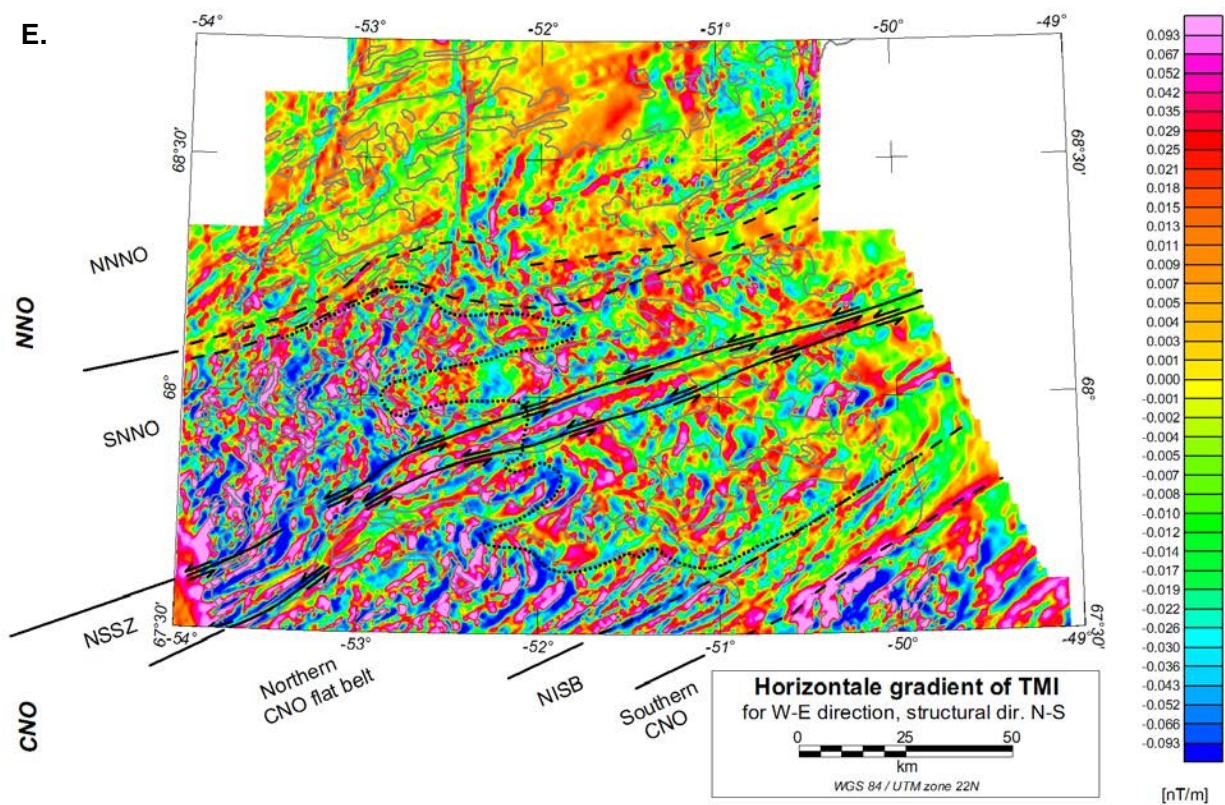


Fig. 52 Continued →

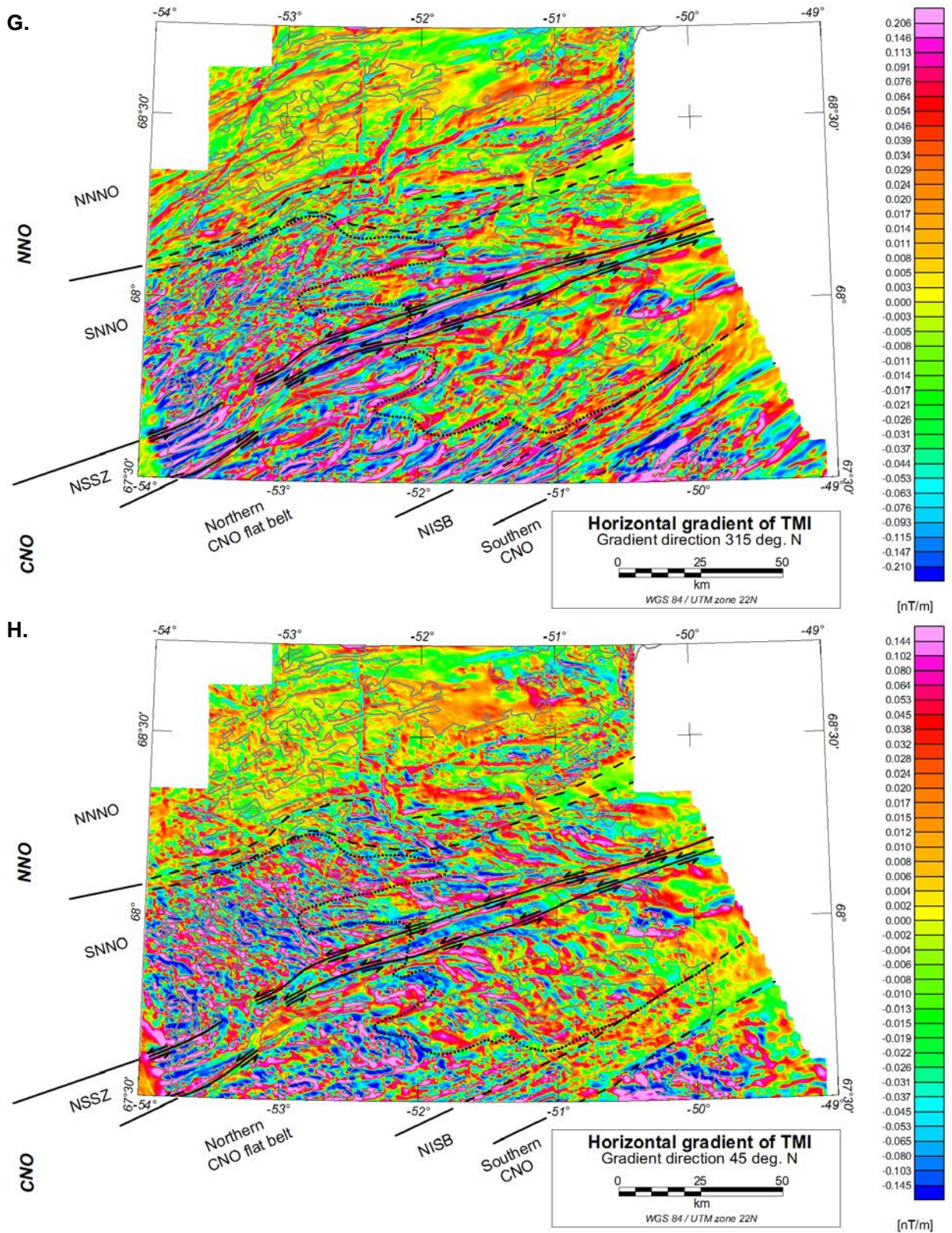


Fig. 52 Continued →

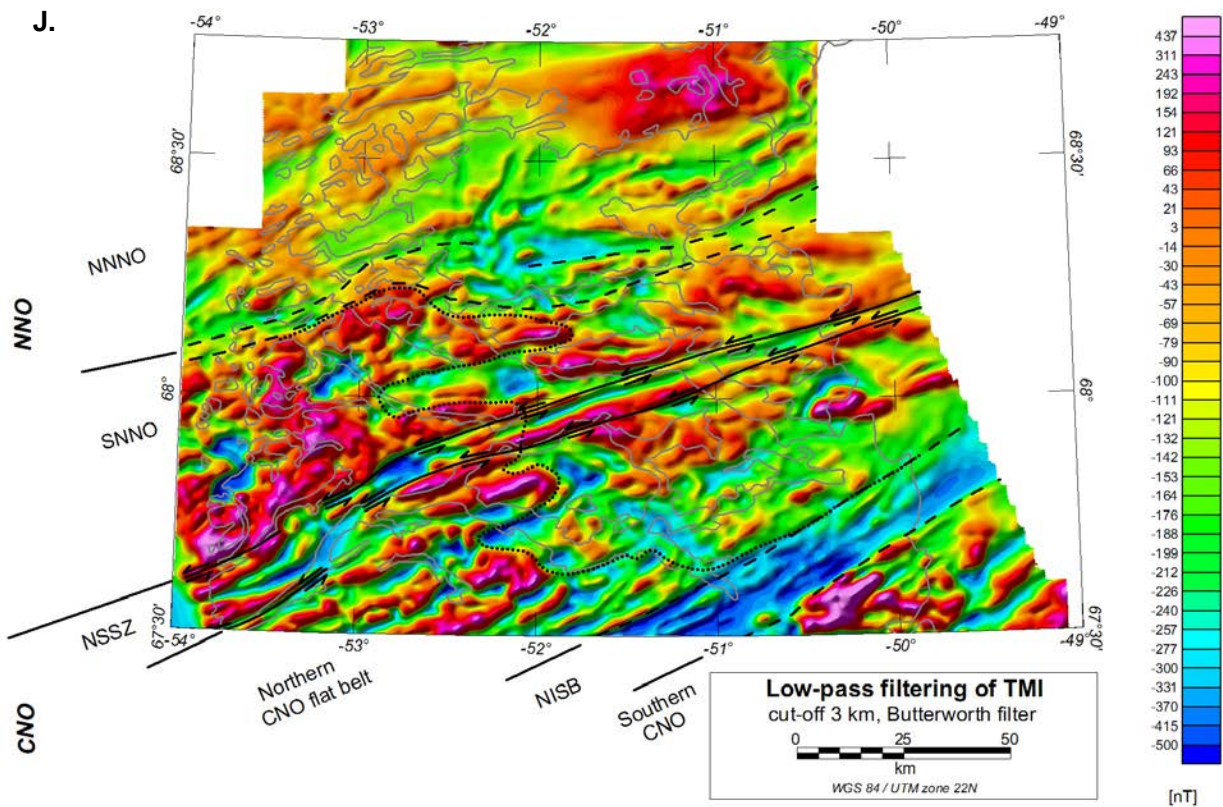
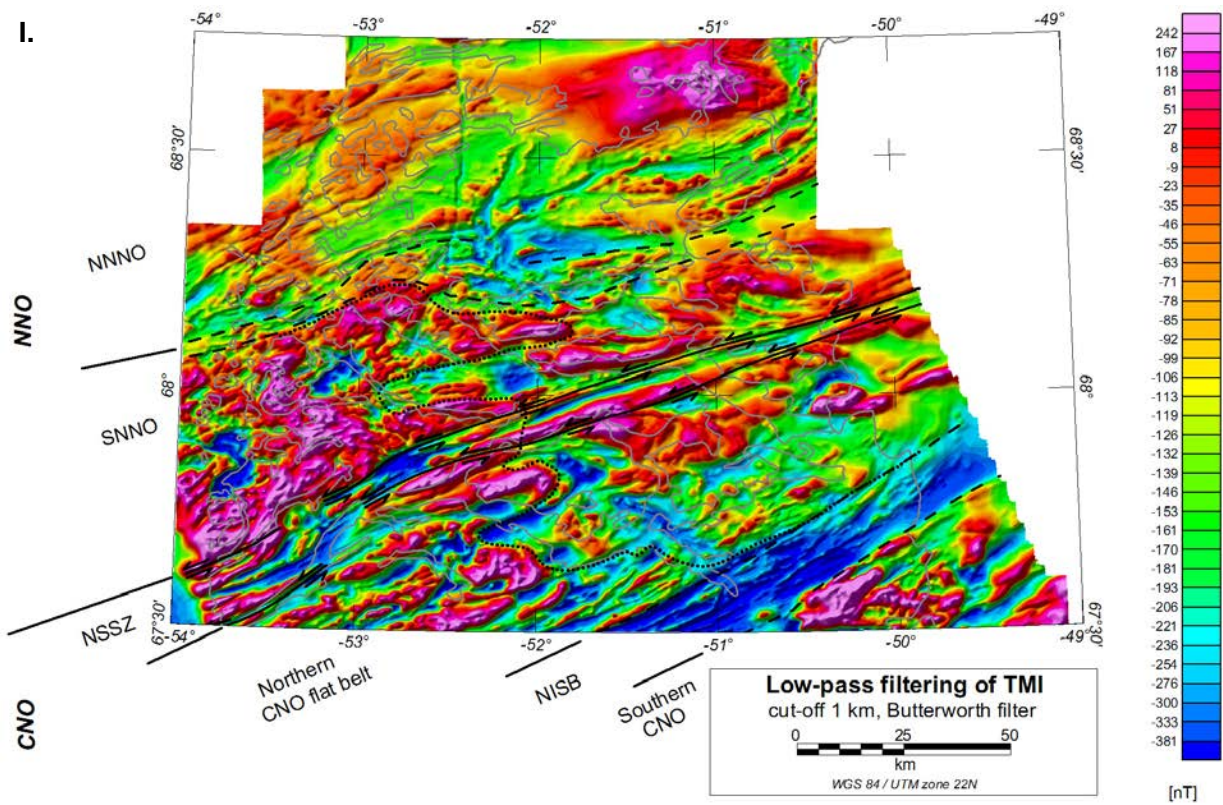
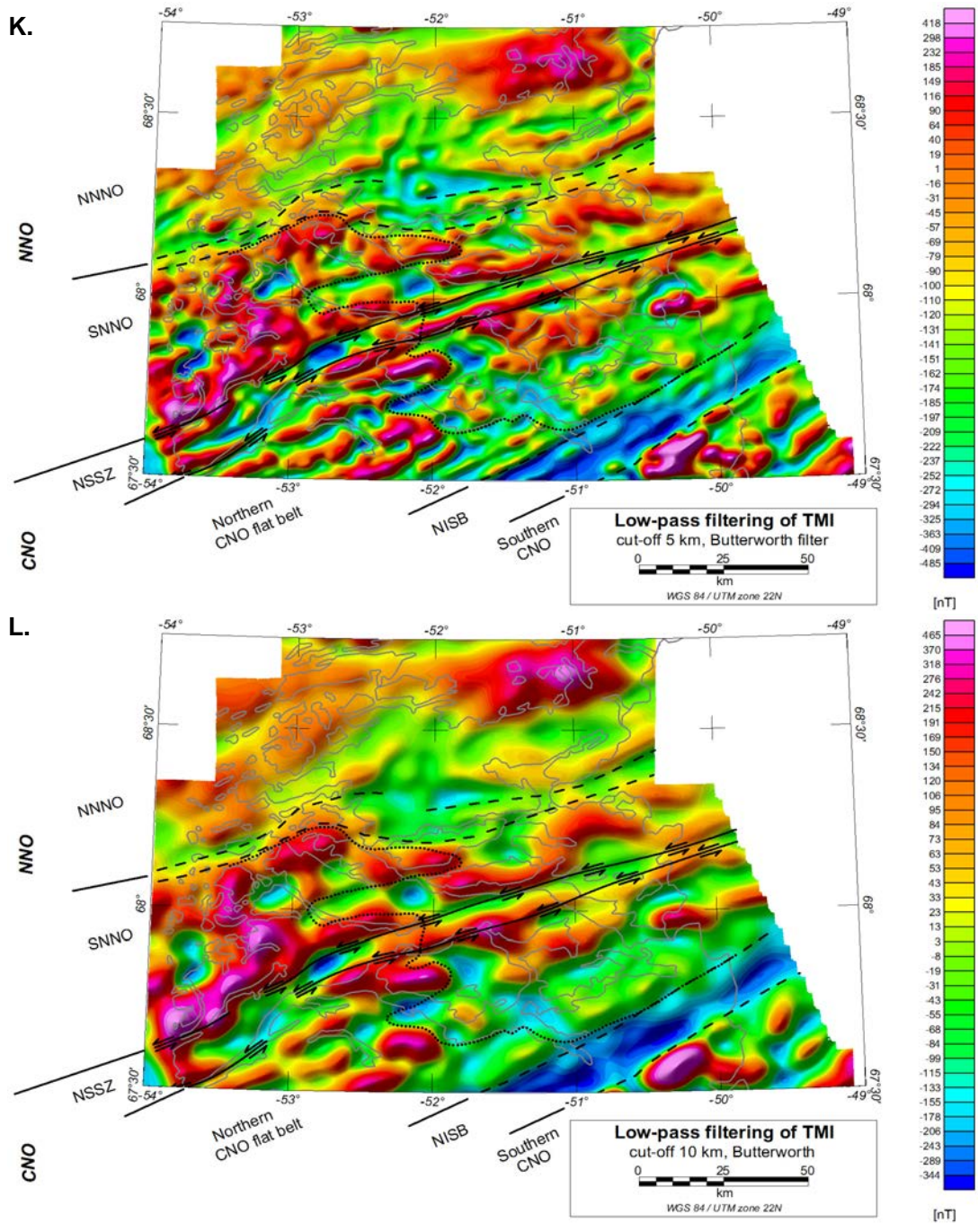


Fig. 52 Continued →



**Figure 52.** Maps showing processed data for the northern segment of the Nagssugtoqidian orogen (NNO). **A.** Total magnetic field intensity (TMI). **B.** Vertical gradient of TMI. **C.** Analytic signal of TMI. **D.** Amplitude of the horizontal gradient of magnetics (the square root of the sum of the squares of the derivatives in the x and y directions). **E.** Horizontal gradient of TMI calculated for W–E direction emphasising N–S structures. **F.** Horizontal gradient of TMI calculated for N–S direction emphasising W–E structures. **G.** Horizontal gradient of TMI calculated for the direction 315°N emphasising structures with a 45°N direction. **H.** Horizontal gradient of TMI calculated for the direction 45°N emphasising structures with a 315°N direction. **I., J., K.** and **L.** Low pass filtering of the TMI with a 1 km, 3 km, 5 km and 10 km as cut-off wavelengths respectively. For abbreviation used, refer to Fig. 11.

## Northern transition zone of the Nagssugtoqidian orogen

The area around and south of Kangersuneq fjord is denoted the Northern transition zone of the Nagssugtoqidian orogen (NTZ).

Sydostbugt (Fig. 11) is dominated by a broad positive magnetic anomaly with considerable amplitude. This anomaly has been interpreted to originate from one or several large intrusives at a depth of 1–2 km (Schacht 1992; Thorning 1993). Similar anomalies are observed north and northeast of Sydostbugt. This might indicate the presence of other intrusives. Especially the area north and east of Ilulissat contains a large positive anomaly. The N–S orientated anomaly in the southern part of Disko Ø with similar response as the above mentioned could also be an intrusive body. However, it can also reflect the uplifted Archean basement (Talbot 1979; Steenfelt 1994; Stendal *et al.* 1999; Steenfelt 2002). The outline of these intrusives is shown by both the Euler deconvolution results and source estimations based on the analytic signal (see Figs. 29, 30 and 36). The results suggest that the intrusives in the Sydostbugt continue beneath the area southwest of Kangersuneq fjord. Depth estimates from the Euler deconvolution are mostly around 1500 m to above 2000 m. This is in agreement with depths found by Schacht (1992).

The NTZ and southernmost Rinkian orogen is divided into smaller sub-domains that are described in the following in separate sections. The definitions of the sub-domains are based on the geophysical anomaly patterns. These sub-domains should not be regarded as confirmed tectonometamorphic domains even though they possibly represent different crustal levels, lithologies, and degrees of tectonic and thermal reworking. The sub-domains, with names taken from major place-names, are the Akiamiut domain, the Orpissuup Nunaa domain and the Kangilinaaq domain (Fig. 53.A).

The observed linear features bounding the sub-domains are related to faults or shear zones. In the NTZ, the shearing is concentrated along the limbs of large-scale folds. Based on the magnetic pattern the structures in the western part of the NTZ can be extended to the western part of the northern NNO.

### **Akamiut domain – continuation of the Northern NNO**

Trends in the anomaly pattern (Figs. 53.B, 53.C, 53.F and 53.I) and large-scale domains with similar magnetic variations (Figs. 53.B, 53.H, 53.K, 53.L and 53.M) suggest that the eastern part of the NTZ constitute a continuation of the NNO. This domain is denoted Akiamiut domain (Figs. 52 and 53.A). The pronounced E–W trend of the magnetic anomalies in the NNO swings into a more northern trend in the southern part of Akiamiut, but swings around into a more NNW to WNW orientated trend again in the northern part of the Akiamiut domain. To the west the domain is characterised by an abrupt change in magnetisation from low magnetisation in the formerly described eastern part of the NTZ to more magnetised conditions to the west (Figs. 53.A and 53.B). The central western part of the domain is dominated by some low amplitude anomalies. These reflect an amphibolite rich supracrustal sequence in this area. A N–S orientated short-wavelength anomaly in the middle of the domain (Figs. 53.A, 53.C, 53.Q and 53.R) correlates with a 15 to 20 m thick vertical dolerite dyke.

The area north of the peninsula north of Kangersuneq fjord is interpreted to be a part of the Akiamiut domain and many of the NNW–SSE orientated structures in this area continues eastward into structures located in the Akiamiut domain. A pronounced low magnetic lineament is situated in the Tasiusuaq fjord. This lineament delineates a possible fault zone that continues northeastward and bends to the north into Jakobshavn Isfjord or the north orientated fjord north of Jakobshavn Isfjord.

### **Orpissuup Nunaa domain**

A large vertical fold dominates the Orpissuup Nunaa domain. The northern limb of the fold is parallel with a pronounced magnetic ESE–WNW orientated lineament, which reflect a shear zone. In addition, the southern limb is characterised by a low magnetic lineament, which can be related to another mapped shear zone (J.A.M. van Gool, GEUS, personal communication, Sep. 2003). This domain is denoted the Orpissuup Nunaa domain. The southwestern corner of the Sydostbugt is dominated by a broad high anomaly (Fig. 53.H and 53.K), which, as described in the former sections, outlines an intrusive body. The anomaly continues beneath the Orpissuup Nunaa domain and in the outer and central part of the Kangersuneq fjord. In the outer part of Kangersuneq fjord a coarse-grained porphyritic granodiorite with a weak foliation granite and a high content of magnetite was found during fieldwork. This suggests that the intrusive in the Sydostbugt could be granodioritic. However, other common highly magnetised intrusive lithologies in the area such as ultramafic to mafic rocks have been found. Though, observations in the Rodebay domain (Garde & Steenfelt 1999a, will be described separately later) north of Jakobshavn Isfjord, which have similar anomalies as the one in Sydostbugt and is dominated by a coarse-grained porphyritic granodiorite, is in support for a granodioritic composition of the intrusives in Sydostbugt. The northern shore of Kangersuneq fjord is characterised by a marked change in magnetisation. The change in magnetisation is associated with a mylonitic shear zone.

### **Kangilinaaq domain**

The peninsula north of Kangersuneq fjord is low magnetised (Fig. 53.B) reflecting the supracrustal belt that dominates the peninsula. This domain is denoted Kangilinaaq domain. The lineaments bounding the Kangilinaaq domain and the change in magnetic pattern can be followed offshore into the Sydostbugt and further west. Consequently, it is interpreted that the supracrustal belt continues westwards and can be linked with the supracrustal rock units at Ikamiut and Aasiaat. The trends of the magnetic patterns in the eastern part of the Kangilinaaq domain change from a NW direction into a northerly direction. To the north is the low magnetised Kangilinaaq domain again characterised by an abrupt change to higher magnetic responses. As well as reflecting a change in lithology to orthogneisses north of the peninsula, the boundary also defines a WNW–ESE orientated fault zone that can be followed as a low magnetised lineament (Figs. 53.B and 53.C).

## **The southernmost part of the Rinkian orogen**

The described tectonometamorphic domains for the southernmost part of the Rinkian orogen (Garde & Steenfelt 1999a) is evident in the magnetic patterns. However, some adjustments and refinements can be made from the potential field data.

### **Nunatarsuaq domain**

The Nunatarsuaq domain shows lithological and structural dissimilarities with the neighbouring Rodebay domain. The deviations and proposed boundaries of the Nunatarsuaq domain are difficult to recognize in the magnetics; conversely, it is not possible to link structures in the one domain with structures in the neighbouring domain. A small decrease in magnetisation (Fig. 53.B) is observed at the northern fjord branch of the Jakobshavn Isfjord, which might represent the western boundary of the domain, but the decrease could also reflect a topographic effect due to the fjord. Towards the north, anomalies similar to those in the Rodebay domain are observed (Figs. 53.Q and 53.R). Low-pass filtering of the magnetic field (Figs. 53.H, 53.K and 53.Q) suggests that the intrusive Rodebay granodiorite possibly continues beneath the Nunatarsuaq domain. The folded Archaean supracrustal rocks in the northern part of the domain are recognized in the magnetic pattern (Fig. 53.C).

### **Rodebay domain**

The Rodebay domain is characterised by broad strong magnetic anomalies (Fig. 53.B). These anomalies reflect the Archaean Rodebay granodiorite. Beside two NE-orientated magnetic lineaments in the southern part of the Rodebay domain (Figs. 53.C and 53.G), which reflects tectonic slices of supracrustal rocks with sheared boundaries (Garde & Steenfelt 1999a) are the lineaments in the domain NW-orientated and related to faults and shear zones. The faults could be related to post-compressional relaxation.

In the central part of the Rodebay domain is the late vertical ESE–WNW-trending Paakitsoq ductile shear zone situated (Knudsen *et al.* 1988; Escher *et al.* 1999; Garde & Steenfelt 1999a). The shear zone is evident as a couple of low magnetised lineaments (Figs. 53.C, 53.J and 53.Q) that can be traced from the Inland Ice to Arveprinsen Ejland. The shear zone has been suggested to be the boundary between the Nagssugtoqidian orogen and the Rinkian orogen (Escher & Pulvertaft 1976). No support, such as abrupt changes in the potential field data or prominent features in the stripping filtered responses, is observed in potential field data.

Proterozoic basic dykes and sills in the central northern part of the Rodebay domain are evident as short wavelength (compared with the broad anomalies from the granodiorite) highly magnetic elongated or small rounded anomalies (Figs. 53.B, 53.D, 53.E and 53.Q).

The high amplitude broad anomalies in the northern part of the Rodebay domain, especially in the northeastern corner of the domain are interpreted to reflect lithologies similar to the Rodebay granodiorite, which are in agreement with the chemical composition of gneisses from this area (Garde & Steenfelt 1999a). Judged from the anomaly pattern of the TMI, it is apparent that the Rodebay granodiorite also continues to Arveprinsen Ejland, especially south of the Paakitsoq shear zone. The lower magnetised area just north of the Paakitsoq

shear zone in the central part of the Rodebay domain (Figs. 53.B, 53.H and 53.K) is interpreted to originate from 'normal' orthogneisses. This low magnetised zone, with Proterozoic basic dykes and sills, appears to continue eastward to Arveprinsen Ejland (Fig. 53.N) and can perhaps be related to an orthogneiss block within the Rodebay granodiorite domain.

### **Ataa domain**

The Ataa domain is generally low magnetised and is characterised by magnetic anomaly patterns without abrupt changes and pronounced lineaments (Figs. 53.A and 53.B). The gentle variations of magnetic field reflect the described lower degree of deformation (Garde & Steenfelt 1999a) compared to the domains to the south.

The Archaean Arveprinsen–Eqi supracrustal rocks (c. 2800 Ma, Kalsbeek & Skjerna 1999) and the Proterozoic Anap Nunâ supracrustal group can be followed and distinguished in the magnetics as belts of high and low magnetic elongated short wavelength anomalies reflecting the different lithologies within the supracrustal rocks (Figs. 53.B, 53.C and 53.Q). The basal unconformity separating the supracrustal sequences is visible in the magnetics as an abrupt change from high magnetisation in Proterozoic supracrustal rocks from the Anap Nunâ group to lower magnetised Archaean supracrustal rocks. The crescent-shaped supracrustal belt from Egi to Arveprinsen Ejland is visible in both the magnetics (Figs. 53.C and 53.Q) and the Bouguer anomaly field (Fig. 53.S). Arveprinsen Ejland and adjacent areas are the only areas with sufficient density of the gravity stations to allow local structures to be investigated by use of the gravity data.

The Ataa domain continues eastward under the Inland Ice (Figs. 53.L and 53.N). The Atâ tonalite (c. 2800 Ma, intruded in Arveprinsen–Eqi supracrustal rocks, younger than the surrounding orthogneiss and cut by c. 2740 Ma granotoid rocks, Kalsbeek *et al.* 1988; Nutman & Kalsbeek 1999) located in the northern part of Arveprinsen Ejland is characterised by low magnetisation and low density. A continuous linear magnetic anomaly in the eastern part of the domain can be related to a mapped 1645 Ma Proterozoic undeformed dolerite dyke (Kalsbeek & Taylor 1986), which continues for more than 400 km northwards. A similar pronounced lineament is located beneath the Inland Ice and is interpreted to be caused by a dolerite dyke.

A. – part 1

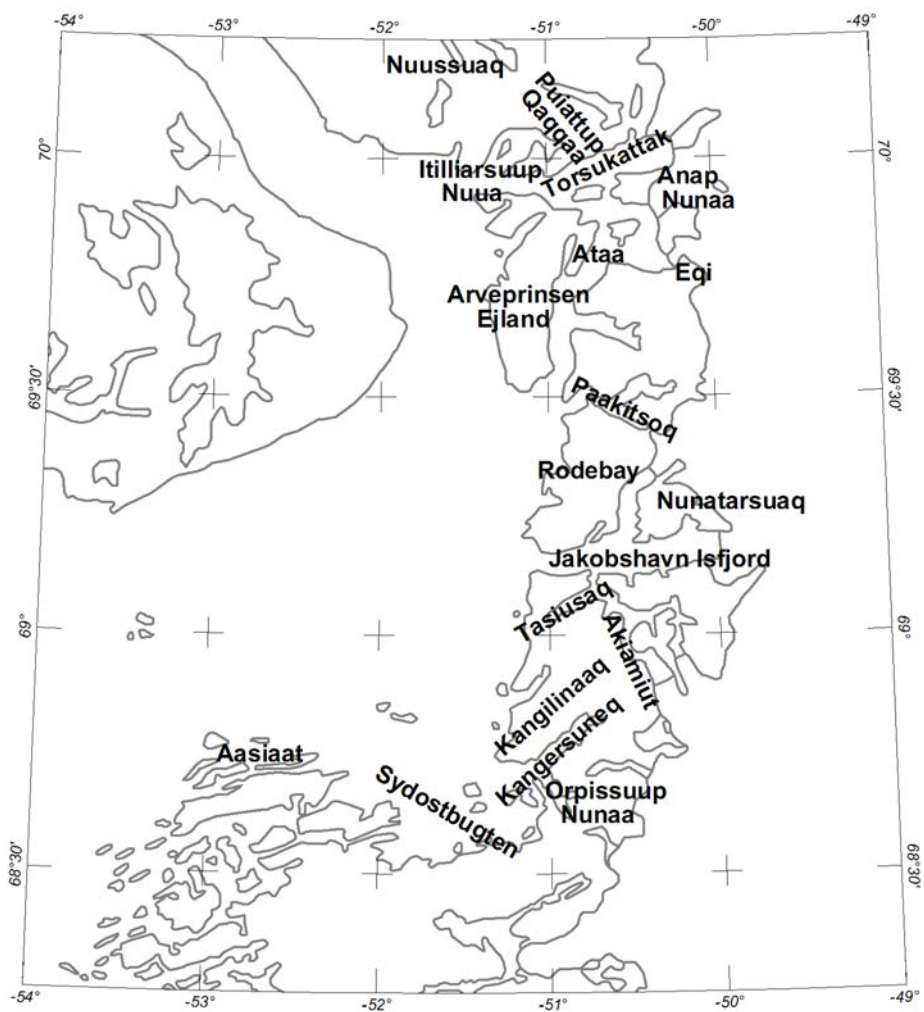


Fig. 53 Continued →

A. – part 2

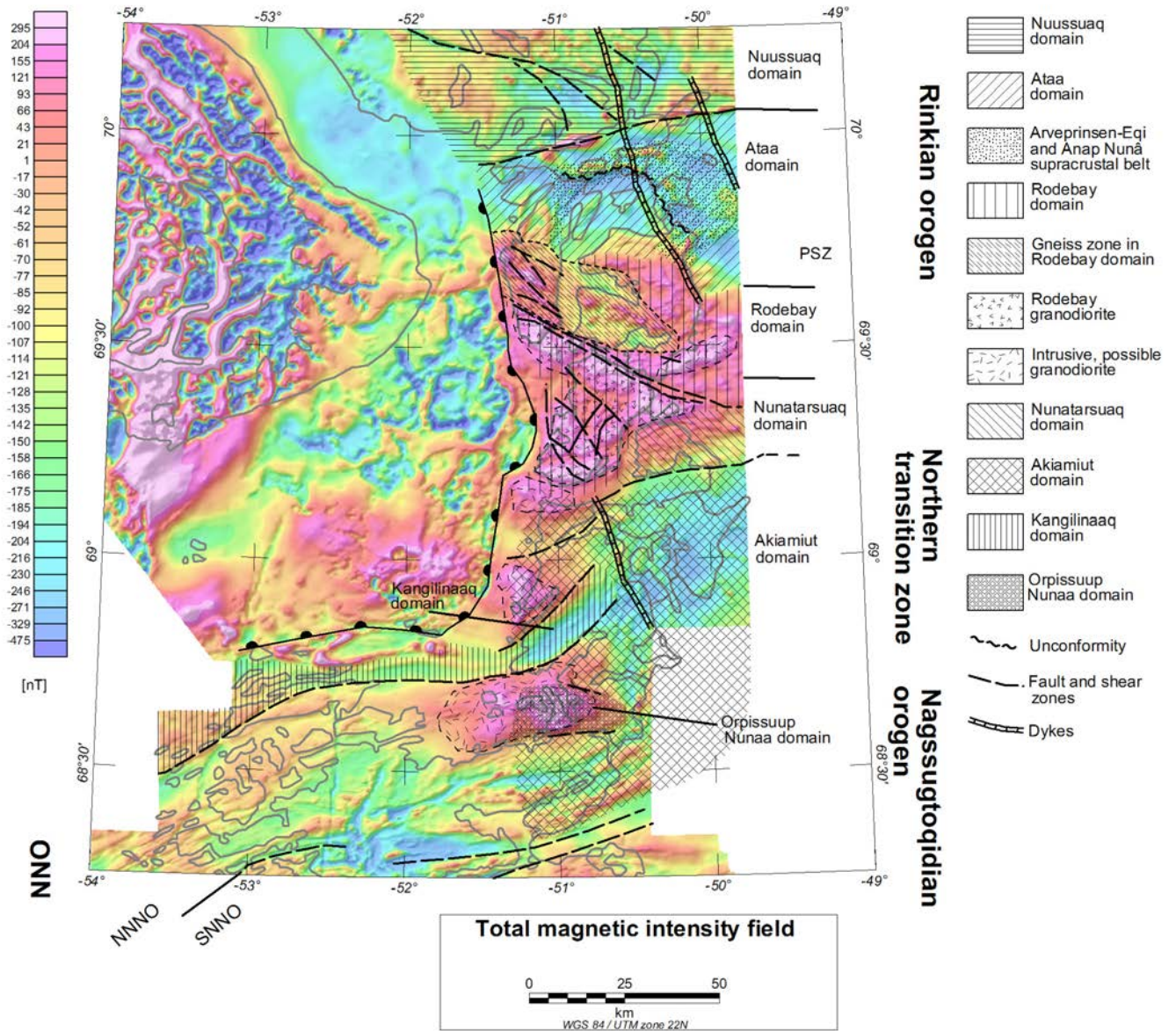


Fig. 53 Continued →



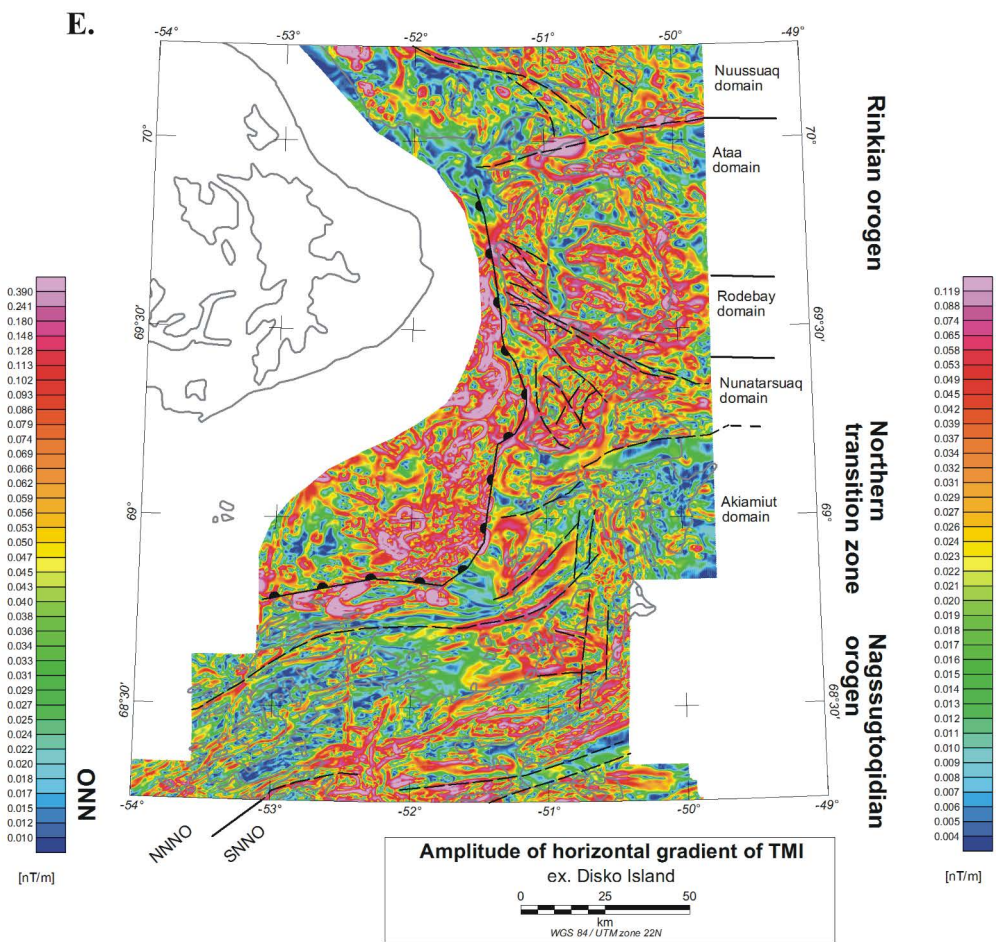
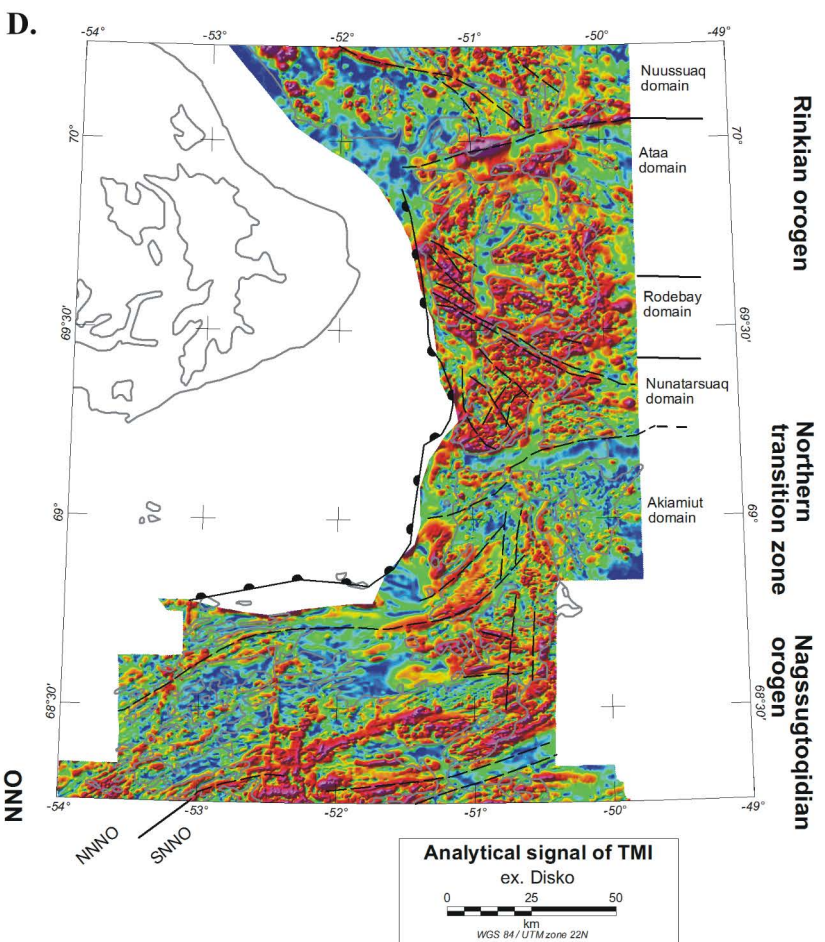


Fig. 53 Continued →

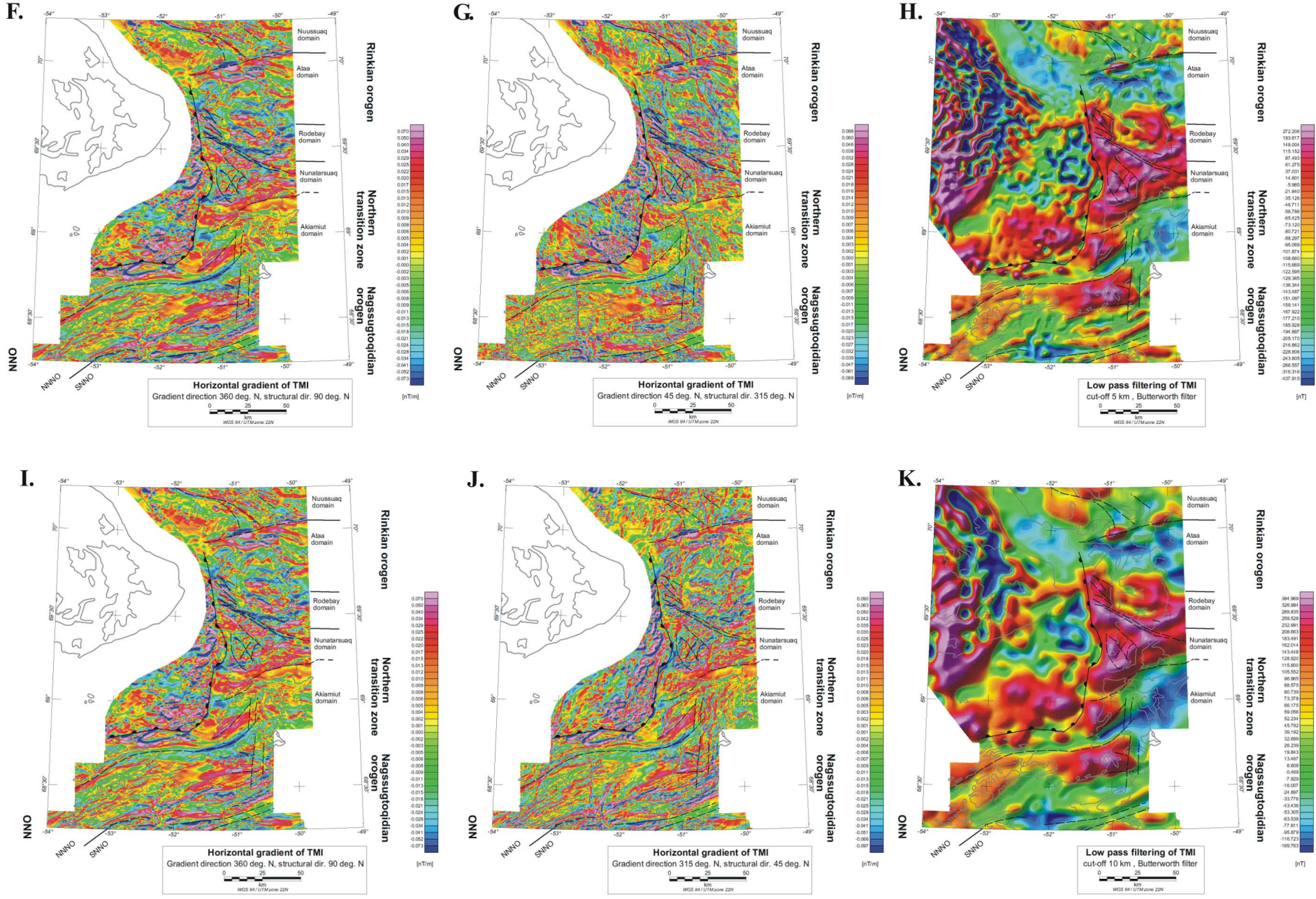


Fig. 53 Continued →

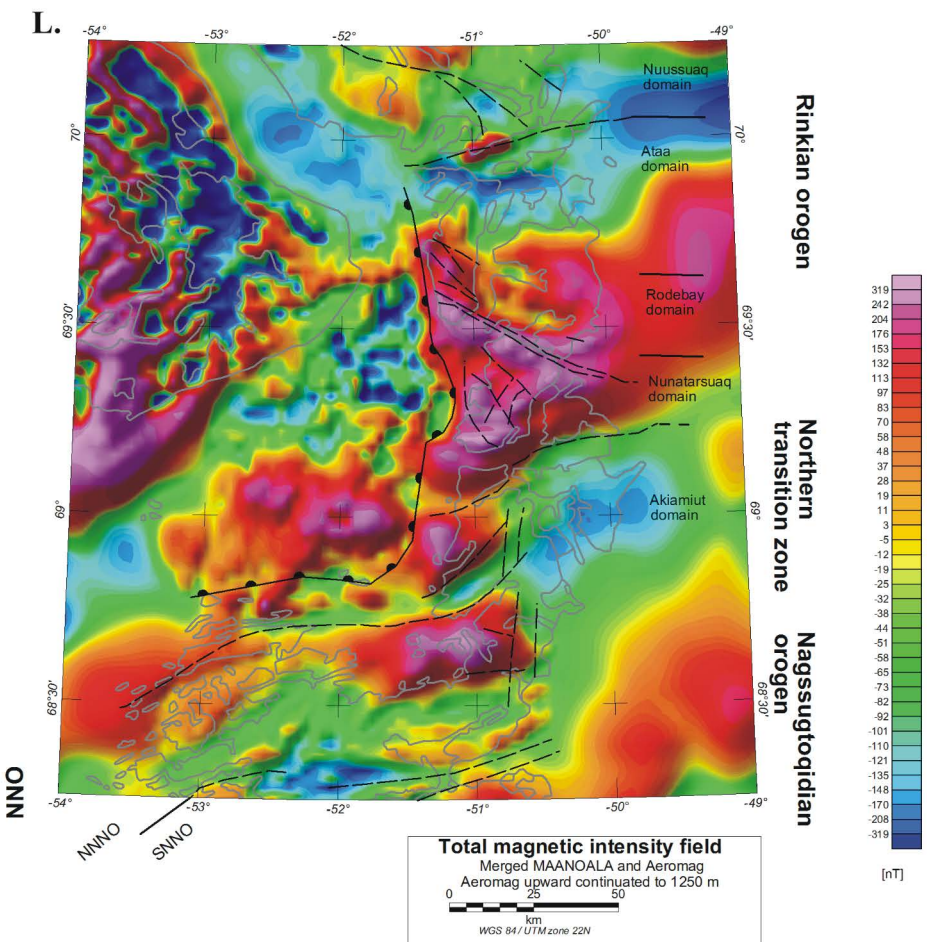
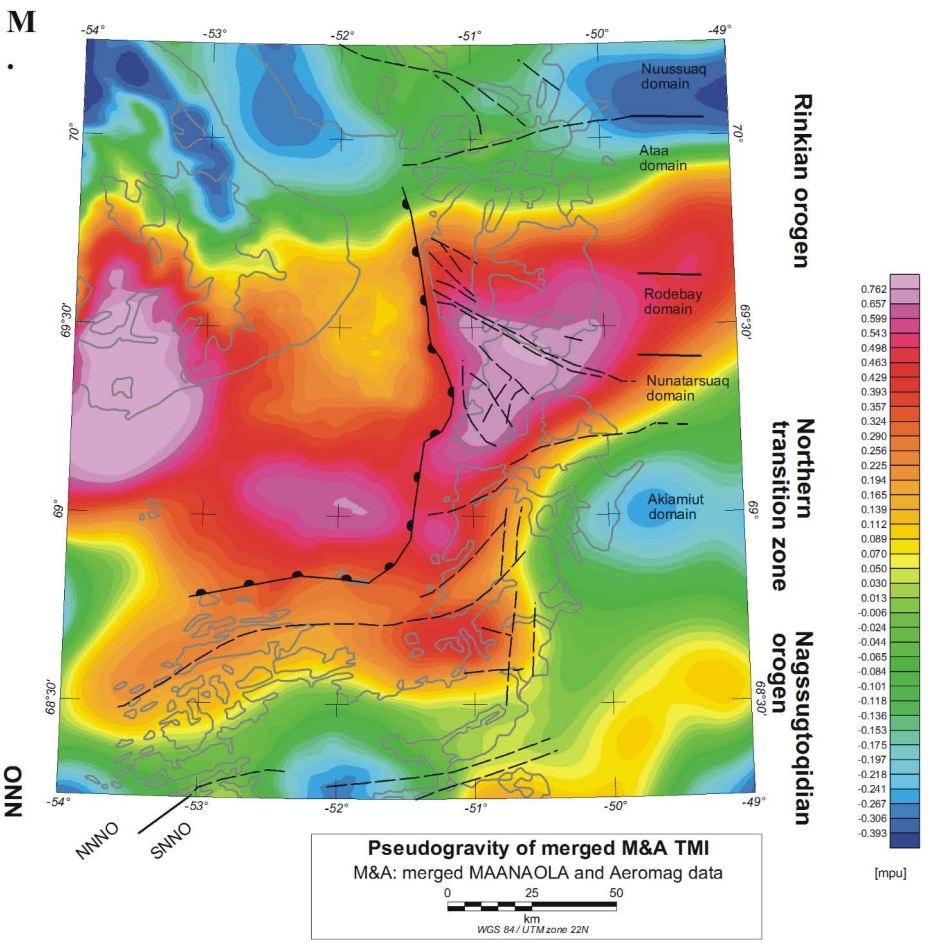


Fig. 53 Continued →

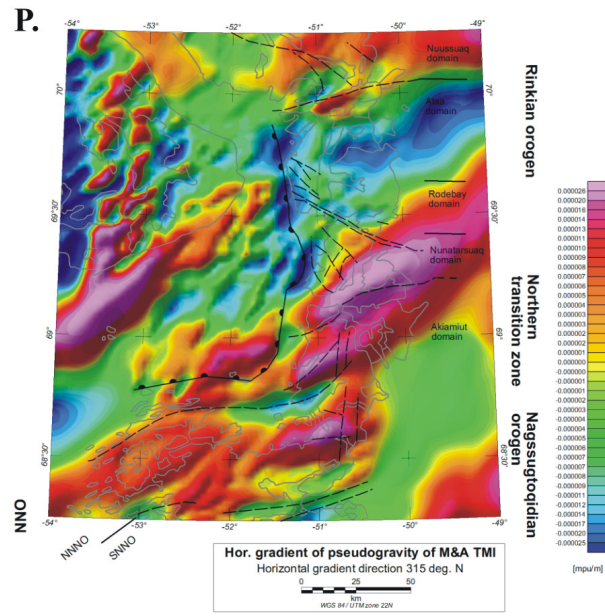
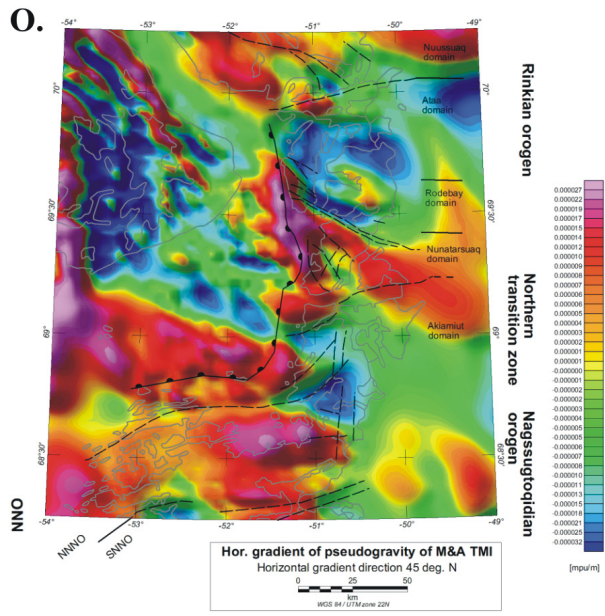
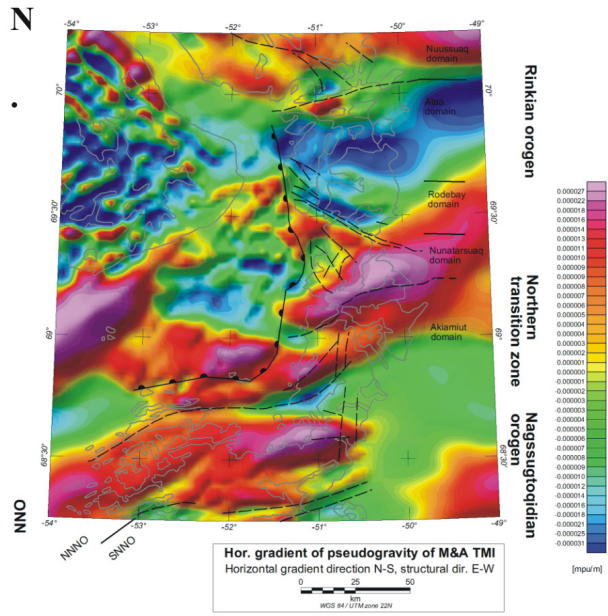


Fig. 53 Continued →

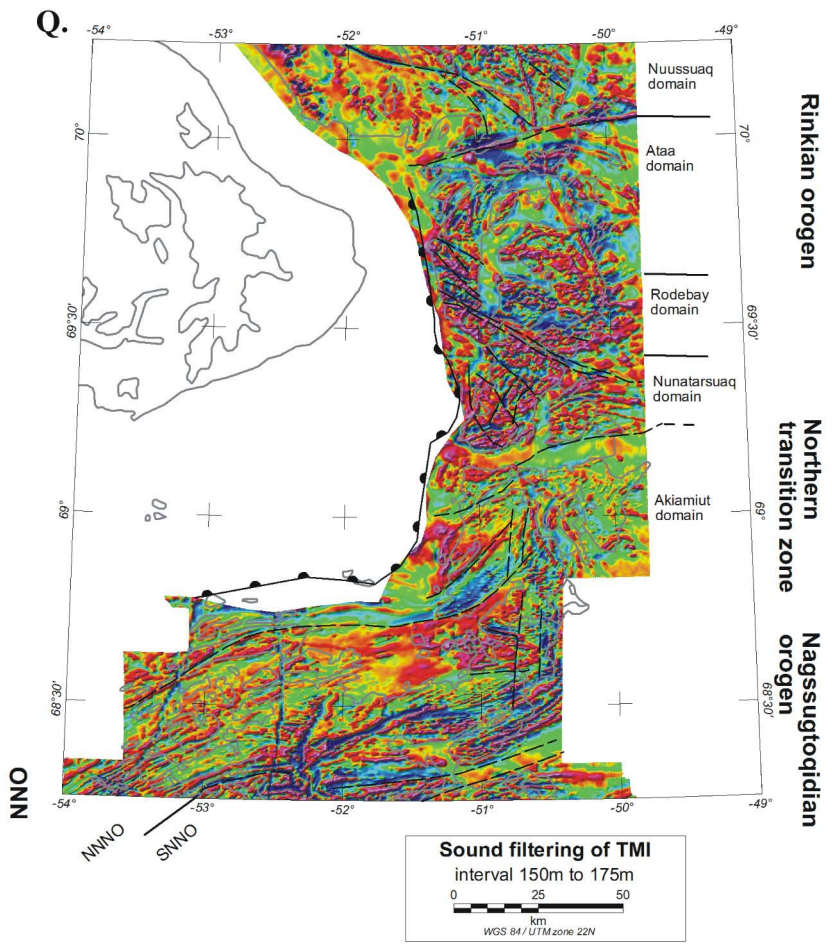
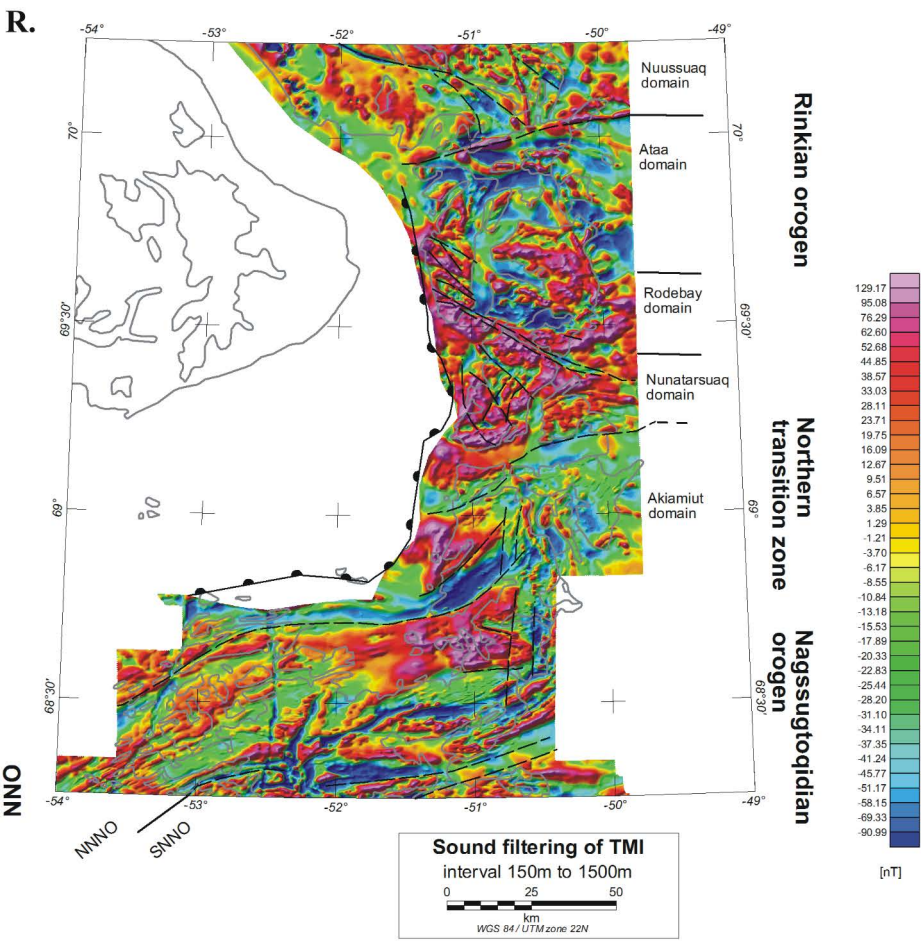
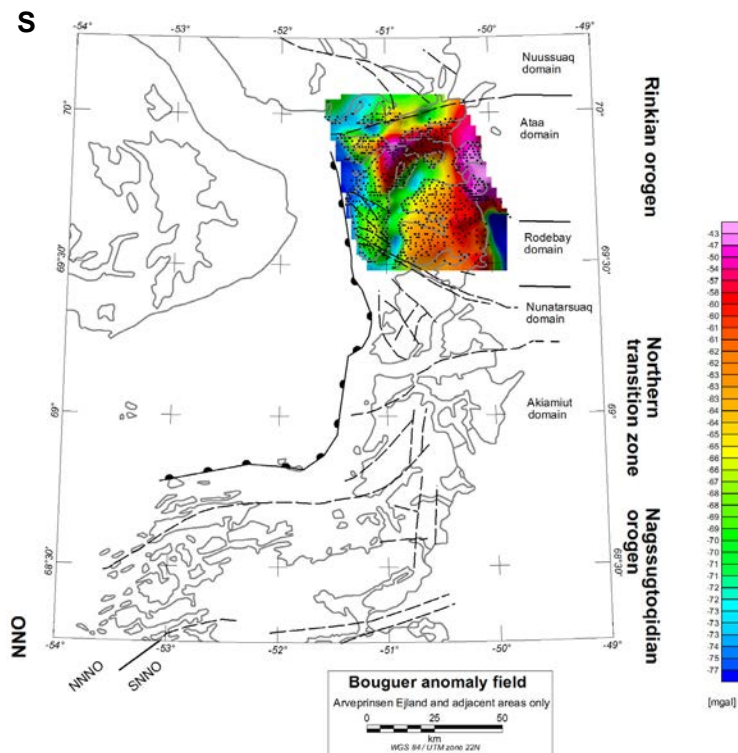


Fig. 53 Continued →



**Figure 53. A.** Interpretations drawn on top of the total magnetic field intensity showing the different domains, boundaries, and magnetic lineaments (possible fault or shear zone related) in the northern transition zone of the Nagssugtoqidian orogen (NTZ) and the southernmost Rinkian orogen. A map with the geographic names used in the text is also given (part 1 of A.). **B.** Total magnetic field intensity (TMI). **C.** Vertical gradient of TMI. **D.** Analytic signal of TMI. **E.** Amplitude of the horizontal gradient of magnetics (the square root of the sum of the squares of the derivatives in the north and east directions). **F.** Horizontal gradient of the TMI calculated for E direction emphasising N–S directed structures. **G.** Horizontal gradient of TMI calculated for N direction emphasising W–E structures. **H.** Horizontal gradient of TMI calculated for the direction 45°N emphasising structures with a 315°N direction. **I.** Horizontal gradient of TMI calculated for the direction 315°N emphasising structures with a 45°N direction. **J.** and **K.** Low pass filtering of the TMI with 5 km and 10 km as cut-off wavelengths respectively. **L.** Total magnetic intensity of merged MAANAOALA and Aeromag (Aeromag data is upward continued to 1250 m, which is the average measurement height of the MAANAOALA data, before the data was merged). **M.** Pseudogravity of the merged Aeromag and MAANAOALA TMI. **N.** Horizontal gradient of the pseudogravity of merged TMI calculated for the direction 0°N enhancing structures with a 90°N orientation. **O.** Horizontal gradient of the pseudogravity of merged TMI calculated for the direction 45°N enhancing structures with a 315°N orientation. **P.** Horizontal gradient of the pseudogravity of merged TMI calculated for the direction 315°N enhancing structures with a 45°N orientation. **Q.** Sound filtering of TMI, depth interval from 150 m to 175 m. **R.** Sound filtering of TMI, depth interval from 150 m to 1500 m. **S.** Bouguer anomaly field for Arveprinsen Ejland and adjacent areas in the Ataa domain. Only this area is considered for detail interpretations as the resolution of the gravity field in other areas only allow regional interpretations. The black dots represent gravity stations.

### **Nuussuaq domain**

The metamorphic low facies Ataa and metamorphic higher facies Nuussuaq domain are described as being separated by a major late oblique extensional shear zone characterised by intense SE-plunging extension fabric; the Torsukattak shear zone (Garde & Steinfeldt 1999a). Unpublished age data on acid volcanic lithologies from Itilliarsuup Nuua yield Archaean ages (K. Thrane and A.A. Garde, personal communication, Sep. 2003).

No marked change in the patterns or lineaments in the potential field data are associated with the Torsukattak shear zone. Nevertheless, the possible presence of a tectonic boundary cannot be rejected based on the potential field data; the fjord and thereby larger distances to the sources attenuates the magnetic field and the identification of a shallow dipping structure in the potential field data is problematic.

From the magnetics (Figs. 53.C and 53.Q) it is likely that the supracrustal belt in the Ataa domain continues across the Torsukattak fjord. However, the gravity data outlines the supracrustal rocks in the Ataa domain (Figs. 53.S) and display no support for a possible connection between the supracrustal rocks north and south of Torsukattak fjord. This observation is in agreement with the described differences in metamorphic facies, lithologies of supracrustal rocks and age. Discrete elongated or rounded high magnetic anomalies (Figs. 53.A, 53.B and 53.Q) in the supracrustal belt at Itilliarsuup Nuua are interpreted to originate from metagabbro and banded iron formations. From the magnetics the occurrence of supracrustal rocks can be extended eastwards. Several high magnetic discrete anomalies similar to those at Itilliarsuup Nuua are seen.

Beside the Torsukattak shear zone is a major NW–SE orientated shear zone located in the middle part of the domain; the Puiattup Qaqqaa shear zone (Garde & Steinfeldt 1999a). The shear zone gives rise to a compressional flower structure, with opening to the south. The boundaries and internal structures are expressed in the magnetics (Figs. 53.C, 53.J and 53.Q). The width of the shear zone narrows towards northeast and from the magnetics it is interpreted that the zone merge into a single thin low magnetised lineament that continues further towards west.

### **Mesozoic sedimentary basins**

The transition from the continental part of the crust to the oceanic part is seen as a sharp transition from a high Bouguer anomaly over the oceanic crust to a low Bouguer anomaly over the continental parts of the region (see Fig. 40). An anomalous low Bouguer and Free Air anomaly (see Fig. 42) is seen offshore between Nordre Strømfjord and Nordre Isortoq. A Mesozoic sedimentary basin causes this anomaly. A clear change in the magnetic patterns exists from the basement to the Mesozoic basins (Chalmers *et al.* 1998) in the Disko Bugt (Figs. 53.A and 53.B). Several magnetic anomalies within this basin can be related to sills and dykes from Tertiary activities. The faulting, separating the Cretaceous–Tertiary basin from the basement, are seen by W–E and N–S orientated lineaments in the southern and eastern part of the Disko Bugt.

## Conclusions

By analysis and interpretation of the processed geophysical data the major tectonic features, domains and characteristics for central West Greenland are delineated and interpreted. The results and interpretations can be used as input to the geological models for the region. The unravelled tectonic features are generally in good agreement with the model involving a full Wilson cycle as presented by van Gool *et al.* (2002) for the Nagssugtoqidian orogen. Some of the main conclusions are given below.

The geological domains based on geological data are in agreement with the main domains interpreted and outlined by the geophysical data. The main domains are characterised by distinct anomaly patterns and the boundaries of the domains are reflected as marked changes in the field variations. The differences between the domains are enhanced by use of different processing techniques. Both differences in lithologies, structures, metamorphic facies, and deformation phases across the boundaries of the domains are interpreted by use of the processed geophysical data. The subdivisions of the main domains are also reflected in the geophysical data.

The southern boundary of the Nagssugtoqidian orogen, the SNF, is found to be a very pronounced feature in the magnetic and gravity fields. The SNF is seen as a major regional feature and the boundary is interpreted to continue to great depths. It is interpreted that the SNF is associated with the collision in the Nagssugtoqidian orogen. Gravity data indicate that the crust of the region south of the front is thickened. The southern foreland is characterised by a high density of faults with main directions NNW–SSE to NW–SE. These faults are at high angles to the SNF.

The middle and eastern part of the SNO is dominated by low magnetic responses, reflecting the persistent reworking under retrograde amphibolite facies. A large granodiorite body marked by low Bouguer anomaly and a magnetic low is located in the southwestern corner of the middle SNO. Different deformation phases are also reflected in the magnetics. The magnetic patterns of the western part of the SNO resemble the patterns observed in the southern foreland. The western SNO is furthermore characterised by a high density of lineaments that are interpreted as fault zones. Two distinct E–W orientated shear zones are observed as well.

The magnetic field associated with the CNO is dominated by a distinct segmentation, which reflects the different geological sub-domains of the CNO. The major tectonic features, the Ikertôq thrust zone and the Nordre Strømfjord shear zone, stand out as very pronounced zones in the magnetics. The Ikertôq thrust zone is in the magnetics characterised by several lineaments, possibly reflecting panels of supracrustal rocks or thrust faults. The Ikertôq thrust zone is furthermore defined by a change in the Bouguer anomaly field. From the potential field data is the Ikertôq thrust zone interpreted to be a deep-seated zone. From the magnetics, large 'augen' structures with less deformed lithologies can be deduced in the Nordre Strømfjord shear zone. The possible linking of the 'augen' structures with other structures can be used to constrain the displacement of the shear zone. In the southern CNO the Sisimiut charnockite suite can be outlined from the aeromagnetic data. The central CNO is characterised by a pronounced low magnetised anomalous area stretching from

the coast to the Inland Ice. This reflects a large cursorily mapped supracrustal belt and possibly also several panels of E–W shearing or faulting. A couple of gravity anomalies in the southern SNO reflect dense material, possibly subducted oceanic crust or intrusives.

From the magnetic anomaly patterns in the southwestern corner of the NNO an Attu magmatic suite is suggested. Furthermore several NW–SE orientated lineaments in the magnetics (coinciding with many of the fjords) are interpreted to be related to faults, which reflect a block faulting, associated with the regional east-ward tilting of the region. The tilting of the crust is reflected in both the magnetic and gravity field. Based on the magnetic anomaly patterns the NNO is divided into a southern and northern part (SNNO and NNNO respectively). The boundary is interpreted to reflect a rheological and metamorphic boundary of two autochthonous blocks associated with localisation of strain and folding.

The area southeast of Sydostbugt and south of Jakobshavn Isfjord is denoted the Nagssugtoqidian transition zone. The western part of this area is interpreted from the magnetic anomaly patterns to be an extension of the NNNO. This extension is denoted the Akiamiut domain. To the west two other domains are inferred: the Kangilinaaq and the Orpissuup Nunaa domain. The Kangilinaaq domain is characterised by a low magnetic response reflecting a large upright antiform fold of a supracrustal sequence, the Kangilinaaq supracrustal belt. The domain, or the limbs of the antiform folded supracrustal belt, is bounded by two NE–SW orientated magnetic lineaments. These lineaments can be correlated to a fault zone to the north and a shear zone to the south. The Orpissuup Nunaa domain reflects a vertical fold. As for the fold north of this domain is the limbs defined by a change in the magnetic patterns and associated with magnetic lineaments.

The southernmost Rinkian orogen is interpreted to consist of a collage of different domains bounded by zones of tectonic deformation. No persistent trend among the domains is observed and the degree of deformation and tectonic reworking within the domains seems to be lower compared to the Nagssugtoqidian orogen. A boundary between the Nagssugtoqidian orogen and Rinkian orogen is not reflected by the magnetics.

Petrophysical measurements, both *in situ* and laboratory determined, from the region are also presented and analysed. These data play an important role in the control on the interpretation of the potential field data and should always be considered when dealing with potential field data from the region. The main results arising from this analysis are:

- Supracrustal rocks are characterised by lower magnetic susceptibility values compared to basement gneiss.
- The magnetic susceptibility values generally increase for various lithologies in the following order: marble/calc-silicate, quartzite, felsic granite, schist, quartz-diorite, gneiss (very dispersed values), mafic magnetite-bearing granite, amphibolite, mafic rocks, ultramafic rocks, banded iron formations.
- Densities in the range 2600 kg/m<sup>3</sup> to 2700 kg/m<sup>3</sup> reflect mostly intermediate to felsic rocks (gneisses, granites, charnockite, quartz diorites, schist, quartzite, marble and calc-silicates). Rocks with a density above 2700 kg/m<sup>3</sup> are mainly found for mafic rocks (amphibolites, mafic and ultramafic rocks). The highest

densities (up to  $4026 \text{ kg/m}^3$ ) are represented by rock samples of banded iron formations and massive iron sulphides.

- The ratio of remanence to induced magnetisation, the Königsberger ratio  $Q$ , was below 1 in 55% of the analysed rocks.

## Acknowledgements

The authors would like to thank Agnete Steenfelt and Karsten Secher, both Geological Survey of Denmark and Greenland (GEUS), for their constructive comments, suggestions and critical review of the report. The National Survey and Cadastre of Denmark (Kort & Matrikel Styrelsen) is thanked for providing the gravity data. Mette Svane Jørgensen is thanked for her assistance in preparing the accompanying CD-ROM.

The work presented here is a part of a Ph.D. project by Bo Møller Nielsen, funded by the Danish Research Agency and GEUS. This report is a contribution to the second performance contract (2000–2003) between GEUS and the Ministry of the Environment.

## References

- Airo, M.-L. 1999: Aeromagnetic and petrophysical investigations applied to tectonic analysis in the northern Fennoscandian shield. Geological Survey of Finland, Report of Investigation **145**, 51 pp.
- Airo, M.-L. & Ruotoistenmäki, T. 2000: Magnetic signatures of Finnish bedrock and their relationship with geological boundaries. Modified from talk: Magnetic signatures of Finnish bedrock and their relationship with geological boundaries. In: Pesonen, L., Korja, A. & Hjelt, S.-E. (eds): Lithosphere 2000, Report S-41.: Institute of Seismology, University of Helsinki.
- Allaart, J.H. 1982: Geological map of Greenland, 1:500 000, Frederikshåb Isblink - Søndre Strømfjord, sheet 2. Copenhagen: Geological Survey of Greenland.
- Allaart, J.H. & Jensen, S.B. 1979: Compilation of 1:500 000 reconnaissance mapping in the Precambrian of the Evighedsfjord - Søndre Strømfjord - Itivleq region, southern West Greenland. Rapport Grønlands Geologiske Undersøgelse **95**, 72–76.
- Bak, J., Korstgård, J. & Sørensen, K. 1975a: A major shear zone within the Nagssugtoqidian of West Greenland. Tectonophysics **27**, 191–209.
- Bak, J., Sørensen, K., Grocott, J., Korstgård, J.A., Nash, D. & Watterson, J. 1975b: Tectonic implications of Precambrian shear belts in western Greenland. Nature **254**, 566–569.
- Blakely, R.J. 1996: Potential theory in gravity and magnetic applications, 441 pp. Cambridge, United Kingdom: Cambridge University Press.
- Bridgwater, D., Escher, A. & Watterson, J. 1973a: Tectonic displacements and thermal activity in two contrasting Proterozoic mobile belts from Greenland. Philosophical Transactions of the Royal Society of London **A 273**, 513–533.
- Bridgwater, D., Escher, A., Nash, D.F. & Watterson, J. 1973b: Investigations on the Nagssugtoqidian boundary between Holsteinsborg and Kangâmiut, central West Greenland. Rapport Grønlands Geologiske Undersøgelse **55**, 22–25.
- Bridgwater, D., Mengel, F., Fryer, B., Wagner, P. & Hansen, S.C. 1995: Early Proterozoic mafic dykes in the North Atlantic and Baltic cratons: field setting and chemistry of distinctive dyke swarms. In: Coward, M.P. & Ries, A.C. (eds): Early Precambrian Processes **95**, 193–210. Geological Society Special Publication (London).
- Cadman, A.C., Tarney, J., Bridgwater, D., Mengel, F., Whitehouse, M.J. & Windley, B.F. 2001: The petrogenesis of the Kangâmiut dyke swarm, W. Greenland. Precambrian Research **105**, 183–203.
- Carmichael, R.S. 1982: Magnetic properties of minerals and rocks. In: Carmichael, R.S. (ed.): Handbook of Physical Properties of Rocks **2**, 229–287. Boca Raton: CRC Press.
- Chalmers, J.A., Pulvertaft, T.C.R., Marcussen, C. & Pedersen, A.K. 1998: New structure maps over the Nuussuaq Basin, central West Greenland. Geology of Greenland Survey Bulletin **180**, 18–27.
- Christensen, N.I. & Mooney, W.D. 1995: Seismic velocity structure and composition of the continental crust: A global view. Journal of Geophysical Research **100**, 9761–9788.
- Clark, D.A. 1997: Magnetic petrophysics and magnetic petrology: aids to geological interpretation of magnetic surveys. AGSO Journal of Australian Geology and Geophysics **17**, 83–103.
- Clark, D.A. & Emerson, D.W. 1991: Notes on rock magnetization characteristics in applied geophysical studies. Exploration Geophysics **22**, 547–555.
- Connelly, J. & van Gool, J.A.M. 2002: Tectonic evolution of the North Atlantic region - an overview from a West Greenland perspective. In: Nielsen, B.M. & Thrane, K. (eds): Workshop on Nagssugtoqidian and Rinkian geology, West Greenland - abstract volume **2002/9**, 13–14. Copenhagen: Geological Survey of Denmark and Greenland.
- Connelly, J.N. & Mengel, F.C. 2000: Evolution of Archaean components in the Paleoproterozoic Nagssugtoqidian orogen, West Greenland. Geological Society of America Bulletin **112**, 747–763.
- Connelly, J.N., van Gool, J.A.M. & Mengel, F. 2000: Temporal evolution of a deeply eroded orogen: the Nagssugtoqidian Orogen, West Greenland. Canadian Journal of Earth Sciences **37**, 1121–1142.

- Cordell, L. & Grauch, V.J.S. 1985: Mapping basement magnetization zones from aeromagnetic data in the San Juan basin, New Mexico. In: Hinze, W.J. (ed.): The utility of regional gravity and magnetic anomaly maps, 181–197. Tulsa, OK: Society of Exploration Geophysicists.
- Cordell, L. & McCafferty, A.E. 1989: A terracing operator for physical property mapping with potential field data. *Geophysics* **54**, 621–634.
- Ellis, S. & Beaumont, C. 1999: Models of convergent boundary tectonics: implications for the interpretation of Lithoprobe data. *Canadian Journal of Earth Sciences* **36**, 1711–1741.
- Ellitsgaard-Rasmussen, K. 1951: A West Greenland globule dike. *Meddelelser fra Dansk Geologisk Forening* **12**, 83–101.
- Escher, A. 1971: Geological Map of Greenland, 1:500 000, Søndre Strømfjord - Nûgssuaq, sheet 3. Copenhagen: Geological Survey of Greenland.
- Escher, A. & Pulvertaft, T.C.R. 1976: Rinkian mobile belt of West Greenland. In: Escher, A. & Watt, W.S. (eds): *Geology of Greenland*, 104–119. Copenhagen, Denmark: Geological Survey of Greenland.
- Escher, A., Escher, J.C. & Watterson, J. 1975: The reorientation of the Kangâmiut dyke swarm, West Greenland. *Canadian Journal of Earth Sciences* **12**, 158–173.
- Escher, J.C., Ryan, M.J. & Marker, M. 1999: Early Proterozoic thrust tectonics east of Atâ Sund, north-east Disko Bugt, West Greenland. *Geology of Greenland Survey Bulletin* **181**, 171–179.
- Fowler, C.M.R. 1995: *The Solid Earth - An introduction to Global Geophysics*, 472 pp. Cambridge: Cambridge University Press.
- Garde, A.A. & Steenfelt, A. 1999a: Precambrian geology of Nuussuaq and the area north-east of Disko Bugt, West Greenland. *Geology of Greenland Survey Bulletin* **181**, 7–40.
- Garde, A.A. & Steenfelt, A. 1999b: Proterozoic tectonic overprinting of Archaean gneisses in Nuussuaq, West Greenland. *Geology of Greenland Survey Bulletin* **181**, 141–154.
- Garde, A.A., Connelly, J.N., Krawiec, A.W., Piaolo, S. & Thrane, K. 2002: A coastal survey in the southern part of the Palaeoproterozoic Rinkian fold belt, central West Greenland. *Geology of Greenland Survey Bulletin* **191**, 33–38.
- Grant, F.S. 1985: Aeromagnetism, geology, and ore environments, I. Magnetite in igneous, sedimentary and metamorphic rocks: an overview. *Geoexploration* **23**, 303–333.
- Grauch, V.J.S. & Cordell, L. 1987: Limitation of determining density or magnetic boundaries from the horizontal gradient of gravity or pseudogravity data. *Geophysics* **52**, 118–121.
- Grocott, J. 1977: The relationship between Precambrian shear belts and modern fault systems. *Journal of the Geological Society, London* **133**, 257–262.
- Grocott, J. 1979: Shape fabrics and superimposed simple shear strain in a Precambrian shear belt, W Greenland. *Journal Geological Society, London* **136**, 471–488.
- Grocott, J. & Davies, S.C. 1999: Deformation at the southern boundary of the large Archean Atâ tonalite and the extent of Proterozoic reworking of the Disko terrane, West Greenland. In: *Geology of Greenland Survey Bulletin* **181**, 155–169.
- Hageskov, B. 1995: Structural evolution of the southern Nagssugtoqidian front and the role of the Kangâmiut dykes. *Terra Nova* **7**(Abstract supplement), 107 only.
- Hanmer, S., Mengel, F., Connelly, J. & van Gool, J. 1997: Significance of crustal-scale shear zones and synkinematic mafic dykes in the Nagssugtoqidian orogen, SW Greenland: a reexamination. *Journal of Structural Geology* **19**, 59–75.
- Henkel, H. 1991: Petrophysical properties (density and magnetization) of rocks from the northern part of the Baltic Shield. *Tectonophysics* **192**, 1–19.
- Henkel, H. 1994: Standard diagrams of magnetic properties and density - a tool for understanding magnetic petrology. *Journal of Applied Geophysics* **32**, 43–53.
- Henkel, H. & Guzmán, M. 1977: Magnetic features of fracture zones. *Geoexploration* **15**, 173–181.
- Hildenbrand, T.G., Berger, B., Jachens, R.C. & Lundington, S. 2001: Utility of magnetic and gravity data evaluation regional controls on mineralization: examples from the Western United States. *Society of Economic Geologists Reviews* **14**, 75–109.
- Hoepfl, M.C. 1997: Choosing Qualitative Research: A primer for technology education researchers. *Journal of Technology Education* **9**, 31–46.
- Jacobsen, B.H. 1987: A case for upward continuation as a standard separation filter for potential-field maps. *Geophysics* **52**, 1138–1148.

- Kalsbeek, F. 2001: Geochemical comparison between Archaean and Proterozoic orthogneisses from the Nagssugtoqidian orogen, West Greenland. *Precambrian Research* **105**, 165–181.
- Kalsbeek, F. & Taylor, P.N. 1986: Chemical and isotopic homogeneity of a 400 km long basic dyke in central West Greenland. *Contributions to Mineralogy and Petrology* **93**, 439–448.
- Kalsbeek, F. & Nutman, A.P. 1996a: Anatomy of the Early Proterozoic Nagssugtoqidian orogen, West Greenland, explored by reconnaissance SHRIMP U-Pb zircon dating. *Geology* **24**, 515–518.
- Kalsbeek, F. & Nutman, A.P. 1996b: New reconnaissance SHRIMP U-Pb zircon age determinations from the Nagssugtoqidian Orogen, West Greenland. In: 2nd DLC Workshop in Nagssugtoqidian geology. Proceedings, 80–85. Copenhagen: Danish Lithosphere Centre.
- Kalsbeek, F. & Skjerna, L. 1999: The Archaean Atâ intrusive complex (Atâ tonalite), north-east Disko Bugt, West Greenland. *Geology of Greenland Survey Bulletin* **181**, 103–112.
- Kalsbeek, F. & Taylor, P.N. 1999: Review of isotope data for Precambrian rocks from the Disko Bugt region, West Greenland. *Geology of Greenland Survey Bulletin* **181**, 41–47.
- Kalsbeek, F., Pidgeon, R.T. & Taylor, P.N. 1987: Nagssugtoqidian mobile belt of West Greenland; a cryptic 1850 Ma suture between two Archaean continents; chemical and isotopic evidence. *Earth and Planetary Science Letters* **85**, 365–385.
- Kalsbeek, F., Taylor, P.N. & Pidgeon, R.T. 1988: Unreworked Archaean basement and Proterozoic supracrustal rocks from northeastern Disko Bugt, West Greenland; implications for the nature of Proterozoic mobile belts in Greenland. *Canadian Journal of Earth Sciences* **25**, 773–782.
- Knudsen, C., Appel, P.W.U., Hageskov, B. & Skjerna, L. 1988: Geological reconnaissance in the Precambrian basement of the Atâ area, central West Greenland. *Rapport Grønlands Geologiske Undersøgelse* **140**, 9–17.
- Korstgaard, J., Ryan, B. & Wardle, R. 1987: The boundary between Proterozoic and Archaean crustal blocks in central West Greenland and northern Labrador. In: Tarney, J. (ed.): *Evolution of the Lewisian and comparable Precambrian high grade terrains*. **27**, 247–259. London, United Kingdom: Geological Society of London.
- Korstgård, J. 1979a: Seminar on Nagssugtoqidian geology - an introduction. *Rapport Grønlands Geologiske Undersøgelse* **89**, 5–7.
- Korstgård, J.A. 1979b: Metamorphism of the Kangâmiut dykes and the metamorphic and structural evolution of the southern Nagssugtoqidian boundary in the Itivdeq - Ikertôq region, West Greenland. *Rapport Grønlands Geologiske Undersøgelse* **89**, 63–75.
- Larsen, L.M. & Rex, D.C. 1992: A review of the 2500 Ma span of alkaline-ultramafic, potassic and carbonatitic magmatism in West Greenland. *Lithos* **28**, 367–402.
- Marker, M., Mengel, F., van Gool, J. & field party 1995: Evolution of the Palaeoproterozoic Nagssugtoqidian orogen: DLC investigations in West Greenland. *Rapport Grønlands Geologiske Undersøgelse* **165**, 100–105.
- Mengel, F., van Gool, J.A.M., Krogstad, E. & the 1997 field crew 1998: Archaean and Palaeoproterozoic orogenic processes: Danish Lithosphere Centre studies of the Nagssugtoqidian orogen, West Greenland. *Geology of Greenland Survey Bulletin* **180**, 100–110.
- Murphy, F. & Coyle, M. 1997: Project report. High Resolution Aeromagnetic Survey. Aeromag '97 - Disko Bay, Greenland: Unpublished report by Sander Geophysics Ltd. available from Geological Survey of Denmark and Greenland, 26 pp.
- Nabighian, M.N. 1972: The analytic signal of two-dimensional magnetic bodies with polygonal cross-section: Its properties and use for automated interpretation. *Geophysics* **37**, 507–517.
- Nabighian, M.N. 1974: Additional comments on the analytic signal of two-dimensional magnetic bodies with polygonal cross section. *Geophysics* **39**, 85–92.
- Nielsen, B.M. & Rasmussen, T.M. 2002: Geological correlation of magnetic susceptibility and profiles from Nordre Strømfjord, southern West Greenland. *Geology of Greenland Survey Bulletin* **191**, 48–56.
- Nutman, A.P. & Kalsbeek, F. 1999: SHRIMP U-Pb zircon ages for Archaean granitoid rocks, Ataa area, north-east Disko Bugt, West Greenland. *Geology of Greenland Survey Bulletin* **181**, 49–54.

- Nutman, A.P., Friend, C.R.L., Baadsgaard, H. & McGregor, V.R. 1989: Evolution and assembly of Archean gneiss terranes in the Godthaabsfjord region, southern West Greenland; structural, metamorphic, and isotopic evidence. *Tectonics* **8**, 573–589.
- O'Connor, K. 1999: Project Report. High Sensitivity Aeromagnetic Survey. Southern West Greenland 1999: Unpublished report by Sander Geophysics Ltd. available from Geological Survey of Denmark and Greenland, 26 pp.
- Olesen, N.Ø. 1984: Geological map of Greenland, 1:100 000, Agto 67 V.1 Nord. Copenhagen: Grønlands Geologiske Undersøgelse.
- Olesen, O., Henkel, H., K., K. & Tveten, E. 1991: Petrophysical properties of a prograde amphibolite-granulite facies transition zone at Sigerfjord, Vesterålen, northern Norway. *Tectonophysics* **192**, 33–39.
- Parasnis, D.S. 1986: Principles of Applied Geophysics, 393. London, U.K.: Chapman & Hall.
- Pedersen, L.B. 1991: Relations between potential fields and some equivalent sources. *Geophysics* **56**, 961–971.
- Piazolo, S., Alsop, G.I., van Gool, J.A.M. & Nielsen, B.M. 2002: Unravelling high strain zone patterns in high grade terranes using GIS based geological and geophysical datasets: a case study from West Greenland. Transport and flow processes in shear zones. Tectonic Studies Group 2003 AGM, Liverpool 2002. Programme and abstracts, 69 only.
- Piazolo, S., Alsop, G.I., Nielsen, B.M. & van Gool, J.A.M. 2004: The application of GIS to unravel patterns of deformation in high grade terrains: a case study from West Greenland. In: Alsop, G.I. & Holdsworth, R.E. (eds): Flow Processes in Faults and Shear Zones. Geological Society, London, Special Publications **224**, 63–78. London, U.K.: The Geological Society of London.
- Puranen, R. 1989: Susceptibilities, iron and magnetite content of Precambrian rocks in Finland. Geological Survey of Finland, Report of Investigation **90**, 45 pp.
- Ramberg, H. 1948: On the petrogenesis of the gneiss complexes between Sukkertoppen and Christianshaab, West-Greenland. Bulletin of the Geological Society of Denmark = Meddelelser fra Dansk Geologisk Forening **1**, 312–327.
- Rasmussen, T.M. 2002: Aeromagnetic survey in central West Greenland: project *Aeromag 2001*. Geology of Greenland Survey Bulletin - Review of Greenland activities 2001 **191**, 67–72.
- Rasmussen, T.M. & van Gool, J.A.M. 2000: Aeromagnetic survey in southern West Greenland: project *Aeromag 1999*. Geology of Greenland Survey Bulletin **186**, 73–77.
- Reid, A.B., Allsop, J.M., Granser, H., Millett, A.J. & Somerton, I.W. 1990: Magnetic interpretation in three dimensions using Euler deconvolution. *Geophysics* **55**, 80–91.
- Roest, W.R., Verhoef, J. & Pilkington, M. 1992: Magnetic interpretation using the 3-D analytic signal. *Geophysics* **58**, 116–25.
- Rosing, M.T., Nutman, A.P. & Løfqvist, L. 2001: A new fragment of the early earth crust: the Aasivik terrane of West Greenland. *Precambrian Research* **105**, 115–128.
- Rutland, R.W., Kero, L., Nilsson, G. & Stølen, L.K. 2001: Nature of a major tectonic discontinuity in the Svecofennian province of northern Sweden. *Precambrian Research* **112**, 211–237.
- Schacht, B. 1992: Report of a high resolution aeromagnetic survey over the Lersletten area of central West Greenland for the Geological Survey of Greenland: Unpublished survey report by Geoterrex available from Geological Survey of Denmark and Greenland, 18 pp.
- Schjøth, F. & Steinfeld, A. 2004: Mineral resources of the Precambrian shield of central West Greenland (66° to 70°15' N). Part 1. Compilation of geoscience data.: Danmarks og Grønlands Geologiske Undersøgelse Rapport. **2004/16**, 1 DVD.
- Schlenger, C.M. 1985: Magnetization of lower crust and interpretation of regional magnetic anomalies: example from Lofoten and Vesterålenm Norway. *Journal of Geophysical Research* **90**, 11484–11504.
- Secher, K. 1986: Exploration of the Sarfartôq carbonatite complex, southern West Greenland. Rapport Grønlands Geologiske Undersøgelse **128**, 89–101.
- Shive, P.N., Blackely, R.J., Frost, B.R. & Fountain, D.M. 1992: Magnetic properties of the lower continental crust. In: Fountain, D.M., Arculus, R. & Kay, R.W. (eds): Continental Crust **23**, 145–177. Amsterdam: Elsevier.

- Skilbrei, J.R., Skyseth, T. & Olesen, O. 1991: Petrophysical data and opaque mineralogy of high-grade and retrogressed lithologies: implications of the interpretation of aeromagnetic anomalies in Northern Vestranden, Central Norway. *Tectonophysics* **192**, 21–31.
- Sørensen, K. 1983: Growth and dynamics of the Nordre Strømfjord shear zone. *Journal of Geophysical Research* **88**, 3419–3437.
- Steenfelt, A. 1994: Crustal structure in West and South Greenland reflected by regional distribution of calcium and potassium in stream sediments. *Rapport Grønlands Geologiske Undersøgelse* **161**, 11–20.
- Steenfelt, A. 1996: Syenitic rocks within the Nagssugtoqidian orogen: distribution, age and relation to Proterozoic granitoids. 2nd DLC Workshop on Nagssugtoqidian geology - Proceedings, Copenhagen 1996, 30–38.
- Steenfelt, A. 2002: Geochemical variation from Nagssugtoqidian to Rinkian. In: Nielsen, B.M. & Thrane, K. (eds): Workshop on Nagssugtoqidian and Rinkian geology, West Greenland. Abstract volume, 38 only.
- Steenfelt, A. & Dam, E. 1991: Reconnaissance geochemical exploration of map sheet 67 V 2 (67° to 68°N, 49°30' to 52°W), West Greenland. *Open File Series Grønlands Geologiske Undersøgelse* **91/8**, 10 pp.
- Stendal, H. & Schönwandt, H.K. 2003: Precambrian supracrustal rocks and mineral occurrences, Northeast Disko Bugt - A review and new data. *Danmarks og Grønlands Geologiske Undersøgelse Rapport* **2003/24**, 57 pp.
- Stendal, H., Knudsen, C., Marker, M. & Thomassen, B. 1999: Gold mineralisation at Eqi, northeast Disko Bugt, West Greenland. *Geology of Greenland Survey Bulletin* **181**, 129–140.
- Stendal, H., Nielsen, B.M., Secher, K. & Steenfelt, A. 2004: Mineral resources of the Precambrian shield of central West Greenland (66° to 70°15' N). Part 2. Mineral occurrences. *Danmark og Grønlands Geologiske Undersøgelse Rapport* **2004/20**, 212 pp.
- Strauss, A. & Corbin, J. 1990: Basics of qualitative research: Grounded theory procedures and techniques, 270. Newbury Park, California, U.S.: Sage Publications, Inc.
- Talbot, C.J. 1979: A klippe of Nagssugtoqidian supracrustal rocks at Sarfartúp nunâ, central West Greenland. *Rapport Grønlands Geologiske Undersøgelse* **89**, 23–42.
- Telford, W.M., Geldart, L.P. & Sheriff, R.E. 1998: *Applied Geophysics*, 770 pp. Cambridge, U.K.: Cambridge University Press.
- Thompson, D.T. 1982: EULDPH: a new technique for making computer-assisted depth estimates from magnetic data. *Geophysics* **47**, 31–37.
- Thorning, L. 1984: Aeromagnetic maps of parts of southern and central West Greenland: acquisition, compilation and general analyses of data. *Rapport Grønlands Geologiske Undersøgelse* **122**, 36 pp.
- Thorning, L. 1993: Project AEROMAG-92: a new high resolution aeromagnetic survey of the Lersletten area, central West Greenland (68°15' to 68°55'N, 50°25' to 53°35'W). *Open File Series Grønlands Geologiske Undersøgelse* **93/2**, 36 pp.
- van Gool, J., Marker, M., Mengel, F. & field party 1996: The Palaeoproterozoic Nagssugtoqidian orogen in West Greenland: current status of work by the Danish Lithosphere Centre. *Bulletin Grønlands Geologiske Undersøgelse* **172**, 88–94.
- van Gool, J.A.M., Kriegsman, L.M., Marker, M. & Nichols, G.T. 1999: Thrust stacking in the inner Nordre Strømfjord area, West Greenland. Significance for the tectonic evolution of the Palaeoproterozoic Nagssugtoqidian orogen. *Precambrian Research* **93**, 71–86.
- van Gool, J.A.M., Connelly, J.N., Marker, M. & Mengel, F.C. 2002: The Nagssugtoqidian Orogen of West Greenland: tectonic evolution and regional correlations from a West Greenland perspective. *Canadian Journal of Earth Sciences* **39**, 665–686.
- Verhoef, J., Roest, W.R., Macnab, R. & Arkani-Hamed, J. 1996: Magnetic anomalies of the Arctic and north Atlantic oceans and adjacent land areas. *Geological Survey of Canada Open File* **3125**, 225 pp.
- Wardle, R.J., James, D.T., Scott, D. & Hall, J. 2002a: The southeastern Churchill Province: synthesis of a Paleoproterozoic transpressional orogen. *Canadian Journal of Earth Sciences* **39**, 639–663.
- Wardle, R.J., Gower, C.F., James, D.T., St-Onge, M.R., Scott, D.J., Garde, A.A., Culshaw, N., van Gool, J.A.M., Connelly, J.N., Perreault, S. & Hall, J. 2002b: Correlation chart of the Proterozoic assembly of the northeastern Canadian-Greenland Shield. *Canadian Journal of Earth Sciences* **39**, 895 only.

- Watterson, J. 1978: Proterozoic intraplate deformation in the light of South-east Asian neotectonics. *Nature, London* **273**, 636–640.
- Zhang, C., Mushayandebvu, M.F., Reid, A.B., Fairhead, J.D. & Odegard, M.E. 2000: Euler deconvolution of gravity tensor gradient data. *Geophysics* **65**, 512–520.

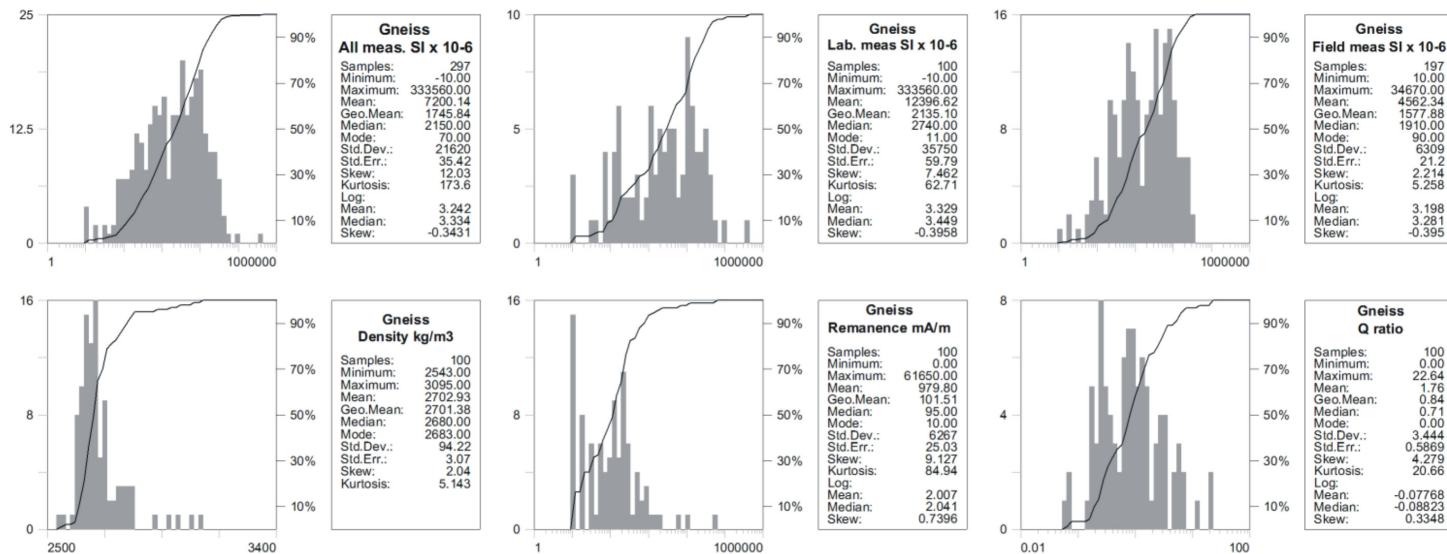


**Figure 54.** Frequency diagrams and statistics showing the magnetic susceptibility, density, magnetic remanence, and calculated Königsberger ratio (Q ratio) of gneiss lithologies from the assessment region. A histogram where both the measured magnetic susceptibility in the field and in the laboratory (denoted All SI x 10<sup>-6</sup>) included is given. Separate histograms of either field (denoted field meas.) or laboratory (denoted lab. meas.) measurements are also given in order to make sure that the results from the two measurement methods can be combined. The Q ratio is calculated as the remanent magnetisation divided by the induced magnetisation (expressed as the product of the strength of the magnetic field; in the region 55500 nT ≈ 44.178 mA/m) and the measured magnetic susceptibility.

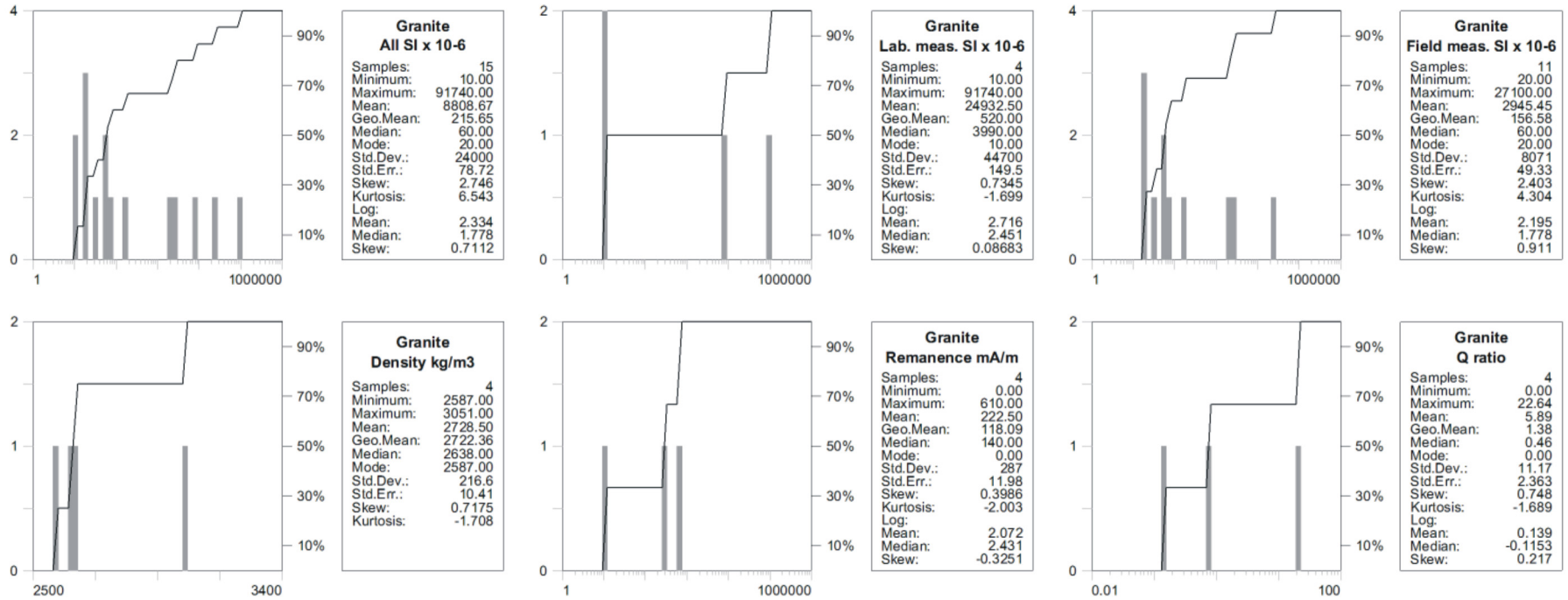


**Figure 55.** Frequency diagrams and statistics of measured magnetic susceptibility, density, magnetic remanence, and calculated Königsberger ratio (Q ratio) of granite lithologies from the assessment region. Histograms included and calculation of Q ratio as described in Fig. 54.

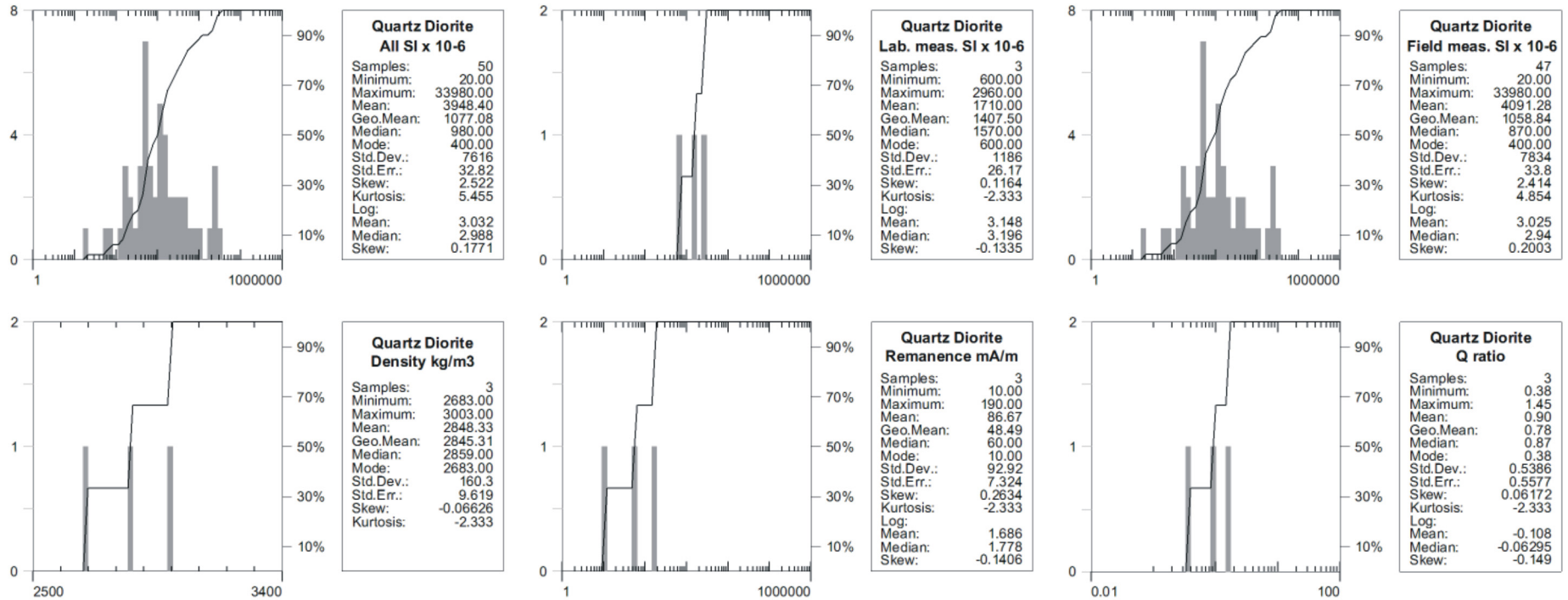


**Figure 56.** Frequency diagrams and statistics of measured magnetic susceptibility, density, magnetic remanence, and calculated Königsberger ratio (Q ratio) of Arfersiorfik quartz diorite lithologies from the assessment region. Histograms included and calculation of Q ratio as described in Fig. 54.

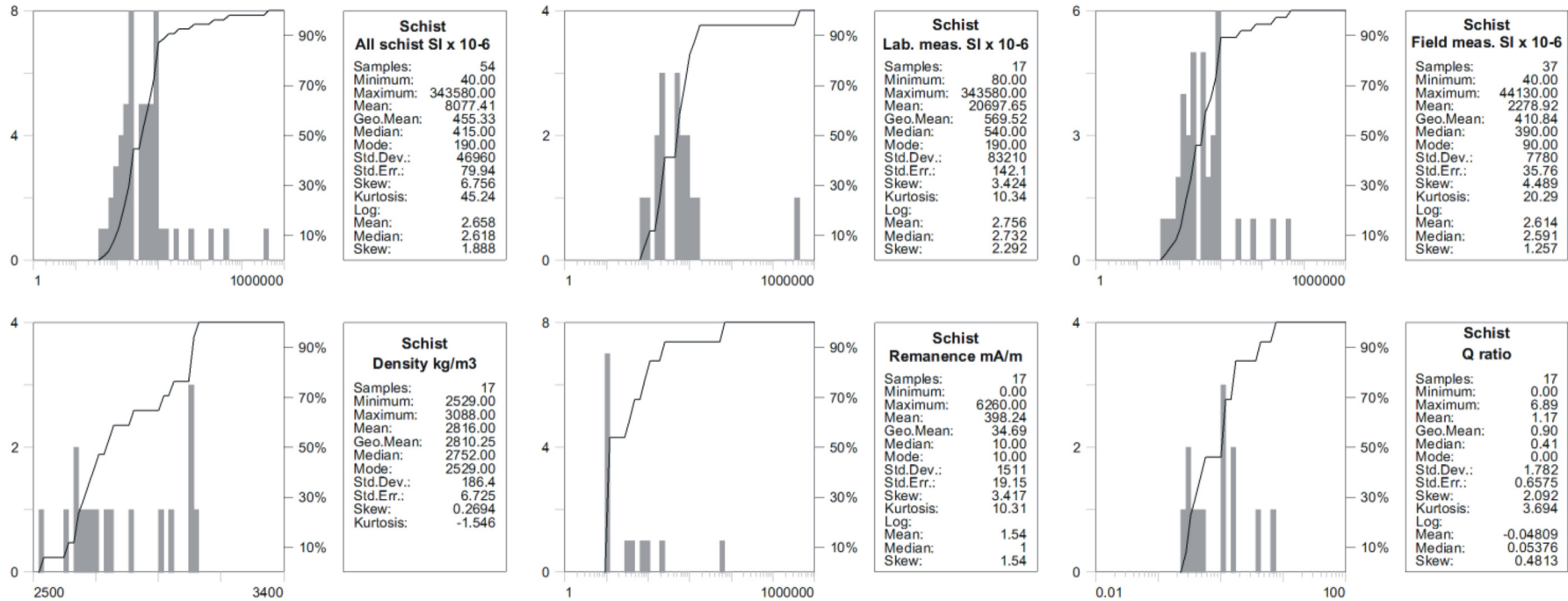


**Figure 57.** Frequency diagrams and statistics of measured magnetic susceptibility, density, magnetic remanence, and calculated Königsberger ratio (Q ratio) of schist lithologies from the assessment region. Histograms included and calculation of Q ratio as described in Fig. 54.

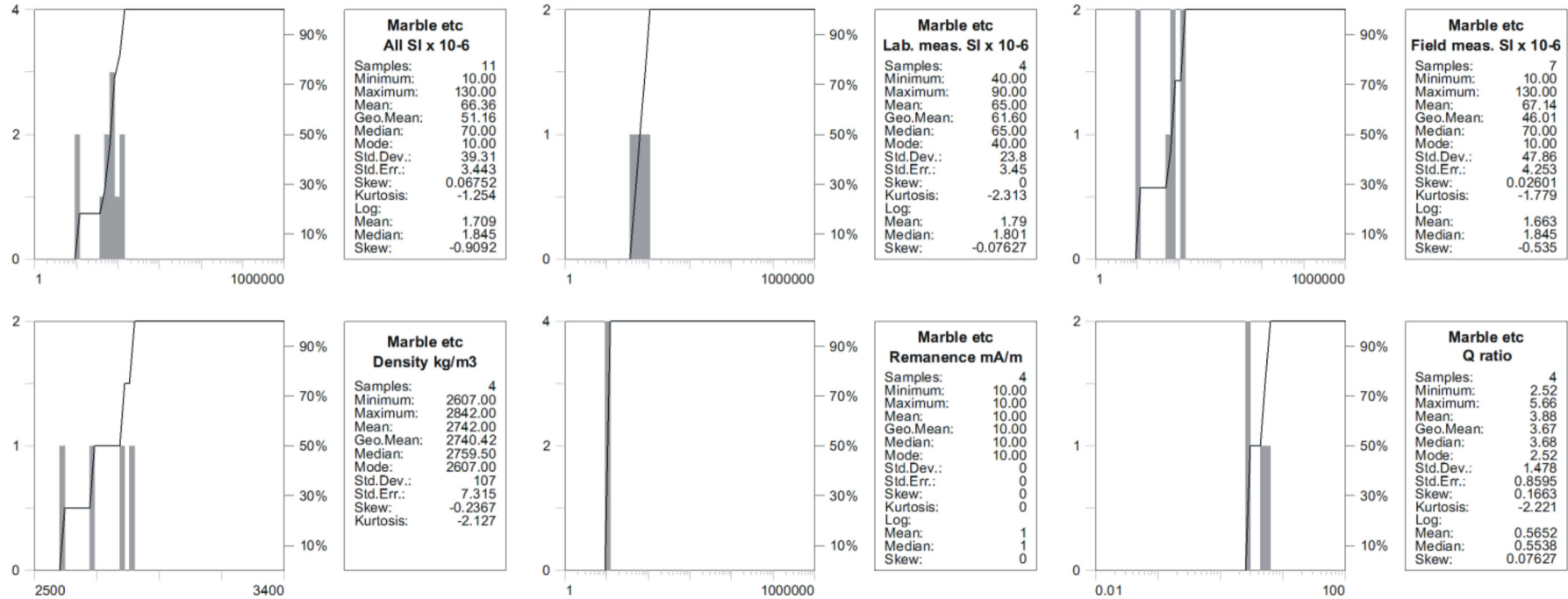


**Figure 58.** Frequency diagrams and statistics of measured magnetic susceptibility, density, magnetic remanence, and calculated Königsberger ratio (Q ratio) of marble, calc-silicate, and dolomite (marble etc) lithologies from the assessment region. Histograms included and calculation of Q ratio as described in Fig. 54.

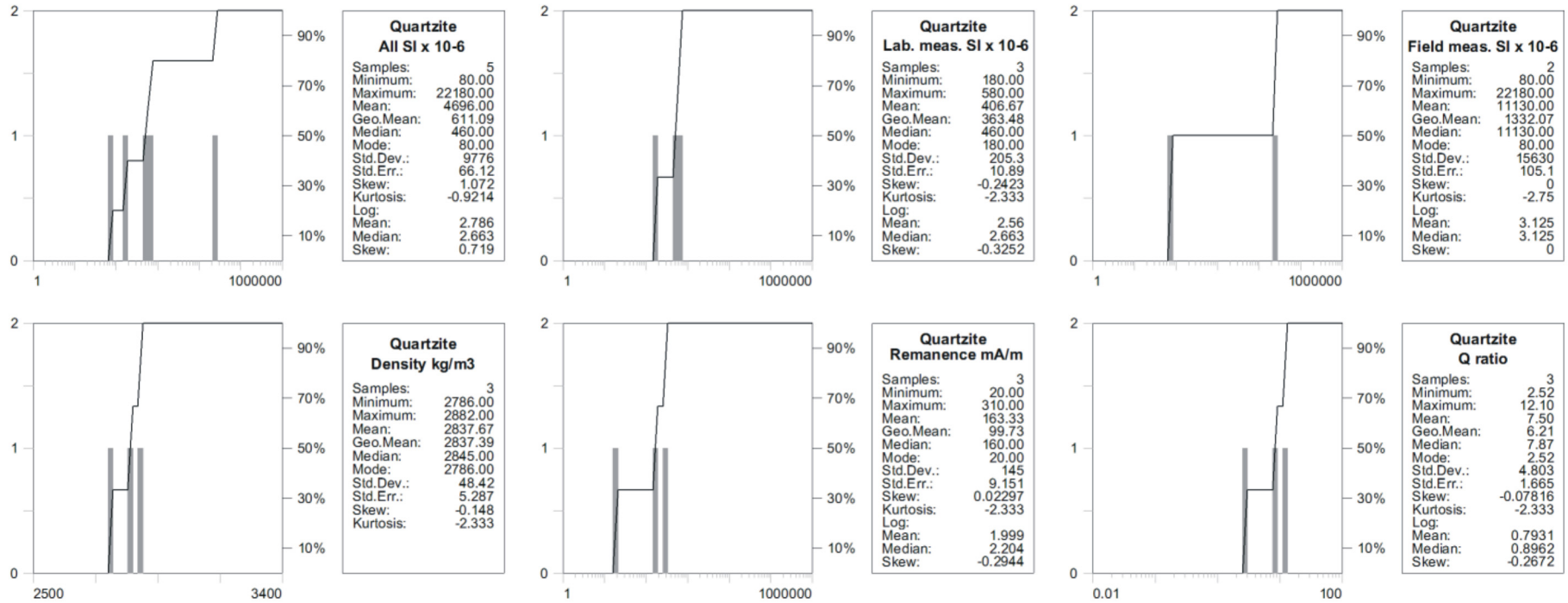


**Figure 59.** Frequency diagrams and statistics of measured magnetic susceptibility, density, magnetic remanence, and calculated Königsberger ratio (Q ratio) of quartzite lithologies from the assessment region. Histograms included and calculation of Q ratio as described in Fig. 54.

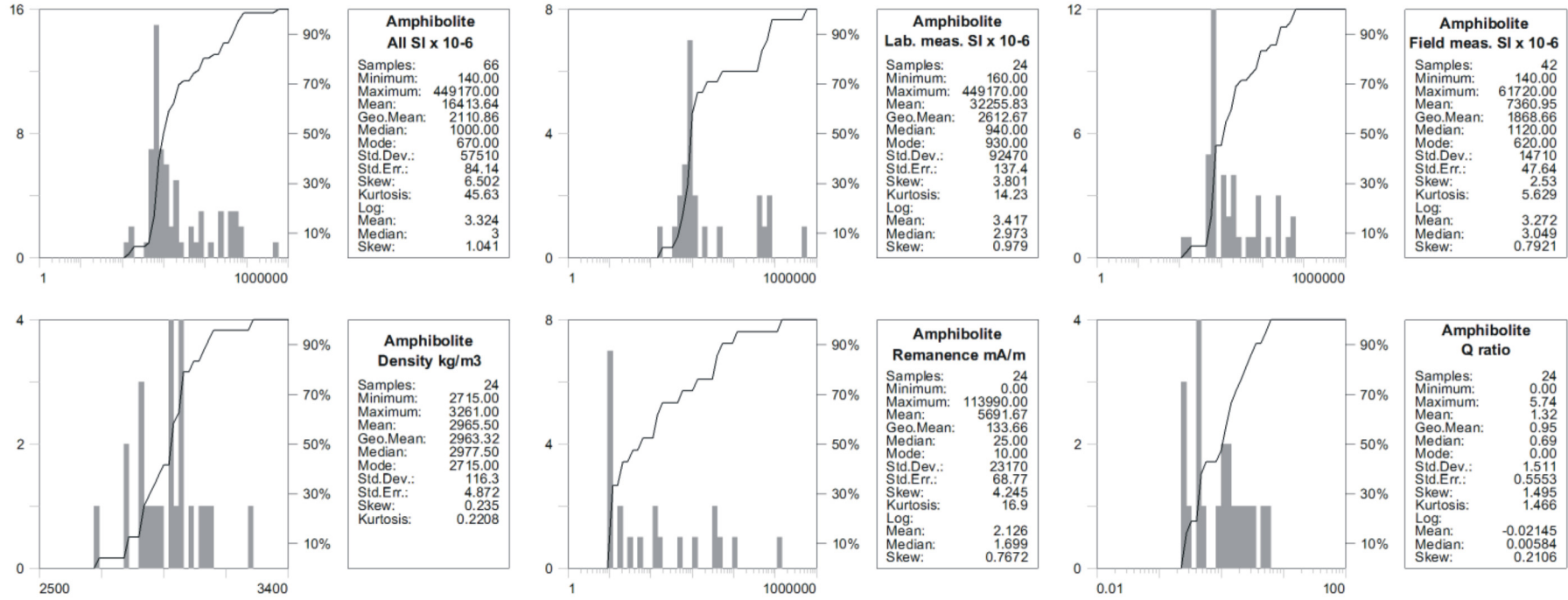


**Figure 60.** Frequency diagrams and statistics of measured magnetic susceptibility, density, magnetic remanence, and calculated Königsberger ratio (Q ratio) of amphibolite lithology from the assessment region. Histograms included and calculation of Q ratio as described in Fig. 54.

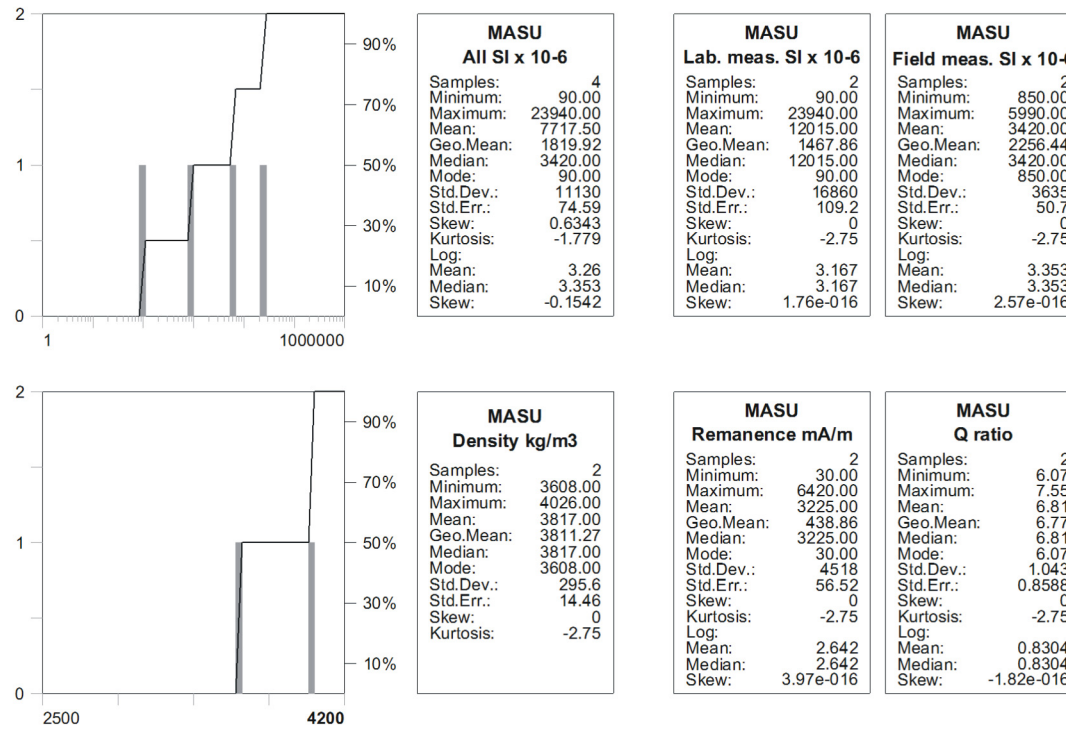


**Figure 61.** Frequency diagrams and statistics for four measured magnetic susceptibility for massive sulphide rocks (massive sulphides; both laboratory and field measurements) are given together with frequency diagrams for two laboratory determined densities of the massive sulphide rocks. Tables for laboratory-determined remanence calculated Königsberger ratio (Q ratio) and field measurements of magnetic susceptibility. Calculation of Q ratio as described in Fig. 54.

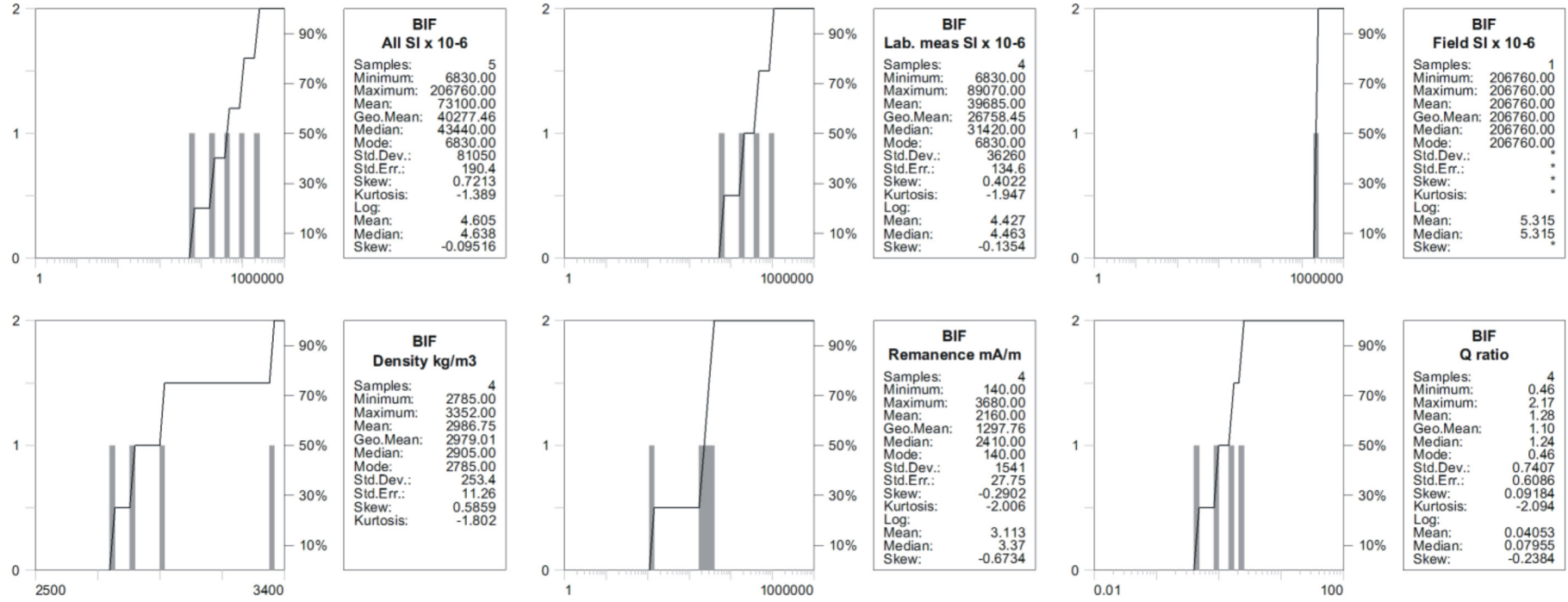


**Figure 62.** Frequency diagrams and statistics of measured magnetic susceptibility, density, magnetic remanence, and calculated Königsberger ratio (Q ratio) of banded iron formations (BIF) from the assessment region. Histograms included and calculation of Q ratio as in Fig. 54.

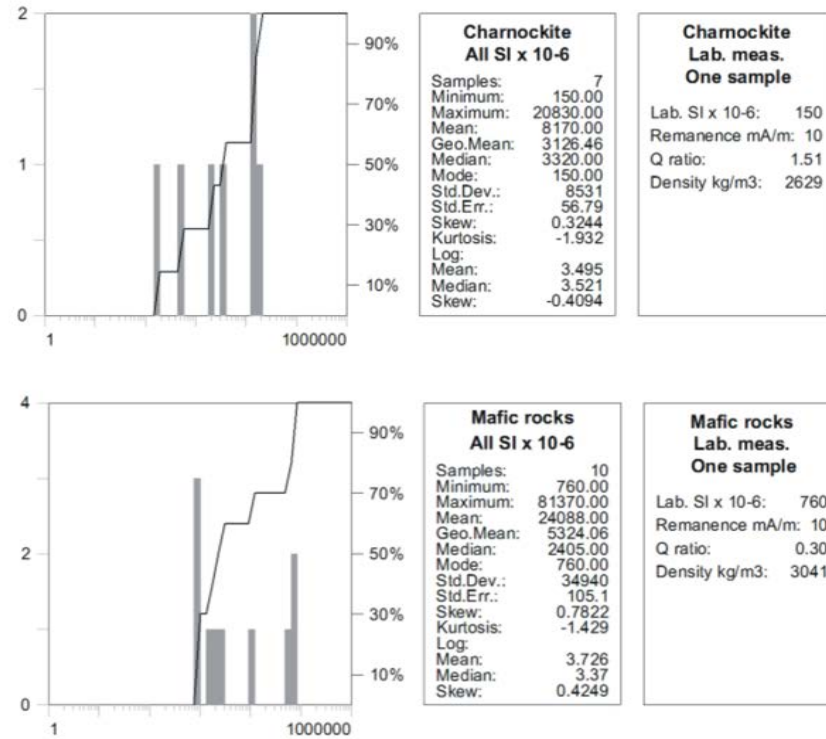


**Figure 63.** Frequency diagrams and statistics of measured magnetic susceptibility for charnockite and mafic rock lithologies. Laboratory determination of the petrophysical properties are only carried out for one sample of each lithology. The results from this determination are given in separate tables. Calculation of Q ratio as described in Fig. 54.

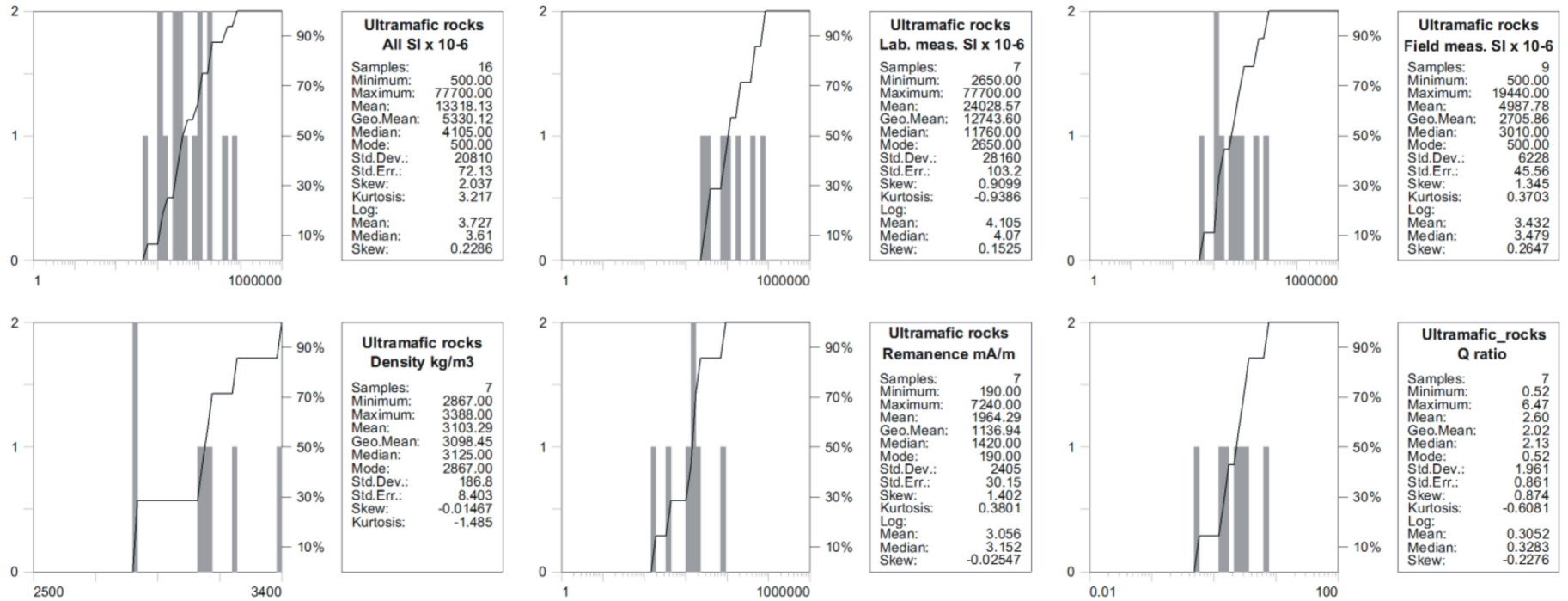


**Figure 64.** Frequency diagrams and statistics of measured magnetic susceptibility, density, magnetic remanence, and calculated Königsberger ratio (Q ratio) of ultramafic rock lithologies from the assessment region. Histograms included and calculation of Q ratio as described in Fig.54.

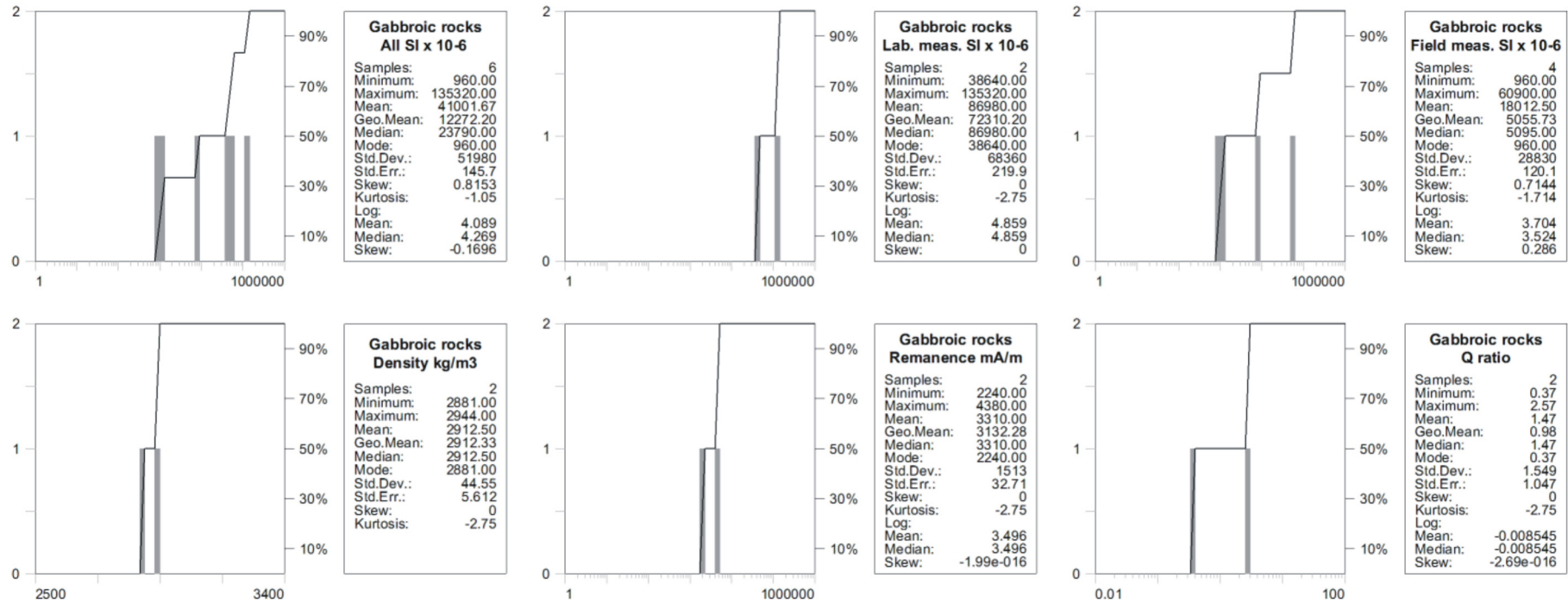


**Figure 65.** Frequency diagrams and statistics showing the magnetic susceptibility, density, magnetic remanence, and calculated Königsberger ratio (Q ratio) of gabbroic rocks lithologies from the assessment region. Histograms included and calculation of Q ratio as described in Fig. 54.

# Appendix B – CD-ROM with selected images of potential field data from West Greenland

## Data presentation

Most of the processed potential field data presented as figures in the report are included on the accompanying CD-ROM in order to make it possible for the reader to investigate the data further. The A4 paper-size in the report hinder in some cases the accessibility to the details in many of the processed geophysical data. The accompanying digital maps on the CD-ROM should remedy this. Software for viewing the maps is enclosed.

## Directory structure of the CD-ROM

The directory structure of the CD-ROM is shown in Figure 66.

'Geophysical\_Images\_West\_Greenland' directory

The individual images of the different views of potential field data included in the maps. The images are stored as geographic referred .tif files. Coastlines (in scale 1:2,500,000) are also included in each data image.

'Geophysical\_Maps\_West\_Greenland' directory'

The maps in this directory contain the selected images of the potential field data (and associated legends) from West Greenland. The data are stored as data layers in OASIS montaj™ map format.

It is recommended to copy the content of the directories 'Geophysical\_Maps\_West\_Greenland' and 'Geophysical\_Images\_West\_Greenland' from the CD-ROM into a directory on your own computer. Furthermore, the directory structures between these two directories should be maintained.

'Oasis\_montaj\_Interface' directory

The maps are opened, copied and printed using the OASIS montaj™ Interface software, which are freely distributed by Geosoft Inc. and is included on the CD-ROM in this directory.

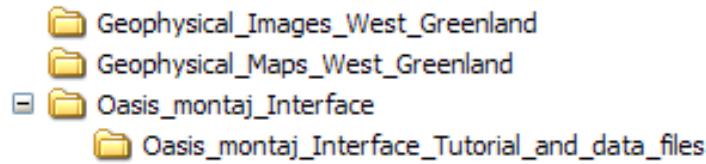


**Figure 66.** Directory structure of the CD-ROM with geophysical maps from West Greenland and software for viewing the maps.

## Installing OASIS montaj™ Interface and Adobe Acrobat® Reader

The following software and hardware is required to install and run OASIS montaj™ Interface (version 5.1.8):

- Windows NT® 4.0, Windows 95®, Windows 98®, Windows 2000® required (Windows 2000® is recommended). Do not currently support Windows ME.
- A Pentium CPU required.
- RAM memory: 128 Mb or more recommended, 32 Mb minimum.
- 24-bit graphics card with 3-D acceleration is recommended and required for full colour imaging. Recommend 64Mb Ram on card.
- Any Windows® supported colour printer. Hewlett Packard® large-format ink-jet plotters are recommended.
- To use the Internet capabilities in Oasis montaj™, you will need to install Internet Explorer 5.0 or later. This does not mean that you have to have Internet Explorer as your default browser; Oasis montaj™ just uses the Internet connection technology supplied in IE5 to connect to the internal help systems html pages.

The files for OASIS montaj™ Interface is located in the directory 'OASIS\_montaj\_Interface'. The directory contains the file 'Oasismontaj\_5.1.8.exe'. To install the software, open the above-mentioned directory and double-click on the self-extracting file 'Oasismontaj\_5.1.8.exe' by using Windows Explorer® or go to 'Start | Run'. Then follow the install-wizard instructions. Updated versions of Oasis montaj™ software are located on the homepage of Geosoft Inc. <http://www.geosoft.com/>

OASIS montaj™ Interface can only be installed on your local drives. It is not recommended to install this on any network drive. It is recommended that Oasis montaj™ is installed off a root directory and not off the 'Program Files'-directory or directories with space characters in the name.

If you are not familiar with the Oasis montaj™ software is a tutorial provided by Geosoft Inc. The tutorial gives an introduction to the possibilities and environment of the OASIS montaj™ Interface. The tutorial and associated files are included in the subdirectory 'OASIS\_montaj\_Interface\_Tutorial\_and\_data\_file' in the directory containing the file for installing the OASIS montaj™ Interface. The file 'InterfaceTutorial.pdf' (opened with Acrobat® Reader) will give further instructions how to carry out the tutorial.

The files for installing Acrobat® Reader can be located on the homepage of Adobe <http://www.adobe.com/products/acrobat/readermain.html> Click on the button 'Get Adobe Reader' and follow the instructions.

## **Opening of maps and toggling between different geophysical data – using Oasis montaj™ Interface**

### **Create a workspace**

Before opening of any of the supplied maps on the CD-ROM with the Oasis montaj™ Interface software, a *workspace* is required.

For the purpose of displaying the information on the CD-ROM, the workspace file can be interpreted as a container that holds all the maps plus information that tells the software about the state in which the maps were left the last time you used it.

The workspace is stored in files with extension *.gws*. More information about workspaces, as well as information on other subjects, can be found by clicking the 'help'-button when the Oasis montaj™ window is opened.

It is recommended to place the workspace files in separate directories. A workspace is created by clicking the 'File | Open Workspace ...'-button in the Oasis montaj™ window followed by entering a workspace (file) name within an appropriate directory. New directories can also be created from the menu. Note that it is not possible to create any directories or files on the drive containing the CD-ROM.

When creating a new workspace, a message may appear that the software is unable to load some menus due to unavailable licence information. This message can be disregarded. By clicking the 'Workspace comments' -button in the 'file' -menu and typing a description in the file opened by the editing software, information about the specific workspace that has been created can be entered and stored. The name of the file is '*\_gws\_comments.rtf*'. The Oasis montaj™ software returns to its idle mode when the editing software is closed.

### **Open a geophysical map**

It is possible to read the maps directly from the CD-ROM into the Oasis montaj™ window. However, for a faster opening and processing of the maps on your own computer it is recommended to copy the content of the directories 'Geophysical\_Maps\_West\_Greenland' and 'Geophysical\_Images\_West\_Greenland' from the CD-ROM into a directory on your own computer, but be sure that the directory structure between these two are kept. Furthermore, the Oasis montaj™ software will display messages such as the map is write protected when read directly from the CD-ROM. This will not be the case if data in the two directories are copied to your own computer.

Four maps of geophysical data are included in the directory 'Geophysical\_Maps\_West\_Greenland'. The names of the four maps refer to the area they cover.

**Table 5.** Overview of the geophysical maps and the area that are covered by the maps. All four maps are included in the directory 'Geophysical\_Maps\_West\_Greenland' on the CD-ROM. All maps are stored in the Geosoft Oasis montaj™ map format.

Name of geophysical map	Area covered
NTZ_southernmost_Rinkian_GEUS	Nagssugtoqidian transition zone (between Sydosstbugt and Jakobshavn Isfjord) and the southernmost part of the Rinkian orogen
NNO_GEUS	Northern Nagssugtoqidian orogen
CNO_GEUS	Central Nagssugtoqidian orogen
SNO_GEUS	Southern Nagssugtoqidian orogen

The opening of the geophysical maps is done by using the 'Map | Open Map ...'-menu and selecting one of the maps in the directory 'Geophysical\_Maps\_West\_Greenland' at a time. The 'Map | Open Map ...'-menu is located in the top-menu in the Geosoft Oasis montaj™ window. All maps can be displayed simultaneously in the same workspace.

If two versions of the same map is wanted (e.g. if the user would like to view two different geophysical data sets at the same time for the same region) you just open the original map twice. The user will then be asked to give the second version of the map a different name, e.g. a suffix \_ver2.

### Toggling between different geophysical data

The reader is referred to the on-line 'Help'-utility in Oasis montaj™ for obtaining information on specific functions provided with the software. However, the most common and important functions for using the geophysical maps included are given here below.

The most commonly used functions are likely to be the View/Group manager (see Fig. 67) and the zoom-function in combination with the dynamic linking utility (shadow cursors icon) (see Fig. 67). This allows the user to display multiple maps simultaneously and visualise the same anomaly-location for different data types (i.e. images of different type of processed magnetic data together). By clicking the shadow cursors icon in the Oasis montaj™ window, it activates the dynamic link when the maps are opened. When the 'All maps'-icon is activated, application of the zoom-utility in one window will be mirrored in all other opened maps.

Different images of geophysical data and associated titles and legend bars are selected for viewing by clicking the function-button *View/Group manager* () in the left side menu while the open map window is active (by clicking on the window). By clicking this button will a View/Group manager window open (Fig. 68). It is also possible to access this command by clicking the right mouse button on a map and select *Groups* and the then select *View/Group manager* from the popup menu.

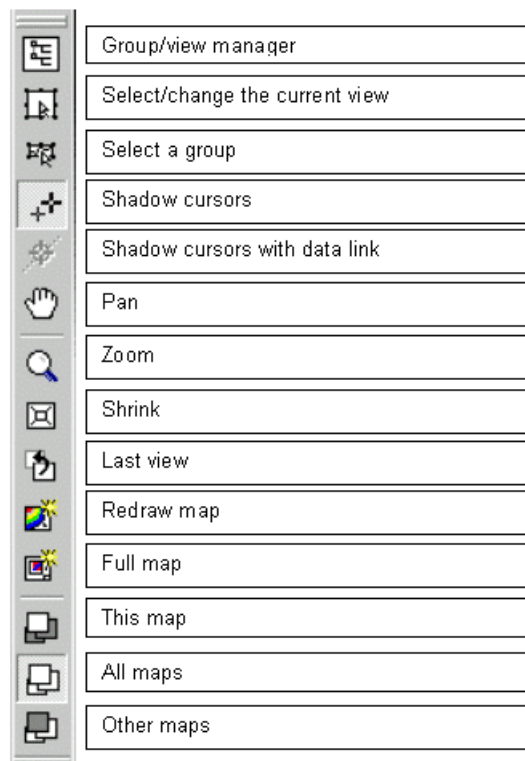


**Figure 67.** *The left-side push-buttons menu used to control the appearance of maps in the Oasis montaj™ window. Information on the use of the push-buttons can be found in the Oasis montaj™ help-documents in the sections ‘Map viewing tools’ and ‘Mode selection tools’.*

The View/Group manager window gives a tree-list of the different information and material contained in the map (Fig. 68).

A View divides the information on a map into a Base view, which uses paper coordinates, and a Data view, which uses ground coordinates.

Information and material contained in the mapped is denoted groups. The group on the top layer of the map (closest to the front) is listed first (e.g. A\_VGM in Fig. 68), followed by group of the next layer behind it (e.g. A\_TMI\_s in Fig. 68), followed by the rest of the groups representing the layers to the bottom layer of the map at the end of the list.

Each group in a view shows an icon (see Fig. 68) beside its name that identifies the group as either a map object (📄) or an aggregate (🌈). A blank icon (☐) indicates that the group is hidden in the map (the group is presently not viewed in the map). Check the box ‘Render images (AGGs) first’ to draw the aggregate groups first on top of all other layers in the map.

The different abbreviations used for the different groups indicate the data that are included in the opened geophysical map. A listing and explanation of the abbreviations used in the maps are given in the next sections.

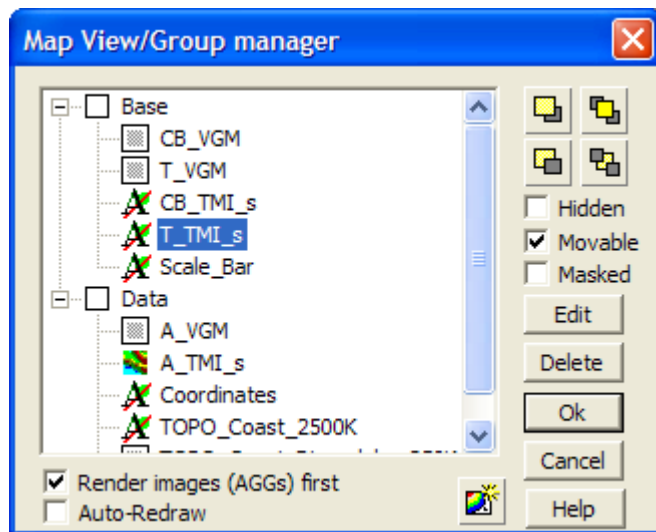


**Figure 68.** The Map View/Group manager window showing the content of the selected map. For the abbreviations used in the description of the content please refer to the Tables 4, 5 and 6 in Appendix B (this appendix).

Use the scroll bar on the right side of the View/Group manager window (Fig. 68) to scroll up and down in the list. In the top right corner of the View/Group manager window are three check boxes. If you check the '*Hidden*' box the selected group in the list (select the group by clicking it) will be hidden (not displayed) in the map. If you check the *Moveable* box this will enable you to move the group around on the map using the cursor. If a group has a mask associated with it, check the '*Masked*' box to apply (turn on the mask).

The '*Hidden*' check-box is very important. Images of different processed data and their associated legends and titles are shown or hidden by the use of this function.

Both in the View/Group window manager (Fig. 68) and in the main menu in left side of the

Oasis montaj window (Fig. 67) is a '*Redraw Map Window*' button (  ). By clicking this button will the map window be refreshed/redrawn. If the maps are edited or new groups are hidden/selected to be shown should this button be clicked in order to redrawn/refresh the map to shown the latest changes. If the Auto-Redraw option is on will the map automatically be redrawn/refreshed. However, this is not always wanted. It is also possible to access this command by clicking the right mouse button on a map and selecting '*Redraw*' from the popup menu.

It is recommended to use the '*File | Close workspace*'-menu before exiting the Oasis montaj™ software.

## Data included in the maps

### Coordinates and scale bar

Coordinates	The coordinates marks, text and frame for the maps can also be found in the end of the Data list. These are named Coordinates.
Scale_Bar	The scale bar for the map is named Scale_Bar in the end of the Base or Data list.

### Prefix descriptions

i\_ Images of the different processed geophysical grid data are marked with i\_ as prefix in the list of 'Data'.

The abbreviation following the prefix i\_ will describe the geophysical grid data it represents. The different abbreviations used for the different types of processed geophysical data are given in Table 6 in Appendix B. The abbreviations used after the selected prefix i\_, CB\_ and T\_ should be the same in order to get the right combination of features in the map.

CB\_ The colour bar legend associated with the processed data is marked with CB\_ as prefix in the list of 'Base'. The abbreviation behind the prefix CB\_ will describe, which geophysical data the colour bar legend is associated with. The different abbreviations used for the different types of processed geophysical data are given in Table 6 in Appendix B. The abbreviations used after the selected prefix i\_, CB\_ and T\_ should be the same in order to get the right combination of features in the map.

T\_ The title associated with the processed data is marked with CB\_ as prefix in the list of 'Base'. The text behind the prefix T\_ will describe, which geophysical grid data the title is associated with. The different abbreviations used for the different types of processed geophysical data are given in Table 6 in Appendix B. The abbreviations used after the selected prefix i\_, CB\_ and T\_ should be the same in order to get the right combination of features in the map.

Symb\_ If symbol/point data is used, e.g. to represent gravity measurement stations or depth estimates from the analysis of the analytic signal, will the prefix Symb\_ denotes this. The different abbreviations used after the prefix Symb\_ for the different symbol data are given in Table 6 in Appendix B. The abbreviations used after

the selected prefix Symb\_, CB\_ and T\_ should be the same abbreviations in order to get the right combination of features in the map.

M\_ M denote the thematic layers with interpretations, geographic names, text, etc. Explanation of the different abbreviations used after the prefix M\_ are given in Table 6 in Appendix B.

## Suffix descriptions

_s	The suffix _s denotes that the geophysical data is shown with a shadow effect. Unless otherwise stated is the shadow done with inclination 45° and declination 315°.
_ex_disko	For maps of the Disko Bugt area will the suffix _ex_disko denote that Disko Island and adjacent sea is excluded from the data in order to give more dynamic to the imaging of the different data.
_scs1	In special cases is it appropriate to use the same colour scaling when representing different processed data. The suffix _scs1 denote that the same colour scale no.1 is used – the corresponding CB will therefore be CB_SCS1 and should be used for all data with the suffix _scs1.
_m&a	In special cases have the data from Aeromag and MAANAOALA been merged. The suffix _m&a denote this.
_only_arveprinsen_area	In one case is it appropriate only to show the Bouguer anomaly field at Arveprinsen Ejland and adjacent areas (in the northern part of Disko Bugt). This is denoted by the suffix Only_Arveprinsen_area.

## Abbreviations of thematic maps; M\_

**Table 6.** Abbreviations following the prefix M\_ for the thematic layers showing interpretations, geological information, etc.

<b>Abbreviations</b>	<b>Meaning</b>
Major_text	The text that denotes the major geological features and boundaries
Major_features_boundaries	Polygons and lines that show the major geological features and boundaries.
Interpretation_map	More detailed interpretation delineating the important geological features, boundaries, domains etc.
Legend_interp_map	Legend for the Interpretation map
Geographic_names	Geographic names included in the maps

## Abbreviations of geophysical image data; i\_ and associated CB\_ and T\_

The abbreviations in Table 7 are used for the different types of processed geophysical data. The abbreviations following the prefix i\_, CB\_ and T\_.

**Table 7.** Abbreviations used behind the prefix i\_, and associated CB\_ and T\_ prefix, for the different types of processed geophysical grids.

Abbreviation	Meaning
amp_hg_tmil	Amplitude of the horizontal gradient of the total magnetic field intensity
amp_hg_psgrav_tmi	Amplitude of the horizontal gradient of the pseudo-gravity of the total magnetic field intensity.
amp_hg_psgrav_tmi_m&a	Amplitude of the horizontal gradient of the pseudo-gravity of the total magnetic field intensity from merged Aeromag and MAANAOALA data. The merged field is upward continued to a common height of 1250 m.
asm	Calculated analytic signal of the total magnetic field intensity
ba	Bouguer anomaly field
butw_lpas_tmi_wc##km	Butterworth low-pass filtering of the total magnetic field intensity with wavelength cut-off at ## km.
hg360_sdir90_tmi	Horizontal gradient calculated in direction 360°N, which enhance structures with the direction 90°N (E-W), for the total magnetic field intensity.
hg315_sdir45_tmi	Horizontal gradient calculated in direction 315°N, which enhance structures with the direction 45°N (NE-SW), for the total magnetic field intensity.
hg90_sdir360_tmi	Horizontal gradient calculated in direction 90°N, which enhance structures with the direction 360°N (N-S), for the total magnetic field intensity.
hg45_sdir315_tmi	Horizontal gradient calculated in direction 45°N, which enhance structures with the direction 315°N (NW-SE), for the total magnetic field intensity.
hg45_sdir315_psgrav_tmi_m&a	Horizontal gradient calculated in direction 45°N, which enhance structures with the direction 315°N (NW-SE), of the pseudogravity field of the total magnetic field intensity from merged Aeromag and MAANAOALA data.
hg360_sdir90_psgrav_tmi_m&a	Horizontal gradient calculated in direction 360°N, which enhance structures with the direction 90°N (E-W), of the pseudogravity field of the total magnetic field intensity from merged Aeromag and MAANAOALA data.

hg315_sdir45_psgrav_tmi_m&a	Horizontal gradient calculated in direction 315°N, which enhance structures with the direction 45°N (NE–SW), of the pseudogravity field of the total magnetic field intensity from merged Aeromag and MAANAOALA data.
tmi	Total magnetic field intensity
tmi_sound_###m_###m	Sounding filtering of the total magnetic field intensity for the field between ### m and ### m (or km if indicated) below the surface.
psgrav_of_tmi	Pseudogravity of the total magnetic field intensity.
psgrav_of_tmi_m&a	Pseudogravity of the total magnetic field intensity from merged Aeromag and MAANAOALA data.
vg_psgrav_tmi	Calculated vertical gradient of the pseudogravity field of the total magnetic field intensity.
vgm	Vertical gradient of the total magnetic field intensity.
2nd_vgm	The second vertical derivative of the total magnetic field intensity.

### Abbreviations of point/symbol data; Symb\_ and associated CB\_ and T\_

**Table 8.** Abbreviations used behind the prefix S\_, and associated CB\_ and T\_ prefixes, for the different types of point/symbol data used in the maps.

Abbreviations	Meaning
grav_station_arveprinsen	Points showing locations of measurements of gravity.

## **Copyright of the data on the CD-ROM**

The Geological Survey of Denmark and Greenland (GEUS) retains copyright of all data in the CD-ROM. The topographic base map in scale 1:2,500,000 included in the images on the CD-ROM originate from the G/2.5 M Vector copyright KMS/GEUS 1997. There are restrictions on the use of the data. In short, the digital map must only be used in conjunction with the CD-ROM and must not be copied or distributed in anyway. For further information see page 2 of the report.